

NORTHWESTERN UNIVERSITY

Resource Efficient Microbial Bioprocesses for Shortcut Nitrogen and Phosphorus Removal from  
Wastewater

A DISSERTATION

SUBMITTED TO THE GRADUATE SCHOOL IN PARTIAL FULFILLMENT OF THE  
REQUIREMENTS

for the degree

DOCTOR OF PHILOSOPHY

Field of Civil and Environmental Engineering

By

Paul Roots

EVANSTON, ILLINOIS

June 2020

## ABSTRACT

Excess loading of reactive nitrogen and phosphorus into the environment from human activities has resulted in widespread eutrophication and the degradation of surface water quality and wildlife habitat. Wastewater is the dominant point source of nutrient loading into waterways, and thus represents a critical opportunity for treatment and prevention of downstream pollution. However, conventional biological processes for nutrient removal from wastewater are energy intensive; wastewater treatment currently consumes 3% of the total electrical energy demand in the United States. Emerging processes in biological wastewater treatment include energy saving methods for shortcut nitrogen removal such as anaerobic ammonia oxidation (anammox) via the partial nitrification/ anammox (PN/A) process, and the nitrification-denitrification process, both of which require less organic carbon and aeration than conventional processes. Application of these processes to mainstream wastewater, subject to low temperatures and fluctuations in flow due to wet weather events, remains a challenge due to the growth of undesirable nitrite oxidizing bacteria (NOB) at low temperatures and the low growth rate of anammox. My research focuses on the integration of shortcut nitrogen removal processes with biological phosphorus removal (which can facilitate phosphorus recovery via struvite precipitation) in the challenging environment of mainstream wastewater. I have investigated two treatment trains; a one-stage process (single reactor) and a two-stage process (separate reactors for nitrogen and phosphorus removal), both of which demonstrated robust combined nitrogen and phosphorus removal at lower energy demand than conventional processes.

The first treatment train, a single sludge method for combined shortcut nitrogen, phosphorus and carbon removal, was the first to demonstrate the compatibility and consistent

performance of nitrification-denitrification and biological phosphorus removal at the moderate mainstream wastewater temperature of 20 °C. Shortcut nitrogen removal likely improved biological phosphorus removal performance due to the increased nitrogen removal (due to lower carbon requirements) and resulting lower concentrations of oxidized nitrogen recycled to the anaerobic zone. Another important finding of this study was the contribution of organic carbon to the suppression of NOB, namely by providing a nitrite sink through denitrification in anoxic zones.

The second treatment train was a two-stage process, and the A-stage comprised a high rate biological phosphorus reactor for combined phosphorus and carbon removal. This reactor advanced understanding of low solids retention time (SRT) biological phosphorus removal systems by being the first to demonstrate a washout SRT for *Candidatus Accumulibacter* polyphosphate accumulating organisms (PAOs) in real mainstream wastewater. Moreover, it was the first to investigate their diversity in low SRT systems via the clade-level dynamics of *Accumulibacter*. *Accumulibacter* clades IIA, IIB and IID dominated the PAO community at the lowest SRT values, while clades IA and IC were washed out, suggesting that certain clades may have higher growth rates and thus be better adapted to low SRT operation.

An integrated fixed-film activated sludge system comprised one of the B-stage reactors of the second treatment train and demonstrated the robust nature of anammox biofilms and their long-term compatibility with low temperature, low concentration environments such as mainstream wastewater. The challenge of NOB out-competition in mainstream deammonification was clearly illustrated in this process, which limited nitrogen removal due to excess nitrate production. Nitrogen removal dramatically improved by rerouting 10% of the

influent flow around the A-stage reactor, thus increasing the influent sCOD-to-ammonia ratio by 35%. This provided an additional nitrite sink via denitrification (the other being anammox) that, like the one-stage nitrification-denitrification reactor discussed above, aided in NOB out-competition and contributed to total nitrogen removal. This reactor illustrated the critical role of organic carbon in mainstream deammonification, which lacks the usual selective pressures for AOB over NOB that exist in the sidestream (high temperatures and elevated free ammonia).

A parallel B-stage reactor for the second treatment train also demonstrated the difficulty of NOB out-competition in mainstream deammonification, but also led to the first clear demonstration of *Nitrospira* comammox as the dominant ammonia oxidizers in a wastewater bioreactor. This discovery suggested that the very conditions of mainstream deammonification – low temperatures, long solids retention times, low dissolved oxygen and ammonia concentrations – may inadvertently select for comammox. Comammox seem to offer a relatively low-energy path for nitrification due to their success in this low dissolved oxygen reactor and may even be compatible with anammox given the increasing research into denitrification-anammox.

In all, these results suggest that the application of shortcut nitrogen removal technologies coupled with biological phosphorus removal holds potential for decreasing the carbon and ecological footprint of wastewater treatment.

**Thesis Adviser**

Dr. George F. Wells, Department of Civil and Environmental Engineering

**Final Examination Committee**

George F. Wells

Aaron I. Packman

Neal Blair

Haydée De Clippeleir

Fenghua Yang

## ACKNOWLEDGEMENTS

So many people contributed to my research in so many varying ways that I know I will fail to list them all, and that my expression of gratitude here will fall short of what is truly deserved. The work contained in this dissertation is my summary of a collaborative project including individuals far beyond the walls of Northwestern and the Metropolitan Water Reclamation District of Greater Chicago (MWRDGC). To present the enclosed work as mine alone would be a gross misrepresentation, and so I submit it with humility, and hope to acknowledge the many individuals that have shaped me and this work over the past five years.

First and foremost, this PhD would not have been possible without my advisor, George Wells. I owe him many thanks for welcoming me into his research group, introducing me to my project, offering thoughtful feedback and research knowledge, finding extra research hands when I needed them, and encouraging me to interact with larger research field through conferences and collaborations.

Alex Rosenthal, who was a postdoc with George when I entered the group, contributed immensely to the work contained in this dissertation. In addition to helping write the proposal and scope of work for the Shortcut Biological Nitrogen Removal project (i.e. the project that would eventually turn into this dissertation) along with George to the MWRDGC, he played a lead role in designing and building the reactor layout that I used for the next four years. Alex also turned out to be (and continues to be) a great friend and mentor, and this dissertation would not be possible without him.

Another Northwestern colleague that deserves special mention is Yubo Wang. Yubo joined George's group as a postdoc near the beginning of my third year, which was a stressful

time for me due to the research workload. Yubo immediately helped by lending her time and expertise in microbial ecology and contributed an enormous amount of work to Chapter 5 of this thesis via DNA extraction, all qPCR assays, gene sequencing sample preparation/data analysis, and FISH sample preparation. She also conducted, along with Jim Griffin, 16S rRNA gene sequencing analysis in other chapters of this thesis.

PhD students that preceded me in George's lab and offered invaluable support and guidance include Jim Griffin, Han Gao, and Morgan Petrovich. Thank you for welcoming me into the lab! Other Northwestern students and post docs that worked directly with me and spent hours in the lab include Zhen Jia, Fabrizio Sabba, Jianing Li, Qiteng Feng, Lachelle Brooks, and John Docter. Quan Yuan, a visiting PhD student from Tsinghua University in China, dedicated much of her year at Northwestern to working with me and contributed both lab work and ideas to my project. Thank you, Quan, for encouraging and helping me to do nitrogen isotope testing! Andrew Masterson in the Northwestern stable isotope laboratory was extremely patient and helpful in measuring isotopes of nitrogen gas from our anammox vs. denitrification batch tests.

Jeff DeCicco of ILS Automation installed the programmable logic control system for our reactor suite, but he went above and beyond his duties as a contractor. With incredible patience and a surprisingly positive attitude he taught me coding and systems integration over several long days, without so much as suggesting that he ought to be properly compensated for his time! My subsequent ability to test sensor-based and other conditional controls on the reactors is entirely thanks to Jeff.

The MWRDGC contributed much more than just funding for my project. They provided a research space at the O'Brien Water Reclamation Plant and I am indebted to the staff and

operators for logistical and mechanical help, including occasionally fixing our floods. MWRDGC researchers that contributed to the initial design and ongoing feedback for this project included Fenghua Yang, Joseph Kozak, and Heng Zhang. Fenghua Yang in particular worked closely with me throughout the past four years, kept me in tune with the needs of wastewater utilities, and served on my dissertation committee. Other MWRDGC staff that helped along the way include Dale MacDonald, Robert Swanson, Thota Reddy, Thaís Pluth, Conor Heffernan and others. MWRDGC interns Christian Landis, Adam Bartecki and George Velez assisted with reactor sampling, batch testing, biomass archiving and more. I am also grateful to the members of my dissertation committee that I have not yet mentioned: Neal Blair, Aaron Packman and Haydee De Clippeleir, for their time and valuable feedback.

Emotional support outside of research was critical to my success within research, and for that I am most indebted to my wife, Sarah, for her incredible support. My parents, friends, and Northwestern CAPS also played a big role in helping me through the most difficult period of my PhD. And many sincere thanks and my apologies to those I have inevitably forgotten to mention! Funding for my research and degree came from Northwestern University, the MWRDGC, and the National Science Foundation (grant number DGE-1842165.)

## TABLE OF CONTENTS

List of Figures .....	13
List of Tables .....	19
Chapter 1: Introduction .....	20
1.1 Problem Statement .....	20
1.1.1 Microbial Nitrogen cycling and Conventional Biological Nitrogen Removal .....	20
1.1.2 Shortcut Nitrogen Removal .....	22
1.1.3 Enhanced Biological Phosphorus Removal .....	24
1.2 Technical Background .....	25
1.2.1 Challenges in shortcut N removal: NOB Out-competition .....	25
1.2.2 Challenges in Deammonification – Promoting Anammox Activity and Biomass Retention .....	28
1.2.3 EBPR Background and Integration with Nitrification-Denitrification .....	30
1.2.4 EBPR and Integration with Carbon Diversion and Recovery .....	32
1.3 Research Approach .....	34
1.4 Layout of Chapters .....	35
Chapter 2: Integrated shortcut nitrogen and biological phosphorus removal from mainstream wastewater: process operation and modeling <sup>1</sup> .....	38
2.1 Introduction .....	39
2.2 Materials and Methods .....	42
2.2.1 Reactor inoculation and operation .....	42
2.2.2 Batch activity assays .....	46
2.2.3 Process Modeling .....	47
2.2.4 Biomass sampling and DNA extraction .....	50
2.2.5 16S rRNA gene amplicon sequencing .....	51
2.2.6 Quantitative Polymerase Chain Reaction (qPCR) .....	51
2.3 Results and Discussion .....	52
2.3.1 Nitrogen, AOO and NOO .....	52
2.3.2 P removal and PAOs .....	65
2.3.3 Functional Guild Analysis: PAO, NOO, and AOO .....	69
2.4 Conclusions .....	73

	10
2.5 Supporting Information.....	74
2.5.1 Supporting Information: Methods.....	74
2.5.2 Process Modeling Reproduces Key Elements of Process Performance .....	81
2.5.3 Supporting Tables .....	82
2.5.4 Supporting Figures.....	84
Chapter 3: Pushing the limits of solids retention time for enhanced biological phosphorus removal: Process characteristics and Accumulibacter population structure <sup>1</sup> .....	91
3.1 Introduction.....	92
3.2 Materials and Methods.....	95
3.2.1 Reactor Operation .....	95
3.2.2 SRT Control.....	96
3.2.3 P Assimilation Calculation .....	97
3.2.4 Reactor Sampling.....	98
3.2.5 <i>In situ</i> Batch Activity Assays.....	98
3.2.6 Reactor Biomass Archiving and DNA Extraction.....	98
3.2.7 16S rRNA Gene Amplicon Sequencing .....	99
3.2.8 Quantitative Polymerase Chain Reaction (qPCR).....	100
3.3 Results.....	101
3.3.1 SRT Optimization and Reactor Performance .....	101
3.3.2 Evidence for P Removal via EBPR .....	106
3.3.3 Accumulibacter vs. GAO Abundance from 16S rRNA Gene Sequencing.....	106
3.3.4 Clade-Specific Accumulibacter Abundance via qPCR.....	107
3.4 Discussion.....	110
3.4.1 Exploring the Limits of High Rate EBPR.....	110
3.4.2 PAO Abundance and GAO Suppression in High Rate EBPR.....	113
3.4.3 Accumulibacter Diversity in High Rate EBPR.....	114
3.4.4 Nitrification in low SRT EBPR Systems.....	115
3.5 Conclusions.....	115
3.6 Supporting Information.....	116
3.6.1 Sludge Volume Index .....	116
3.6.2 Supplementary Figures .....	117

Chapter 4: Practical optimization of the carbon to nitrogen ratio for mainstream deammonification and its impact on aggregate structure <sup>1</sup> .....	120
4.1 Introduction.....	121
4.2 Materials and Methods.....	123
4.2.1 Reactor Operation .....	123
4.2.2 Reactor Sampling, SRT Control, and Batch Activity Assays.....	126
4.2.3 Nitrogen Isotope Testing.....	127
4.2.4 Biomass Sampling, DNA Extraction, qPCR and 16S rRNA Gene Sequencing.....	127
4.3 Results and Discussion .....	128
4.3.1 Phase 1 Reactor Performance .....	128
4.3.2 Long term retention of robust anammox activity under low-concentration mainstream conditions.....	131
4.3.3 Performance Improvement after Addition of 10% PE in Feed and Nitrifier Shift from Carriers to Suspension .....	132
4.3.4 Reactor Performance during the Phase 2 Temperature Decline .....	136
4.3.5 Community analysis via 16S rRNA gene sequencing and qPCR.....	138
4.3.6 Quantification of anammox vs denitrification contribution to N removal .....	140
4.3.7 Implications for Practice .....	143
4.4 Supporting Information.....	143
4.4.1 Batch Activity Assays.....	143
4.4.2 Nitrogen Isotope Testing.....	146
4.4.3 Biomass sampling .....	147
4.4.4 16S rRNA Gene Sequencing .....	148
4.4.5 qPCR.....	149
4.4.6 Supplementary Figures .....	149
Chapter 5: Comammox Nitrospira are the dominant ammonia oxidizers in a mainstream low dissolved oxygen nitrification reactor <sup>1</sup> .....	155
5.1 Introduction.....	156
5.2 Methods.....	159
5.2.1 SBR operation/control, inoculation, online sensors, and batch activity assays .....	159
5.2.2 Full-scale secondary treatment at O'Brien WRP .....	161
5.2.3 Analytical methods .....	162

5.2.4 Biomass sampling and DNA extraction.....	162
5.2.5 Quantitative PCR and comammox <i>amoA</i> cloning.....	162
5.2.6 16S rRNA, <i>amoA</i> , and <i>nxrB</i> gene amplicon sequencing.....	163
5.2.7 Quantitative Fluorescence <i>in situ</i> Hybridization (qFISH).....	164
5.3 Results.....	164
5.3.1 Bioreactor performance.....	164
5.3.2 16S rRNA gene sequencing demonstrates strong enrichment of <i>Nitrospira</i> and decline in AOB.....	168
5.3.3 Functional gene quantification reveals dominance of comammox over canonical AOB.....	170
5.3.4 qFISH confirms <i>Nitrospira</i> enrichment.....	174
5.3.5 Functional gene sequencing.....	175
5.4 Discussion.....	178
5.4.1 High NOB to AOM ratios.....	181
5.5 Conclusions.....	184
5.6 Supporting Information.....	185
5.6.1 Methods.....	185
5.6.2 Analysis of FISH probe Ntspa476 specificity.....	193
5.6.2 Supporting Tables and Figures.....	196
Chapter 6: Summary and Future Work.....	203
6.1 Summary of Key Findings.....	203
6.1.1 Single Sludge Nitrification-Denitrification with EBPR.....	203
6.1.2 High Rate EBPR.....	205
6.1.3 Deammonification IFAS.....	207
6.1.4 Comammox SG.....	208
6.2 Future Work.....	209
References.....	212

## LIST OF FIGURES

Figure 1.1 Major nitrogen removal pathways. O <sub>2</sub> demand and reducing equivalents are per mole N removed as reported in Gao et al., (2014), and are based on typical SRT and yield of each process.....	22
Figure 1.2 Simplified schematic of the polyphosphate accumulating organism (PAO) metabolism under anaerobic (left), aerobic (top right), and anoxic (bottom right) conditions. Image by Han Gao and used with permission. ....	25
Figure 1.3 Reactor operation timeline and relation to chapter content. ....	37
Figure 2.1 Reactor performance over time from composite sampling (2 – 3 samples/week) over the entire study. A) Influent (primary effluent) NH <sub>4</sub> <sup>+</sup> and effluent NH <sub>4</sub> <sup>+</sup> , NO <sub>2</sub> <sup>-</sup> , and NO <sub>3</sub> <sup>-</sup> . B) Influent and effluent orthophosphate. C) Nitrite accumulation ratio (NAR) and percent removal of NH <sub>4</sub> <sup>+</sup> , orthophosphate and TIN. ....	53
Figure 2.2 A) and B) Two react cycles on days 328 and 414, respectively, that demonstrate efficient P and N removal, selective nitrification, and variability in aerated react length. Cycle A included measurements for rbCOD and VFAs, and cycle B was run with an N <sub>2</sub> O sensor in the reactor. C) SBR cycle as modeled in SIMBA#. rbCOD as shown was calculated as soluble COD <sub>t</sub> – soluble COD <sub>effluent</sub> .....	56
Figure 2.3 Maximum specific AOO and NOO activity as measured by <i>ex situ</i> batch testing. Error bars represent the standard deviation of the method replicates. ....	57
Figure 2.4 Comparison plot between high resolution within-cycle reactor sampling (A) and modeled results (B, C, D) for the intermittently aerated react period of SBR operation (minutes 65 – 105, beginning 20 minutes after the start of aeration). A) Results of grab sampling from a reactor cycle on day 258 of operation. Selective nitrification rather than nitrification during aerated phases (gray shading) is evident and produced NO <sub>2</sub> <sup>-</sup> is then denitrified in anoxic phases. The scan optical DO sensor is rated for a 60-second response time, and a ~1-minute delay is evident in comparison to the model plot B. B) Modeled concentration dynamics including on/off switching for aeration control. C) Modeled AOO and NOO net specific growth rates including decay. D) Modeled PAO specific growth rates associated with P uptake via O <sub>2</sub> , NO <sub>2</sub> <sup>-</sup> and NO <sub>3</sub> <sup>-</sup> . Decay and growth not associated with P uptake are not included. ....	59
Figure 2.5 P uptake rates in the presence of O <sub>2</sub> , NO <sub>2</sub> <sup>-</sup> , and NO <sub>3</sub> <sup>-</sup> from <i>ex situ</i> batch tests. ....	67
Figure 2.6 Relative AOO and NOO abundance based on 16S rRNA gene amplicon sequencing through the first 421 days of reactor operation. Day “0” represents the inoculum, which was sampled before reactor operation began. ....	71
Figure 2.S1 Process representation in the Simba# 3.0 software. ....	84
Figure 2.S2 Total and aerobic dynamic SRT over time in the SBR. The average total and aerobic SRT during Phase 1 was 11 ± 7 and 4.5 ± 3.0 days, and the average total and aerobic SRT during	

Phase 2 was $9.2 \pm 1.8$ and $3.6 \pm 0.9$ days, respectively. *Mixed liquor wasting was suspended from days 158 – 195 to recover AOO activity.....	85
Figure 2.S3 In-cycle N and P removal rates from least-squares regression of the linear portions of in-cycle grab samples for $\text{NH}_4^+$ , $\text{NO}_2^-$ , $\text{NO}_3^-$ , and $\text{PO}_4^{3-}$ . Error bars represent standard errors of the slopes.....	86
Figure 2.S4 Relative <i>Accumulibacter</i> , <i>Tetrasphaera</i> , and <i>Competibacter</i> abundance through the first 421 days of reactor operation according to 16S rRNA gene sequencing. Day “0” represents the inoculum, which was sampled before reactor operation began. ....	87
Figure 2.S5 Ammonia oxidizing bacterial <i>amoA</i> gene abundance normalized to total bacterial 16S rRNA genes through the first 421 days of reactor operation according to qPCR. ....	87
Figure 2.S6 Reactor influent and effluent alkalinity concentrations from composite sampling. .	88
Figure 2.S7 Reactor influent and effluent total phosphorus concentrations from composite sampling.....	88
Figure 2.S8 Reactor mixed liquor TSS and VSS concentrations.....	89
Figure 2.S9 Reactor influent and effluent filtered COD from composite sampling. Samples were filtered through a 1.2 $\mu\text{m}$ pore size membrane. ....	89
Figure 2.S10 Reactor influent and effluent total COD concentrations from composite sampling. ....	90
Figure 2.S11 Reactor influent and effluent TKN concentrations from composite sampling. ....	90
Figure 3.1 Hydraulic retention time (HRT), total solids retention time (SRT) and aerobic SRT throughout the study. ....	103
Figure 3.2 Reactor influent and effluent orthophosphate from daily composite samples throughout the study. ....	103
Figure 3.3 Two representative in-cycle batch tests from Phase 2, A = day 457 and B = day 485. ....	105
Figure 3.4 Relative abundance of PAO and GAO taxonomic groups according to 16S rRNA gene amplicon sequencing. <i>Ca. Competibacter</i> was the most abundant GAO identified; other GAOs present at some time points and included in “Total GAO” above were <i>Ca. Contendobacter</i> , <i>Micropruina</i> , <i>Propionivibrio</i> , and <i>Deftuviicoccus</i> . Relative abundance of nitrifiers from 16S rRNA gene sequencing is shown separately in Figure 3.S2. ....	107
Figure 3.5 Abundance of <i>Ca. Accumulibacter</i> Clades IA, IC, IIA, IIB and IID relative to total bacteria according to qPCR. Clades detected but at negligible abundance (<0.3% at all time points) and not shown in this plot include clades IB, ID, IE, IIC and IIF. Standard deviations for clade-specific data points are shown in Figure 3.S5.....	109

- Figure 3.6 Non-metric multidimensional scaling (NMDS) ordination of *Accumulibacter* clade population structure, calculated from clade-specific qPCR data. The SRT for each sample is the average of 3 measurements (taken over about 1 week) prior to the sample date. The inoculum (day 0) came from an EBPR process with an SRT around 8 days, which is not represented on the SRT scale bar. The significance of the ordination is represented by the stress value of 0.07. ... 109
- Figure 3.S1 Influent ammonium ( $\text{NH}_4^+$ ) and effluent ammonium and nitrite + nitrate ( $\text{NO}_x$ )... 117
- Figure 3.S2 Reactor mixed liquor total suspended solids (TSS) and volatile suspended solids (VSS)..... 117
- Figure 3.S3 Orthophosphate (P) release and uptake rates from *in situ* batch activity assays. Error bars represent the standard error of the fitted linear slope..... 118
- Figure 3.S4 Relative abundance of nitrifiers detected from 16S rRNA gene sequencing. The presence of nitrifiers was generally associated with the presence of  $\text{NO}_x$  in the effluent (see Figure 3.S1)..... 118
- Figure 3.S5 Abundance of *Accumulibacter* clades relative to total bacteria according to qPCR. Clades detected but at negligible abundance (<0.3% at all time points) and not shown in this plot include clades IB, ID, IE, IIC and IIF. “Total *Accumulibacter*” represents the sum of the individual clades. .... 119
- Figure 4.1 Reactor temperature and performance over 1,128 days of reactor operation. A: Average daily reactor temperature and suspended SRT. The higher frequency of SRT data points beginning on day 358 is due to implementation of variable react length based on the online ammonia sensor, at which point the SRT value was calculated on a per-cycle basis. B: Reactor volatile solids (VS) on the carriers and in the suspension. C: Influent  $\text{NH}_4^+$  and effluent  $\text{NH}_4^+$ ,  $\text{NO}_x$  ( $\text{NO}_2^- + \text{NO}_3^-$ ) (all shown as ~2-week rolling average) and  $\text{NO}_2^-$  (shown as discrete measurements) concentrations as measured from composite sampling. D:  $\text{NH}_4^+$  and total inorganic nitrogen (TIN) removal (both shown as ~2-week rolling averages) calculated from composite sampling measurements. E: Ratio of  $\text{NO}_3^-$  produced to  $\text{NH}_4^+$  removed as calculated from composite sampling measurements. The ratio of 0.11, shown in the graph, represents the theoretical combined stoichiometry of nitrification-anammox..... 129
- Figure 4.2 Relative abundance of key functional groups in the attached growth biomass (panel A) and suspended growth biomass (panel B) according to 16S rRNA gene sequencing. Genera detected included *Nitrosomonas* for AOB, *Nitrospira*, *Nitrolancea* and *Nitrotoga* (in order of abundance) for NOB, and *Candidatus Brocadia* for anammox. Panel C shows the anammox hydrazine synthase (*hzsA*) gene copy number from carrier biomass according to qPCR, normalized to ng DNA..... 130
- Figure 4.3 Maximum anammox activity from *in situ* activity tests along with associated test temperatures. The reactor total N loading rate was calculated as a weekly average. .... 132

Figure 4.4 Maximum AOB and NOB activities in the suspended biomass and on the carriers as measured in <i>ex situ</i> batch activity assays from day 800 to the end of the project. The entire dataset of AOB and NOB activity measurements is shown in Figure 4.S1.....	133
Figure 4.5 Results from nitrogen isotope testing, which was performed to quantify relative contributions of anammox (which produce $^{29}\text{N}_2$ in this test) and denitrification (which produce $^{30}\text{N}_2$ ) to N removal. The testing schematic is shown in the top panel and results from day 1,128 are shown on the bottom panel. ....	141
Figure 4.S1 Maximum AOB and NOB activities in the suspended biomass and on the carriers as measured in <i>ex situ</i> batch activity assays over the entire project. The red box outlines the data shown in Figure 4.4.....	150
Figure 4.S2 Hydraulic retention time (HRT) and daily average reactor temperature throughout the study. Variable HRT began on day 358 upon implementation of ammonia-based control, whereupon the aerated portion of the cycle was terminated when the target effluent ammonia concentration of 2 mg $\text{NH}_4^+$ -N/L was reached. After day 358 the HRT was calculated on a per-cycle basis. ....	150
Figure 4.S3 Arrhenius plot of 15 maximum specific anammox activity tests (normalized to total carrier biomass) during Phase 2 (days 904 – 1,121). The activation energy calculated from the slope was $71 \pm 8$ kJ/mol ( $\pm$ standard error of the slope), though this should not be interpreted as a strict activation energy considering possible temperature adaptation and shifts in the microbial community over the 217 days. ....	151
Figure 4.S4 Non-metric multidimensional scaling (NMDS) ordination of all carrier and suspended biomass samples as calculated from genus-level 16S rRNA gene sequencing data. In order to facilitate convergence of the solution, the data was first trimmed to remove the least abundant genera comprising 0.09% of the total abundance. The significance of the ordination is represented by the stress value of 0.096. ....	151
Figure 4.S5 Two representative in-cycle tests during Phase 2 from (A) day 909 at 18.9 °C and (B) day 1107 at 21.1 °C. Reactor fill (not shown) occurred in less than 2 minutes, and cycle time = 0 is defined as the completion of fill. ....	152
Figure 4.S6 Relative abundance of the 14 most abundant bacterial genera in the carrier biomass according to 16S rRNA gene sequencing. Amplicon sequence variants that were unclassified at the genus level are presented with the corresponding lowest annotable taxonomy: p_ = phylum, c_ = class, o_ = order, f_ = family, g_ = genus. ....	153
Figure 4.S7 Relative abundance of the 14 most abundant bacterial genera in the suspended biomass according to 16S rRNA gene sequencing. Amplicon sequence variants that were unclassified at the genus level are presented with the corresponding lowest annotable taxonomy: o_ = order, f_ = family, g_ = genus. ....	154
Figure 5.1 Nitrogen concentrations in reactor influent and effluent over time. All parameters are shown as a two-week rolling average. “ $\text{NO}_3^-$ ” was measured as $\text{NO}_3^- + \text{NO}_2^-$ , but weekly effluent	

NO<sub>2</sub><sup>-</sup> measurements revealed that NO<sub>2</sub><sup>-</sup> comprised <1% of NO<sub>3</sub><sup>-</sup> + NO<sub>2</sub><sup>-</sup> on average (max 6%).  
 ..... 165

Figure 5.2 Maximum specific activities for aerobic ammonia oxidation rate, nitrite oxidation rate, and anaerobic ammonia oxidation (anammox) rate in reactor biomass over time from batch assays. Rates were measured under non-limiting substrate concentrations..... 166

Figure 5.3 Relative abundance of total *Nitrospira*, total AOB (all *Nitrosomonas*) and total anammox (all *Brocadia*), based on 16S rRNA gene amplicon sequence analysis. Relative abundance for *Nitrospira* is shown on the left y-axis, and AOB and anammox are shown on the right y-axis. *Nitrospira* OTU2 and OTU4 together comprise 95.3 – 99.8% of total *Nitrospira* for all time points..... 169

Figure 5.4 Abundance of *Nitrospira nxrB* (squares), AOB *amoA* (circles), and comammox *amoA* (diamonds), as measured by qPCR. Results are normalized to total bacterial 16S rRNA gene copies. *Nitrospira* results are shown on the left y-axis, and AOB and comammox results are shown on the right y-axis..... 171

Figure 5.5 Phylogenetic affiliation of comammox *amoA* gene sequences from the low DO nitrification reactor via cloning and sanger sequencing and via high throughput amplicon sequencing (173 bp fragment). Scale bars indicate estimated change per nucleotide sequence. a) Maximum likelihood tree showing the phylogenetic relationship of the 3 clone sequences and 8 amplicon sequence variants (ASV) from sequencing (circled in above tree) with other *amoA* gene superfamily members (167 sequences). b) Maximum likelihood tree showing phylogenetic relationship between the 3 comammox *amoA* clone sequences and 8 comammox *amoA* ASV from amplicon sequencing (black, names beginning with NU\_comammox) with NCBI database-derived comammox *amoA* gene sequences. The *amoA* gene from *Nitrosococcus watsonii* C-113 was applied as the outgroup. The heatmap indicates the relative abundance of the 8 comammox *amoA* ASV we detected in reactor biomass at the six time-points. Genome-derived comammox *amoA* genes are in magenta and other database-derived comammox *amoA* genes are in light gray. Nodes with the bootstrap value > 70% have all been marked with a gray circle, and the size of the circle is in positive correlation with the bootstrap value. .... 173

Figure 5.6 qFISH results of Ntspa476 probe (see text section 3.4 and (van Kessel et al., 2015), total *Nitrospira*, total AOB, and total bacteria. See Supporting Information regarding the specificity of the Ntspa476 FISH probe to comammox..... 174

Figure 5.7 Maximum-likelihood phylogenetic tree of *Nitrospira nxrB* gene sequences (453 bp fragment). The *nxrB* gene from *Nitrobacter hamburgensis* X14 was applied as the outgroup. Nodes with the bootstrap value > 70% have all been marked with a gray circle, and the size of the circle is in positive correlation with the bootstrap value. 30 *nxrB* ASV recovered in this study on day 407 of reactor operation are shown in bold as “NU *nxrB* ###”. In magenta are *nxrB* genes from known comammox *Nitrospira* genomes, and in purple are *nxrB* genes of known non-comammox *Nitrospira* genomes. Percentages to right of the tree indicate relative abundance of *nxrB* clusters relative to total *nxrB* in the low DO nitrification reactor. The red to white heatmap

indicates the percentage of each NU *nxB* ASV relative to the overall *Nitrospira* in the reactor. No *nxB* genes from currently available genomes cluster with the 10 and 38% abundance NU *nxB* clusters, so the three closest non-genome database sequences are shown as “[*accession #*] activated sludge”..... 177

Figure 5.S1 Relative abundance of the 15 most abundant bacterial genera at each time point according to 16S rRNA gene sequencing data. Sampling time point is shown on the x axis. The OTUs that were unclassified at the genus level are presented with the corresponding lowest annotable taxonomy names; ‘f\_’ indicate ‘Family’, and ‘o\_’ indicates ‘Order.’ ..... 198

Figure 5.S2 Principle Coordinate Analysis of weighted unifracs distances between samples, based on 16S rRNA gene amplicon sequencing analyses. Samples from the low DO bench-scale reactor are indicated by circles, and a single sample for comparison in the parallel full-scale high DO nitrifying activated sludge bioreactor is indicated by a square. Samples are color coded by time of sampling..... 199

Figure 5.S3 Maximum-likelihood phylogenetic tree of the 5 *Nitrospira* 16S rRNA gene amplicon sequence variants (ASV) (370 bp fragment) in the two dominant OTUs (OTU2 and OTU4, clustered to 97% identity). The heatmap shows the abundance of each of the 5 ASV against the total number of the 16S rRNA gene reads. .... 200

Figure 5.S4 Representative FISH micrograph of showing co-aggregation of *Nitrospira*, *Nitrosomonas* and Ntspa476-hybridized *Nitrospira* in the low DO bench scale nitrification reactor consortium on day 407. DAPI counterstaining is in grey, and probes specific for *Nitrospira* (Ntspa662 and Ntspa712, blue), a subset of *Nitrospira* that includes known comammox (Ntspa476, red; red + blue = magenta), and *Nitrosomonas* (AOB mix: NEU, Nso1225, Cluster6a192; green) ..... 201

Figure 5.S5 Maximum-likelihood phylogenetic tree of the 16S rRNA genes that could be targeted by FISH probe Ntspa476 (originally designed to target specific comammox taxa) and *Nitrospira* FISH probe mix (Ntspa662 and Ntspa712). Magenta indicates sequences predicted to hybridize with both Ntspa476 and the *Nitrospira* probe mix; blue indicates sequences predicted to hybridize with only the *Nitrospira* probe mix; pink indicates the 16S rRNA genes from three comammox genomes; and black indicates the five *Nitrospira* 16S rRNA gene ASV that were dominant in the reactor consortium of this study, with the relative abundance of each indicated in the heatmap. Numbers in parentheses after taxonomy names indicate the number of 16S rRNA genes that are predicted to hybridize with the *Nitrospira* FISH probes (Ntspa662 or Ntspa712) in the corresponding taxa. The heatmap indicates the abundance of each the *Nitrospira* 16S rRNA gene ASV against the total number of the 16S rRNA gene reads. .... 202

## LIST OF TABLES

Table 2.1 SBR cycle timing (gravity fill, anaerobic reactor, aerobic react, wasting, settling, and decant) and reactor control details. The end of the SBR aerobic (intermittently aerated) react phase was determined based on an $\text{NH}_4^+$ setpoint shown in the table. ....	43
Table 2.2 Arithmetic mean $\pm$ standard deviation of composite sampling results for influent (primary effluent) and reactor effluent concentrations. Results from Phase 1 are highlighted in light gray and results from Phase 2 are highlighted in dark gray. Process model predictions are for Phase 2 only. Additional information regarding influent COD fractionation can be found in Table 2.S2. ....	54
Table 2.3 Summary of $\text{N}_2\text{O}$ emission measurements reported in the literature for conventional and shortcut N removal processes. Conventional nitrogen removal processes (nitrification-denitrification) are highlighted in grey while shortcut nitrogen removal processes (nitritation-denitrification and nitritation-anammox) are highlighted in white. ....	64
Table 2.S1 Sampling frequency and target analytes (per APHA, 2005) for daily composite samples. All samples listed are of reactor influent and effluent except $\text{NO}_2^-$ -N (effluent only) and mixed liquor TSS and VSS (sampled in-reactor). ....	82
Table 2.S2 Influent (primary effluent) COD fractionation and COD-to-nutrient ratios. ....	83
Table 2.S3 $\text{N}_2\text{O}$ emissions test results for 8 cycles during Phase 2. ....	83
Table 3.1 Reactor influent (O'Brien WRP primary effluent) average values over the entire study and reactor effluent values averaged over the three phases. ....	102
Table 3.2 Comparison table for key studies of low sludge age EBPR processes. ....	112
Table 4.1 Average reactor influent and effluent concentrations over the two phases. ....	134
Table 5.1 Low DO nitrification reactor influent (A-stage effluent) and effluent average composition, along with primary effluent and parallel full-scale (O'Brien WRP) nitrifying activated sludge bioreactor effluent concentrations. ....	160
Table 5.S1 16S rRNA-targeted oligonucleotide FISH probes used in this study. ....	196
Table 5.S2 GenBank accession numbers for <i>Nitrospira nxrB</i> and comammox <i>amoA</i> amplicon sequence variants, comammox <i>amoA</i> clone sequences, and raw sequencing data. ....	197

## CHAPTER 1: INTRODUCTION

### 1.1 Problem Statement

Nitrogen (N) and phosphorus (P) are two key nutrients that limit primary productivity (i.e. of plants, algae and certain bacteria) in aquatic environments. Bacterial and algal blooms harmful to aquatic life and human health have increased in both fresh water and marine habitats due nutrient pollution from agriculture and wastewater effluent. The problem is both local and global: Of nine planetary boundaries identified by Steffen et al., the biogeochemical flows of both N and P have already been exceeded “beyond the zone of uncertainty” and pose a high risk to the stability of the earth system (Steffen et al., 2015). The dominant *point* source (i.e. from a discrete, treatable location) of N and P to the environment is wastewater, so their removal is an increasingly critical and stringently enforced objective of municipal wastewater treatment. Unfortunately, conventional wastewater treatment demands a significant amount of energy – currently ~3% of the electrical supply in the U.S. (Scherson and Criddle, 2014) – making it a major contributor to another planetary boundary: climate change.

#### 1.1.1 Microbial Nitrogen cycling and Conventional Biological Nitrogen Removal

Biological wastewater treatment systems are engineered mixed culture microbial ecosystems designed to remove chemical oxygen demand (COD) and nutrients such as N and P. We are only beginning to understand the phylogenetic diversity of these mixed communities, which contain up to trillions of cells per milliliter. Some of what we do know about conventional biological N removal, termed nitrification-denitrification, is as follows: ammonia-oxidizing microorganisms (AOM, which can be both bacteria and archaea) oxidize ammonium ( $\text{NH}_4^+$ ) to

nitrite ( $\text{NO}_2^-$ ), and nitrite-oxidizing bacteria (NOB) oxidize  $\text{NO}_2^-$  to nitrate ( $\text{NO}_3^-$ ). The coupled activity of AOM and NOB is termed nitrification. Both AOM and NOB are aerobic and require oxygen for growth and activity. It should also be noted that **complete ammonia oxidizers** (comammox), discovered in 2015 (Daims et al., 2015; van Kessel et al., 2015), are able to completely nitrify  $\text{NH}_4^+$  to  $\text{NO}_3^-$ , but their role in biological N removal processes is at present little understood. Denitrifying bacteria then reduce  $\text{NO}_3^-$  to nitrogen gas ( $\text{N}_2$ ) under anoxic conditions (long-dashed green arrows in Figure 1.1). Conventional nitrification-denitrification processes require energy intensive aeration to supply  $\text{O}_2$  as the electron acceptor for nitrification and electron donors typically in the form of COD for denitrification. Aeration in the form of blowers is generally the major energy consuming process in a wastewater treatment plant – about 50% of total energy – so strategies to reduce aeration requirements are highly desirable. The COD requirement represents a loss of the  $1.66 \text{ kWh/m}^3$  of chemical energy in municipal wastewater (Scherson and Criddle, 2014), so utilities are looking to maximize COD redirection to energy/resource recovery processes to achieve energy neutral or energy positive treatment.

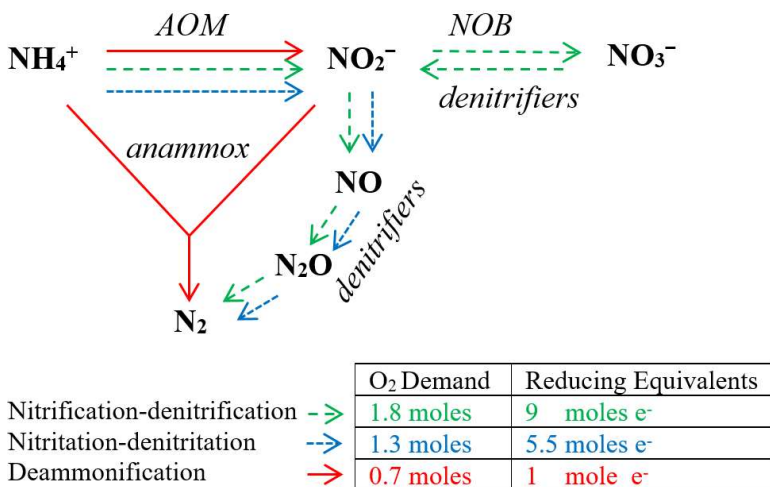


**Figure 1.1** Major nitrogen removal pathways. O<sub>2</sub> demand and reducing equivalents are per mole N removed as reported in Gao et al., (2014), and are based on typical SRT and yield of each process.

### 1.1.2 Shortcut Nitrogen Removal

Promising energy-saving strategies in wastewater treatment include shortcut N removal bioprocesses, which dramatically reduce energy requirements and decouple COD from N removal. Two strategies for shortcut N removal will be investigated here: nitritation-denitritation and deammonification.

1. The nitritation-denitritation N removal pathway (also called nitrite-shunt) is similar to conventional nitrification-denitrification, with the exception that NO<sub>2</sub><sup>-</sup> is never oxidized to NO<sub>3</sub><sup>-</sup>. Rather, NO<sub>2</sub><sup>-</sup> produced by AOM is reduced directly by denitrifiers to N<sub>2</sub>. Compared to conventional nitrification-denitrification, the nitritation-denitritation pathway can reduce oxygen requirements by ~28% (thereby substantially reducing energy demand) and COD requirements by nearly 40% (Gao et al., 2014).

2. In the deammonification bioprocess, anammox (**anaerobic ammonium oxidation**) bacteria oxidize  $\text{NH}_4^+$  directly to  $\text{N}_2$  in the presence of  $\text{NO}_2^-$  (solid red arrows in Figure 1.1). Therefore, the oxidation of  $\text{NO}_2^-$  to  $\text{NO}_3^-$  by NOB and reduction back to  $\text{NO}_2^-$  by denitrifiers is bypassed. Partial nitrification, the oxidation of  $\text{NH}_4^+$  to  $\text{NO}_2^-$  by AOM, is still necessary to provide  $\text{NO}_2^-$  for anammox. Compared to conventional nitrification/denitrification, the nitrification-anammox process can reduce oxygen requirements by ~60% and COD requirements by nearly 100%, thereby enabling rerouting of endogenous COD to the sidestream for energy or value-added product generation.

Selective nitrification (via NOB washout) has been demonstrated via the SHARON (**single reactor high activity ammonia removal over nitrite**) process (Hellings et al., 1998) in the relatively high temperatures of digester centrate. Similarly, the deammonification bioprocess is a proven strategy for N removal from relatively concentrated ( $>300$  mg  $\text{NH}_4\text{-N/L}$ ) waste streams, such as anaerobic digester centrate, with over 100 full-scale processes implemented worldwide (Lackner et al., 2014). Application of nitrification-denitrification or deammonification to mainstream wastewater flows is still in the research stage but could maximize the impact of these savings, as 80-85% of a typical plant's total N load is not directed to the sludge handling side stream (Fux et al., 2002). Moreover, the organic carbon savings can be redirected via a high-rate activated sludge "A" stage process for energy recovery (Rahman et al., 2015), for value added product generation, or to support enhanced biological phosphorus removal (EBPR) processes for facilities with total P limits. An enhanced phosphorus recovery process also provides the opportunity for recovery and reuse of this limited resource (Yuan et al., 2012).

### 1.1.3 Enhanced Biological Phosphorus Removal

Biological phosphorus removal from wastewater is possible via polyphosphate accumulating organisms (PAOs) in the EBPR process. Under anaerobic conditions, PAOs take up readily biodegradable COD (rbCOD) such as acetate and propionate and convert it to intracellular polyhydroxyalkanoates (PHAs) at the expense of internally stored polyphosphate, which is released into the bulk water in the form of orthophosphate (Figure 1.2). When said anaerobic conditions are followed by aerobic conditions, PAOs will oxidize the stored PHAs to take up excess orthophosphate and store it internally as polyphosphate. By removing biomass from the reactor at the end of this aerobic phase, P can be both removed from the waste stream and potentially recovered from the biomass (Yuan et al., 2012). While EBPR is a widely applied technology in wastewater treatment, an unexplored challenge is how to maximize COD diversion and recovery in tandem with P removal and shortcut N removal. Biological methods for recovering both COD and P will be explored in this study along with shortcut N removal.

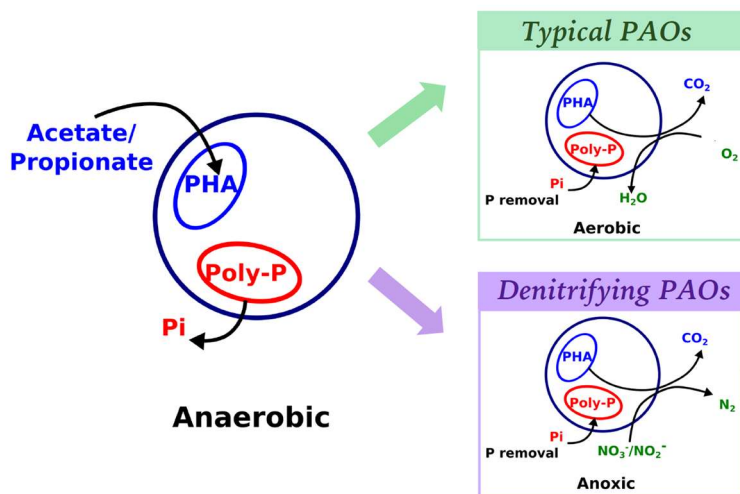


**Figure 1.2** Simplified schematic of the polyphosphate accumulating organism (PAO) metabolism under anaerobic (left), aerobic (top right), and anoxic (bottom right) conditions. Image by Han Gao and used with permission.

## 1.2 Technical Background

### 1.2.1 Challenges in shortcut N removal: NOB Out-competition

NOB out-competition is key to the N removal performance and efficiency of both nitrification-denitrification and deammonification, and nitrifier diversity and metabolic versatility is critical to understanding and anticipating successful NOB out-competition strategies. In engineered systems, the dominant genus-level NOB are *Nitrospira* and *Nitrobacter*. *Nitrospira* are typically considered K-strategists (it should be noted that this is an oversimplification to give a sense of relative niches), in that they have a relatively high affinity for oxygen and NO<sub>2</sub><sup>-</sup>, while *Nitrobacter* are r-strategists (another oversimplification) and typically have a relatively low affinity for oxygen and NO<sub>2</sub><sup>-</sup> (Nowka et al., 2015). The *Nitrospira* genus also contains various comammox *Nitrospira* species, the first of which were discovered in 2015 (Daims et al., 2015; van Kessel et al., 2015), which are able to oxidize NH<sub>4</sub><sup>+</sup> all the way to NO<sub>3</sub><sup>-</sup>. At least one species

of comammox *Nitrospira* is known to have an especially high affinity for  $\text{NH}_4^+$  (Kits et al., 2017). It is not well known how significant a role comammox *Nitrospira* play in engineered N removal systems. AOM contain both bacteria, which include the genera *Nitrosomonas* and *Nitrosospira*, as well as archaea, which are usually not as abundant in wastewater treatment systems as ammonia oxidizing bacteria (Wells et al., 2009).

In conventional nitrification-denitrification processes, NOB activity unnecessarily increases oxygen demand (relative to AOM activity alone) and organic carbon demand (for the subsequent heterotrophic denitrification of  $\text{NO}_3^-$  to  $\text{NO}_2^-$ ), and thus may limit N removal due to COD limitation. Many conventional nitrification-denitrification systems are COD limited, and therefore supplement organic carbon to promote complete denitrification. Sidestream conditions naturally favor AOM selection over NOB in the following ways:

1. AOM exhibit faster growth rates and higher oxygen affinity than NOB at elevated temperatures (Hellings et al., 1998), typically around 30°C for digester centrate, such that NOB can be selectively washed out with SRT control.
2. Free ammonia concentrations of 0.08 – 0.8 mg  $\text{NH}_3\text{-N/L}$  and free nitrous acid concentrations of 0.07 – 0.83 mg  $\text{HNO}_2\text{-N/L}$  are thought to partially inhibit NOB growth (Anthonisen et al., 1976), and one or both ranges are exceeded under most sidestream operating conditions. Taken together, (1) and (2) allow for selective enrichment of AOM and washout of NOB in suspension, and out-competition of NOB by AOM in biofilms for space and dissolved oxygen (DO).

In contrast, NOB out-competition is an enduring challenge for successful operation of mainstream deammonification and nitrification-denitrification processes because neither high

temperatures that favor AOM nor elevated concentrations of inhibitors are generally achieved; temperatures are generally below 20°C and free ammonia concentrations are generally below 0.08 mg NH<sub>4</sub><sup>+</sup>-N/L. A diversity of strategies that have been proposed in the literature for favoring AOM growth over NOB in the mainstream include the following:

1. Maintaining an NH<sub>4</sub><sup>+</sup> residual of 2 mg N/L or higher (Stinson et al., 2013) coupled with low NO<sub>2</sub><sup>-</sup> in the reactor is thought to aid in selection of AOM over NOB. Elevated NH<sub>4</sub><sup>+</sup> residual is thought to aid NOB out-competition by maintaining a high AOM growth rate (Stinson et al., 2013), or in the case of biofilms, by increasing AOM oxygen consumption at the biofilm surface (i.e. avoid NH<sub>4</sub><sup>+</sup> limitation) and limiting the depth at which NOB are able to survive within the biofilm (Poot et al., 2016).
2. Intermittent aeration has been found to partially inhibit NOB growth (Wett et al., 2015). Gilbert et al. found that *Nitrospira* NOB experience a lag phase in metabolic activity after an anoxic period greater than 15 minutes, while AOM do not (Gilbert et al., 2014a). This lag phase was found to last from 10 to 15 minutes, offering a potential window for selective NO<sub>2</sub><sup>-</sup> drawdown by anammox and/or denitrifiers.
3. Particle selection through sieving, hydrocyclones, or biofilms with tight SRT control of flocs can aid NOB washout, which are thought to favor growth in loose floccules, while maintaining denser and larger granules that tend to harbor anammox (Han et al., 2016b).
4. Segregation of NOB into the suspended biomass and off of biocarriers has been modeled by maintaining a greater suspended biomass concentration (Hubaux et al., 2015) and demonstrated in a bench-scale integrated fixed film activated sludge (IFAS) process

(Laureni et al., 2019). This segregation may then allow for NOB washout by SRT control of the suspended biomass.

Despite the many strategies available, there is a lack of consensus in the literature as to the efficacy of these approaches, especially given the wide range of conditions found in mainstream wastewater. In fact, given this difficulty, in recent years some researchers have abandoned efforts to suppress NOB and have turned towards systems for full nitrification, denitrification (i.e. production of  $\text{NO}_2^-$  from denitrifier  $\text{NO}_3^-$  reduction) and anammox. Such systems may operate in a single compartment with intermittent aeration (Zheng et al., 2016), with separate compartments for nitrification and denitrification/anammox (B. Ma et al., 2017a) or a combination thereof (Le et al., 2019a). While such systems will lose some of the metabolic efficiency of pure nitrification/anammox, they may be easier to maintain without the need for tight SRT control for NOB washout.

Which strategies do/do not work in what combinations and under what conditions is a subject of ongoing research. Of interest to this study is the effectiveness of different strategies for NOB out-competition in biofilm vs. suspended growth bioprocesses, or under what conditions their presence is compatible with high N removal.

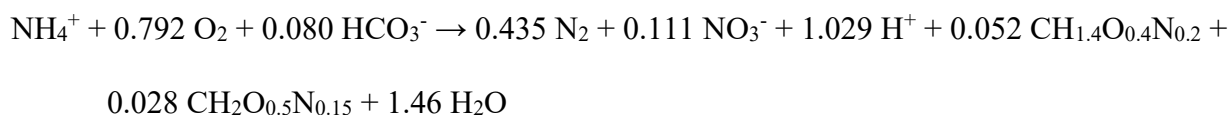
### **1.2.2 Challenges in Deammonification – Promoting Anammox Activity and Biomass**

#### **Retention**

Despite widespread research into mainstream deammonification, challenges abound that stall application to full-scale systems. Anammox are slow growing and more sensitive to temperature reduction than AOM, NOB, and heterotrophs (Lotti et al., 2015c), implying reduced process stability at low temperatures that are typical of the mainstream when compared to

nitrification/denitrification. Even at moderate temperatures, anammox have notably low growth rates; the highest growth rate reported of  $0.33 \text{ d}^{-1}$  at  $30^\circ\text{C}$  (doubling time of 2.1 days, Lotti et al., 2015a) was for a free-cell suspension in a membrane bioreactor, well below reported growth rates of  $\sim 0.8 \text{ d}^{-1}$  at  $20^\circ\text{C}$  (doubling time  $< 1$  day) for AOM and NOB (Rittmann and McCarty, 2001). More commonly reported maximum growth rate values for anammox range from  $0.05$ - $0.1 \text{ d}^{-1}$  at  $20^\circ\text{C}$  (Koch et al., 2000; Ni et al., 2009; Volcke et al., 2010), which translates into a minimum doubling time of 7-14 days. Anammox biomass retention is therefore a critical challenge under mainstream conditions, where growth rates are expected to be well below those seen in sidestream deammonification processes.

In addition, both AOM and anammox bacteria are autotrophic, and can face competition from faster growing ordinary heterotrophic organisms (OHO) and denitrifying heterotrophic organisms in mainstream conditions, which typically contain higher COD:N ratios than seen under sidestream conditions. The theoretical stoichiometry of combined nitrification-anammox (without any activity by NOB or heterotrophic denitrifiers) is as follows (Vlaeminck et al., 2012):



Excessive OHO activity can reduce AOM activity due to competition for oxygen, and excessive denitrification can reduce anammox activity due to competition for  $\text{NO}_2^-$ . Also note from the above stoichiometry that a small amount of  $\text{NO}_3^-$  is produced (as part of the anammox metabolism, specifically). Ratios higher than 0.5 COD:N (in gCOD/gN) can induce competition from denitrifiers (Jenni et al., 2014), though some amount of denitrification can enhance N

removal efficiency, as denitrifiers can remove  $\text{NO}_3^-$  produced by anammox and provide additional selective pressure against NOB due to the removal of  $\text{NO}_2^-$  and competition for oxygen, given that most denitrifiers are facultative aerobes. A biodegradable-COD:N ratio of around 2.0 has been suggested for mainstream processes (Han et al., 2016a) as conducive to a beneficial level of denitrification that does not lead to out-competition of anammox, though systems designed for full nitrification and denitrification/anammox may tolerate higher ratios (Le et al., 2019a; B. Ma et al., 2017a). It should be noted that absolute minimization of the COD:N ratio can be detrimental to total N removal; Malovany et al. (2015) found that N removal decreased by 18% when the COD:N ratio decreased from 1.8 to 1.3 g sCOD/ g  $\text{NH}_4^+$ -N. Despite the apparent sensitivity of mainstream deammonification to the relative quantity of COD, few suggestions for adjusting its ratio in practice (without VFA dosing) have been made.

### 1.2.3 EBPR Background and Integration with Nitrification-Denitrification

Biological phosphorus removal from wastewater (beyond the typical stoichiometric P requirements for cell synthesis) was first observed at a wastewater treatment plant in San Antonio, Texas in 1967 (Barnard, 1976). Since then, much has been learned about the metabolism of so-called polyphosphate accumulating organisms (PAOs), the key microbial functional group in the process that has been termed “enhanced biological phosphorus removal” (EBPR). A general overview of PAO diversity in wastewater treatment systems is as follows:

Canonical PAOs are affiliated with as-yet-uncultivated *Candidatus Accumulibacter phosphatis*, which can further be delineated into 14 clades based on phylogenetic inference of the functional gene *ppk1* (Camejo et al., 2016). *Accumulibacter* takes up volatile fatty acids (VFAs) in the anaerobic phase and stores the carbon internally as PHA, meanwhile expending

polyphosphate as an energy source. Alternative PAOs that have gained more attention recently include the genus *Tetrasphaera*, which appear to dominate the PAO community in some full scale plants (Nguyen et al., 2011). *Tetrasphaera* PAOs are rather diverse in their metabolic pathways, and have been found to variously take up acetate, amino acids and/or glucose during the anaerobic phase, with similar P-uptake activity in the aerobic phase. Additional genera of bacteria have been proposed to be capable of high levels of P uptake but are not widely observed in wastewater treatment systems.

Competitors to PAOs are glycogen accumulating organisms (GAOs), so called because under anaerobic conditions they are able to hydrolyze glycogen, consume VFAs and internally store PHAs (Zeng et al., 2003c). They do not, however, take up phosphate under subsequent aerobic conditions, and thus represent a competitor to PAOs and the EBPR process in general. Because they compete for reducing equivalents but do not contribute to P removal, GAOs are considered undesirable in EBPR.

N removal through nitrification-denitrification and P removal through the EBPR process share a common substrate: biodegradable COD. While both processes aid in the treatment goal of COD removal before discharge to receiving water bodies, they can also act as competitors where COD is limiting. Since both processes require aeration, ordinary heterotrophic oxidation of COD in the aerobic phase may reduce COD concentration to the point that N and P removal goals are no longer achievable. Moreover, Tasli et. al. found that COD removal in the anoxic/anaerobic phase of a sequencing batch reactor exceeded stoichiometric requirements for EBPR and denitrification alone, indicating that non-PAO storage of intercellular carbon may further exacerbate the issue of carbon limitation (Tasli et al., 1999). In fact, about 200

wastewater treatment plants in the US add methanol as a substrate for denitrification (“Wastewater Treatment,” 2017), and many more use non-organic means to remove P, such as chemical precipitation via salts of iron or aluminum. Both methanol and salts can be a significant cost to treatment plants.

If chemical additions are to be avoided to reduce cost and environmental impact, the COD present in the influent must be used efficiently to target N and P removal. There are two primary strategies for reducing the COD demand of these processes, both of which also reduce oxygen (and therefore energy) requirements:

1. Perform nitrite shunt, such that denitrification from  $\text{NO}_3^-$  to  $\text{NO}_2^-$  is not required.
2. Promote the activity of denitrifying phosphorus accumulating organisms (DPAOs).

Point (1) was discussed above, and point (2) takes advantage of the observation that some PAOs are able to accumulate phosphorus as intercellular polyphosphate under anoxic conditions (in addition to aerobic conditions) in the presence of  $\text{NO}_3^-$  or  $\text{NO}_2^-$  (Ahn et al., 2001; Kern-Jespersen and Henze, 1993). DPAO activity over aerobic PAO activity reduces the DO required for P uptake, thereby conserving energy, and reduces COD demand via a single metabolic pathway for N and P removal.

#### **1.2.4 EBPR and Integration with Carbon Diversion and Recovery**

The conventional activated sludge (CAS) process, while a reliable 100+ year old technology, is inefficient due to COD losses to mineralization (i.e. oxidation of organic carbon to inorganic forms, such as  $\text{CO}_2$  gas) and to biomass production. A typical CAS plant loses an average of 50% of influent COD (influent here means “primary effluent,” that is, after the

primary settling tanks) to mineralization, and the microbial biomass produced from most of the remaining COD loss has low methane yields in anaerobic digestion (Wan et al., 2016). The high-rate activated sludge (HRAS) process, first proposed in 1944 (Chase and Eddy, 1944), aims to reduce mineralization and increase the digestibility of diverted COD by minimizing both HRT and SRT, thereby minimizing footprint and maximizing carbon diversion to sidestream anaerobic digestion. In the HRAS process, a primary goal is to entrain colloidal and particulate COD into the suspended flocs – before it can be oxidized or hydrolyzed – for removal via waste sludge to anaerobic digesters or other energy recovery methods.

More recently, increasing research efforts have focused on incorporating P removal into the HRAS process (Ge et al., 2015; Valverde-Pérez et al., 2016). This inevitably leads to some loss of efficiency in COD recovery due to the rbCOD required by PAOs for storage of intracellular carbon as PHAs. However, the potential for simultaneous recovery of COD and P has made the HRAS-P (HRAS + phosphorus removal) process an attractive option. A proposed theoretical maximum growth rate of PAOs,  $\mu_{\text{PAO}} = 1.0 \text{ d}^{-1}$  (Gujer et al., 1995) at 20 °C, indicates that without any safety factor the theoretical minimum SRT is 1 day, making the typically aggressive HRAS SRTs of 1 day or less not possible. To date, researchers have demonstrated effective P removal via EBPR at SRTs between 2 – 4 days and temperatures between 16 – 25 °C (Chan et al., 2017; Ge et al., 2015; Valverde-Pérez et al., 2016; Yang et al., 2017). Despite these advances, there remain critical gaps in the understanding of low SRT EBPR systems, including the diversity of *Accumulibacter* PAOs and minimum SRT for EBPR when using real wastewater.

In addition to the intrinsic benefits of a high rate EBPR process (i.e. COD and P removal and potential recovery), the effluent is suitable for use in a downstream deammonification process. A low SRT process EBPR process can result in washout of nitrifiers, resulting in process effluent with a low COD:N ratio ideal for autotrophic N removal via deammonification. Such a A-stage/B-stage setup was used in my research, as detailed below.

### 1.3 Research Approach

The objective of my research is to assess energy saving bench-scale biological processes for combined COD, N and P removal from real mainstream wastewater. To facilitate this, I ran four reactors at the Terrence J. O'Brien Water Reclamation Plant from 2016 to 2019 and used effluent from the plant's primary clarifiers as process influent. Process sustainability and feasibility for scale-up were two key goals of this project, so chemical dosing and bioaugmentation were avoided when possible. Broadly speaking, two separate treatment trains were investigated, both with the goal of total N, P and COD removal (bold lettering corresponds to the reactor names in Figure 1.3, which includes operation timelines).

- ❖ Treatment Train 1: Single-stage **nitritation-denitritation with EBPR**. A single 56-L suspended sludge sequencing batch reactor (SBR) was operated with anaerobic – aerobic (with intermittent aeration during the aerobic period) cycling to facilitate simultaneous P and shortcut N removal.
- ❖ Treatment Train 2: A-stage high rate biological P removal followed by two parallel B-stage deammonification reactors.

- A-stage, **high rate EBPR**: A 56-L suspended sludge SBR was operated with anaerobic-aerobic cycling and short hydraulic and solids retention times to target COD and P removal and potential recovery.
- B-stage 1, **deammonification IFAS**: A 12-L integrated fixed-film activated sludge (IFAS, i.e. with both biofilm and suspended biomass) SBR was operated for N removal via deammonification.
- B-stage 2, **comammox SG**: A 12-L suspended growth (SG) SBR was operated for N removal via deammonification to facilitate comparison between biofilm (above reactor) and suspended growth morphologies for mainstream deammonification. The serendipitous comammox enrichment observed in this reactor led to its given name.

#### 1.4 Layout of Chapters

Chapter 2 provides results for treatment train 1, that is, the single-stage nitrification-denitrification with EBPR reactor. This chapter is published in *Environmental Science: Water Research and Technology*: Roots, P., Sabba, F., Rosenthal, A.F., Wang, Y., Yuan, Q., Rieger, L., Yang, F., Kozak, J.A., Zhang, H., Wells, G.F., 2019. Integrated shortcut nitrogen and biological phosphorus removal from mainstream wastewater: process operation and modeling. *Environ. Sci.: Water Res. Technol.* 10.1039.C9EW00550A.

Chapter 3 details the performance of the A-stage process of treatment train 2, that is, the high-rate EBPR reactor. This Chapter is from a manuscript in preparation: Roots, P., Rosenthal, A.F., Wang, Y., Sabba, F., Jia, Z., Yang, F., Kozak, J.A., Zhang, H., Wells, G.F. Pushing the

limits of solids retention time for enhanced biological phosphorus removal: Process characteristics and *Accumulibacter* population structure.

Chapter 4 describes the biofilm-based B-stage process of treatment train 2, or deammonification IFAS. This Chapter is from a manuscript under review in *Environmental Science & Technology*: Roots, P., Rosenthal, A.F., Yuan, Q., Wang, Y., Yang, F., Kozak, J.A., Zhang, H., Wells, G.F., 2020. Practical optimization of the carbon to nitrogen ratio for mainstream deammonification and its impact on aggregate structure.

Chapter 5 details the comammox enrichment observed in the suspended growth-based B-stage process of treatment train 2. This Chapter is published in *Water Research*: Roots, P., Wang, Y., Rosenthal, A.F., Griffin, J.S., Sabba, F., Petrovich, M., Yang, F., Kozak, J.A., Zhang, H., Wells, G.F., 2019. Comammox *Nitrospira* are the dominant ammonia oxidizers in a mainstream low dissolved oxygen nitrification reactor. *Water Research* 157, 396–405.  
<https://doi.org/10.1016/j.watres.2019.03.060>.

Chapter 6 provides a summary of conclusions and prospects for future work.

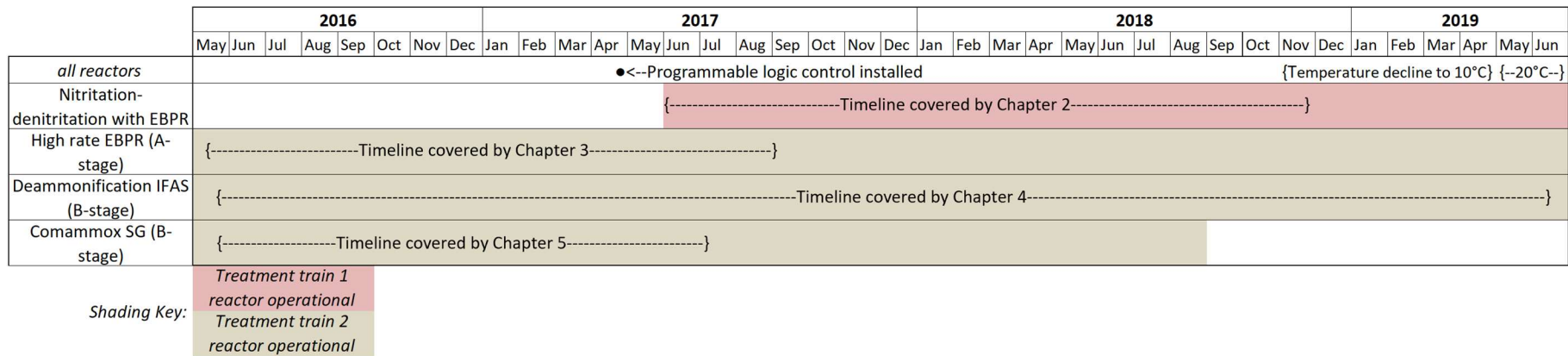
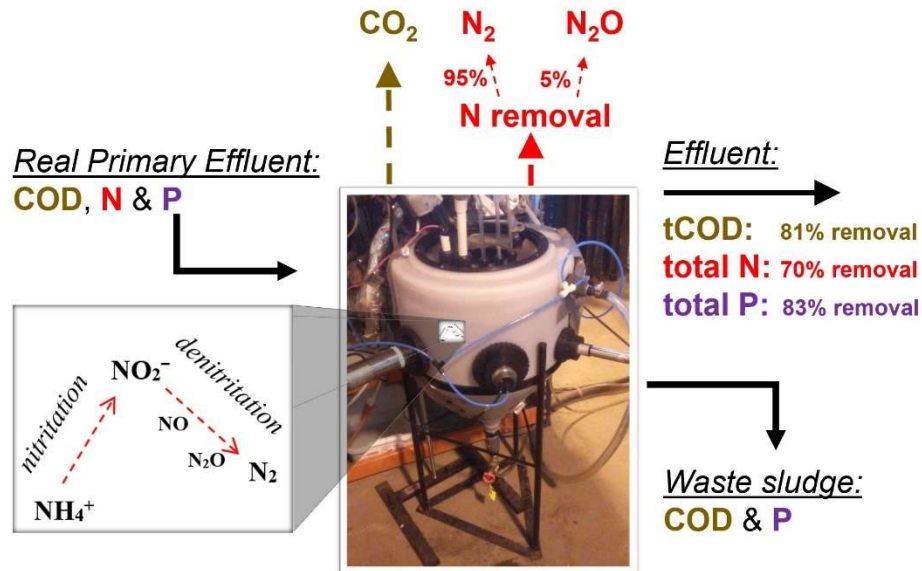


**Figure 1.3** Reactor operation timeline and relation to chapter content.

## CHAPTER 2: INTEGRATED SHORTCUT NITROGEN AND BIOLOGICAL PHOSPHORUS REMOVAL FROM MAINSTREAM WASTEWATER: PROCESS OPERATION AND MODELING<sup>1</sup>



### Abstract

While enhanced biological phosphorus removal (EBPR) is widely utilized for phosphorus (P) removal from wastewater, understanding of efficient process alternatives that allow combined biological P removal and shortcut nitrogen (N) removal, such as nitritation-denitritation, is limited. Here, we demonstrate efficient and reliable combined total N, P, and chemical oxygen demand removal (70%, 83%, and 81%, respectively) in a sequencing batch reactor (SBR) treating real mainstream wastewater (primary effluent) at 20°C. Anaerobic – aerobic cycling (with intermittent oxic/anoxic periods during aeration) was used to achieve consistent removal rates, nitrite oxidizing organism (NOO) suppression, and high effluent quality. Importantly, high resolution process monitoring coupled to *ex situ* batch activity assays demonstrated that robust biological P removal was coupled to energy and carbon efficient nitritation-denitritation, not simultaneous nitrification-denitrification, for the last >400 days of

<sup>1</sup>Roots, P., Sabba, F., Rosenthal, A.F., Wang, Y., Yuan, Q., Rieger, L., Yang, F., Kozak, J.A., Zhang, H., Wells, G.F., 2019. Integrated shortcut nitrogen and biological phosphorus removal from mainstream wastewater: process operation and modeling. *Environ. Sci.: Water Res. Technol.* 10.1039/C9EW00550A. <https://doi.org/10.1039/C9EW00550A>

531 total days of operation. Nitrous oxide emissions of 2.2% relative to the influent TKN (or 5.2% relative to total inorganic nitrogen removal) were similar to those measured in other shortcut N bioprocesses. No exogenous chemicals were needed to achieve consistent process stability and high removal rates in the face of frequent wet weather flows and highly variable influent concentrations. Process modeling reproduced the performance observed in the SBR and confirmed that nitrite drawdown via denitrification contributed to suppression of NOO activity.

## 2.1 Introduction

Nitrogen (N) and phosphorus (P) are key limiting nutrients in surface waters, and their removal from wastewater is becoming increasingly important due to widespread eutrophication in both marine and lacustrine environments. While denitrification with exogenous carbon addition to remove N as well as chemical precipitation to remove P are well-established methods to meet nutrient discharge limits, utilities are seeking more efficient and cost-effective methods to meet their permits. Enhanced biological P removal (EBPR) is increasingly implemented as an economical alternative to chemical P precipitation, and emerging innovations in shortcut N removal processes, including nitrification coupled to heterotrophic denitrification via out-competition of nitrite oxidizing organisms (NOO) (Corominas et al., 2010), offer a route to low-energy, low-carbon biological N removal (Gao et al., 2014). However, the drivers that select for NOO out-competition in shortcut N removal processes and their impact on biological P removal are little understood.

While several studies have proposed 2-stage systems with separate sludge for N and P removal from mainstream wastewater (Chan et al., 2017; Klaus et al., 2019; Ma et al., 2013; Yang et al., 2017; Zhang et al., 2018), single sludge systems simplify operations and

maintenance and can reduce both capital and ongoing costs over 2-stage systems. A limited number of lab-scale studies have used single-sludge systems to incorporate shortcut N removal with P removal from synthetic wastewater feed (Lee et al., 2001; Tsuneda et al., 2006; Zeng et al., 2003a). Given that chemical oxygen demand (COD) can be limiting in nutrient removal systems, it is important to note that all three of the referenced studies used readily biodegradable acetate in the synthetic feed as their primary carbon source in 10:1 g acetate-COD:gN and 27:1 g acetate-COD:gP ratios or higher. While promising proof of concepts, use of synthetic feed at such high VFA:N and VFA:P ratios is not representative of the dynamics in N, P, and COD composition commonly found in real wastewater.

Investigations of combined shortcut N and P removal from real wastewater without exogenous carbon or chemical addition for P precipitation are limited to two lab-scale reactors (Zeng et al., 2014; Zhao et al., 2018) and two full scale processes (Cao et al., 2016; Jimenez et al., 2014), but one of the lab-scale and both full scale processes had average wastewater temperatures between 26 and 30 °C. Such elevated temperatures confer a significant advantage to ammonia oxidizing organisms (AOO, which can include both ammonia oxidizing bacteria and archaea) over NOO, thereby greatly facilitating NOO out-competition (Hellinga et al., 1998), but are not representative of conditions found in WWTPs in temperate regions. In the lab-scale reactor with high temperature cited above, for instance, (Zeng et al., 2014) lost NOO out-selection when the wastewater temperature dropped below 23 °C as winter approached. The other lab-scale process was operated at a more moderate temperature range of 18 – 26 °C, but was hampered by long hydraulic retention times (HRT) of 17.5 – 55 hours due to its reliance on post endogenous denitrification for N removal (Zhao et al., 2019, 2018). Research into combined

shortcut N and EBPR processes with real wastewater at moderate temperatures (i.e.  $\leq 20$  °C), where NOO suppression is significantly more challenging (Ma et al., 2015), is currently lacking. Intermittent aeration is one promising strategy for NOO suppression at moderate temperatures. Explanations for its efficacy range from a metabolic lag phase of *Nitrospira* NOO compared to AOO upon exposure to oxygen (Gilbert et al., 2014a) to transient exposure to free ammonia due to pH shifts in biofilms (Y. Ma et al., 2017a), as free ammonia has a greater inhibitory effect on NOO than AOO (Anthonisen et al., 1976; Seuntjens et al., 2018). However, the mechanism and efficacy of intermittent aeration for NOO suppression at moderate temperatures, with or without integration of biological P removal, is currently not well understood.

Process modeling of combined shortcut N and P removal systems is very limited due to the novelty of such systems; none of the above-cited studies included whole-system models. Some modeling efforts to date have focused on NOB out-competition in shortcut N systems (Dold et al., 2015; Hubaux et al., 2015; Laurenzi et al., 2019), but integration with biological phosphorus removal is limited. Of interest in the present study is whether a commercially available modeling platform can replicate observed nutrient dynamics in an integrated shortcut N and P removal process, and thus providing a valuable tool for insight and interpretation.

The propensity for shortcut N removal systems to produce nitrous oxide ( $N_2O$ ), a potent greenhouse gas, is little understood, though reports suggest that  $N_2O$  production may exceed that of conventional N removal biotechnologies (Desloover et al., 2011; Domingo-Félez et al., 2014; Joss et al., 2009; Kampschreur et al., 2008). For example, in one of the lab scale studies cited above, (Zeng et al., 2003a),  $N_2O$  production exceeded  $N_2$  production from a lab-scale nitrification-denitrification process by more than 3-fold. However, none of the above studies using real

wastewater (Cao et al., 2016; Jimenez et al., 2014; Zeng et al., 2014) measured N<sub>2</sub>O emissions. Therefore, N<sub>2</sub>O measurements on shortcut N removal systems integrated with biological P removal from real wastewater are of interest to accurately assess their net impact on greenhouse gas emissions.

Here, we demonstrate efficient and reliable combined shortcut N, P, and COD removal in a sequencing batch reactor (SBR) treating real mainstream wastewater (primary effluent) at 20°C. In contrast to the synthetic studies cited above, the primary effluent used here as influent contained average ratios of 1:1 gVFA-COD:gTKN and 8.2:1 gVFA-COD:gTP, comprising a challenging environment for total nutrient removal. Importantly, EBPR was coupled to nitrification-denitrification for energy and carbon-efficient N removal. A simple kinetic explanation for the out-competition of NOO via intermittent aeration and SRT control was illustrated via batch tests and process modeling. No exogenous chemicals were needed to achieve consistent process stability and high removal rates in the face of frequent rain events and highly variable influent concentrations.

## **2.2 Materials and Methods**

### **2.2.1 Reactor inoculation and operation**

A 56-L reactor was seeded with activated sludge biomass from another pilot EBPR bioreactor (grown on the same wastewater) on June 15, 2017 (day 0 of reactor operation) and fed primary settling effluent from the Terrance J. O'Brien WRP in Skokie, IL for 531 days. Online sensors included the ammo::lyser™ eco+pH ion-selective electrode for NH<sub>4</sub><sup>+</sup> and pH, the oxi::lyser™ optical probe for dissolved oxygen (DO), and the redo::lyser™ eco potentiometric probe for oxidation-reduction potential (ORP) (s::can, Vienna, Austria). The reactor was

operated with code-based Programmable Logic Control (PLC) (Ignition SCADA software by Inductive Automation, Fulsom, CA, USA, and TwinCAT PLC software by Beckhoff, Verl, Germany) as a sequencing batch reactor (SBR) with cycle times detailed in Table 2.1. An anaerobic react period followed by an intermittently aerated period was chosen with the intent to select for integrated biological P removal and nitrification/denitrification via suppression of NOO activity. The reactor was temperature-controlled to target 20°C (actual temperature = 19.8 ± 1.0°C) via a heat exchange loop to evaluate performance at moderate temperatures. The pH was not controlled and varied between 7.0 and 7.8.

**Table 2.1** SBR cycle timing (gravity fill, anaerobic reactor, aerobic react, wasting, settling, and decant) and reactor control details. The end of the SBR aerobic (intermittently aerated) react phase was determined based on an  $\text{NH}_4^+$  setpoint shown in the table.

	<i>Phase 1</i>	<i>Phase 2</i>
Days of operation	0 to 246	247 to 531
Gravity fill (min)	3 to 6	
Anaerobic react (min)	45	
Aerobic react via intermittent aeration (min)	317 ± 146	206 ± 105
Wasting (min)	0 to 2.2	
Settling (min)	30 to 40	
Decant of 5/8 volume fraction (min)	4.5 to 6.0	
Online $\text{NH}_4^+$ -based control target effluent concentration ( $\text{mgNH}_4^+\text{-N/L}$ )	3 to 5	1.5 to 2
Total SRT (days)	11 ± 7	9.2 ± 1.8
Aerobic SRT (days)	4.5 ± 3.0	3.6 ± 0.9
HRT (hours)	9.7 ± 3.9	6.8 ± 2.8

The variable-length aerated react period was terminated if either a maximum allowable react time was reached (usually between 300 – 480 minutes) or if the target  $\text{NH}_4^+$  concentration was

reached according to the online sensor. Intermittent aeration was used during the aerated react period with the following loop:

1. 4 or 5 minutes of aeration with proportional-integral (PI) control to target  $1 \text{ mgO}_2/\text{L}$  via the online DO probe. PI control managed the percent-open time of an air solenoid valve, which, when open, provided compressed air at 7 – 15 liters per minute through a 5-inch diameter aquarium stone disk diffuser at the bottom of the reactor. (Compressed air was provided via a California Air Tools model 5510SE air compressor [San Diego, CA, USA]. The 7 – 15 LPM flow rate was selected based on expected oxygen demand and modified to allow for rapid realization of the  $1 \text{ mgO}_2/\text{L}$  target DO level.)
2. After aeration, shut air solenoid valve and wait until DO drops to  $< 0.05 \text{ mgO}_2/\text{L}$ .
3. Run “anoxic” timer for 0 – 3 minutes. At end of timer, return to Step 1.

Due to variable oxygen uptake rates (OUR) and changes to the anoxic timer, the total aerobic/anoxic interval lengths typically varied between 10 – 20 minutes. Because react length varied with influent  $\text{NH}_4^+$  concentration (due to  $\text{NH}_4^+$  sensor-based control), the SBR loading rate followed that of the full-scale plant, i.e. with shortened SBR cycles and increased flow during wet-weather events.

The process timeline is split into 2 phases to simplify reporting: Phase 1 (days 0 - 246) and Phase 2 (days 247 – 531), the latter of which represents lower target effluent N concentrations ( $1.5 - 2 \text{ mgNH}_4^+-\text{N}/\text{L}$ , vs.  $3 - 5 \text{ mgNH}_4^+-\text{N}/\text{L}$  during Phase 1) and better N-removal performance. Phase 1 was used as a process optimization period to determine the optimal SRT for NOO washout with AOO retention.

SRT was controlled via timed mixed liquor wasting after the aerated react phase, and solids losses in the effluent were included in the dynamic SRT calculation, following the methodology of (Laureni et al., 2019). Using an operational definition of “aerobic” as  $> 0.2 \text{ mgO}_2/\text{L}$ , an analysis of 4 cycles from Phase 2 showed that an average 48% of the time within the intermittently aerated react period is aerobic. See the Supporting Information for details regarding SRT control and calculations.

Composite sampling as summarized in Table 2.S1 was initiated on day 27 after an initialization period to allow the accumulation of AOO as measured by ammonia oxidation activity. Beginning on day 114 and to the end of the study, influent COD fractionation analysis was conducted once per week with the following definitions (Melcer, 2004):

- Particulate COD = Total COD – 1.2- $\mu\text{m}$  filtered COD
- Colloidal COD = 1.2- $\mu\text{m}$  filtered COD – floc-filtered COD
- Soluble COD (not including VFAs) = floc-filtered COD – VFA
- VFA COD = VFA

Floc-filtered COD was measured as described in Mamais et al. (1993) and total COD, filtered COD and VFAs were analyzed per Standard Methods (APHA, 2005). On average, the total COD and VFA to nutrient ratios of the influent were (Table 2.S2):

- 8.3:1 g total COD:g TKN
- 1:1 g VFA-COD:g TKN
- 67:1 g totalCOD:g totalP
- 8.2:1 g VFA-COD:g totalP

## 2.2.2 Batch activity assays

### 2.2.2.1 In-cycle batch activity assays

Seventeen in-cycle batch activity assays were conducted throughout the study to monitor *in situ* dynamics of  $\text{NH}_4^+$ ,  $\text{NO}_2^-$ ,  $\text{NO}_3^-$ ,  $\text{PO}_4^{3-}$  (all tests), readily biodegradable COD (rbCOD - two tests) and volatile fatty acids (VFAs – one test) via Standard Methods (APHA, 2005) and (Mamais et al., 1993) for rbCOD. Samples were taken every 15 – 45 minutes for a full SBR cycle, except in the case of two high-frequency tests, in which samples were taken every one to two minutes for 40 minutes in the aerated portion of the cycle to investigate high time resolution nutrient dynamics during intermittent aeration.

### 2.2.2.2 Ex situ batch activity assays

*Ex situ* maximum batch activity assays for AOO and NOO were performed as previously described (Laureni et al., 2016; Roots et al., 2019b). *Ex situ* activity assays were also employed to quantify biological P uptake of polyphosphate accumulating organisms (PAOs) under aerobic and denitrifying conditions. Relative P-uptake rates via different electron acceptors under typical in-reactor conditions was desired (as opposed to maximum P-uptake rates), so external carbon was not added. 250-mL aliquots of mixed liquor were removed from the reactor following the anaerobic phase (i.e. after P release and VFA uptake) and placed in air-tight 250-mL serum bottles. The sealed bottles were injected with sodium nitrite or potassium nitrate stock solutions to approximately 9 mgN/L of  $\text{NO}_2^-$  or  $\text{NO}_3^-$  for the anoxic (denitrifying) uptake tests or opened and bubbled with air through an aquarium diffusor stone for aerobic tests. A replicate for the aerobic test was provided by the 56-L reactor itself, which was also aerated continuously (with a resulting DO concentration of 2 mg/L) and sampled in parallel with the aerated serum bottle. A

control assay utilized biomass with no electron acceptors ( $O_2$ ,  $NO_3^-$ , or  $NO_2^-$ ) provided. Serum bottles were mixed by a Thermo Scientific MaxQ 2000 shaker table (Waltham, MA) at 150 RPM and at ambient temperature near  $20^\circ C$ . P uptake was quantified via a least squares regression of the  $PO_4^{3-}$  measurement from 3 – 5 samples taken every 20 minutes and normalized to the reactor VSS. The results represent the average  $\pm$  standard deviation of three total replicates for each electron acceptor from days 237 and 286.

#### *2.2.2.3 In-cycle batch activity assays for quantification of $N_2O$ emissions*

$N_2O$  emissions from the reactor were estimated during Phase 2 by measuring the aqueous  $N_2O$  concentration over 8 separate cycles from days 414 to 531 with a Unisense  $N_2O$  Wastewater Sensor equipped with the E- $N_2O$  Head with a working range of 0 – 1.5 mg  $N_2O$ -N/L (Aarhus, Denmark).  $N_2O$  emissions were calculated from the aqueous concentration following Domingo-Félez et al. (2014) after measuring the  $N_2O$  stripping rate during aeration with mixing and during mixing alone.  $NH_4^+$ ,  $NO_2^-$  and  $NO_3^-$  were measured concurrently at the beginning and end of cycles (APHA, 2005) to calculate TIN removal.  $N_2O$  emissions were then quantified relative to TIN removal and the TKN load for each of the eight cycles.

#### **2.2.3 Process Modeling**

To evaluate mechanisms of NOO suppression and the balance between aerobic PAO and denitrifying PAO (DPAO) activity, the SIMBA#3.0.0 wastewater process modeling software (ifak technology + service, Karlsruhe, Germany) was used to simulate performance of the reactor during Phase 2 of operation. We utilized the inCTRL activated sludge model (ASM) (ifak, 2018;

Schraa et al., 2019), an established engineering model applied extensively in the field and which is based on (Barker and Dold, 1997) with the addition of two-step nitrification-denitrification, methanotrophs, and other extensions. The objective of modeling was to see if an established engineering model could predict observed behavior without adjustment of kinetic or stoichiometric parameters, and thus provide insight into the operation and optimization of the modeled reactor. Default Monod half-saturation constants of particular relevance to this study include oxygen affinity of AOO ( $K_{O_2, AOO} = 0.25 \text{ mgO}_2/\text{L}$ ) and NOO ( $K_{O_2, NOO} = 0.15 \text{ mgO}_2/\text{L}$ ), substrate affinity of AOO ( $K_{NH_x, AOO} = 0.7 \text{ mgNH}_x\text{-N/L}$ ;  $\text{NH}_x = \text{NH}_4^+ + \text{NH}_3$ ) and NOO ( $K_{NO_2, NOO} = 0.1 \text{ mgNO}_2\text{-N/L}$ ), and maximum specific growth rate of AOO ( $\mu_{AOO} = 0.9 \text{ d}^{-1}$ ) and NOO ( $\mu_{AOO} = 0.7 \text{ d}^{-1}$ ). All default values listed above from the inCTRL ASM were intentionally left unmodified, but due to their importance in modeling nitrite-shunt systems, a brief discussion is in order. The commonly used parameter values from (Wiesmann, 1994) suggest a higher oxygen and substrate affinity of *Nitrosomonas* AOO than *Nitrobacter* NOO, but more recent measurements demonstrate the high  $\text{NO}_2^-$  affinity ( $K_{NO_2, NOO} = 0.1 - 0.4 \text{ mgNO}_2\text{-N/L}$  (Nowka et al., 2015) and oxygen affinity ( $K_{O_2, NOO} = 0.09 \text{ mgO}_2/\text{L}$  (Law et al., 2019) of *Nitrospira* NOO (*Nitrospira* were found in this study via 16S rRNA gene sequencing, along with *Nitrotoga* NOO). More recent measurements of *Nitrosomonas* AOO (also found in this study) substrate and oxygen affinity (Park and Noguera, 2007) confirm those measured by (Wiesmann, 1994) and are similar to those used here. The implications of higher substrate and oxygen affinities for NOO than AOO is that modeled NOO out-competition will be relatively more difficult to achieve. The exception to this AOO advantage is the slightly higher modeled maximum specific growth rate

of AOO over NOO, though this is supported by (Law et al., 2019), wherein *Nitrosomonas* AOO were shown to have a much higher maximum specific growth rate than *Nitrospira* NOO.

SBR control of the reactor was simulated directly using a petri net approach, with sequence control shown as green blocks in Figure 2.S1. To avoid rounding errors and to improve simulation speed, the reactor was modeled with a 56 m<sup>3</sup> working volume as opposed to 56 L. As in the reactor, the modeled anoxic period was fixed at 45 minutes and the aerobic period ended when soluble NH<sub>X</sub> (i.e. NH<sub>4</sub><sup>+</sup> + NH<sub>3</sub>, which is approximately equal to NH<sub>4</sub><sup>+</sup> at the pH values encountered of 7.0 – 7.8) was < 2 mgN/L. Modeled intermittent aeration during the aerobic period was controlled as described in the Supporting Information, though a slightly longer “anoxic” timer of 3 min 45 seconds in the model was used (vs. 0 – 3 minutes in the actual SBR) to account for the DO sensor delay in the actual SBR. Modeled mixed liquor wasting was adjusted until the calculated model SRT (which included effluent solids) matched the SRT of the reactor during Phase 2. 5/8 volume decant was performed at the end of the cycle and average primary effluent (reactor influent) values from Phase 2 were used as model influent. The initialization procedure involved running the model for 150 days to achieve quasi steady-state conditions. Modeled specific growth rates for AOO, NOO, and PAOs were quantified throughout the SBR cycles with rate equations and parameter values from the SIMBA# inCTRL ASM matrix.

$$\begin{aligned}\mu_{AOO} &= \text{net specific growth rate of AOO (d}^{-1}\text{)} \\ \mu_{NOO} &= \text{net specific growth rate of NOO (d}^{-1}\text{)}\end{aligned}$$

The washout SRT for NOO was calculated from  $\mu_{NOO}$  as detailed in the Supporting Information.

Modeled PAO growth rates as discussed in this paper include growth on PHA associated with P uptake but do not include decay or PAO growth on PHA where  $\text{PO}_4^{3-}$  is limiting. Also, the SIMBA# inCTRL ASM matrix considers only a single PAO population with an anoxic growth factor ( $\eta_{anox,PAO} = 0.33$ ) in the DPAO rate equations to estimate anoxic P uptake (see Supporting Information for full rate equations). The three growth rates below therefore represent growth of a single functional group split between 3 electron acceptors:  $\text{O}_2$ ,  $\text{NO}_2^-$ , and  $\text{NO}_3^-$ .

$$\begin{aligned}\mu_{PAO,O_2} &= \text{PAO growth associated with } O_2 \text{ (d}^{-1}\text{)} \\ \mu_{PAO,NO_2} &= \text{PAO growth associated with } NO_2^- \text{ (d}^{-1}\text{)} \\ \mu_{PAO,NO} &= \text{PAO growth associated with } NO_3^- \text{ (d}^{-1}\text{)}\end{aligned}$$

Rate equations and parameters values for the above modeled growth rates, along with the process representation in SIMBA#, can be found in the Supporting Information.

#### 2.2.4 Biomass sampling and DNA extraction

Reactor biomass was archived biweekly for sequencing-based analyses. Six 1 mL aliquots of mixed liquor were centrifuged at 10,000g for 3 minutes, and the supernatant was replaced with 1 mL of tris-EDTA buffer. The biomass pellet was then vortexed and centrifuged at 10,000g for 3 minutes after which the supernatant was removed, leaving only the biomass pellet to be transferred to the  $-80^\circ\text{C}$  freezer. All samples were kept at  $-80^\circ\text{C}$  until DNA extraction was performed with the FastDNA SPIN Kit for Soil (MPBio, Santa Ana, CA, USA) per the manufacturer's instructions.

### 2.2.5 16S rRNA gene amplicon sequencing

16S rRNA gene amplicon library preparations were performed using a two-step multiplex PCR protocol, as previously described (Griffin and Wells, 2017). All PCR reactions were performed using a Biorad T-100 Thermocycler (Bio-Rad, Hercules, CA). The V4-V5 region of the universal 16S rRNA gene was amplified in duplicate from 20 dates collected over the course of reactor operation using the 515F-Y/926R primer set (Parada et al., 2016). Further details on thermocycling conditions, reagents, and primer sequences can be found in Supporting Information.

All amplicons were sequenced using a MiSeq system (Illumina, San Diego, CA, USA) with Illumina V2 (2x250 paired end) chemistry at the University of Illinois at Chicago DNA Services Facility and deposited in GenBank (accession number for raw data: PRJNA527917). Procedures for sequence analysis and phylogenetic inference can be found in the Supporting Information.

### 2.2.6 Quantitative Polymerase Chain Reaction (qPCR)

qPCR assays were performed targeting the ammonia oxidizing bacterial *amoA* gene via the *amoA*-1F and *amoA*-2R primer set (Rotthauwe et al., 1997), and total bacterial (universal) 16S rRNA genes via the Eub519/Univ907 primer set (Burgmann et al., 2011). All assays employed thermocycling conditions reported in the reference papers and were performed on a Bio-Rad C1000 CFX96 Real-Time PCR system (Bio-Rad, Hercules, CA, USA). Details on reaction volumes and reagents can be found in the Supporting Information. After each qPCR assay, the specificity of the amplification was verified with melt curve analysis and agarose gel electrophoresis.

## 2.3 Results and Discussion

### 2.3.1 Nitrogen, AOO and NOO

#### 2.3.1.1 Overall Performance and Nitrogen Removal

To demonstrate feasibility and evaluate optimal operational conditions for integrated biological P and shortcut N removal via NOO out-selection at moderate temperatures, we operated lab-scale reactor fed with real primary effluent for 531 days. Reactor operation proceeded in two phases. Reactor performance across both phases is shown in Figure 2.1 and summarized in Table 2.2. Phase 1 (days 0-246) established proof-of-concept for the compatibility of N removal via nitrification-denitrification via intermittent aeration with EPBR and allowed for optimization of SRT and the aeration regime (intermittent aeration). P removal was consistent during Phase 1 (average  $\text{PO}_4^{3-}$  removal = 83%) excepting aeration failures from reactor control issues around days 80 – 90. Because SRT control was utilized as one of the strategies for NOO out-selection, partial washout of AOO during Phase 1 was occasionally observed when mixed liquor wasting was too aggressive (i.e. total SRT less than 5 days,  $\text{SRT}_{\text{AER}}$  less than 2 days, see Figure 2.S2 and Table 2.1), resulting in lower  $\text{NH}_4^+$  oxidation rates and higher effluent  $\text{NH}_4^+$ , after which wasting would be suspended to restore AOO mass. The average TIN removal during Phase 1 was 42% but reached >60% during periods of peak performance. The average TSS during Phase 1 was  $1,362 \pm 623$  mg/L, the VSS was  $1,052 \pm 489$  mg/L, and the HRT was  $9.7 \pm 3.9$  hours not including settling and decant.

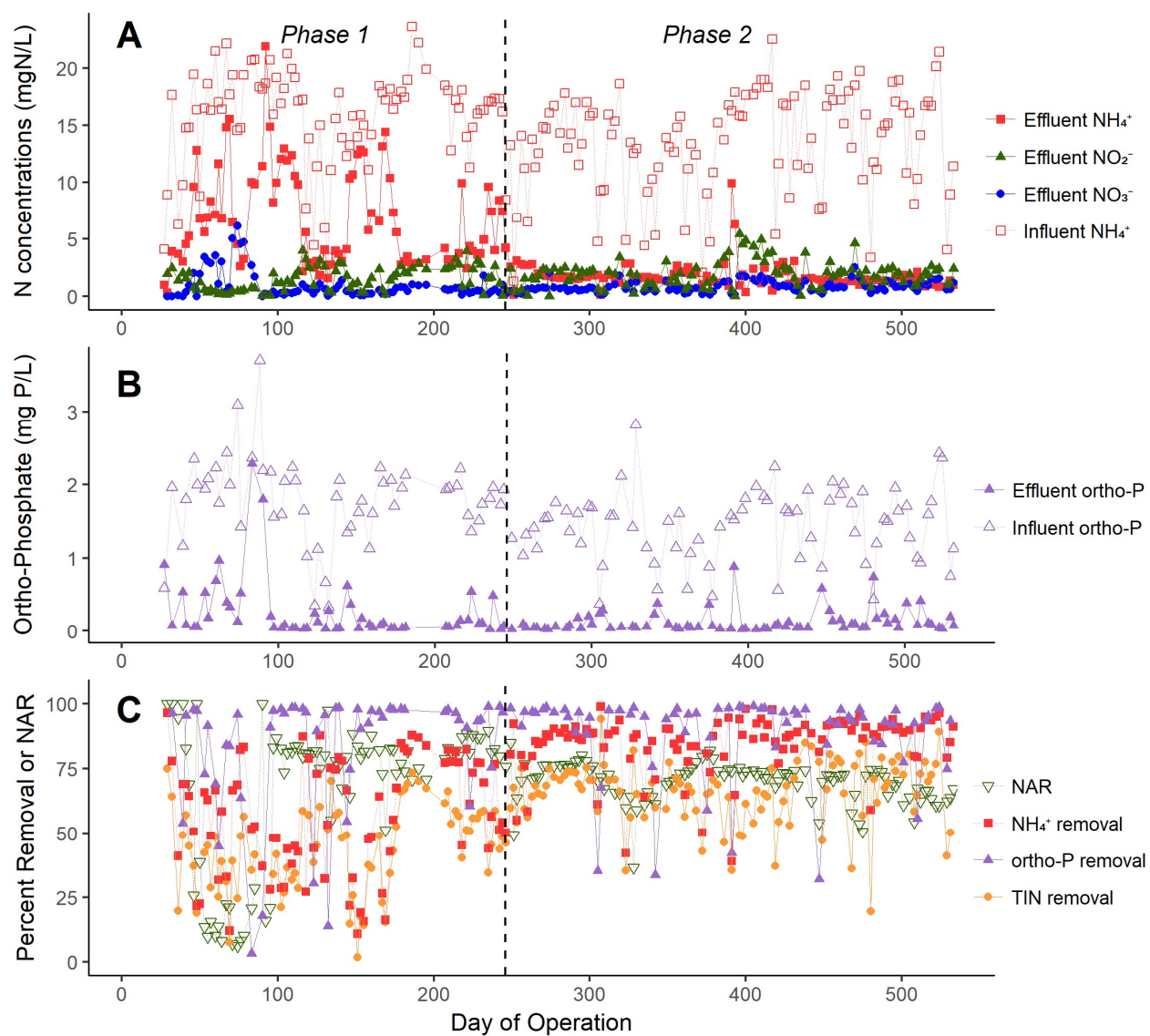


**Figure 2.1** Reactor performance over time from composite sampling (2 – 3 samples/week) over the entire study. A) Influent (primary effluent)  $\text{NH}_4^+$  and effluent  $\text{NH}_4^+$ ,  $\text{NO}_2^-$ , and  $\text{NO}_3^-$ . B) Influent and effluent orthophosphate. C) Nitrite accumulation ratio (NAR) and percent removal of  $\text{NH}_4^+$ , orthophosphate and TIN.

**Table 2.2** Arithmetic mean  $\pm$  standard deviation of composite sampling results for influent (primary effluent) and reactor effluent concentrations. Results from Phase 1 are highlighted in light gray and results from Phase 2 are highlighted in dark gray. Process model predictions are for Phase 2 only. Additional information regarding influent COD fractionation can be found in Table 2.S2.

	Phase 1: Days 0 - 246				Phase 2: Days 247 - 531				Reactor Percent Removal	Modeled Percent Removal <sup>a</sup>
	Influent		Reactor Effluent		Influent		Reactor Effluent			
TKN (mgN/L)	21.3 $\pm$ 5.1	8.4 $\pm$ 4.7	17.9 $\pm$ 5.3	2.8 $\pm$ 1.2	4.4	85%	76%			
NH <sub>4</sub> <sup>+</sup> (mgN/L)	15.8 $\pm$ 4.2	6.9 $\pm$ 4.2	13.5 $\pm$ 4.5	1.7 $\pm$ 1.1	2.0	87%	85%			
NO <sub>2</sub> <sup>-</sup> (mgN/L)	--- <sup>b</sup>	1.5 $\pm$ 1.1	--- <sup>b</sup>	1.9 $\pm$ 1.1	0.3	not applicable				
NO <sub>3</sub> <sup>-</sup> (mgN/L)	--- <sup>b</sup>	0.9 $\pm$ 1.2	--- <sup>b</sup>	0.8 $\pm$ 0.5	0.05	not applicable				
NAR <sup>c</sup> (%)	62%		70%		85%	not applicable				
PO <sub>4</sub> <sup>3-</sup> (mgP/L)	1.8 $\pm$ 0.6	0.3 $\pm$ 0.4	1.4 $\pm$ 0.5	0.1 $\pm$ 0.2	0.16	91%	89%			
Total P (mgP/L)	2.6 $\pm$ 0.6	0.4 $\pm$ 0.5	2.2 $\pm$ 0.7	0.4 $\pm$ 0.5	1.0	83%	56%			
Total COD (mgCOD/L)	176 $\pm$ 55	30 $\pm$ 24	150 $\pm$ 46	28 $\pm$ 11	47	81%	69%			
Filtered COD <sup>d</sup> (mgCOD/L)	107 $\pm$ 31	27 $\pm$ 17	94 $\pm$ 32	24 $\pm$ 6	27	74%	72%			
Alkalinity (meq/L)	4.6 $\pm$ 0.9	3.8 $\pm$ 0.7	4.7 $\pm$ 0.6	3.8 $\pm$ 0.7	4.1	20%	13%			
TSS (mg/L)	50 $\pm$ 27	12 $\pm$ 28	72 $\pm$ 47	18 $\pm$ 19	23	75%	68%			

<sup>a</sup> Average primary effluent values from Phase 2 were used as influent to the process model

<sup>b</sup> 79% of influent NO<sub>x</sub><sup>-</sup> (NO<sub>2</sub><sup>-</sup> + NO<sub>3</sub><sup>-</sup>) measurements were below the detection limit of 0.15 mgN/L

<sup>c</sup> NAR = nitrite accumulation ratio

<sup>d</sup> "Filtered COD" indicates filtration through 1.2  $\mu$ m filter, not to be confused with "floc-filtered COD" (see Methods)

During Phase 2 (days 247-531), SRT control was optimized (total SRT =  $9.2 \pm 1.8$  days, SRT<sub>AER</sub> =  $3.6 \pm 0.9$  days) and consistent NH<sub>4</sub><sup>+</sup> and TKN removal ( $41 \pm 24$  mgN/L/d and  $54 \pm 29$  mgN/L/d, respectively, considering influent and effluent values with HRT during Period 2) was achieved while maintaining NOO out-selection (described in section 3.1.2). The average HRT of  $6.8 \pm 2.8$  hours (not including settling and decant) was lower than Phase 1 ( $9.7 \pm 3.9$  hours) due to improved AOO activity. Average TIN and PO<sub>4</sub><sup>3-</sup> removal during Phase 2 was 68% and 91%,

respectively (Table 2.2). Biological P removal was not impacted by N removal, and the P uptake rate consistently exceeded the  $\text{NH}_4^+$  removal rate during the aerated portion of the cycle (see Figure 2.2.A&B for  $\text{PO}_4^{3-}$  and  $\text{NH}_4^+$  concentration profiles through typical cycles). This may have contributed to COD limitation for N removal via denitrification, as COD was most depleted at the end of the SBR cycles (Figure 2.2.A). This in turn may explain  $\text{NO}_2^-$  accumulation near the end of most cycles and higher P removal than N removal rates. Figure 2.2.A and 2.2.B also demonstrates the variability in react length that was often observed throughout the study due to differences in the  $\text{NH}_4^+$  oxidation rate, possibly caused by fluctuations in AOO concentrations in the reactor. During Phase 2, the average TSS was  $1,773 \pm 339$  mg/L and the VSS was  $1,344 \pm 226$  mg/L.

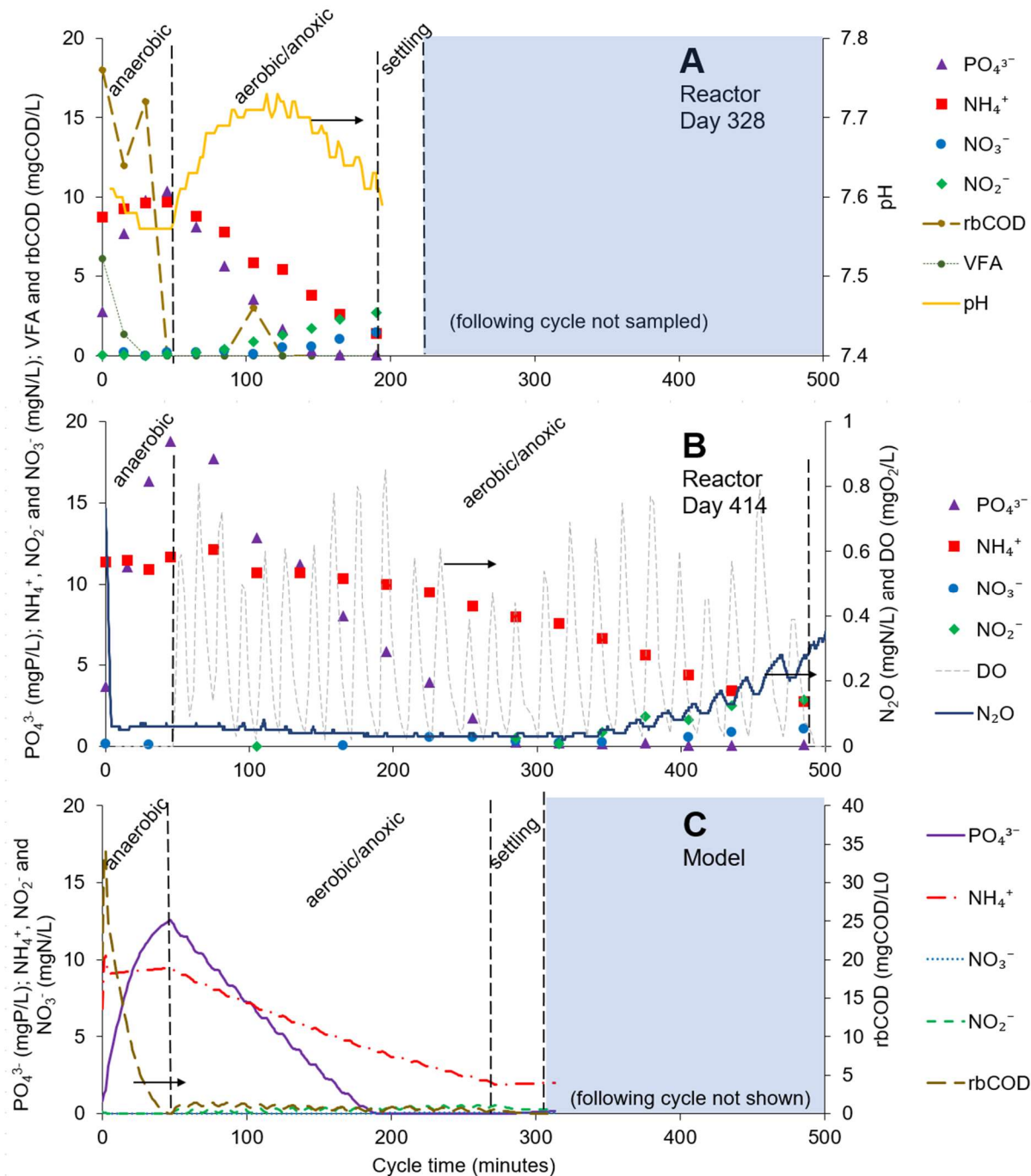


**Figure 2.2** A) and B) Two react cycles on days 328 and 414, respectively, that demonstrate efficient P and N removal, selective nitrification, and variability in aerated react length. Cycle A included measurements for rbCOD and VFAs, and cycle B was run with an  $\text{N}_2\text{O}$  sensor in the reactor. C) SBR cycle as modeled in SIMBA#. rbCOD as shown was calculated as soluble COD<sub>i</sub> – soluble COD<sub>effluent</sub>.

### 2.3.1.2 NOO Out-selection

A crucial challenge to all shortcut N removal processes, including the nitrification-denitrification with EBPR process that we focus on here, is suppression of NOO activity. To address this challenge, we employed a combination of tight SRT control with intermittent aeration to limit substrate ( $\text{NO}_2^-$ ) accumulation. Process monitoring results demonstrated an elevated nitrite accumulation ratio (NAR) of 70% during Phase 2, suggesting successful suppression of NOO activity (Table 2.2 and Figure 2.1). This observation was corroborated by fifteen in-cycle concentration profiles demonstrating  $\text{NO}_2^-$  accumulation greater than  $\text{NO}_3^-$  throughout the cycle (see Figure 2.2.A&B for two representative cycles). In addition, routine maximum activity assays for AOO and NOO demonstrated that during Phase 2 (optimized, stable reactor operation), maximum AOO activity was 3 to 4-fold greater than NOO (Figure 2.3).

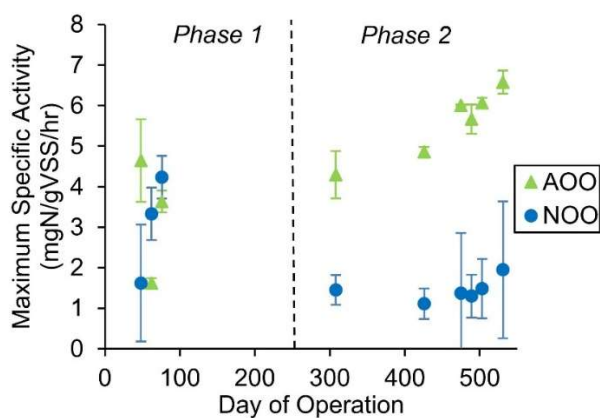


**Figure 2.3** Maximum specific AOO and NOO activity as measured by *ex situ* batch testing. Error bars represent the standard deviation of the method replicates.

To better understand NOO out-selection and nutrient dynamics during intermittent aeration and to provide additional support for suppression of NOO activity in this process, high frequency sampling (1 grab sample/minute for 40 minutes for measurement of  $\text{NH}_4^+$ ,  $\text{NO}_2^-$ ,  $\text{NO}_3^-$ , and  $\text{PO}_4^{3-}$ ) was conducted during two typical SBR cycles on days 202 and 258 (Figure 2.4.A, data from day 258 only shown). The resulting concentration profiles show  $\text{NO}_2^-$  accumulation with very little  $\text{NO}_3^-$  accumulation during aeration. Two complete intermittent aeration intervals are shown in the early part of the cycle (note that intermittent aeration begins 45 minutes into the cycle), during which  $\text{NO}_2^-$  accumulates up to 0.4 mg $\text{NO}_2^-$ -N/L following 5 minutes of aeration, while  $\text{NO}_3^-$  does not get above 0.1 mg $\text{NO}_3^-$ -N/L. The NAR during the nitrite peak of these two aeration intervals was 84% and 95%, which demonstrates NOO suppression via selective nitrification. Then, in the subsequent anoxic intervals, the accumulated  $\text{NO}_2^-$  is drawn down via denitrification. This denitrification provides a robust nitrite sink and one of the methods for NOO out-selection, such that  $\text{NO}_2^-$  is not available for NOO in the following interval.

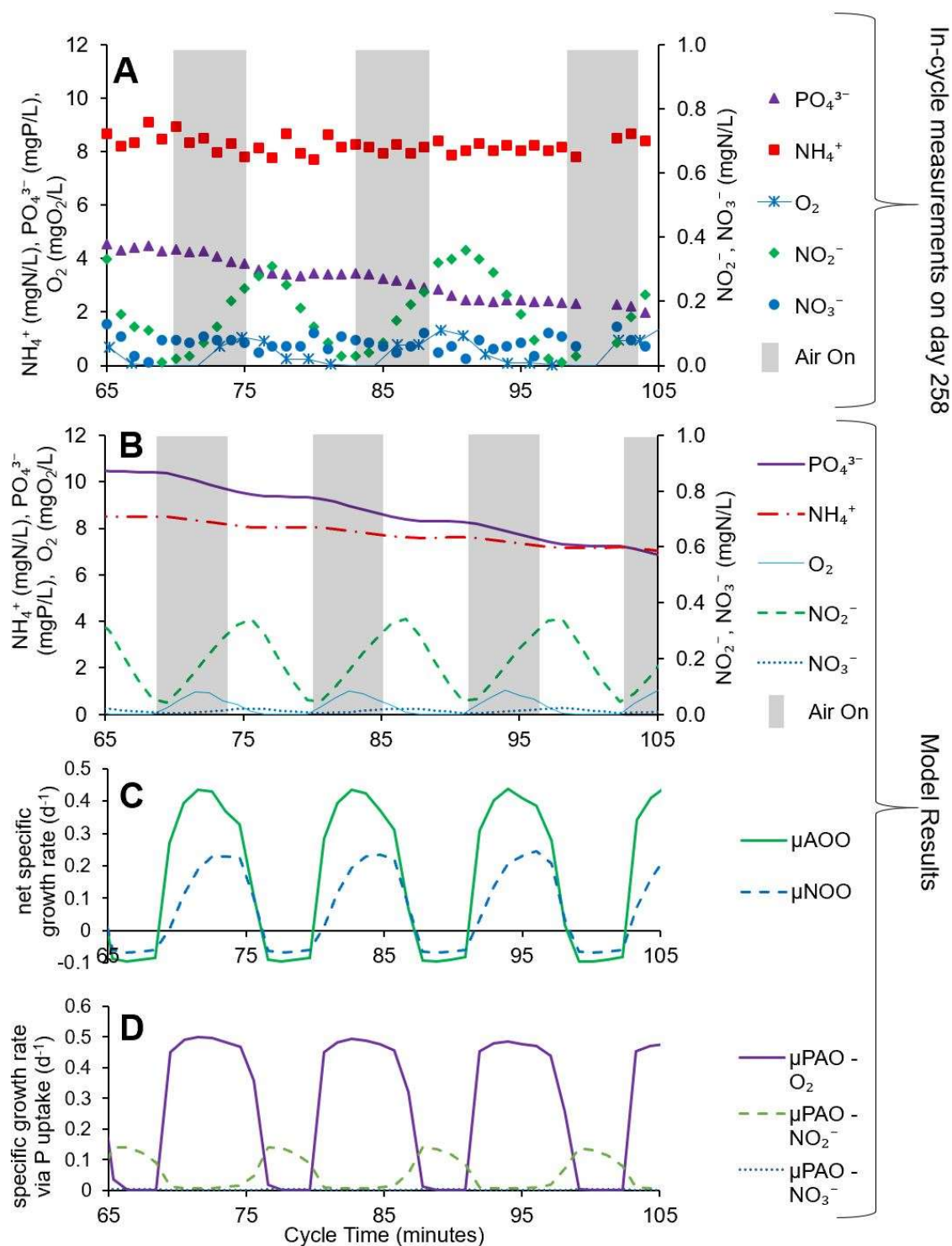


**Figure 2.4** Comparison plot between high resolution within-cycle reactor sampling (A) and modeled results (B, C, D) for the intermittently aerated react period of SBR operation (minutes 65 – 105, beginning 20 minutes after the start of aeration). A) Results of grab sampling from a

reactor cycle on day 258 of operation. Selective nitrification rather than nitrification during aerated phases (gray shading) is evident and produced  $\text{NO}_2^-$  is then denitrified in anoxic phases. The optical DO sensor is rated for a 60-second response time, and a ~1-minute delay is evident in comparison to the model plot B. B) Modeled concentration dynamics including on/off switching for aeration control. C) Modeled AOO and NOO net specific growth rates including decay. D) Modeled PAO specific growth rates associated with P uptake via  $\text{O}_2$ ,  $\text{NO}_2^-$  and  $\text{NO}_3^-$ . Decay and growth not associated with P uptake are not included.

Process model results validate the nutrient dynamics observed as seen in Figures 2.2 and 2.4, where key state variable profiles from the model match experimental measurements: the average  $\text{NH}_4^+$  oxidation and  $\text{PO}_4^-$  uptake rates, very little  $\text{NO}_3^-$  accumulation but strong  $\text{NO}_2^-$  accumulation under aerobic conditions with subsequent drawdown under anoxic conditions, rbCOD consumption in the anaerobic phase, and  $\text{PO}_4^{3-}$  removal only under aerobic conditions. The process model offers additional insight into the mechanism for NOO out-selection. The net specific growth rates of AOO and NOO were calculated from model data output according to rate equations from the inCTRL ASM matrix (see Supporting Information), and are plotted in parallel with the intermittent aeration intervals in Figure 2.4.C. Due to differences in substrate availability (i.e. high  $\text{NH}_4^+$  and low  $\text{NO}_2^-$ ),  $\mu_{\text{NOO}}$  was less than  $\mu_{\text{AOO}}$  at the beginning of each aeration interval and remained below it throughout the 5 minutes of aeration. This specific growth rate differential was maintained throughout much of the cycle, but  $\mu_{\text{NOO}}$  roughly equaled  $\mu_{\text{AOO}}$  by the end of the intermittently aerated react phase due to the accumulation of  $\text{NO}_2^-$  (data not shown). However, the differential in net specific growth rates in the early part of the SBR cycle ensures that AOO can be maintained in the reactor at a lower SRT than NOO. The modeled average net specific growth rate (including decay) over the cycle can be used to infer a theoretical SRT for NOO to avoid washout, which in this case was 13.2 days ( $\text{SRT}_{\text{AER}} = 5.3$

days). A similar calculation using the average net specific growth rate of AOO gives an SRT of 8.2 days ( $SRT_{AER} = 3.3$  days), which affirms that AOO are retained via the modeled SRT of 9.5 days. This differential in theoretical SRT (13.2 days for NOO, 8.2 days for AOO) was found with standard kinetic modeling that did not invoke metabolic lag times of NOO (i.e. Gilbert et al., 2014), indicating that substrate limitation alone is sufficient to explain NOO out-competition in this process. The average reactor SRT during Phase 2 was  $9.2 \pm 1.8$  days ( $SRT_{AER} = 3.6 \pm 0.9$  days) which, because it is in between the theoretical AOO and NOO SRT values indicated above, reinforces experimental data indicating that SRT control was optimized to washout NOO and retain AOO. Both reactor and modeling results therefore confirm that a combination of intermittent aeration and SRT control can be used to maintain nitrification-denitrification under mainstream conditions. Furthermore, these results suggest that NOO suppression via intermittent aeration and SRT control can be explained by simple substrate (kinetic) limitations alone without invoking more complex mechanisms such as metabolic lag time (Gilbert et al., 2014a) or free ammonia inhibition (Y. Ma et al., 2017a).

While intermittent aeration was the primary strategy to suppress NOO activity, the reactor was operated at generally low DO levels between 0 and 1 mgO<sub>2</sub>/L. Whether low DO operation itself (aside from the effects of intermittent aeration) confers an advantage to AOO over NOO is unclear. AOO have historically been thought to have a higher affinity for oxygen than NOO (Wiesmann, 1994), but recent studies have countered that assumption by measuring the opposite, that is, with  $K_{O_2,NOO} < K_{O_2,AOO}$  (Regmi et al., 2014; Stinson et al., 2013). The apparent  $K_{O_2}$  values measured in those studies were likely affected by floc and microcolony size, which can govern whether AOO or NOO are conferred a competitive advantage at low DO concentrations

(Piciooreanu et al., 2016). In addition, low DO values may promote simultaneous nitrification-denitrification or nitrification-denitrification (Hocaoglu et al., 2011), thus providing a nitrite sink similar to the anoxic periods during intermittent aeration as discussed above. Low peak DO may therefore contribute to NOO suppression based on both competition for O<sub>2</sub> and by promoting nitrite limitation, which supports the argument above that simple kinetics (based only on substrate limitation) can explain NOO out-competition.

### *2.3.1.3 N<sub>2</sub>O Emissions*

N<sub>2</sub>O emissions were measured during 8 separate cycles during steady performance in Phase 2 (between days 414 – 531) and ranged from 0.2 to 6.2% of the influent TKN load, with an average of  $2.2 \pm 2.0\%$  (Table 2.S3). N<sub>2</sub>O emissions relative to TIN removal averaged  $5.2 \pm 4.5\%$ . N<sub>2</sub>O accumulation in the reactor generally paralleled NO<sub>2</sub><sup>-</sup> accumulation near the end of the aerated portion of the cycle. For example, on the N<sub>2</sub>O test on day 414 (Figure 2.2.B), grab sampling throughout the cycle revealed that by the time NO<sub>2</sub><sup>-</sup> first accumulated above 0.1 mgNO<sub>2</sub>-N/L at 285 minutes, 57% of the TIN removal for that cycle had occurred while only 20% of the N<sub>2</sub>O had been emitted, indicating that relative N<sub>2</sub>O emissions increased in the presence of elevated NO<sub>2</sub><sup>-</sup>.

The above measurements are comparable to reported N<sub>2</sub>O emission rates for conventional biological nutrient removal (BNR) processes. (Ahn et al., 2010) reported a range of 0.01 – 1.8% N<sub>2</sub>O emitted relative to influent TKN at 12 full-scale wastewater treatment plants (WWTPs), which included both conventional BNR and non-BNR processes. Foley et al., 2010 reported a much larger range of 0.6 – 25% N<sub>2</sub>O emitted relative to TIN removed at 7 full-scale conventional BNR WWTPs. See Table 2.3 for a comparison of N<sub>2</sub>O emissions as measured in

various treatments processes found in the literature. Both studies found that  $\text{N}_2\text{O}$  emissions were correlated with high  $\text{NO}_2^-$  concentrations, as was the case in our reactor (Figure 2.2.B). In fact, of the eight cycles analyzed for  $\text{N}_2\text{O}$  emissions, the four tests with the highest effluent  $\text{NO}_2^-$  also had the four highest  $\text{N}_2\text{O}$  emissions. Ahn et al. emphasized that the bulk of  $\text{N}_2\text{O}$  emissions occur in aerobic zones due to air stripping of  $\text{N}_2\text{O}$ ; indeed, in our reactor 92% of the  $\text{N}_2\text{O}$  emitted from the in-cycle test on day 414 (for example) occurred during aeration.  $\text{N}_2\text{O}$  mass transfer (i.e. stripping) coefficients for our reactor were 40 times higher during aeration and mixing than during mixing alone ( $0.0688 \text{ min}^{-1}$  and  $0.0017 \text{ min}^{-1}$ , respectively). On average, over the course of one cycle 76% of the  $\text{N}_2\text{O}$  production in the reactor was emitted into the gaseous phase while 24% remained in the liquid phase.

**Table 2.3** Summary of N<sub>2</sub>O emission measurements reported in the literature for conventional and shortcut N removal processes. Conventional nitrogen removal processes (nitrification-denitrification) are highlighted in grey while shortcut nitrogen removal processes (nitritation-denitrification and nitritation-anammox) are highlighted in white.

	Nitrogen removal method	Reactor configuration	N <sub>2</sub> O Emissions (%N <sub>2</sub> O-N / TKN load)	N <sub>2</sub> O Emissions (%N <sub>2</sub> O-N / N removed)	Reference
Conventional	Nitrification-denitrification or none	12 full-scale WWTPs (BNR & non-BNR)	0.01 to 1.8	0.01 to 3.3	Ahn et al. (2010)
	Nitrification-denitrification	7 full-scale BNR WWTPs	---	0.6 to 25	Foley et al. (2010)
	Denitrification (varying C:N ratios)	1 lab-scale semi-continuous	0.005 to 0.5	---	Chung and Chung (2000)
Shortcut Nitrogen	Nitritation-anammox (two stage)	1 full-scale 4-stage "New Activated Sludge"	5.1 to 6.6	---	Desloover et al. (2011)
	Nitritation-anammox (two stage)	1 full-scale process	2.3	---	Kampschreur et al. (2008)
	Nitritation-anammox (single stage)	2 lab-scale SBRs	---	1.7 to 10.9	Domingo-Feléz et al. (2014)
	Nitritation-denitrification	1 lab-scale SBR	2.2 ± 2.0	5.2 ± 4.5	<i>This study</i>

*Definitions: BNR = Biological nutrient removal, WWTP = wastewater treatment plant, SBR = sequencing batch reactor*

Other shortcut N removal biotechnologies, such as PN/A, have been found to have elevated N<sub>2</sub>O production levels over conventional methods for biological N removal (Desloover et al., 2011; Domingo-Feléz et al., 2014; Joss et al., 2009; Kampschreur et al., 2008). Both Desloover et al. (2011) and Kampschreur et al. (2008) (who measured 5.1 – 6.6% and 2.3% N<sub>2</sub>O production relative to influent TKN, respectively; see Table 2.3) found that a separate nitritation step (as opposed to simultaneous nitritation and anammox) caused increased N<sub>2</sub>O production by AOO, which may be due to elevated NO<sub>2</sub><sup>-</sup> concentrations. However, it is not clear that AOO are

causing the bulk of  $\text{N}_2\text{O}$  production in our system or other nitrification-denitrification systems, as low COD concentrations can induce incomplete denitrification and lead to elevated  $\text{N}_2\text{O}$  production (Chung and Chung, 2000; Law et al., 2012; Sabba et al., 2018). Low COD conditions (along with low DO) have also been shown to increase  $\text{N}_2\text{O}$  emissions from nitrifier denitrification (Wrage et al., 2001). Indeed,  $\text{NO}_2^-$  and  $\text{N}_2\text{O}$  accumulation occurs at the end of the SBR cycles (Figure 2.2.B) where COD is most depleted from aeration. This suggests that  $\text{N}_2\text{O}$  emissions from this reactor could be mitigated by a step-feed process, i.e. by filling additional primary effluent to prevent a low COD:N ratio and avoid  $\text{NO}_2^-$  and  $\text{N}_2\text{O}$  accumulation at the end of the cycle. Additional research is required to test the effects of this strategy.

An additional potential benefit of a step-feed modification could be a reduction in the effluent  $\text{NO}_2^-$  concentration. Elevated  $\text{NO}_2^-$  concentrations in discharge to surface waters is undesirable in part due to its toxicity to fish and other aquatic life (Lewis and Morris, 1986). Aside from a step-feed system, potential solutions to elevated  $\text{NO}_2^-$  include a final nitrification step (for oxidation of  $\text{NO}_2^-$  to  $\text{NO}_3^-$ ) or an anammox polishing step (as suggested by (Regmi et al., 2015)). It should be noted that anammox on seeded biocarriers similar to those in the ANITA<sup>TM</sup>Mox process (Christensson et al., 2013) could be incorporated into the same reactor for increased N removal, thus eliminating the need for a two-stage system.

### **2.3.2 P removal and PAOs**

Consistent P removal was achieved in Phase 2 and most of Phase 1 (Figure 2.1, Table 2.2). EBPR performance was not negatively impacted by long-term nitrification-denitrification; in fact, the P uptake rate exceeded the  $\text{NH}_4^+$  removal rate throughout the study (see Figure 2.2.A&B for two representative cycles), indicating that SRT and HRT control to optimize AOO activity

(while minimizing NOO activity) ensured sufficient retention and react times for PAOs. The total P removal rate during Phase 2 was  $6.8 \pm 2.7$  mgP/L/d when considering the entire SBR cycle. The P uptake rate from in-cycle testing during Phase 2 was  $105 \pm 34$  mgP/L/d (or  $3.4 \pm 1.1$  mgP/gVSS/hour) when considering the linear portion of P uptake during the aerated react phase (Figure 2.S3).

High frequency sampling (Figure 2.4.A) and model results (Figure 2.4.B) both demonstrate P removal during aeration coupled to little to no P removal during periods of anoxia. Importantly, this indicates that P release did not occur in the absence of oxygen, verifying that intermittent aeration with periods of anoxia is compatible with EBPR technologies. However, it also indicates that relatively little denitrifying P uptake occurred, even under anoxic conditions when  $\text{NO}_2^-$  was present. This suggests that P uptake by aerobic PAO metabolism rather than by denitrifying PAOs (DPAOs) was the predominant driver of P removal. Figure 2.4.D shows the modeled specific PAO/DPAO growth rates associated with P uptake. Kinetic insights from the process model, which models PAOs as a single group capable of using  $\text{O}_2$ ,  $\text{NO}_2^-$  and  $\text{NO}_3^-$  as electron acceptors for P uptake, show that the combination of low  $\text{NO}_2^-$  and inhibition due to  $\text{O}_2$  prevented appreciable DPAO activity during intermittent aeration. Modeled P uptake via  $\text{NO}_2^-$  was only 16% of total P uptake, and modeled P uptake via  $\text{NO}_3^-$  was even lower at only 0.7% of total P uptake due to limited  $\text{NO}_3^-$  accumulation. The process model suggests that the presence of residual DO, rather than a lack of  $\text{NO}_2^-$  or  $\text{NO}_3^-$ , was the primary inhibitor of DPAO activity. Figure 2.4.D shows that peak DPAO growth in the model occurred not at the maximum  $\text{NO}_2^-$  concentration (i.e. 75 minutes) but when DO had reached near zero (i.e. 78 minutes), at which point  $\text{NO}_2^-$  was at about half of the maximum concentration. Finally, while in-reactor, in-cycle

measurements of DPAO activity are difficult to make, *ex situ* measurements of P uptake rates via  $O_2$ ,  $NO_2^-$  and  $NO_3^-$  showed that the P uptake via  $NO_2^-$  was 17% relative to  $O_2$ , while that of  $NO_3^-$  was 14% relative to  $O_2$  (Figure 2.5). The high frequency sampling plots, DPAO modeling and *ex situ* P uptake tests all indicate that DPAO activity likely plays a relatively minor role in P removal in this reactor.

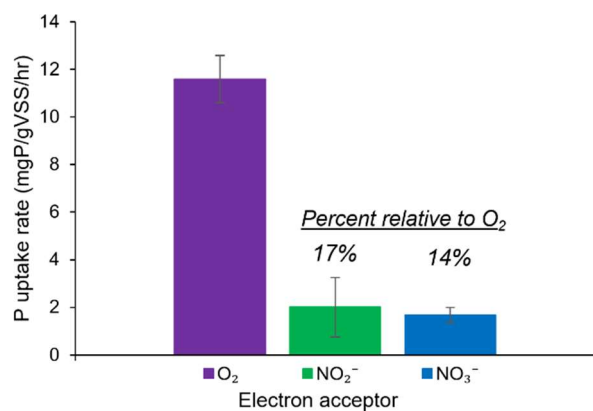


**Figure 2.5** P uptake rates in the presence of  $O_2$ ,  $NO_2^-$ , and  $NO_3^-$  from *ex situ* batch tests.

The minor role of DPAOs in this process countered our original expectation that frequent periods of anoxia coupled to the presence of  $NO_2^-$  would select for a significant DPAO population. DPAOs are considered advantageous in combined N and P removal processes because they offer the opportunity to reduce carbon demand and aeration requirements (Carvalho et al., 2007). Lee et al. (2001) were able to achieve 64% DPAO activity (relative to total P uptake) by introducing a single long anoxic phase (with both  $NO_2^-$  and  $NO_3^-$  present) in the middle of the aerobic phase, which suggests that longer intermittent aeration intervals may select for more DPAO activity (but perhaps at the expense of NOO out-selection). However, preference for DO does not explain the low P uptake via  $NO_2^-$  or  $NO_3^-$  in the absence of  $O_2$  (Figure 2.5)

from *ex situ* batch tests in our reactor. Zeng et al. (2003b) observed that *Accumulibacter* PAOs (which were also identified in this study, see Section 2.3.3) previously acclimated to aerobic P uptake exhibited a 5-hour lag phase in P-uptake when exposed to anoxic conditions ( $\text{NO}_3^-$ ) in place of aeration. A metabolic lag phase is unlikely to explain low maximum P uptake via  $\text{NO}_2^-$  or  $\text{NO}_3^-$  in this reactor, however, given that linear drawdown of  $\text{NO}_2^-$  or  $\text{NO}_3^-$  was observed in all *ex situ* batch tests. A large majority of *Candidatus Accumulibacter phosphatis* genomes sequenced to date have contained the gene encoding nitrite reductase (responsible for reducing  $\text{NO}_2^-$  to nitric oxide [NO]) (Camejo et al., 2019), suggesting that most, if not all, *Accumulibacter* PAOs harbor genomic machinery necessary for denitrifying P uptake via  $\text{NO}_2^-$ . Whether the lack of DPAO activity in this reactor and others is due to the types of PAOs present (and thus the presence or absence of denitrifying genes) or due to the relative expression/inhibition of denitrifying genes present in the PAOs requires further study.

As previously stated, shortcut N removal via nitrification-denitrification did not negatively impact EBPR in this study. Instances of relatively poor P removal were instead usually associated with wet weather flows. Rain not only dilutes the influent but may also induce higher redox conditions in the collection system, indicating a lack of fermentation and little formation of the VFAs that are beneficial to the EBPR process. On sampling days when primary effluent VFAs were at or below the detection limit of 5 mg acetate/L ( $n = 21$ ), the average  $\text{PO}_4^{3-}$  removal of 63% was significantly lower ( $p$  value = 0.003) than the average  $\text{PO}_4^{3-}$  removal of 93% on days when VFAs were greater than 5 mg acetate/L ( $n = 81$ ). For areas with permit requirements below the average of  $0.4 \pm 0.5$  mgTP/L achieved in the reactor effluent, the effects of wet weather flows would need to be mitigated by either occasional exogenous VFA addition or, preferably,

primary sludge or return activated sludge fermentation (Skalsky and Daigger, 1995). However, it is commonly considered difficult to achieve  $< 0.5$  mgTP/L with EBPR alone, so for low effluent limits chemical precipitation and/or filtration are often used (Pagilla et al., 2006).

Shortcut N removal systems can be problematic for EBPR if  $\text{NO}_2^-$  accumulation leads to elevated concentrations of its conjugate acid, nitrous acid ( $\text{HNO}_2$ ).  $\text{HNO}_2$  concentrations above  $0.5 \times 10^{-3}$  mg $\text{HNO}_2$ -N/L can lead to inhibition of *Candidatus Accumulibacter* PAOs (Pijuan et al., 2010), which were the dominant PAO identified in this study (see Section 2.3.3). In the extreme case, the maximum  $\text{NO}_2^-$  concentration in the effluent of our reactor (e.g. end of the SBR cycle) of 5.4 mg $\text{NO}_2^-$ -N/L combined with the minimum pH of 7.0 (which did not actually occur simultaneously) corresponds to  $0.96 \times 10^{-3}$  mg  $\text{HNO}_2$ -N/L with  $\text{pK}_a$  of 3.25 for  $\text{HNO}_2$  (Rumble, 2018). This indicates that  $\text{HNO}_2$  was rarely, if ever, above the reported PAO inhibition concentration in our reactor. Moreover, the highest  $\text{NO}_2^-$  concentrations occurred near the end of the cycle when the majority of  $\text{PO}_4^{3-}$  had already accumulated intracellularly as polyphosphate, and residual  $\text{NO}_2^-$  from the end of the cycle was rapidly depleted after filling at the top of the following cycle.

### 2.3.3 Functional Guild Analysis: PAO, NOO, and AOO

We used 16S rRNA gene sequencing to evaluate diversity and relative abundance of PAOs, NOO, and AOO in the reactor. *Candidatus Accumulibacter* was the dominant genus of PAO in the SBR throughout the study and ranged in relative abundance from 6.6% to 12.0% (Figure 2.S4). *Tetrasphaera* was detected at most time points but always below 0.3% relative abundance. Glycogen accumulating organisms (GAOs) in the genus *Candidatus Competibacter*, which are potential competitors to PAOs, were consistently less abundant than PAOs, and varied from

below the detection limit to 2.4% relative abundance. Other putative GAOs, such as the genera *Defluviicoccus* and *Propionivibrio* (Stokholm-Bjerregaard et al., 2017), were found at even lower abundance than *Candidatus Competibacter* (data not shown).

Regarding the successful suppression of GAOs in this process, possible influencing factors include SRT, temperature, DO and carbon load. GAOs are thought to effectively compete with PAOs at long SRTs above 20 days (Wang et al., 2001), which is well above the average SRTs of 11 days (Phase 1) and 9.2 days (Phase 2) of this reactor. PAOs are also known to compete more effectively with GAOs at lower temperatures (Erdal et al., 2003; Lopez-Vazquez et al., 2009), so the moderate temperature of 20 °C utilized in this study may also have assisted GAO suppression. Lower DO concentrations have also been shown to favor PAO activity over GAO activity (Carvalho, 2014), perhaps due to higher oxygen affinities of PAOs. Finally, the relatively low carbon load in this study (8.2:1 g VFA-COD:g totalP in the influent, and considering the additional demand for carbon for denitrification) may suppress GAO growth. López-Vázquez et al. (2008) found that high influent COD concentrations were positively associated with higher GAO concentrations in full-scale WWTPs and speculated that the excess carbon (not needed for PAO PHA production) allowed for GAO proliferation.

*Nitrotoga* and *Nitrospira* alternately dominated the NOO population according to 16S rRNA gene sequencing (Figure 2.6). The reason for the alternation is unknown as the timing of succession did not clearly correlate with reactor control or performance, although Keene et al. (2017) observed a similar phenomenon. *Nitrospira* dominated at the beginning of Phase 2, and although the NOO population shifted to *Nitrotoga* over the next 100 – 200 days, there was no corollary change in nitrification-denitrification performance, the NAR, or N removal. This result

suggests that the observed robust suppression of NOO activity in this process does not depend upon complete washout of either *Nitrospira* or *Nitrotoga*.

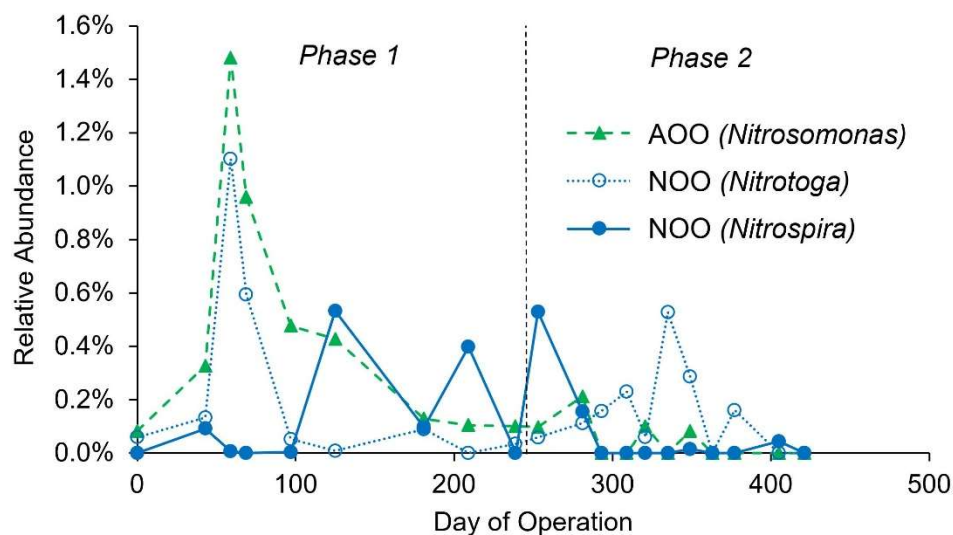


**Figure 2.6** Relative AOO and NOO abundance based on 16S rRNA gene amplicon sequencing through the first 421 days of reactor operation. Day “0” represents the inoculum, which was sampled before reactor operation began.

*Nitrosomonas*-affiliated Betaproteobacteria were the dominant AOO throughout the study according to 16S rRNA gene sequencing but were present at surprisingly low relative abundance for the 2<sup>nd</sup> half of Phase 1 and all of Phase 2 of reactor operation. Interestingly, the relative abundance of *Nitrosomonas* based on 16S rRNA gene sequencing was below the detection limit for selected samples between days 293 – 431 (Phase 2, Figure 2.6). No other known AOO were detected during that time; ammonia oxidizing archaea were detected at only two timepoints before day 100 and at low abundance (< 0.04%). Other potential AOO genera, such as *Nitrospira* and *Nitrosococcus*, were not detected in any 16S rRNA gene sequencing samples. *Nitrospira* can include complete ammonia oxidizing (comammox) clades (Daims et al., 2015),

and comammox can in some cases be the dominant AOO (Roots et al., 2019b) in wastewater treatment. However, *Nitrospira* were not detected or were at low abundance (< 0.04%) after day 293. The decline in AOO was confirmed by qPCR via the functional bacterial *amoA* gene (Figure 2.S5), although AOO were still detected at all time points via qPCR with a minimum of 0.15% relative abundance on day 421. Although the  $\text{NH}_4^+$  oxidation rate was variable throughout Phase 2 (Figure 2.S3),  $\text{NH}_4^+$  oxidation activity was maintained throughout the experimental period. This suggests that either *Nitrosomonas* AOO can maintain effective  $\text{NH}_4^+$  oxidation rates at very low abundance or an as-yet unidentified organism contributed to  $\text{NH}_4^+$  oxidation (Fitzgerald et al., 2015).

## 2.4 Conclusions

This study is the first to demonstrate robust combined shortcut N and P removal from real wastewater without exogenous carbon or chemical addition at the moderate average wastewater temperature of 20°C. Mainstream nitrification-denitrification was achieved for more than 400 days via intermittent aeration and SRT control, with an average NAR of 70% during Phase 2. Process modeling reproduced this performance and confirmed that NOO activity was suppressed with a combination of  $\text{NO}_2^-$  drawdown via denitrification and washout via SRT control, and provided possible explanations for the relative lack of DPAO activity. Importantly, neither  $\text{NO}_2^-$  accumulation nor periods of anoxia in intermittent aeration adversely affected EBPR performance, and consistent and integrated shortcut TIN and biological P removal were achieved for more than 400 days.  $\text{N}_2\text{O}$  emissions were in line with observations of other shortcut N removal systems and were primarily associated with  $\text{NO}_2^-$  accumulation at the end of the cycle. The single-sludge nutrient removal process examined here, as compared to two-stage systems with separate sludges, could reduce operating cost and complexity while meeting nutrient removal goals. Low DO intermittent aeration as utilized in this study can also reduce aeration demands, thereby reducing electrical costs along with the total carbon footprint of treatment. Moreover, effective removal of limiting nutrients will reduce N and P loads to surface waters, thus potentially reducing the negative effects of eutrophication such as biodiversity loss.

## 2.5 Supporting Information

### 2.5.1 Supporting Information: Methods

#### 2.5.1.1 Process Modeling

Modeled specific growth rates for AOO, NOO, and PAOs were quantified throughout the SBR cycles with rate equations and parameter values from the Simba# inCTRL ASM matrix.

Rate equations and parameters values (at 20°C) discussed in the text are as follows:

$$\begin{aligned}
 \text{net specific growth rate of AOO (d}^{-1}\text{)} &= \mu_{AOO} \\
 &= \hat{\mu}_{AOO} \frac{S_{NHx}}{S_{NHx} + K_{NHx,AOO}} \frac{S_{O2}}{S_{O2} + K_{O2,AOO}} \frac{S_{PO4}}{S_{PO4} + K_{PO4,ANO}} \frac{S_{ALK}}{S_{ALK} + K_{ALK,AOO}} \\
 &\quad - \hat{b}_{AOO,O2} \frac{S_{O2}}{S_{O2} + K_{O2,AOO}} - \hat{b}_{AOO,NOx} \frac{S_{NO3} + S_{NO2}}{S_{NO3} + S_{NO2} + K_{NOx,ANO}} \frac{K_{O2,AOO}}{S_{O2} + K_{O2,AOO}} \\
 &\quad - \hat{b}_{AOO,ANA} \frac{K_{NOx,ANO}}{S_{NO3} + S_{NO2} + K_{NOx,ANO}} \frac{K_{O2,AOO}}{S_{O2} + K_{O2,AOO}}
 \end{aligned}$$

Where:

$$\hat{\mu}_{AOO} = \text{maximum specific growth rate of AOO (d}^{-1}\text{)} = 0.9$$

$$S_{NHx} = \text{concentration of } NH_4^+ + NH_3 \left( \frac{mgN}{L} \right)$$

$$K_{NHx,AOO} = \text{AOO half saturation coefficient for } (NH_4^+ + NH_3) \left( \frac{mgN}{L} \right) = 0.7$$

$$S_{O2} = \text{concentration of dissolved } O_2 \left( \frac{mgO_2}{L} \right)$$

$$K_{O2,AOO} = \text{AOO half saturation coefficient for dissolved } O_2 \left( \frac{mgO_2}{L} \right) = 0.25$$

$$S_{PO} = \text{concentration of } PO_4^{3-} \left( \frac{mgP}{L} \right)$$

$$K_{PO4,ANO} = \text{nitrifier nutrient half saturation coefficient for } PO_4^{3-} \left( \frac{mgP}{L} \right) = 0.001$$

$$S_{ALK} = \text{concentration of alkalinity} \left( \frac{meq}{L} \right)$$

$$K_{ALK,AOO} = \text{AOO half saturation coefficient for alkalinity} \left( \frac{meq}{L} \right) = 0.5$$

$$\hat{b}_{AOO,O2} = \text{maximum specific aerobic decay rate of AOO (d}^{-1}\text{)} = 0.17$$

$$\hat{b}_{AOO,NOx} = \text{maximum specific anoxic decay rate of AOO (d}^{-1}\text{)} = 0.1$$

$$S_{NO3} = \text{concentration of } NO_3^- \left( \frac{mgN}{L} \right)$$

$$S_{NO_2} = \text{concentration of } NO_2^- \left( \frac{mgN}{L} \right)$$

$$K_{NOx,ANO} = \text{nitrifier half saturation for anoxic conditions} \left( \frac{mgN}{L} \right) = 0.03$$

$$\hat{b}_{AOO,ANA} = \text{maximum specific anaerobic decay rate of AOO} (d^{-1}) = 0.05$$

$$\begin{aligned} & \text{net specific growth rate of NOO} (d^{-1}) = \mu_{NOO} \\ &= \hat{\mu}_{NOO} \frac{S_{NO_2}}{S_{NO_2} + K_{NO_2,NOO}} \frac{S_{O_2}}{S_{O_2} + K_{O_2,NOO}} \frac{S_{NHx}}{S_{NHx} + K_{NHx,ANO}} \frac{S_{PO_4}}{S_{PO_4} + K_{PO_4,ANO}} \frac{S_{ALK}}{S_{ALK} + K_{ALK,NOO}} \\ &- \hat{b}_{NOO,O_2} \frac{S_{O_2}}{S_{O_2} + K_{O_2,NOO}} - \hat{b}_{AOO,NOx} \frac{S_{NO_3} + S_{NO_2}}{S_{NO_3} + S_{NO_2} + K_{NOx,ANO}} \frac{K_{O_2,NOO}}{S_{O_2} + K_{O_2,NOO}} \\ &- \hat{b}_{NOO,ANA} \frac{K_{NOx,ANO}}{S_{NO_3} + S_{NO_2} + K_{NOx,ANO}} \frac{K_{O_2,NOO}}{S_{O_2} + K_{O_2,NOO}} \end{aligned}$$

Where (in addition to above):

$$\hat{\mu}_{NOO} = \text{maximum specific growth rate of NOO} (d^{-1}) = 0.7$$

$$K_{NO_2,NOO} = \text{NOO half saturation coefficient for } (NO_2^-) \left( \frac{mgN}{L} \right) = 0.1$$

$$K_{O_2,NOO} = \text{NOO half saturation coefficient for dissolved } O_2 \left( \frac{mgO_2}{L} \right) = 0.1$$

$$K_{NHx,ANO} = \text{Nitrifier nutrient half saturation coefficient for } (NH_4^+ + NH_3) \left( \frac{mgN}{L} \right) = 0.001$$

$$K_{ALK,NOO} = \text{NOO half saturation coefficient for alkalinity} \left( \frac{meq}{L} \right) = 0.5$$

$$\hat{b}_{NOO,O_2} = \text{maximum specific aerobic decay rate of NOO} (d^{-1}) = 0.15$$

$$\hat{b}_{NOO,NOx} = \text{maximum specific anoxic decay rate of NOO} (d^{-1}) = 0.07$$

$$\hat{b}_{NOO,ANA} = \text{maximum specific anaerobic decay rate of NOO} (d^{-1}) = 0.04$$

### AOO and NOO washout SRT calculation

The modeled SRT to avoid washout for NOO was calculated by taking the inverse of average modeled  $\mu_{NOO}$  values (as shown above, calculated approximately every minute) over one cycle, i.e.:

$$\text{washout } SRT_{NOO} = \frac{1}{\text{mean}(\mu_{NOO})}$$

A similar calculation was done for AOO to affirm that modeled SRT was sufficiently high to retain AOO. The aerobic fraction of the resulting SRT for AOO and NOO was then calculated by assuming that 48% of the intermittently aerated react phase was aerobic – see Section 2.1 for details.

$$SRT_{AER} = SRT * \frac{0.48(t_{AER})}{t_{AN} + t_{AER}} = SRT * 0.399$$

Where:

$SRT_{AER}$  = aerobic SRT

$t_{AER}$  = length of modeled intermittently aerated react phase (minutes)  
= 222 (variable in the actual reactor)

$t_{AN}$  = length of anaerobic react phase (minutes)  
= 45 (same in the actual reactor)

### PAO-Related Rate Equations

**specific growth rate of PAOs on PHA and  $O_2$  ( $d^{-1}$ ) =  $\mu_{PAO,O_2}$**

$$= \hat{\mu}_{PAO} \frac{\frac{X_{PHA}}{X_{PAO}}}{\frac{X_{PHA}}{X_{PAO}} + K_{PHA}} \frac{S_{O_2}}{S_{O_2} + K_{O_2,OHO}} \frac{S_{NHx}}{S_{NHx} + K_{NHx,OHO}} \frac{S_{PO_4}}{S_{PO_4} + K_{PO_4,PAO}} \frac{S_{ALK}}{S_{ALK} + K_{ALK}}$$

Where (in addition to above):

$\hat{\mu}_{PAO}$  = maximum specific growth rate of PAOs ( $d^{-1}$ ) = 0.95

$X_{PHA}$  = concentration of polyhydroxyalkanoates – PHAs  $\left(\frac{mgCOD}{L}\right)$

$X_{PAO}$  = concentration of PAOs  $\left(\frac{mgCOD}{L}\right)$

$K_{PHA}$  = half saturation coefficient for PHA  $\left(\frac{mgCOD}{L}\right)$  = 0.1

$K_{O_2,OHO}$  = OHO and PAO half saturation coefficient for dissolved  $O_2$   $\left(\frac{mgO_2}{L}\right)$  = 0.05

$K_{NHx,OHO}$  = OHO and PAO nutrient half saturation coefficient for  $(NH_4^+ + NH_3)$   $\left(\frac{mgN}{L}\right)$  = 0.001

$K_{PO_4,PAO}$  = PAO half saturation coefficient for  $PO_4^{3-}$   $\left(\frac{mgP}{L}\right)$  = 0.15

$K_{ALK}$  = PAO half saturation coefficient for alkalinity  $\left(\frac{meq}{L}\right)$  = 0.1

$$\begin{aligned}
 & \text{specific growth rate of PAOs on PHA and NO}_2^- \text{ (d}^{-1}\text{)} = \mu_{PAO,NO2} \\
 & = \hat{\mu}_{PAO} \eta_{anox,PAO} \frac{\frac{X_{PHA}}{X_{PAO}}}{\frac{X_{PHA}}{X_{PAO}} + K_{PHA}} \frac{S_{NO2}}{S_{NO2} + K_{NO2,OHO}} \frac{K_{O2,OHO}}{S_{O2} + K_{O2,OHO}} \frac{S_{NHx}}{S_{NHx} + K_{NHx,OHO}} \\
 & \frac{S_{PO4}}{S_{PO4} + K_{PO4,PAO}} \frac{S_{ALK}}{S_{ALK} + K_{ALK}}
 \end{aligned}$$

Where (in addition to above):

$$\eta_{anox,PAO} = \text{PAO anoxic growth factor} = 0.33$$

$$K_{NO2,OHO} = \text{OHO and PAO half saturation coefficient for NO}_2^- \left(\frac{mgN}{L}\right) = 0.05$$

$$\text{specific growth rate of PAOs on PHA and NO}_3^- \text{ (d}^{-1}\text{)} = \mu_{PAO,NO3}$$

$$\begin{aligned}
 & = \hat{\mu}_{PAO} \eta_{anox,PAO} \frac{\frac{X_{PHA}}{X_{PAO}}}{\frac{X_{PHA}}{X_{PAO}} + K_{PHA}} \frac{S_{NO3}}{S_{NO3} + K_{NO3,OHO}} \frac{K_{NO2,OHO}}{S_{NO2} + K_{NO2,OHO}} \frac{K_{O2,OHO}}{S_{O2} + K_{O2,OHO}} \\
 & \frac{S_{NHx}}{S_{NHx} + K_{NHx,OHO}} \frac{S_{PO4}}{S_{PO4} + K_{PO4,PAO}} \frac{S_{ALK}}{S_{ALK} + K_{ALK}}
 \end{aligned}$$

Where (in addition to above):

$$K_{NO3,OHO} = \text{OHO and PAO half saturation coefficient for NO}_3^- \left(\frac{mgN}{L}\right) = 0.1$$

### Additional Equations Governing PHA in the Model

While the three equations above govern PAO growth on PHA associated with P uptake, there are three additional equations that govern PAO growth in  $PO_4^{3-}$ -limited conditions. These three equations are identical to those listed above (i.e. one each for aerobic,  $NO_2^-$  and  $NO_3^-$ ) aside from the following changes:

Substitute  $\hat{\mu}_{PAO}$  with  $\hat{\mu}_{PAO,LIM} = \text{maximum specific growth rate of PAOs, P-limited (d}^{-1}\text{)} = 0.42$

Substitute  $K_{PHA}$  with  $K_{PHA,lim}$

$$= \text{half saturation coefficient for PHA, P-limited} \left(\frac{mgCOD}{L}\right) = 0.05$$

And add the following Monod term:  $\frac{X_{PP,LO}}{X_{PP,LO} + K_{PP,lim}}$

Where:  $X_{PP,LO}$  = *releasable stored polyphosphate*  $\left(\frac{mgP}{L}\right)$

$$K_{PP,lim} = \text{polyphosphate limitation half - saturation} \left(\frac{mgP}{L}\right) = 0.001$$

PHA production is modeled via the following equation:

**Specific PHA storage rate from VFAs by PAOs ( $d^{-1}$ ):**

$$= q_{PAO,PHA} \frac{\frac{X_{PP,LO}}{X_{PAO}}}{\frac{X_{PP,LO}}{X_{PAO}} + K_{PP,LO}} \frac{S_{VFA}}{S_{VFA} + K_{STORE,VFA}} \frac{S_{ALK}}{S_{ALK} + K_{ALK}}$$

Where (in addition to above):

$$q_{PAO,PHA} = \text{PHA storage rate by PAOs} (d^{-1}) = 6$$

$$K_{PP,LO} = \text{polyphosphate half - saturation for storage} \left(\frac{mgP}{mgCOD}\right) = 0.01$$

$$S_{VFA} = \text{concentration of volatile fatty acids} \left(\frac{mgCOD}{L}\right)$$

$$K_{STORE,VFA} = \text{VFA half - saturation for storage} \left(\frac{mgCOD}{L}\right) = 1$$

Aside from the equations above, modeling of PHA in the inCTRL ASM matrix is affected only by the aerobic, anoxic and anaerobic PAO decay rate equations, which causes PHA release proportional to the PHA content of the PAO biomass.

### 2.5.1.2 Solids Retention Time (SRT) Control

SRT was controlled via timed mixed liquor wasting after the aerated react period and before settling. A maximum wasting pump time was set on the PLC, and the actual pumping time for each cycle varied depending on the length of the aerated react phase. For example, if the maximum wasting pump time was set to 1 minute, the maximum aeration time was set to 300 minutes, and the actual aeration time for a given cycle was 150 minutes, the actual pumping time would be  $1 \text{ minute} \times \frac{150 \text{ minutes}}{300 \text{ minutes}} = 0.5 \text{ minutes}$ . Because the aeration time varied on a cycle-

by-cycle basis according to the influent strength and the target effluent  $\text{NH}_4^+$  level, the dynamic SRT value was calculated for each individual cycle, as adapted from (Laureni et al., 2019) and Takács et al., (2008). SRT for each cycle was calculated according to the equation below (Laureni et al., 2019).

$$SRT_{t+\Delta t} = SRT_t \left( 1 - \frac{X_E V_E + X_R V_W}{X_R V_R} \right) + \Delta t$$

Where:

$SRT_{t+\Delta t}$  = Solids retention time of cycle under analysis (days)

$SRT_t$  = Solids retention time of previous cycle (days)

$V_R$  = Volume of reactor (L)

$X_E$  = Effluent VSS concentration for the cycle under analysis (mg/L)

$V_E$  = Effluent volume for the cycle under analysis (L)

$X_R$  = Reactor MLVSS concentration for the cycle under analysis (mg/L)

$V_W$  = Mixed liquor wasting volume for the cycle under analysis (L)

$\Delta t$  = React time of the cycle under analysis, not including settling and decant (days)

### 2.5.1.3. 16S rRNA Gene Amplicon Sequencing

16S rRNA gene amplicon library preparations were performed using a two-step PCR protocol using the Fluidigm Biomark: Multiplex PCR Strategy as previously described (Griffin and Wells, 2017). In the first round of PCR, each 20  $\mu$ L reaction contained 10  $\mu$ L of FailSafe PCR 2X PreMix F (Epicentre, Madison, WI), 0.63 units of Expand High Fidelity PCR Taq Enzyme (Sigma-Aldrich, St. Louis, MO), 0.4  $\mu$ M of forward primer and reverse primer modified with Fluidigm common sequences at the 5' end of each primer, 1  $\mu$ L of gDNA (approximately 100 ng) and the remaining volume molecular biology grade water. The V4-V5 region of the 16S rRNA gene was amplified in duplicate from 10 samples collected over the course of reactor operation using the 515F-Y (5'-GTGYCAGCMGCCGCGGTAA-3') and 926R (5'-CCGYCAATTYMTTTRAGTTT-3') (Parada et al., 2016) primer set. Thermocycling conditions for the 515F-Y/926R primer set were 95°C for 5 minutes, then 28 cycles of 95°C for 30 seconds, 50°C for 45 seconds, and 68°C for 30 seconds, followed by a final extension of 68°C for 5 minutes. Specificity of amplification was checked for all samples via agarose gel electrophoresis.

Samples were then barcoded by sample via a second stage PCR amplification using Access Array Barcodes (Fluidigm, South San Francisco, CA) (Griffin and Wells, 2017). Each 20  $\mu$ L PCR reaction consisted of 10  $\mu$ L of FailSafe PCR 2X PreMix F, 0.63 units of Expand High Fidelity PCR Taq Enzyme, 2  $\mu$ L of template from the first round of PCR, 4  $\mu$ L of sample-specific barcode primers and the remaining volume molecular biology grade water. The conditions for the second round of PCR were 95°C for 5 minutes, then 8 cycles of 95°C for 30 seconds, 60°C for 30 seconds, and 68°C for 30 seconds. Agarose gel electrophoresis was run again after the second round of PCR to verify correct amplification. Sequencing was performed

on an Illumina Miseq sequencer (Illumina, San Diego, CA) using Illumina V2 (2x250 paired end) chemistry.

For amplicon sequence analysis, sequence quality control was performed through DADA2 (Callahan et al., 2016) integrated in QIIME2 version qiime2-2018.8 (Bolyen et al., 2018), which included quality-score-based sequence truncation, primer trimming, merging of paired-end reads, and removal of chimeras. Taxonomy was assigned to each individual sequence variation using the Silva database, release 132.

#### 2.5.1.4 qPCR supermix and reaction conditions

Bio-Rad iQ SYBR Green Supermix (Bio-Rad, Hercules, CA, USA) containing 50 U/ml iTaq DNA polymerase, 0.4 mM dNTPs, 100 mM KCl, 40 mM Tris-HCl, 6 mM MgCl<sub>2</sub>, 20 mM fluorescein, and stabilizers was used for two qPCR assays. Target genes included ammonia oxidizing bacterial *amoA* via the *amoA*-1F and *amoA*-2R primer set (Rotthauwe et al., 1997) and total bacterial (universal) 16S rRNA genes via the Eub519/Univ907 primer set (Burgmann et al., 2011). The final volume of the reaction mix for each PCR and qPCR reaction was 20 µl, in which the DNA template was ~1 ng, and the primer concentrations were 0.2 µM. All assays were performed in triplicate. For each assay, triplicate standard series were generated by tenfold serial dilutions (10<sup>2</sup>-10<sup>8</sup> gene copies/µl).

### 2.5.2 Process Modeling Reproduces Key Elements of Process Performance

Agreement between the process model and our experimental results suggest that the trends in N and P removal from mainstream wastewater that we observed are likely generally applicable to other locations. By closely modeling the influent (primary effluent), reactor control, aeration

control and SRT (model SRT 9.5 days, reactor SRT  $9.2 \pm 1.8$  days) from Phase 2, the resulting model performance closely matched that of the reactor: modeled HRT was 7.2 hours (reactor HRT  $6.8 \pm 2.8$  hours), modeled VSS was 1,245 mg/L (reactor VSS  $1,344 \pm 226$  mg/L) and Figure 2.2, Figure 2.4, and Table 2.2 demonstrate that both in-cycle nutrient dynamics and effluent concentrations were well-matched between the model and reactor performance. Importantly, this was done via a commercially available wastewater process modeling software without modification to the inCTRL ASM matrix.

### 2.5.3 Supporting Tables

**Table 2.S1** Sampling frequency and target analytes (per APHA, 2005) for daily composite samples. All samples listed are of reactor influent and effluent except  $\text{NO}_2^-$ -N (effluent only) and mixed liquor TSS and VSS (sampled in-reactor).

Analyte	Samples per week
Total COD	3
Filtered COD (1.2 $\mu\text{m}$ filter)	3
Alkalinity	3
Total Kjeldahl Nitrogen	3
$\text{NH}_4^+$ -N	3
$\text{NO}_x^-$ -N <sup>1</sup>	3
$\text{NO}_2^-$ -N (effluent only)	3
Total Phosphorus	3
Ortho-Phosphate	2
TSS <sup>2</sup> & VSS <sup>3</sup>	1
Mixed Liquor TSS <sup>2</sup> & VSS <sup>3</sup>	2

<sup>1</sup>  $\text{NO}_x^-$ -N =  $\text{NO}_2^-$ -N +  $\text{NO}_3^-$ -N

<sup>2</sup> TSS = total suspended solids

<sup>3</sup> VSS = volatile suspended solids

**Table 2.S2** Influent (primary effluent) COD fractionation and COD-to-nutrient ratios.

	Primary Effluent	As percent of total COD
Total COD (mgCOD/L) <sup>a</sup>	164.4 ± 46.2	---
Particulate COD (mgCOD/L)	61.7 ± 23.8	37%
Colloidal COD (mgCOD/L)	28.6 ± 18.1	17%
Soluble COD not including VFA (mgCOD/L)	56.4 ± 19.4	34%
VFA (mgCOD/L)	18.8 ± 8.9	11%
COD:TP <sup>b</sup> (gCOD/gP)	67:1	---
COD:TKN <sup>b</sup> (gCOD/gN)	8.3:1	---

<sup>a</sup>Primary effluent COD fractionation was performed weekly from days 114 - 515 (n = 50).

<sup>b</sup>COD:Nutrient ratios are taken from average of all samples from days 27 - 519 (n = 192).

**Table 2.S3** N<sub>2</sub>O emissions test results for 8 cycles during Phase 2.

Day of cycle tested	N <sub>2</sub> O emitted/ influent TKN	N <sub>2</sub> O emitted/ TIN removed	influent TKN (mgN/L)	influent COD (mg/L)	COD/ TKN	Effluent NO <sub>2</sub> <sup>-</sup> (mgN/L)	Average temp (°C)
414	3.8%	11.4%	23	206	9	2.9	20.5
426	6.2%	12.0%	20	204	10	2.7	20.3
428	1.0%	2.3%	12	140	12	1.2	20.5
475	1.0%	2.6%	13	64	5	2.0	20.4
489	2.2%	4.3%	19	183	10	2.4	20.3
503	0.2%	0.2%	14	160	11	0.4	19.4
517	0.8%	1.6%	21	147	7	1.9	19.4
531	1.56%	7.36%	13	144	11	2.1	19.4

## 2.5.4 Supporting Figures

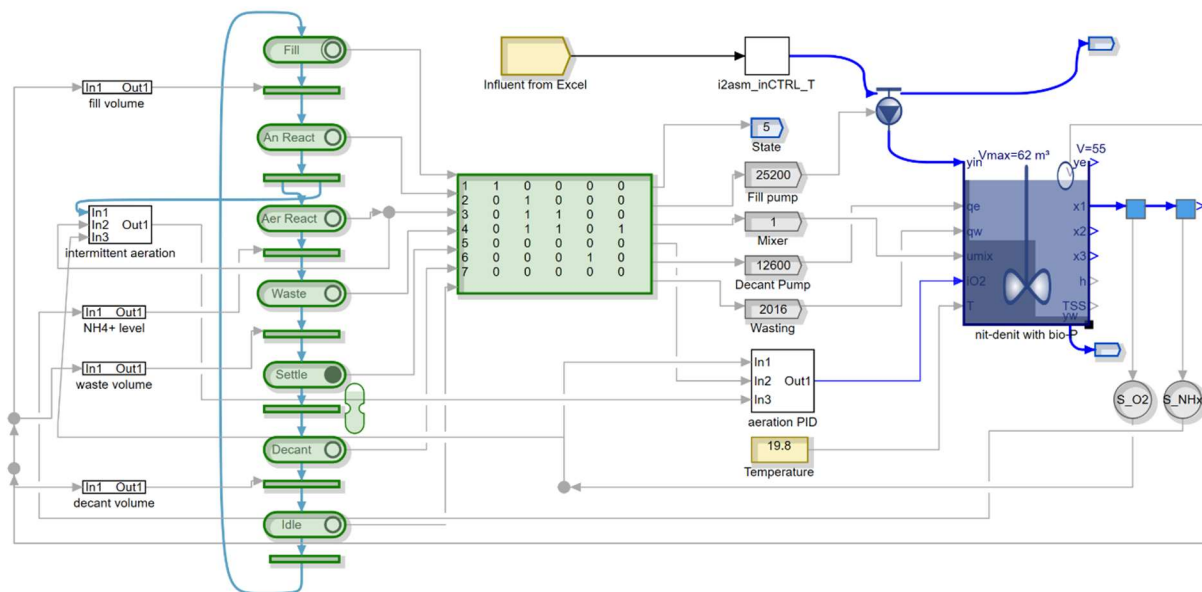
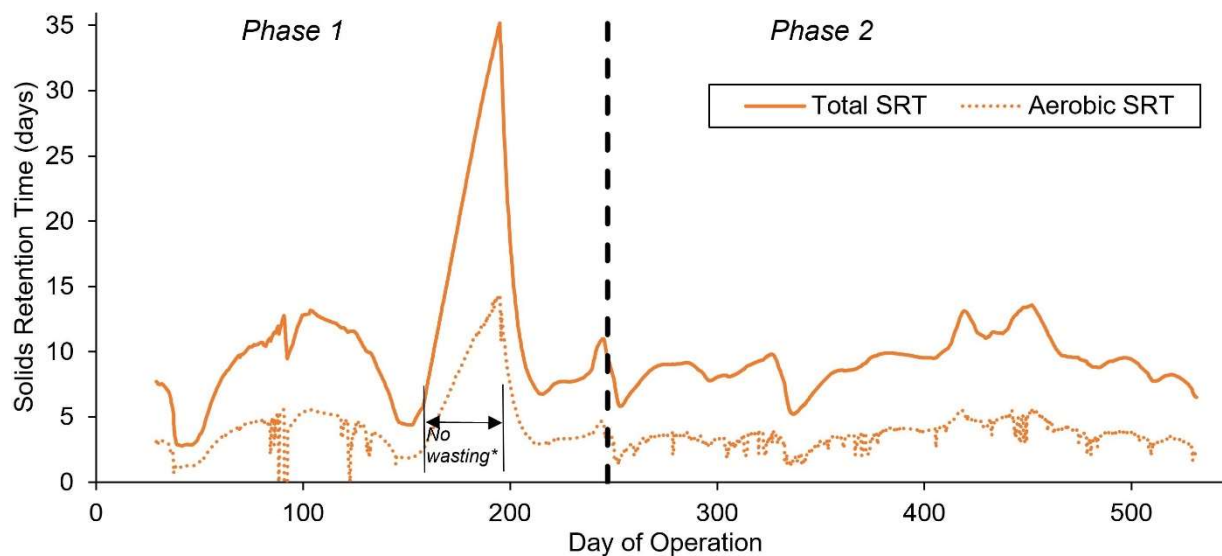
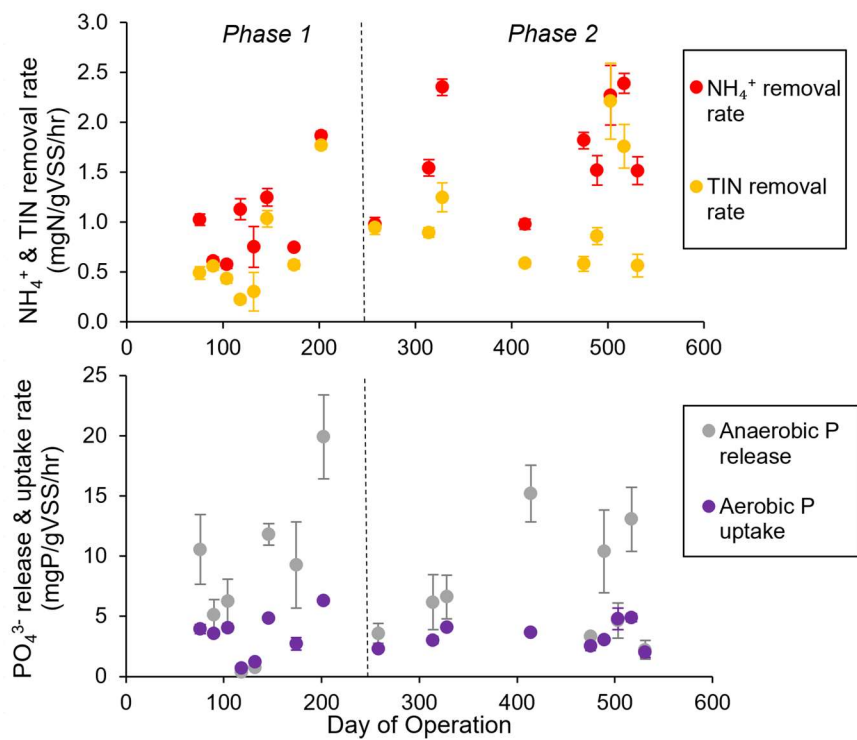


Figure 2.S1 Process representation in the Simba# 3.0 software.



**Figure 2.S2** Total and aerobic dynamic SRT over time in the SBR. The average total and aerobic SRT during Phase 1 was  $11 \pm 7$  and  $4.5 \pm 3.0$  days, and the average total and aerobic SRT during Phase 2 was  $9.2 \pm 1.8$  and  $3.6 \pm 0.9$  days, respectively. \*Mixed liquor wasting was suspended from days 158 – 195 to recover AOO activity.



**Figure 2.S3** In-cycle N and P removal rates from least-squares regression of the linear portions of in-cycle grab samples for NH<sub>4</sub><sup>+</sup>, NO<sub>2</sub><sup>-</sup>, NO<sub>3</sub><sup>-</sup>, and PO<sub>4</sub><sup>3-</sup>. Error bars represent standard errors of the slopes.

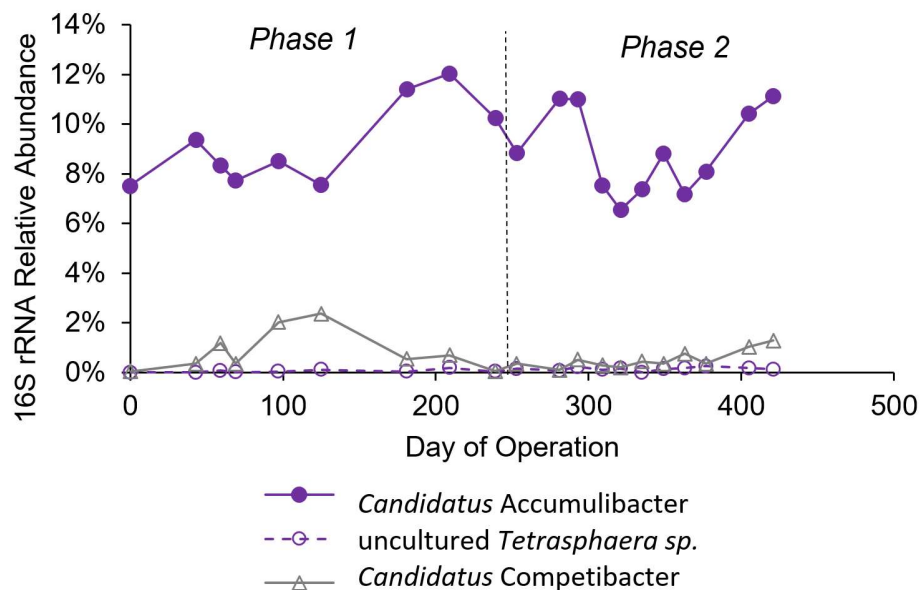


**Figure 2.S4** Relative *Accumulibacter*, *Tetrasphaera*, and *Competibacter* abundance through the first 421 days of reactor operation according to 16S rRNA gene sequencing. Day “0” represents the inoculum, which was sampled before reactor operation began.

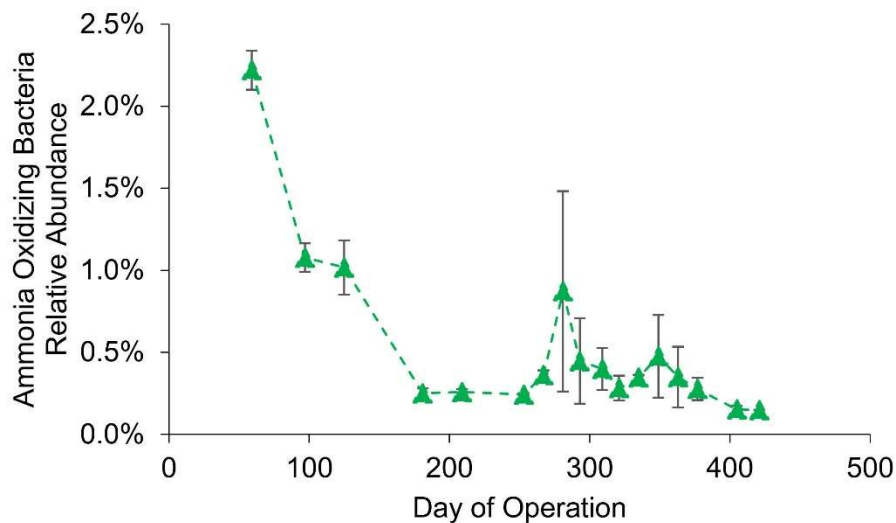


**Figure 2.S5** Ammonia oxidizing bacterial *amoA* gene abundance normalized to total bacterial 16S rRNA genes through the first 421 days of reactor operation according to qPCR.

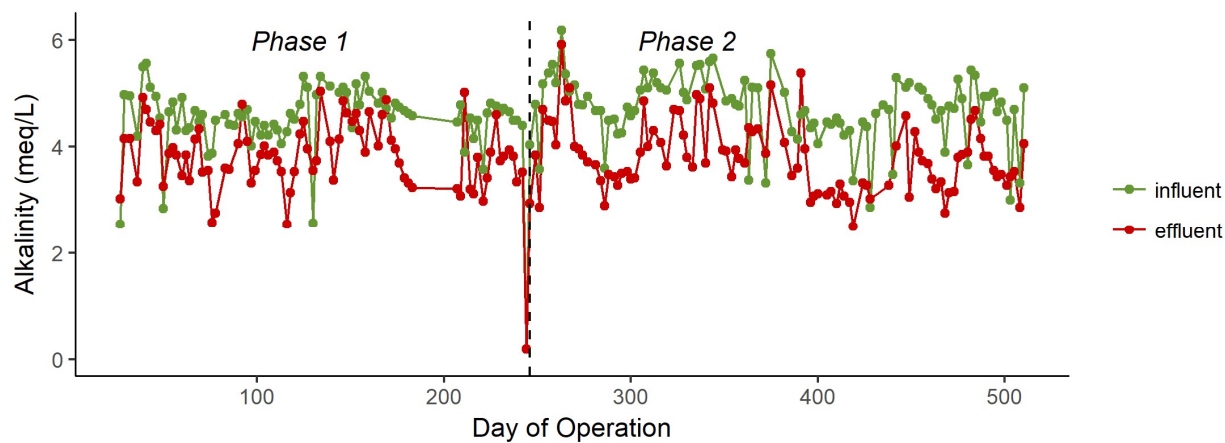


**Figure 2.S6** Reactor influent and effluent alkalinity concentrations from composite sampling.

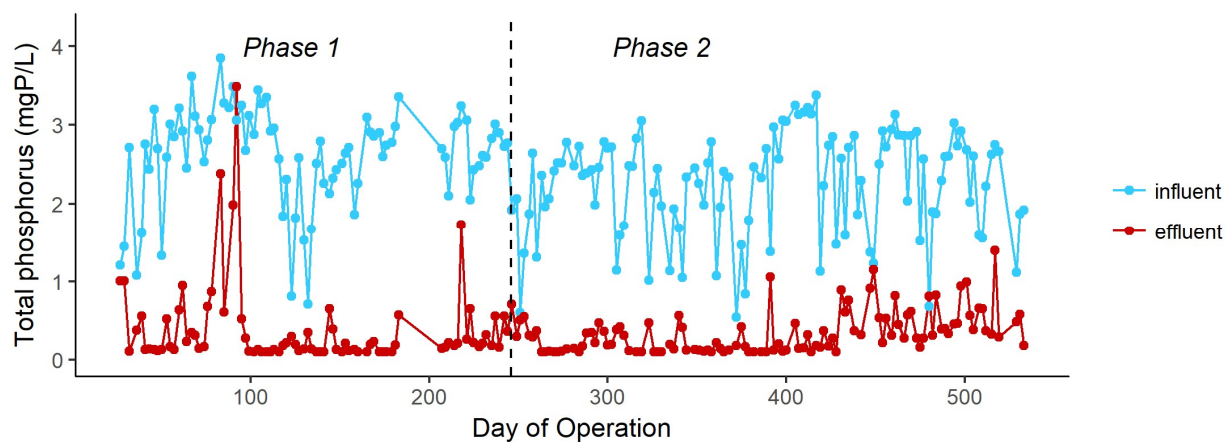


**Figure 2.S7** Reactor influent and effluent total phosphorus concentrations from composite sampling.

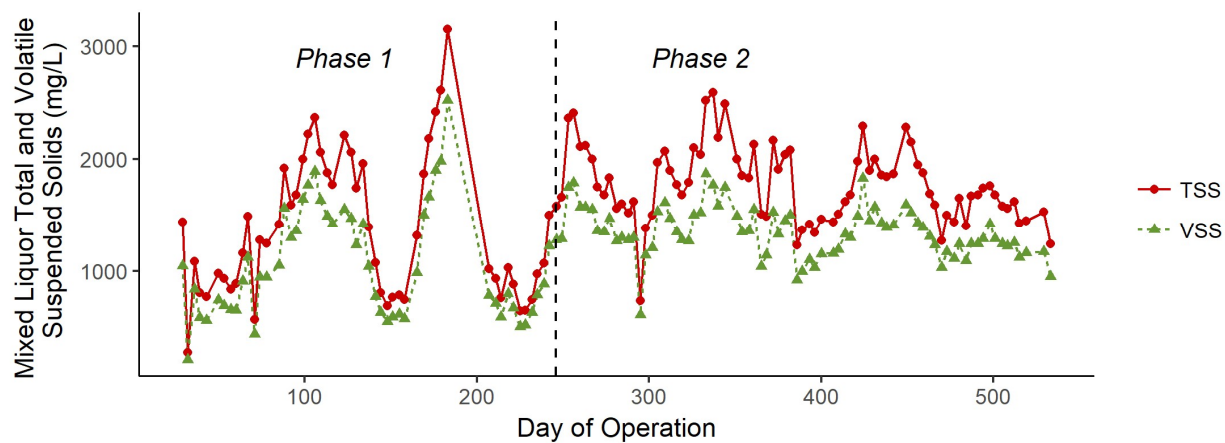


**Figure 2.S8** Reactor mixed liquor TSS and VSS concentrations.

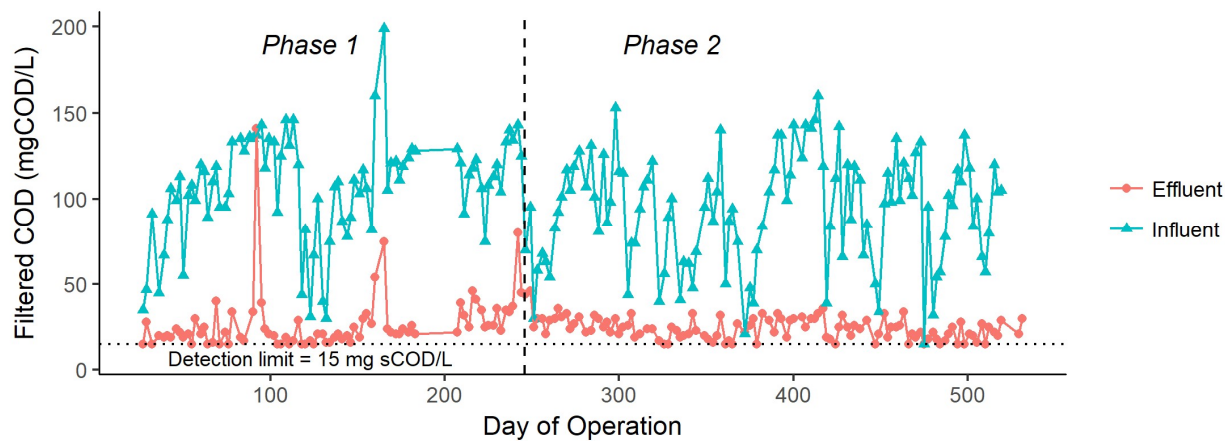


**Figure 2.S9** Reactor influent and effluent filtered COD from composite sampling. Samples were filtered through a 1.2  $\mu\text{m}$  pore size membrane.

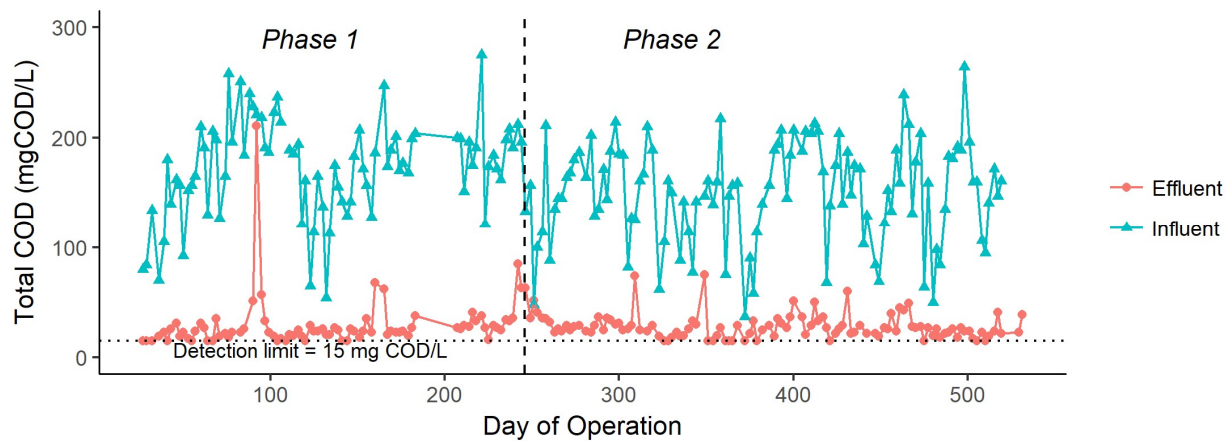


**Figure 2.S10** Reactor influent and effluent total COD concentrations from composite sampling.

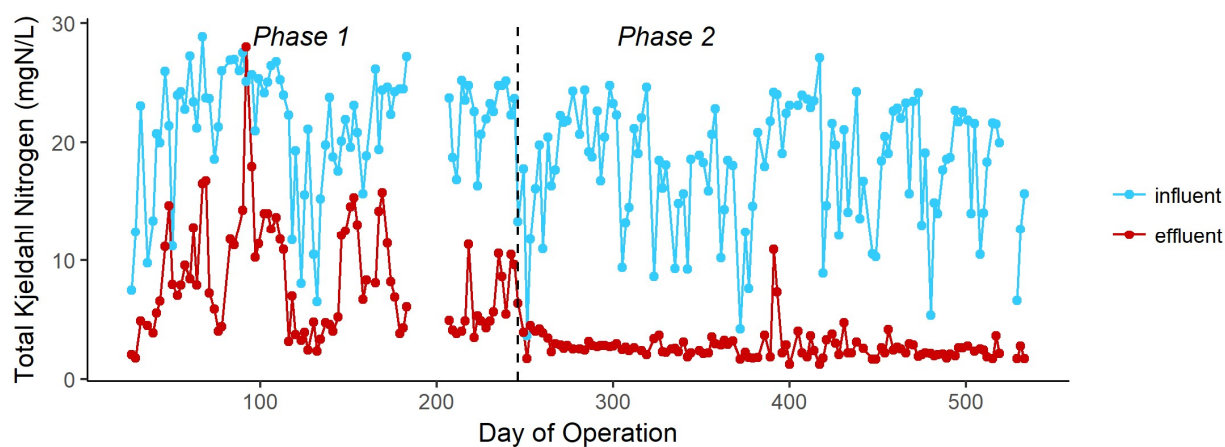
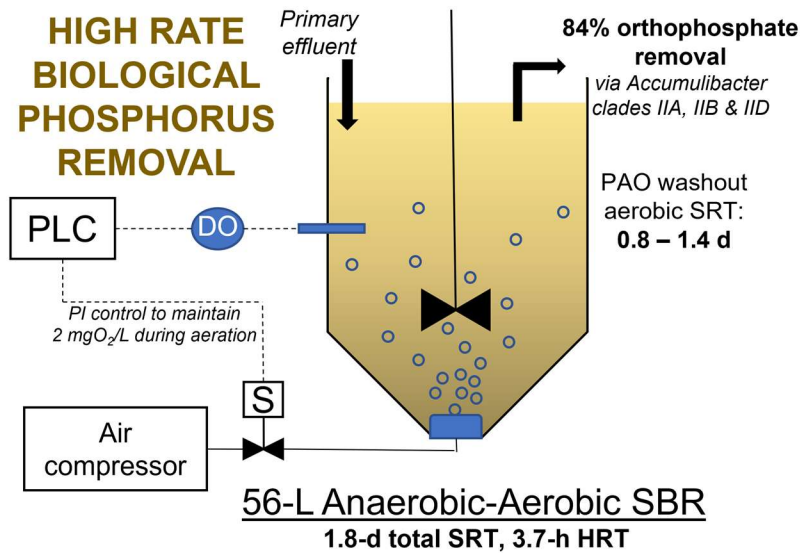


**Figure 2.S11** Reactor influent and effluent TKN concentrations from composite sampling.

### CHAPTER 3: PUSHING THE LIMITS OF SOLIDS RETENTION TIME FOR ENHANCED BIOLOGICAL PHOSPHORUS REMOVAL: PROCESS CHARACTERISTICS AND ACCUMULIBACTER POPULATION STRUCTURE<sup>1</sup>



#### Abstract

Biological treatment processes that maximize organic carbon diversion to the sidestream for energy recovery via anaerobic digestion, such as the high rate activated sludge (HRAS) process, can reduce the carbon footprint of wastewater treatment. By reducing the solids retention time (SRT) of the enhanced biological phosphorus removal (EBPR) process, some of the same benefits of energy recovery can be realized. While carbon recovery in a high rate EBPR process will be less than that of conventional HRAS, determining the washout (i.e. minimum) SRT of polyphosphate accumulating organisms (PAOs) will allow for simultaneous phosphorus and carbon diversion for energy recovery from EBPR systems. However, few studies have investigated the washout SRT of PAOs in real wastewater, and little is known of the diversity of PAOs in high rate EBPR systems. Here we demonstrate efficient phosphorus removal (84% orthophosphate removal) in a high rate EBPR sequencing batch reactor fed real primary effluent

<sup>1</sup> This chapter is from a manuscript in preparation: Roots, P., Rosenthal, A.F., Wang, Y., Sabba, F., Jia, Z., Yang, F., Kozak, J.A., Zhang, H., Wells, G.F. Pushing the limits of solids retention time for enhanced biological phosphorus removal: Process characteristics and *Accumulibacter* population structure.

and operated at 20 °C. Stable operation was achieved at a total SRT of  $1.8 \pm 0.2$  days and hydraulic retention time of 3.7 – 4.8 hours. 16S rRNA gene sequencing data demonstrated that *Accumulibacter* were the dominant PAO throughout the study, with a washout aerobic SRT between 0.8 and 1.4 days. qPCR targeting the polyphosphate kinase gene revealed that *Accumulibacter* clades IIA, IIB and IID dominated the PAO community at low SRT operation, while clade IA was washed out at the lowest SRT values.

### 3.1 Introduction

Despite the large amount of energy typically used to treat wastewater, estimated at 3.2 kJ/g chemical oxygen demand (COD), the theoretical chemical energy contained in typical domestic sewage, 16.2 kJ/g COD, is about 5 times that amount (Wan et al., 2016). The high-rate activated sludge (HRAS) process (Chase and Eddy, 1944) aims to reduce mineralization and increase the digestibility of COD diverted to anaerobic digestion by minimizing both HRT and SRT, thereby minimizing footprint and maximizing carbon diversion to sidestream anaerobic digestion for energy recovery (Ge et al., 2013). While the HRAS process has been widely applied in mainstream wastewater treatment, little research has focused on incorporating enhanced biological phosphorus removal (EBPR) into high rate A-stage processes. The potential for simultaneous recovery of COD and phosphorus (P) makes high rate EBPR processes an attractive option. It should be noted that the minimum SRT required to retain polyphosphate accumulating organisms (PAOs) in a high rate EBPR process may disqualify it as a true HRAS process, which typically operates with  $SRT < 1$  day. Nonetheless, evidence has shown that a relatively low SRT (around 3 days) in an EBPR process achieved a higher biomass yield than

with more typical SRTs of 10 – 20 days (Chan et al., 2017) and, by implication, higher energy recovery in anaerobic digestion. High rate A-stage EBPR in series with a B-stage autotrophic partial nitrification/anammox (PN/A) process for N removal could therefore enable energy efficient total nutrient removal (Gao et al., 2014). However, because conventional EBPR processes are typically operated with SRTs around 10 days or higher, knowledge about performance characteristics, population structure, and the limits of SRT for PAOs in high rate systems is limited.

Of the existing studies on low sludge age EBPR, many were conducted in conditions atypical of mainstream wastewater: Ge et al. (2015) established an optimal SRT of 2 – 2.5 days (aerobic SRT [ $SRT_{aer}$ ] = 1.2 – 1.5 days) for P removal from a strong abattoir waste stream at a temperature of 20 – 22 °C, and Valverde-Pérez et al. (2016) found an optimal SRT of 3 days ( $SRT_{aer}$  = 1.5 days) at 16 – 19 °C for P removal from a primary effluent stream to which propionate had been added to simulate primary fermentation. Chan et al. (2017) found that EBPR performance was maintained at an SRT of 3.6 days ( $SRT_{aer}$  = 2.1 days) when treating synthetic wastewater at 25 °C, and Mamais and Jenkins (1992) found an optimal SRT of 2.3 – 2.6 days ( $SRT_{aer}$  = 1.7 – 2 days) at 20 °C in a bench scale process using primary effluent supplemented with acetate. Only a few studies have used real wastewater without supplemental carbon to investigate low SRT EBPR, which limits our understanding of the boundaries of SRT under real world conditions: Yang et al. (2017) used a 2 – 3 day SRT ( $SRT_{aer}$  = 1.5 – 2.25 days) for successful EBPR at 16 – 24 °C in an A-stage sequencing batch reactor (SBR) treating primary effluent, McClintock et al. (1993) demonstrated good EBPR at an SRT of 2.7 days ( $SRT_{aer}$  = 1.5 days) at 20 °C in a pilot scale process, and Shao et al. (1992) found an optimal SRT of 3 days

( $SRT_{aer} = 2.8$  days) at 23 °C in a full scale process. Three of the above studies preceded the identification and classification of *Accumulibacter* (Hesselmann et al., 1999), and none of the more recent studies that selected for *Accumulibacter* investigated clade-level population dynamics. Fourteen clades of *Accumulibacter* have been identified (Camejo et al., 2016; Mao et al., 2015), and it remains to be investigated if low SRT operation exerts a selective pressure that leads to dominance of specific clades.

Depending upon effluent end-use, an additional motivation to maintain low SRT in the high rate EBPR process is to prevent nitrification by washout of ammonia and nitrite oxidizing bacteria (AOB and NOB). This is the case in the present study, where the effluent of the high rate EBPR (A-stage) reactor fed a mainstream PN/A (B-stage) process that benefits from high ammonia and low COD concentrations. Such an A-B process has promise as an energy saving method for total nutrient removal, with no exogenous chemical additions required. However, growth parameters indicate that maintaining an SRT that retains PAOs and expels nitrifiers may be difficult: typical reported maximum growth rates for AOB and NOB at 20°C are 0.76 and 0.81 d<sup>-1</sup> (Rittmann and McCarty, 2001), respectively, which corresponds to a theoretical minimum  $SRT_{aer}$  of 1.2 – 1.3 days. While this disregards microbial decay and variable reactor conditions, it clearly indicates that selectively washing out nitrifiers while maintaining PAOs will be difficult in practice where precise SRT control is a challenge.

This study addresses the knowledge gap of low sludge age EBPR performance and PAO population diversity in real mainstream wastewater without VFA addition. Our specific objectives were to determine the limits of SRT and HRT for robust EBPR, and to evaluate if low sludge age impacts clade level diversity of *Accumulibacter*. An anaerobic-aerobic SBR was

operated for 500 days with primary effluent as feed at 20 °C. Efficient and stable total P and COD removal (77% of both) was achieved at a very low SRT of  $1.8 \pm 0.2$  days and HRT down to 3.7 hours. The washout  $SRT_{\text{aer}}$  for PAOs was found to be between 0.8 and 1.4 days. 16S rRNA gene sequencing data revealed that *Accumulibacter* was the dominant PAO throughout the study, and qPCR revealed high abundance of *Accumulibacter* clades IIA, IIB and IID under low SRT conditions. The SRT in this process is substantially lower than conventional EBPR processes and suggests the potential of a high rate AO process to recover both energy and P from wastewater.

## 3.2 Materials and Methods

### 3.2.1 Reactor Operation

A 56-L working volume sequencing batch reactor (hereafter called “reactor”) was enriched with suspended growth biomass intended to facilitate high rate COD and biological P removal. The reactor was inoculated with EBPR biomass from the James C. Kirie Water Reclamation Plant (WRP) of the Metropolitan Water Reclamation District of Greater Chicago (MWRD) on May 2, 2016 (day 0). The James C. Kirie WRP operated with an 8-day average SRT in April 2016. The reactor was then fed with primary effluent (PE) (Table 3.1) of the Terrence J. O’Brien WRP of the MWRD and temperature controlled to  $19.7 \pm 1.2$  °C (average  $\pm$  standard deviation over the entire study). SBR operation initially consisted of a  $\approx$ 3-minute gravity fill, 45 minutes of anaerobic mixing, a 135-minute aerobic react phase, 30 – 40 minutes settling (0.41 m/h critical settling velocity), and 62.5% volume decantation ( $\approx$ 5 minutes), yielding an estimated 4.8-hour hydraulic retention time (HRT) excluding settling and decant. On

day 416, react times were shortened to 35 minutes of anaerobic mixing and 105 minutes of aerobic react, yielding an estimated 3.7-hour HRT excluding settling and decant.

SBR control of reactor equipment from inoculation to day 358 was managed with on-off circuit switching via ChronTrol programmable timers (4-circuit, 8-input XT Table Top unit, ChronTrol). Aeration prior to day 358 was controlled manually by throttling a rotameter downstream of an air compressor, with a target dissolved oxygen (DO) concentration of 2 – 4 mg O<sub>2</sub>/L. Starting on day 358 and continuing to the end of the study (day 499), reactor equipment was controlled with code-based Programmable Logic Control (PLC) (Ignition SCADA software by Inductive Automation and TwinCAT PLC software by Beckhoff). Upon PLC implementation aeration control was switched to proportional-integral-derivative (PID) control based on the online oxygen sensor (S::CAN oxi::lyser™ optical probe) signal to target 2 mg O<sub>2</sub>/L. For the purposes of this paper, data is split into three time ranges: Phase 1: days 0 – 357 before PLC control, Phase 2: days 358 – 486 with PLC control, and Phase 3: days 487 – 499 after PAO washout.

### **3.2.2 SRT Control**

The goal of SRT control was to maintain PAOs and EBPR activity while washing out nitrifiers and was controlled by wasting a known volume of mixed liquor near the end of the aerobic phase. Mixed liquor suspended solids were measured twice per week and effluent suspended solids were measured once per week, and the overall SRT was calculated as in the following formula:

$$SRT = \frac{X_R V_R}{X_E Q_E + X_R Q_W} \quad (Eq. 1)$$

Where  $SRT$  = Solids retention time (d)  
 $X_R$  = Volatile suspended solids concentration in the reactor (mgVSS/L)  
 $V_R$  = Volume of reactor (L)  
 $X_E$  = Volatile suspended solids concentration in the reactor effluent (mgVSS/L)  
 $Q_E$  = Effluent flow rate (L/d)  
 $Q_W$  = Wasting flow rate (L/d)

$Q_E$  and  $Q_W$  above were calculated via the react time, which excludes settling and decant.

The aerobic SRT was calculated as follows:

$$SRT_{aer} = SRT \frac{t_{aer}}{t_c} \quad (Eq. 2)$$

Where (in addition to above)

$SRT_{aer}$  = Aerobic solids retention time (d)  
 $t_{aer}$  = Aerobic react time (min)  
 $t_c$  = Cycle time excluding settling and decant (min)

### 3.2.3 P Assimilation Calculation

P removal via non-EBPR biomass assimilation was estimated following methods detailed in Rittmann and McCarty (2001), as follows:

$$P_{assm} = \frac{0.0267 \times Y(1 + (1 - f_d)b\theta_x)\Delta sCOD}{1 + b\theta_x} \quad (Eq. 3)$$

Where:  $P_{assm}$  = P removed through non-EBPR biomass assimilation  
0.0267 = Typical ratio of phosphorus mass to volatile dry mass of activated sludge  
 $Y$  = typical biomass yield, 0.46 mgVSS/mgCOD  
 $f_d$  = biodegradable fraction of new biomass, 0.8  
 $b$  = endogenous decay rate,  $0.1^{-d}$   
 $\theta_x$  = solids retention time, days  
 $\Delta sCOD$  = soluble COD removal, mgCOD/L (as a proxy for BOD removal)

### 3.2.4 Reactor Sampling

Total and soluble chemical oxygen demand (COD), total suspended solids (TSS), volatile suspended solids (VSS), alkalinity, total and soluble Kjeldahl nitrogen (TKN, sTKN),  $\text{NH}_4^+\text{-N}$ , combined  $\text{NO}_3^- + \text{NO}_2^- \text{-N}$  ( $\text{NO}_x\text{-N}$ ), total P, and orthophosphate were monitored 3 to 5 times/week in influent and effluent daily composite samples per Standard Methods (APHA, 2005). Volatile fatty acids (VFA) in the influent were not measured during the study period, but later measurements of the same influent revealed an average VFA:sCOD ratio of  $0.16 \pm 0.7$  ( $n = 143$ , measured October 2017 to May 2019). This translates to an estimated influent VFA concentration of  $14 \pm 6$  mg VFA-COD/L during this study.

### 3.2.5 *In situ* Batch Activity Assays

In-cycle tests to observe phosphate and carbon dynamics were performed on days 65, 79, and weekly to bi-weekly after day 253. No chemical dosing occurred before or during the tests in order to observe typical *in situ* rates of carbon removal and phosphate uptake and release. Grab samples were taken every ~11 minutes during the anaerobic react period and every ~20 minutes during aerobic react period and analyzed for orthophosphate and (for certain tests only) readily biodegradable COD (rbCOD) and VFAs. In-cycle rbCOD was defined as the floc-filtered COD (ffCOD, following the method of Mamais et al., 1993) for a given time point in the cycle minus the ffCOD in the effluent. Phosphate release and uptake rates were measured via a least-squares linear regression of the linear portion ( $R^2 > 0.8$ ) of the phosphate uptake and release curves.

### 3.2.6 Reactor Biomass Archiving and DNA Extraction

Reactor mixed liquor biomass was archived weekly to biweekly with the following procedure: 6 mL of mixed liquor was pipetted from each reactor and separated into six 1-mL

aliquots in 1.5 or 2.0-mL centrifuge tubes. Each tube was centrifuged at 10,000g for 3 minutes, after which the supernatant was removed and replaced with 1 mL of TE buffer. The tubes were centrifuged again at 10,000g for 3 minutes, after which the supernatant was removed, leaving only the biomass pellet. All samples were archived at -80°C. DNA extraction was performed with the FastDNA SPIN Kit for Soil (MPBio), as per the manufacturer's instructions.

### **3.2.7 16S rRNA Gene Amplicon Sequencing**

16S rRNA gene amplicon library preparations were performed using a two-step multiplex PCR protocol, as previously described (Griffin and Wells, 2017). All PCR reactions were performed using a Biorad T-100 Thermocycler (Bio-Rad, Hercules, CA). The V4-V5 region of the universal 16S rRNA gene was amplified in duplicate from 20 dates collected over the course of reactor operation using the 515F-Y/926R primer set (Parada et al., 2016). Thermocycling conditions were 95°C for 5 minutes, 28 cycles of {95°C for 30 seconds, 50°C for 45 seconds, and 68°C for 30 seconds}, followed by a final extension of 68°C for 5 minutes. Specificity of amplification was checked for all samples via agarose gel electrophoresis.

All amplicons were sequenced using a MiSeq system (Illumina, San Diego, CA, USA) with Illumina V2 (2x250 paired end) chemistry at the University of Illinois at Chicago DNA Services Facility and deposited in GenBank (accession number for raw data: PRJNA599575). For amplicon sequence analysis, sequence quality control was performed through DADA2 (Callahan et al., 2016) integrated in QIIME2 version qiime2-2018.8 (Bolyen et al., 2018). Taxonomy was assigned to each unique sequence variant using the Silva database, release 132.

### 3.2.8 Quantitative Polymerase Chain Reaction (qPCR)

qPCR was used to quantify the relative abundance of the 14 known *Ca. Accumulibacter* clades throughout the study via specific primer sets targeting the polyphosphate kinase (*ppk1*) gene developed by Camejo et al. (2016). Total bacterial (universal) 16S rRNA genes were quantified via the Eub519/Univ907 primer set (Burgmann et al., 2011). All assays employed 20  $\mu$ l reaction volumes with thermocycling conditions and primer concentrations reported in the reference papers and were performed on a Bio-Rad C1000 CFX96 Real-Time PCR system (Bio-Rad, Hercules, CA, USA). For the total bacteria 16S rRNA assay, 10  $\mu$ l of the Bio-Rad SsoAdvanced Universal Inhibitor-Tolerant SYBR Green Supermix (Bio-Rad, Hercules, CA, USA) was used. For assays targeting *ppk1* genes, 10  $\mu$ l of Epicenter FailSafe<sup>TM</sup> PCR 2X PreMixF (5  $\mu$ l of 200x SYBR green in DMSO and 2.5  $\mu$ l of 10% Tween-20 were added to 2.5 mL of PreMix F to facilitate use in qPCR) and 1.25 U of Epicenter FailSafe<sup>TM</sup> PCR Enzyme Mix (Lucigen Corporation, Middleton, WI, USA) were used. Each sample date was analyzed with 2 technical replicates of 2 biological replicates (total of 4 replicates) for each assay. Standard series were generated in duplicate by tenfold serial dilutions ( $10^2$ - $10^8$  gene copies/ $\mu$ l) using cloned plasmid DNA or synthesized DNA (IDT Inc, Coralville, IA, USA). The amplification specificity of each qPCR assay was verified with melt curve analysis and agarose gel electrophoresis. For relative abundance quantification, 4.2 copies/cell of the 16S rRNA gene was assumed for total bacteria (Větrovský and Baldrian, 2013) and 1 copy/cell of the *ppk1* gene was assumed for *Accumulibacter* (Camejo et al., 2016; Mao et al., 2015).

### 3.3 Results

#### 3.3.1 SRT Optimization and Reactor Performance

Process optimization occurred during Phase 1 to characterize conditions for EBPR to occur with simultaneous nitrifier washout. A total SRT around 2 – 3 days ( $SRT_{\text{aer}}$  around 1.5 – 2 days) (Figure 3.1) up to day 120 combined with a high target DO of 4 mg  $O_2/L$  in the aerobic phase resulted in  $NO_2^- + NO_3^-$  ( $NO_x$ ) detected in the effluent in days 67 – 150, with a maximum value of 5.1 mg  $NO_x-N/L$  on day 98 (Figure 3.S1). In order to wash out nitrifiers, on day 121 the target total SRT was lowered to 2.2 days ( $SRT_{\text{aer}}$  of 1.7 days) and the target DO level was lowered to 2 mg  $O_2/L$ , which eliminated  $NO_x$  in the effluent by day 150. While  $NO_x$  production and recycle to the anaerobic zone can be detrimental to the EBPR process, P removal did not improve upon washout of nitrifiers, and in fact temporarily worsened (Figure 3.2). During process optimization in Phase 1 P removal was variable (Figure 3.2), with an average orthophosphate removal of 44% in part due to poor DO control with manual adjustment of air flow.

**Table 3.1** Reactor influent (O'Brien WRP primary effluent) average values over the entire study and reactor effluent values averaged over the three phases.

	<i>Influent (PE)</i>		<i>Reactor effluent</i>		
	Days 0 - 499	<i>Number of samples</i>	Phase 1: Days 0-357	Phase 2: Days 358-486	Phase 3: Days 487- 499
Total phosphorus (mgP/L)	2.5±0.7	250	1.3 ± 1.2	0.55 ± 0.77	1.5 ± 0.5
Orthophosphate (mgP/L)	1.9±0.6	186	1.0 ± 0.7	0.31 ± 0.22	1.3 ± 0.3
COD (mgCOD/L)	143±45	249	44 ± 34	32 ± 10	50 ± 11
sCOD (mgCOD/L)	85±23	249	30 ± 11	27 ± 8	41 ± 10
rbCOD (mgCOD/L)	39±25	27	NA	NA	NA
TSS (mg/L)	44±23	59	17 ± 38	7 ± 5	18 ± 0
Reactor HRT (hr)			4.9	4.1	3.8
Reactor SRT (d)			2.2 ± 0.5	1.8 ± 0.2	1.1 ± 0.2
Reactor MLVSS (mg/L)			434±151	528±15	255±73

*Arithmetic mean shown with standard deviation.*

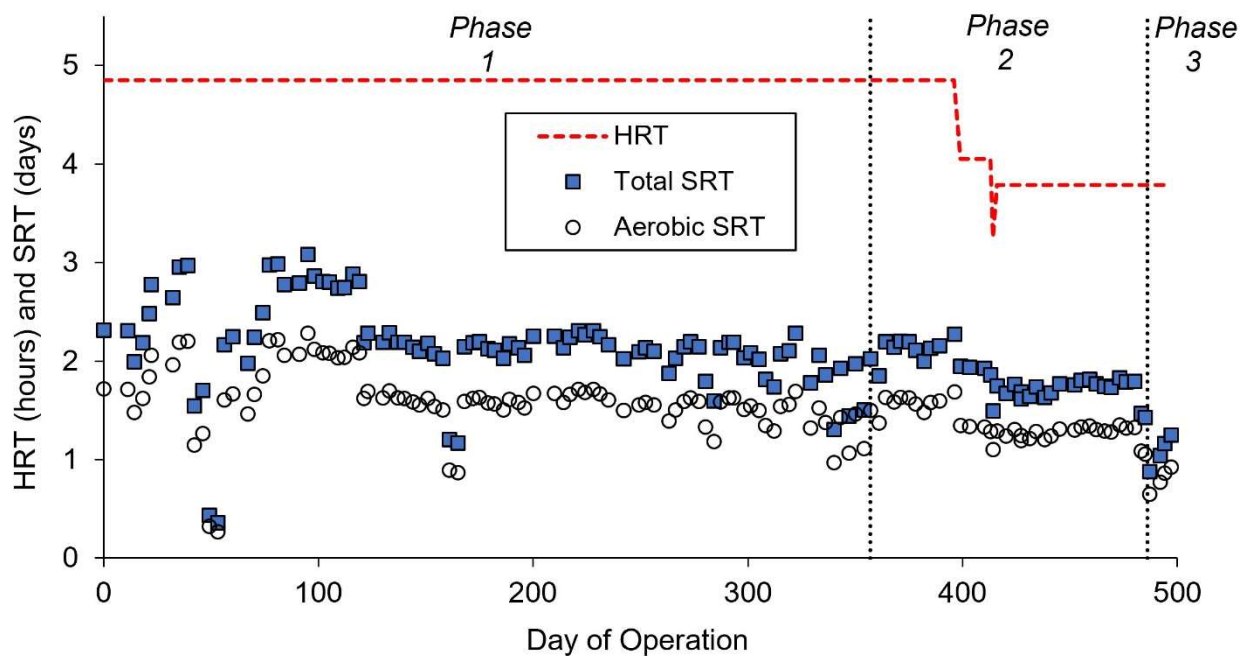


**Figure 3.1** Hydraulic retention time (HRT), total solids retention time (SRT) and aerobic SRT throughout the study.

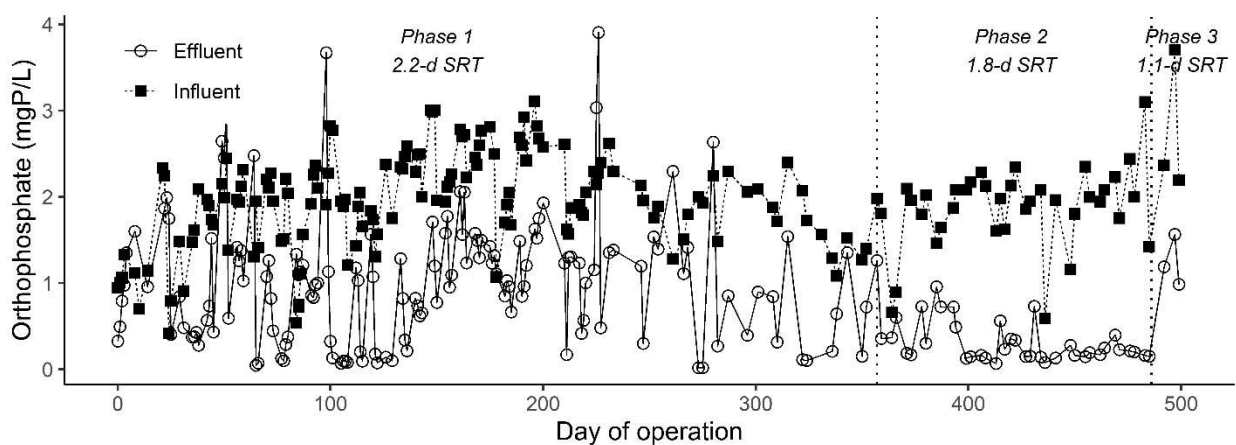


**Figure 3.2** Reactor influent and effluent orthophosphate from daily composite samples throughout the study.

PLC control of reactor equipment was implemented at the beginning of Phase 2 on day 358, which resulted in much more consistent DO control and an improvement in P removal

performance (Figure 3.2 and Figure 3.3 for in-cycle profiles). Average orthophosphate and sCOD removal rates during Phase 2 were  $84 \pm 17\%$  and  $68 \pm 14\%$ , respectively. Surprisingly, despite the low  $SRT_{aer}$  of 1.6 days at the beginning of Phase 2, nitrification was once again observed via  $NO_x$  in the effluent beginning on day 368 (Figure 3.S1). To washout nitrifiers, the  $SRT_{aer}$  was reduced to around 1.3 days on day 399 (Figure 3.1), and by day 415  $NO_x$  was no longer observed in the effluent (Figure 3.S1). The HRT was also reduced to 4 hours (from 4.8 hours) on day 399, and eventually to 3.7 hours by day 414 (Figure 3.1). EBPR performance responded positively to the reductions in HRT and SRT beginning on day 399. The best P removal correlated with these reductions, and average effluent orthophosphate for Phase 2 (days 358 – 485) was  $0.3 \pm 0.2$  mgP/L. The specific total P removal rate for Phase 2 was  $18.3 \pm 7.7$  mgP/gVSS/d, up from  $11.4 \pm 9.5$  mgP/gVSS/d for Phase 1. The average SRT during Phase 2 was  $1.8 \pm 0.2$  days ( $SRT_{aer} = 1.4 \pm 0.2$  days) with a MLVSS of  $529 \pm 155$  mgVSS/L (Figure 3.S2). This low SRT was necessary to wash out nitrifiers, as noted above, and was adequate to maintain stable P removal, as indicated by the low standard deviation ( $\pm 0.2$  mgP/L) in the effluent orthophosphate concentration during Phase 2.

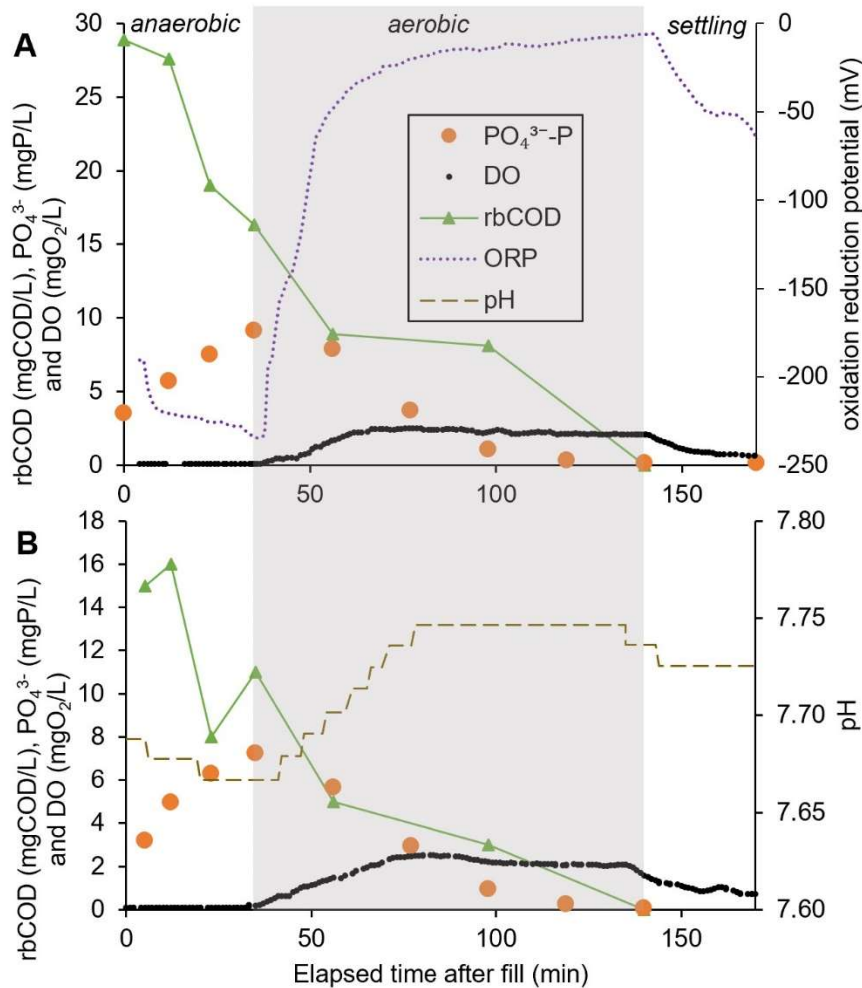


**Figure 3.3** Two representative in-cycle batch tests from Phase 2, A = day 457 and B = day 485.

From day 487 to 499, or Phase 3, the SRT was reduced to  $1.1 \pm 0.2$  days ( $\text{SRT}_{\text{aer}} = 0.80 \pm 0.12$  days, see Figure 3.1). The resulting mixed liquor concentration was  $255 \pm 73$  mgVSS/L, and P removal performance immediately suffered (Figure 3.2). This demonstrated that the Phase 2 SRT of  $1.8 \pm 0.2$  days ( $\text{SRT}_{\text{aer}}$  of  $1.4 \pm 0.2$  days) was nearing the lower limit of *Accumulibacter* PAO retention at 20°C, and that the PAO washout  $\text{SRT}_{\text{aer}}$  lies between 0.8 and 1.4 days.

### 3.3.2 Evidence for P Removal via EBPR

Because P comprises 2 – 3% of non-EBPR activated sludge by dry weight (Rittmann and McCarty, 2001), some P removal can be attributed to typical biomass assimilation alone. An estimate of P removal from assimilation (*Eq. 3*) demonstrates that around 38% of orthophosphate removal during Phase 2 could be attributed to non-EBPR biomass assimilation. In other words, 62% of orthophosphate removal occurred via intracellular polyphosphate accumulation, indicating that EBPR was integral to the P removal performance of this process. Further evidence for EBPR activity included the orthophosphate release to anaerobic rbCOD uptake ratio during Phase 2. Although variable at  $0.43 \pm 0.41$  g P/g COD ( $n = 4$  in-cycle tests without dosing), the average ratio is indicative of the expected ratio from the PAO metabolism of 0.36 g P/g COD (Hesselmann et al., 2000) to 0.56 g P/g COD (Smolders et al., 1994). Also measured during *in situ* tests were P release and uptake rates (Figure 3.S3), which for Phase 2 were  $12.4 \pm 4.1$  mg P/g VSS/hr and  $10.3 \pm 4.8$  mg P/g VSS/hr, respectively. Two representative in-cycle tests without exogenous dosing (i.e. with a typical fill of primary effluent without supplemental carbon) can be seen in Figure 3.3.

### 3.3.3 Accumulibacter vs. GAO Abundance from 16S rRNA Gene Sequencing

Accumulibacter PAOs were highly abundant throughout the study according to 16S rRNA gene sequencing at a  $15 \pm 7\%$  average relative abundance, while putative glycogen accumulating organisms (GAOs) were highly suppressed with a  $0.7 \pm 0.6\%$  relative abundance (Figure 3.4). *Ca. Competibacter* was the most abundant GAO present at  $0.4 \pm 0.4\%$  relative abundance. Other potential GAOs (Stokholm-Bjerregaard et al., 2017) identified at certain time points but at low average abundance ( $<0.3\%$ ) included *Ca. Contendobacter*, *Propionivibrio*,

*Micropruina*, and *Defluviicoccus*. The lack of a significant difference in total *Accumulibacter* abundance between the two phases of reactor operation ( $p$  value = 0.28 on t-test with hypothesis of no difference between means) indicates that the improvement in P removal observed in Phase 2 cannot be explained by better total PAO selection. Rather, the improvement in consistent anaerobic/aerobic conditions and DO control as enabled by PLC implementation and sensor-based aeration control at the beginning of Phase 2 more likely explains the improved performance. Careful control of SRT to facilitate nitrifier washout on day 399, however, did correlate with the best P removal observed in Phase 2 (Figures 3.1 and 3.2).

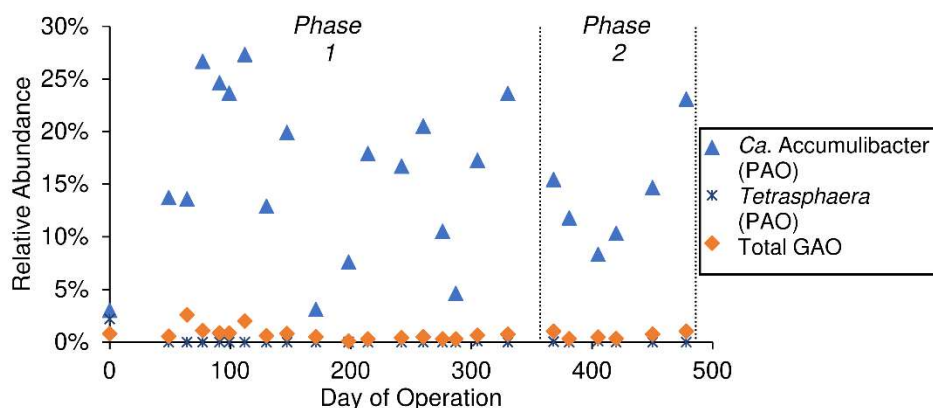


**Figure 3.4** Relative abundance of PAO and GAO taxonomic groups according to 16S rRNA gene amplicon sequencing. *Ca. Competibacter* was the most abundant GAO identified; other GAOs present at some time points and included in “Total GAO” above were *Ca. Contendobacter*, *Micropruina*, *Propionivibrio*, and *Defluviicoccus*. Relative abundance of nitrifiers from 16S rRNA gene sequencing is shown separately in Figure 3.S2.

### 3.3.4 Clade-Specific *Accumulibacter* Abundance via qPCR

In addition to evaluating the feasibility of very low SRT EBPR in an A-stage process, a key objective of this study was to characterize clade-level diversity of PAOs selected at low SRT. Of the 14 known clades (Clades IA-E and IIA-I; Camejo et al., 2016; Mao et al., 2015), 10 were identified as present at some point during operation. The 5 most abundant clades were IA,

IC, IIA, IIB and IID (Figure 3.5), and the other detected clades (IB, ID, IE, IIC and IIF) were at negligible relative abundances (<0.3% in all samples compared to total bacteria). The sum of the clades present relative to total bacteria via qPCR (average throughout the study =  $10 \pm 9\%$ ) confirmed the high abundance of *Accumulibacter* found via 16S rRNA gene sequencing (average throughout the study =  $15 \pm 7\%$ ). We observed higher clade-level *Accumulibacter* diversity during Phase 1 of reactor operation, followed by selection for Clades IIA, IIB and IID at the lowest SRT values during Phase 2 (or in other words, washout of Clades IA and IC, see Figure 3.5). This suggests that clades IIA, IIB and IID may have higher maximum growth rates, although further testing would be required to verify this. An analysis of similarities (ANOSIM) statistical test of *Accumulibacter* clade-level abundance (relative to total *Accumulibacter*, i.e. sum of the clades, based on clade-specific qPCR) indicated a statistically significant difference in *Accumulibacter* population structure between phase 1 and phase 2 of reactor operation ( $R=0.24$ ,  $p=0.03$ ). An accompanying non-metric multidimensional scaling (NMDS) plot, using the same data as the ANOSIM test, visually demonstrates the shift in *Accumulibacter* population structure during reactor operation, as SRT was decreased (Figure 3.6). This study is the first to investigate *Accumulibacter* clade abundance at low SRT values, and suggests that *Accumulibacter* clades IIA, IIB and IID may be better suited for high rate EBPR systems than others.

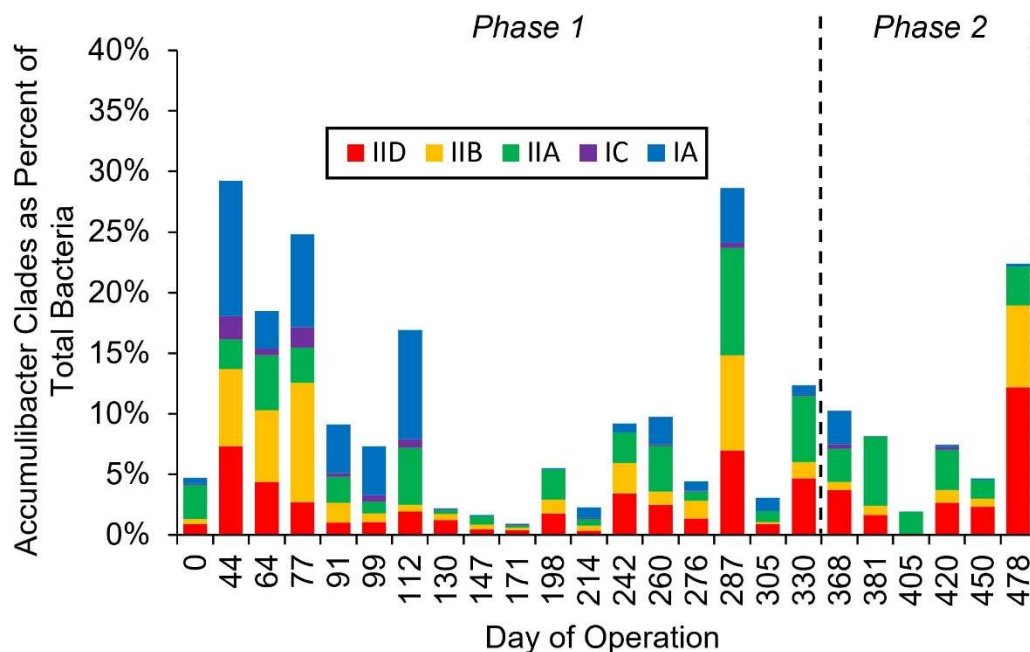


**Figure 3.5** Abundance of *Ca. Accumulibacter* Clades IA, IC, IIA, IIB and IID relative to total bacteria according to qPCR. Clades detected but at negligible abundance (<0.3% at all time points) and not shown in this plot include clades IB, ID, IE, IIC and IIF. Standard deviations for clade-specific data points are shown in Figure 3.S5.

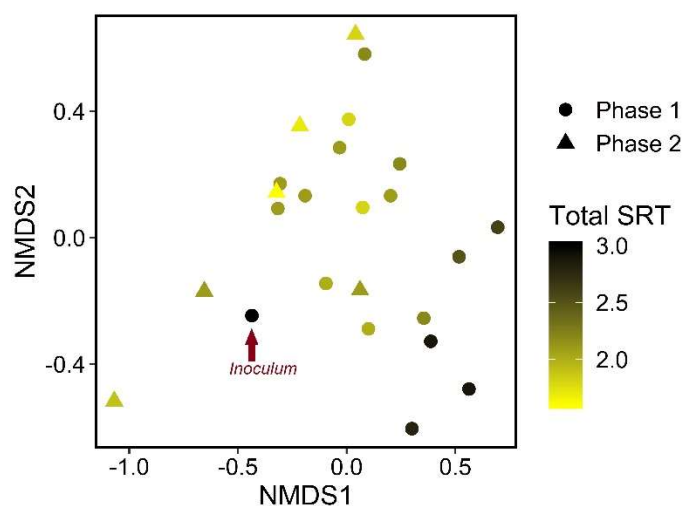


**Figure 3.6** Non-metric multidimensional scaling (NMDS) ordination of *Accumulibacter* clade population structure, calculated from clade-specific qPCR data. The SRT for each sample is the average of 3 measurements (taken over about 1 week) prior to the sample date. The inoculum (day 0) came from an EBPR process with an SRT around 8 days, which is not represented on the SRT scale bar. The significance of the ordination is represented by the stress value of 0.07.

### 3.4 Discussion

#### 3.4.1 Exploring the Limits of High Rate EBPR

Current EBPR process variations generally employ total SRTs of 10 days or longer (although long SRTs are often chosen to retain nitrifiers), and recent work in the literature has demonstrated EBPR at total SRTs down to 2 – 4 days. Here we demonstrate robust and high rate EBPR at the low SRT of  $1.8 \pm 0.2$  days ( $SRT_{\text{aer}} = 1.4 \pm 0.2$  days) with real primary effluent. This provides evidence that the competing goals of low SRT for carbon diversion via HRAS and the carbon requirements of EBPR may be reconcilable, although some compromise in carbon diversion will always occur as compared to a true HRAS process with a  $< 0.5$ -day SRT. To maximize carbon diversion, therefore, knowledge of a washout SRT for PAO, and thus the minimum allowable SRT to maintain the EBPR process, is crucial. The total SRT of  $1.8 \pm 0.2$  days as calculated in this study does not include settling and decant time (*Eq. 1*) in order to better facilitate comparison to plug-flow processes with a separate settling tank. Whether the settling and decant time is included in the SRT calculation of SBRs in other high rate EBPR studies is generally not specified, making direct comparison challenging. At any rate, the aerobic SRT ( $SRT_{\text{aer}}$ ) is independent of the settling and decant time, so  $SRT_{\text{aer}}$  will be utilized in the following discussion of the washout SRT of PAOs.

This study provides evidence that the washout  $SRT_{\text{aer}}$  for *Accumulibacter* PAOs is between 0.8 and 1.4 days at 20 °C (Table 3.2). Ge et al. (2015) found a PAO washout  $SRT_{\text{aer}}$  between 1 and 1.2 days at 20 – 22 °C with 28.2 mg TP/L and 1,000 mg sCOD/L in the influent. Under such high COD concentrations, which differ significantly from typical primary effluent or raw municipal wastewater, they selected for the previously unknown PAO *Comamonadaceae*.

Chan et al. (2017) found a higher *Accumulibacter* PAO washout  $SRT_{\text{aer}}$  between 1.75 and 2.1 days at 25 °C given synthetic wastewater concentrations of 20 mg TP/L and 226 mg sCOD/L (all sCOD as propionic acid). Valverde-Pérez et al. (2016) demonstrated effective EBPR via *Accumulibacter* at  $SRT_{\text{aer}} = 1.5$  days at 16 – 19 °C given substrate conditions of 8 mg TP/L and > 200 sCOD/L (200 mg COD/L of supplemental propionic acid was dosed to the influent to avoid carbon limitation), but did not investigate the PAO washout SRT. Yang et al. (2017) achieved stable EBPR at a 1.5 – 2.3-day  $SRT_{\text{aer}}$  at 16 – 24 °C with real primary effluent (160 mg sCOD/L and 5.9 mg TP/L), although they also did not investigate the PAO washout SRT. Historical studies that investigated the washout  $SRT_{\text{aer}}$  of PAOs but preceded the classification of *Accumulibacter* (Hesselmann et al., 1999) include Mamais and Jenkins (1992), who found a washout  $SRT_{\text{aer}} = 1.5$  days at 20 °C via primary effluent (8.5 mg TP/L and 230 mg sCOD/L, though 50 mg/L of that was supplemental acetate). McClintock et al. (1993) observed a reduction in P removal at  $SRT_{\text{aer}} = 0.9 – 1.5$  days at 20 °C with primary effluent (255 mg tCOD/L, 19 mg TP/L, some phosphate supplemented), and Shao et al. (1992) found a washout  $SRT_{\text{aer}} = 1.4$  days at 23 °C via primary effluent (144 mg BOD<sub>5</sub>/L, 6.3 mg TP/L). The present study is the first to combine the washout SRT of PAOs fed real municipal wastewater with an investigation into the clade-level diversity of *Accumulibacter* selected under low SRT conditions.

**Table 3.2** Comparison table for key studies of low sludge age EBPR processes.

Feed	Scale/ reactor type	Optimal total SRT (d)	Optimal aerobic SRT (d)	Washout aerobic SRT (d)	Primary PAO	Temperature (°C)	Reference
Primary effluent	Bench/SBR	1.8±0.2	1.4±0.2	0.8-1.4	<i>Accumulibacter</i>	19.7 ± 1.2	<i>present study</i>
Primary effluent	Bench/SBR	2-3	1.5-2.3	NA	NA	16 - 24	Yang et al. 2017
Primary effluent	Full/ Plug flow	3	2.8	1.4	NA	23	Shao et al. 1992
Abattoir wastewater	Bench/SBR	2-2.5	1.2-1.5	1-1.2	<i>Comamonadaceae</i>	20 - 22	Ge et al. 2015
Primary effluent + suppl. propionate and phosphate	Bench/SBR	3	1.5	NA	<i>Accumulibacter</i>	16 - 19	Valverde-Perez et al. 2016
Primary effluent + suppl. phosphate	Pilot/ Continuous	2.7	1.5	0.9-1.5	NA	20	McClintock et al. 1993
Primary effluent + suppl. acetate	Bench/ Continuous	2.3-2.6	1.7-2	1.5	NA	20	Mamais & Jenkins 1992
Synthetic wastewater	Bench/SBR	3.6	2.1	1.8-2.1	<i>Accumulibacter</i>	25	Chan et al. 2017

NA = Not Available

Brdjanovic et al. (1998) noted that determining the minimum SRT for PAOs in a given EBPR system is not trivial, and is dependent upon (among other things) the biomass specific VFA to PHA conversion rate (not necessarily limited to acetate as a substrate), the biomass specific yield, and the PHA storage capacity of the biomass. Brdjanovic's model predicted a minimum  $SRT_{\text{aer}}$  for PAOs of 1.0 – 1.6 days, depending on the PHA storage capacity of the biomass, at 20°C. This matches well both with the observed optimal  $SRT_{\text{aer}}$  of  $1.4 \pm 0.2$  days during Phase 2 of the present study, and the observed washout  $SRT_{\text{aer}}$  of  $0.80 \pm 0.12$  days during Phase 3. However, it should be noted Brdjanovic's study used acetate as the sole carbon source. In complex matrices such as mainstream wastewater rbCOD fermentation may become the rate

limiting step in the anaerobic zone. This further complicates efforts to quantify a minimum SRT for PAOs, as influent composition and process characteristics can greatly influence their apparent growth rate. Regardless, the importance of tight aeration control, as observed in the present study with the improvement of P removal upon implementation of PID aeration control, affirms Brdjanovic's observation that retention of PAOs is better determined by a sufficient aerobic time to completely oxidize intracellular PHA than by the more typically used specific growth rate. Conversely, analysis by Barnard et al. (2017) concluded that EBPR failure was often associated with inadequate anaerobic zone design, indicating that proper design of both zones is critical for successful EBPR performance; this may become challenging in full scale systems when HRT and SRT are pushed to the limits.

### **3.4.2 PAO Abundance and GAO Suppression in High Rate EBPR**

Given the relatively poor EBPR performance during Phase 1 of this study (44% average orthophosphate removal), the  $16 \pm 8\%$  average relative abundance of *Accumulibacter* PAOs is surprising. It is possible that this could be explained by the metabolic diversity of *Accumulibacter*, which have been observed to exhibit a GAO-like metabolism under certain conditions (Acevedo et al., 2012; Barat et al., 2006; Erdal et al., 2008; Welles et al., 2014; Zhou et al., 2008). The observed orthophosphate release to anaerobic rbCOD uptake ratio during Phase 1 was  $0.24 \pm 0.22$  g P/g COD (n = 11 in-cycle batch tests without dosing), lower than the expected PAO ratio of 0.36 g P/g COD (Hesselmann et al., 2000) to 0.56 g P/g COD (Smolders et al., 1994). While a GAO-like metabolism of *Accumulibacter* is one potential explanation for these observations, alternate mechanisms include unidentified PHA accumulators and/or noncanonical GAOs.

Low SRT operation in this study may have contributed to the suppression of GAOs, as GAOs are thought to compete more effectively at higher SRTs due to their observed lower growth rates than PAOs (Wang et al., 2001). Also, the low influent rbCOD:TP ratio in this study (16 gCOD:gP) is just above the lower limit of 15 gCOD:gP that has been suggested as necessary for EBPR in systems with minimal fermentation (Barnard et al., 2017). This may contribute to GAO suppression, as higher influent organic carbon levels have been shown to be associated with *Ca. Competibacter* abundance (López-Vázquez et al., 2008), likely due to the availability of rbCOD in the anaerobic zone beyond that required for PHA production via polyphosphate release.

### **3.4.3 Accumulibacter Diversity in High Rate EBPR**

The fact that this study selected for Accumulibacter PAOs as did the reactors run by Chan et al. (2017) and Valverde-Pérez et al. (2016), which used synthetic wastewater to mimic primary effluent and primary effluent with supplemental propionate and phosphate, respectively, suggests that Accumulibacter have a competitive advantage over other PAOs under mainstream conditions at low SRT. All high rate EBPR studies that looked for *Tetrasphaera*, including the present study, have found near-negligible levels (Chan et al., 2017; Ge et al., 2015; Valverde-Pérez et al., 2016); *Tetrasphaera* has been occasionally identified as the dominant PAO in full scale (not high-rate) EBPR systems (Nguyen et al., 2011).

This study further suggests that Accumulibacter Type II, particularly Clades IIA, IIB and IID, are particularly well suited to low SRT operation. Selection against Clade IA was observed at the lowest SRT values. Although no other studies have investigated Accumulibacter clade abundance at low SRT values, other investigations of Accumulibacter clades in wastewater

treatment systems have also observed high diversity (Camejo et al., 2016; Mao et al., 2015). Mao et al. (2015) reported that clades IIC and IID were the most abundant in a survey of 18 wastewater plants, though other studies have demonstrated the dominance of clades IA (Gao et al., 2019), IB (Mao et al., 2014), and IC (Camejo et al., 2016).

#### **3.4.4 Nitrification in low SRT EBPR Systems**

As mentioned in the introduction, washout of nitrifiers at low SRT operation can facilitate a nitrogen-rich and carbon-poor effluent that is ideal for a B-stage autotrophic PN/A process. An additional advantage of preventing nitrification, however, is to limit the production of  $\text{NO}_x$ . With lower  $\text{NO}_x$  in the return sludge, less rbCOD will be consumed by denitrifiers in the anaerobic zone, making more rbCOD available for PHA production by PAOs. Of the eight low SRT studies summarized in Table 3.2 including the present one, five of the eight were able to prevent nitrification with average  $\text{SRT}_{\text{aer}}$  values from 1.3 – 1.9 days with average temperatures 17.5 – 21 °C (Ge et al., 2015; Mamais and Jenkins, 1992; Valverde-Pérez et al., 2016; Yang et al., 2017). Chan et al. (2017) was unable to report on nitrifier washout due to the use of allylthiourea (ATU) to prevent nitrification, and that study utilized the highest  $\text{SRT}_{\text{aer}}$  (2.1 days) and the highest temperature (25 °C). McClintock et al. (1993) observed some nitrification even at the lowest  $\text{SRT}_{\text{aer}}$  tested at 1.5 days at 20 °C. A small amount of nitrification was observed at an  $\text{SRT}_{\text{aer}}$  as low as 1.6 days at 20 °C in the present study.

### **3.5 Conclusions**

- Stable P removal via EPBR from real wastewater (primary effluent) was achieved without chemical dosing at low SRT ( $1.8 \pm 0.2$  days) operation. The washout aerobic SRT for PAOs was shown to lie between 0.8 and 1.4 days at 20 °C.

- Accumulibacter PAOs were highly abundant and Clades IIA, IIB and IID were dominant at the lowest SRT values. GAOs were robustly suppressed with an average relative abundance of < 1.0%.
- Successful EBPR performance depended upon tight aeration and DO control via sensor based PID operation.
- A narrow SRT control window was needed to maintain EBPR and prevent nitrification; NO<sub>x</sub> production was observed at an SRT<sub>aer</sub> as low as 1.6 days.
- The low SRT EBPR process is a promising efficient technology with a small footprint for the diversion of carbon and P to the side-stream, and effluent can be routed downstream to a PN/A process for nitrogen removal.

### 3.6 Supporting Information

#### 3.6.1 Sludge Volume Index

Despite the low mixed liquor solids concentrations observed throughout the project (average MLVSS during Phase 2 =  $529 \pm 155$  mg/L), settling performance was usually good (except for a ~2-day aeration failure during Phase 1, during which effluent solids were elevated). Sludge volume index (SVI) tests performed on days 464, 478, and 483 revealed good settling behavior of the sludge with an average SVI<sub>30</sub> =  $83 \pm 22$  mL/g (n = 3).

### 3.6.2 Supplementary Figures

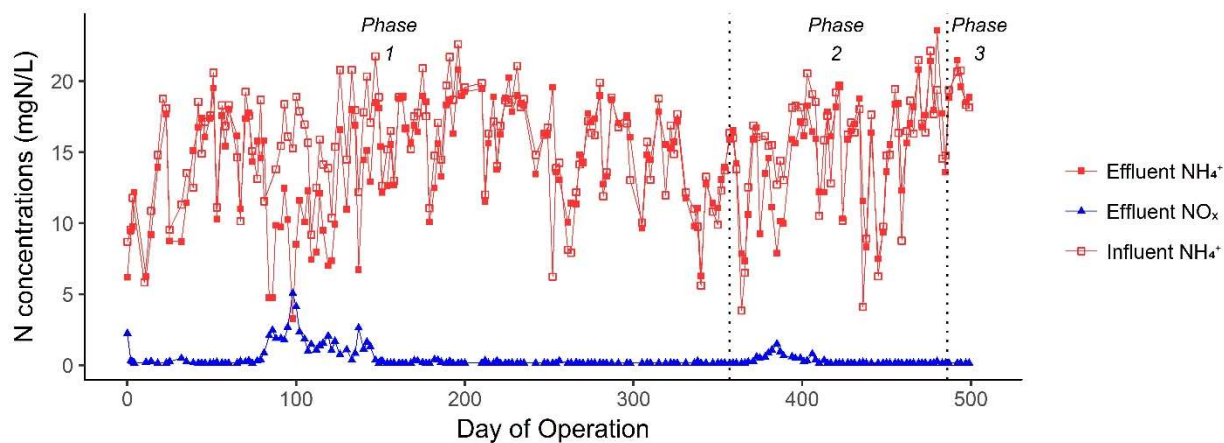


**Figure 3.S1** Influent ammonium ( $\text{NH}_4^+$ ) and effluent ammonium and nitrite + nitrate ( $\text{NO}_x$ ).

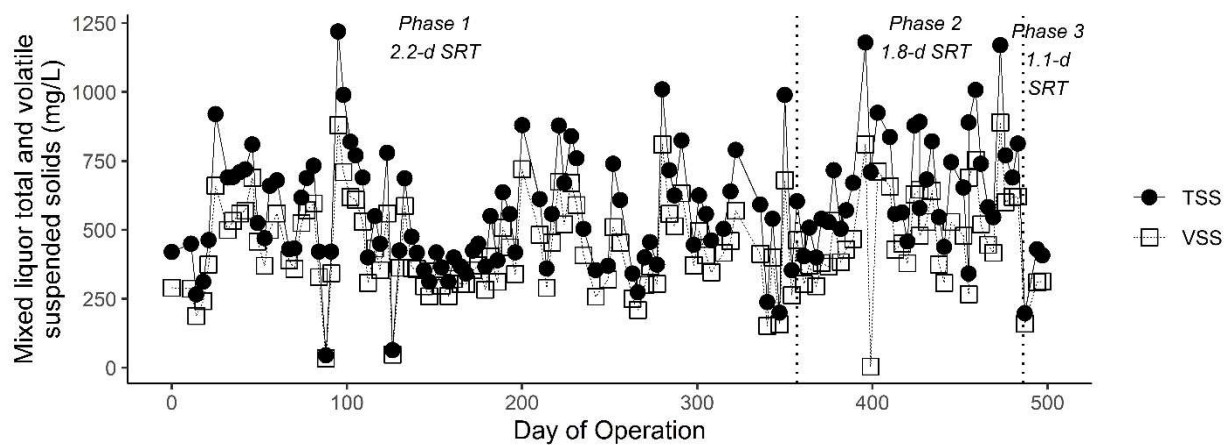


**Figure 3.S2** Reactor mixed liquor total suspended solids (TSS) and volatile suspended solids (VSS).

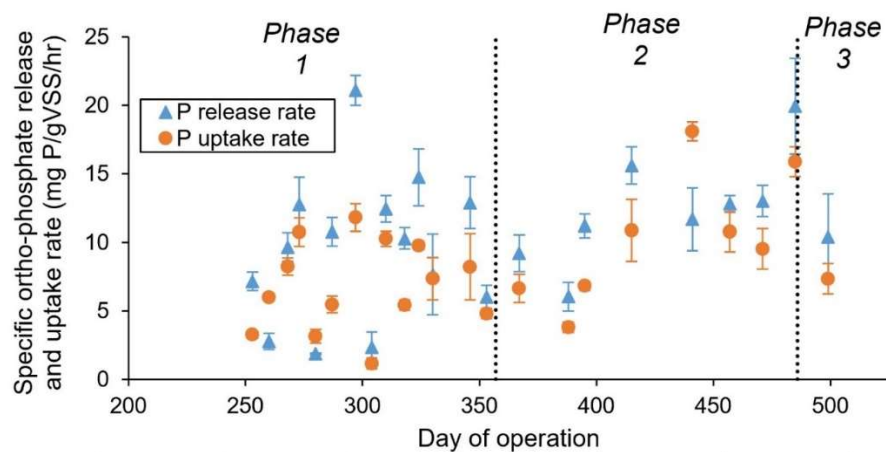


**Figure 3.S3** Orthophosphate (P) release and uptake rates from *in situ* batch activity assays. Error bars represent the standard error of the fitted linear slope.

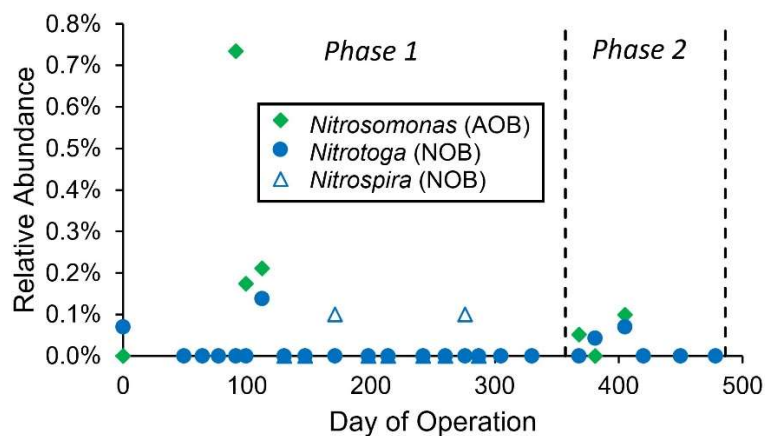


**Figure 3.S4** Relative abundance of nitrifiers detected from 16S rRNA gene sequencing. The presence of nitrifiers was generally associated with the presence of  $\text{NO}_x$  in the effluent (see Figure 3.S1).

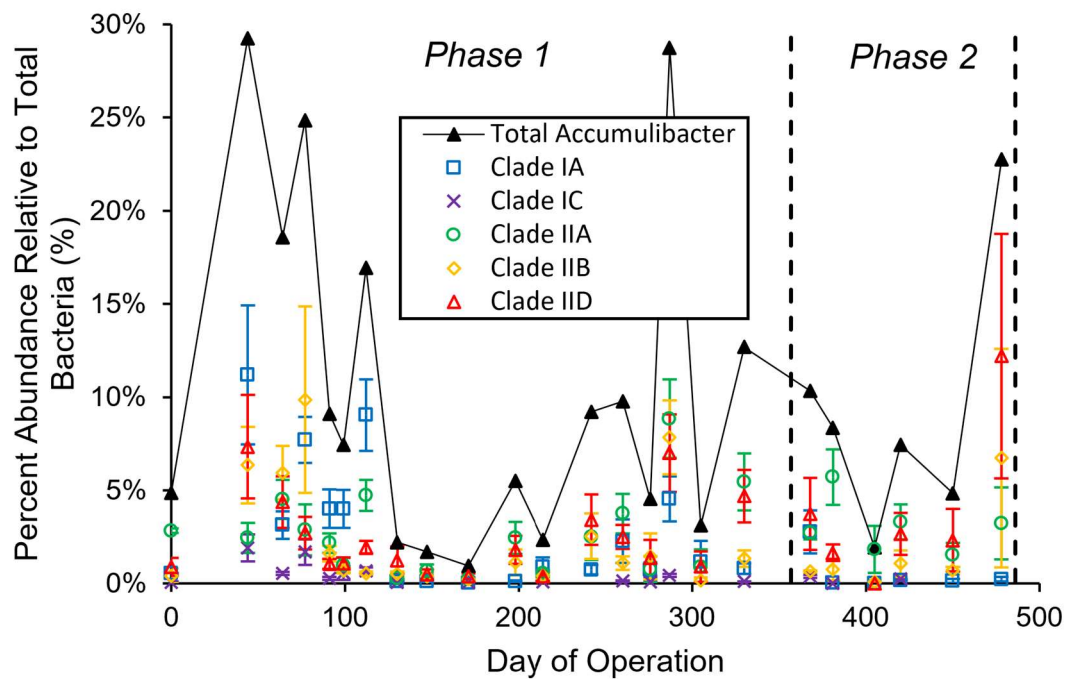
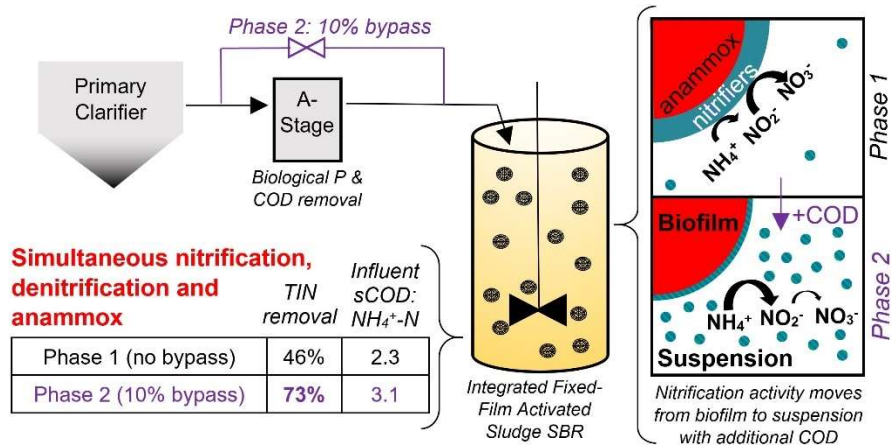


**Figure 3.S5** Abundance of Accumulibacter clades relative to total bacteria according to qPCR. Clades detected but at negligible abundance (<0.3% at all time points) and not shown in this plot include clades IB, ID, IE, IIC and IIF. “Total Accumulibacter” represents the sum of the individual clades.

## CHAPTER 4: PRACTICAL OPTIMIZATION OF THE CARBON TO NITROGEN RATIO FOR MAINSTREAM DEAMMONIFICATION AND ITS IMPACT ON AGGREGATE STRUCTURE<sup>1</sup>



### Abstract

Application of the deammonification process to mainstream wastewater promises energy-efficient nitrogen removal, but has been limited by unwanted activity of nitrite oxidizing bacteria and reduced anammox activity at low temperatures. Research suggests that optimizing the ratio of organic carbon to nitrogen (C:N) in the influent is critical, but most studies to date have used exogenous VFA to adjust C:N. In the present study, N removal in a mainstream integrated fixed-film activated sludge (IFAS) deammonification process increased by 27% to 73% TIN removal by diverting 10% of the primary effluent flow around the A-stage and directly into the deammonification reactor, thus increasing the influent C:N ratio from 2.3 to 3.1 g sCOD/g NH<sub>4</sub><sup>+</sup>-N. This change coincided with a dramatic shift in nitrification activity from the biofilm to the suspension, and the increased carbon enabled a higher suspended solids concentration at a realistic solids retention time of  $7.3 \pm 2.1$  days. Anammox biomass and activity was robustly retained over the entire study (>3 years) and was not negatively impacted by the increase in influent carbon. N isotope testing indicated that cross feeding between denitrifiers and anammox

<sup>1</sup>This chapter is from a manuscript under review: Roots, P., Rosenthal, A.F., Yuan, Q., Wang, Y., Yang, F., Kozak, J.A., Zhang, H., Wells, G.F., 2020. Practical optimization of the carbon to nitrogen ratio for mainstream deammonification and its impact on aggregate structure.

played an important role in N removal and that about 53% of N removal was ultimately routed through the anammox metabolism. Our work demonstrates the impact of small changes in C:N on performance, population structure, and aggregate architecture in mainstream deammonification bioprocesses, and provides a simple approach to control C:N in practice.

#### 4.1 Introduction

Deammonification is a carbon and energy-efficient method for nitrogen (N) removal that combines the activity of aerobic ammonia oxidizing bacteria (AOB) and anaerobic ammonia oxidizing bacteria (anammox) to produce dinitrogen gas (N<sub>2</sub>). Full-scale applications of the deammonification process to sidestream flows in wastewater treatment plants (with process temperatures around 30 °C and influent ammonium (NH<sub>4</sub><sup>+</sup>) > 300 mgN/L) have grown in recent years (Lackner et al., 2014). Application of deammonification to mainstream wastewater that harbors the vast majority of reactive nitrogen in typical municipal wastewater treatment plants is limited, but research efforts have continued (De Clippeleir et al., 2013; Kouba et al., 2016; Lackner et al., 2015; Laurenzi et al., 2016; Lotti et al., 2015b; Malovanyy et al., 2015; Wett et al., 2013) due its potential to transform wastewater treatment from an energy intensive to an energy exporting endeavor. Key challenges that have hindered implementation of deammonification under mainstream conditions include high nitrite oxidizing bacteria (NOB) activity (and thus low total N removal) and low anammox activity at low temperatures (Cao et al., 2017; Xiaojin Li et al., 2018).

Biofilm systems have gained attention under mainstream conditions for their ability to retain anammox biomass and activity (Gilbert et al., 2015; Gustavsson et al., 2020; Lackner et al.,

2015), but their impact on NOB activity is less clear. Sufficient concentrations of suspended solids in biofilm systems can may shift NOB off the biofilms and into the bulk (Hubaux et al., 2015) where they can be selectively washed out via solids retention time (SRT) control, as in Laureni et al. (2019). However, with the low COD loading in that study, accumulation of sufficient suspended solids to induce the shift of NOB from the biofilm required an SRT of >150 days, which is unrealistic for practice.

For this reason and others, suppression of NOB has remained a vexing and persistent challenge in mainstream deammonification studies, leading some researchers to abandon efforts to completely suppress NOB activity and focus on systems for combined nitrification, anammox and denitrification (Le et al., 2019a, 2019b; B. Ma et al., 2017b; Zheng et al., 2016). The impact of organic carbon on competition between functional groups in mainstream processes is critical, given that certain methods for NOB out-selection are only available under sidestream conditions, such as high temperatures (Hellings et al., 1998) and elevated free ammonia (Anthonisen et al., 1976; Jubany et al., 2009; Pambrun et al., 2006). A minimal COD:N ratio has long been assumed to be advantageous in deammonification, as this should favor autotrophs like anammox and AOB over ordinary heterotrophs and denitrifiers (Joss et al., 2009; Ma et al., 2011). However, under sidestream conditions, moderate levels of organic carbon can improve N removal, while excess carbon can lead to anammox suppression via out-competition by denitrifiers and process failure (Chamchoi et al., 2008; Chen et al., 2016, 2009; Ni et al., 2012; Tang et al., 2010, 2013; Zekker et al., 2014; Zhou et al., 2018). Though not required by key functional groups, organic carbon may improve mainstream deammonification by increasing residual N removal via denitrification (Malovanyy et al., 2015), improving cross-feeding to anammox via denitrification (B. Ma et al.,

2017b), and increasing competition for dissolved oxygen (DO), thus reducing nitrate ( $\text{NO}_3^-$ ) production and increasing N removal. However, the influence of influent COD:N on aggregate architecture, population segregation and activity of nitrifiers and anammox in mainstream deammonification systems is poorly understood. Furthermore, a practical means to adjust COD:N has not been demonstrated under real-world conditions.

The objective of this paper is to demonstrate a novel and cost-effective solution for tuning the relative organic carbon content of deammonification systems with upstream A-stage carbon removal, and to demonstrate its influence on aggregate type (biofilms versus flocs), microbial activity, and population structure. N removal in a mainstream IFAS deammonification process operated for >1,000 days improved by diverting 10% of the primary effluent flow around the A-stage and directly into the deammonification reactor. Importantly, this change marked a dramatic shift in nitrification activity from the biofilm to the suspension at a realistic SRT of  $7.3 \pm 2.1$  days, a shift that was not observed during previous IFAS mode without 10% primary effluent in the influent. Anammox biomass and activity was robustly and selectively retained on the biofilm over the entire study (>3 years) and was not negatively impacted by the increase in influent COD. N isotope testing was performed to measure the relative contributions of denitrification and anammox to N removal.

## **4.2 Materials and Methods**

### **4.2.1 Reactor Operation**

A 12-L sequencing batch reactor (SBR, but hereafter referred to as “reactor”) for mainstream deammonification treatment was operated at the Metropolitan Water Reclamation District of Greater Chicago (MWRDGC) O’Brien Water Reclamation Plant (WRP) in Skokie,

Illinois for 1,128 days. The reactor was seeded to a fill ratio of 30% on May 24, 2016 (“day 0” of operation) with anammox-enriched K5 carriers from the Kruger/Veolia Biofarm at James River, VA (equivalent to ~3400mg VSS/L) and ~340 mg VSS/L suspended growth biomass from the full-scale sidestream DEMON® process at the York River treatment plant (Hampton Roads Sanitation District) (equivalent to 10% of the estimated VSS on K5 carriers). Upstream treatment included primary settling tanks and a 56-L activated sludge SBR (“A-stage”) for biological COD and phosphorus removal. From days 0 – 899, 100% of the reactor influent was A-stage effluent, and from day 900 to the end of the study (day 1,128) 90% of reactor influent was A-stage effluent and 10% was untreated primary effluent. Because of the notable change in reactor performance after bypassing 10% of the influent around the A-stage, data reporting in this study is split into Phase 1 (days 0 – 899) and Phase 2 (days 900 – 1,128).

Aside from reactor inoculation on day 0, only 2 bioaugmentation events occurred throughout the study. First, on day 849 additional anammox-enriched K5 carriers were supplemented from the MWRDGC Egan WRP ANITA™ Mox process (Schaumburg, IL, USA) to a final volumetric fill ratio of 38% (up from the original 30%) to increase the anammox population. Second, on day 900, 3 liters of mixed liquor from a 56-L nitrification-denitrification with biological phosphorus removal SBR (Roots et al., 2019a) was added to increase the suspended biomass concentration (by 310 mg VSS/L).

From days 0 to 335 SBR control was managed with ChronTrol programmable timers (4-circuit, 8-input XT Table Top unit, ChronTrol, San Diego, CA, USA), and from days 336 to the end of the study with code-based programmable logic control (PLC) (Ignition SCADA software by Inductive Automation, Fulsom, CA, USA, and TwinCAT PLC software by Beckhoff, Verl,

Germany). Online sensors included the ammonium::lyser™ eco + pH ion-selective electrode for ammonium and pH and the oxii::lyser™ optical probe for dissolved oxygen (DO) (Scan, Vienna, Austria). The reactor was operated in IFAS mode aside from days 132 – 314, when mixed liquor wasting was performed for operation in MBBR mode. Temperature was controlled to about 20 °C from days 0 to 951, gradually reduced to 8 °C from days 952 to 1,076 to stress test performance after achieving optimized N removal in Phase 2, and immediately increased back to around 20 °C from days 1,077 to the end of the study, day 1,128.

SBR control from day 0 to 357 consisted of the following fixed cycle lengths resulting in a fixed 9-hour hydraulic retention time (HRT) not including settling or decant:

- 6-L (50% volume) reactor fill (~2 min)
- Intermittently aerated react period (270 min)
  - (peak DO 0.2 – 2 mg O<sub>2</sub>/L, aeration intervals 8 – 60 min long)
- Settling (40 min)
- 6-L decant (5 min)

On day 358 ammonia-based control was implemented, wherein the aerated portion of the cycle was terminated when the target effluent ammonium concentration of 2 mg NH<sub>4</sub><sup>+</sup>-N/L was reached. SBR control from day 358 to the end of the study, day 1,128, consisted of the following cycle times resulting in a variable 6.2 ± 2.5-hour HRT not including settling or decant:

- 6-L (50% volume) reactor fill (~2 min)
- Anoxic react period (no aeration, 20 min)
- Aerated react period (variable length: 30 – 500 min)
  - Days 358 – 413: Intermittent aeration (peak DO 1 – 2 mg O<sub>2</sub>/L, aeration intervals 8 – 60 min long)
  - Days 414 – 1,128: Low constant aeration (0.05 – 0.2 mg O<sub>2</sub>/L)
- Anoxic react period (no aeration, 20 – 30 min)
- Settling (30 – 50 min)
- 6-L decant (4 – 5 min)

#### 4.2.2 Reactor Sampling, SRT Control, and Batch Activity Assays

Composite influent and effluent samples were collected 3 to 5 times per week and evaluated for total and soluble chemical oxygen demand (COD), total phosphorus, orthophosphate, total and volatile suspended solids (TSS - VSS), alkalinity, total Kjeldahl nitrogen (TKN), ammonium ( $\text{NH}_4^+$ -N), combined nitrate + nitrite ( $\text{NO}_3^- + \text{NO}_2^- = \text{NO}_x^-$ -N), and  $\text{NO}_2^-$ -N (one time per week) per Standard Methods (APHA, 2005). Carrier biomass was scraped off of whole K5 carriers in duplicate once per month and analyzed for total and volatile dry solids per Standard Methods (APHA, 2005).

The SRT of suspended biomass in the reactor was calculated by accounting for solids losses through both mixed liquor wasting (which occurred only from days 132 – 314, during which the reactor was effectively a MBBR) and in the effluent. The presence of floating biocarriers often prevented effective settling of suspended biomass, so settled solids were occasionally returned from the effluent (composite sampling) tank to the reactor when high suspended SRT values were targeted. In these cases, effluent VSS concentrations were measured from the overflow of the composite sampling tank for use in SRT calculations.

Batch kinetic assays were performed to determine maximum activities of anammox, AOB, and NOB functional groups under non-limiting substrate conditions as previously described (Laureni et al., 2016; Roots et al., 2019b), and maximum activity of AOB and NOB was measured separately for suspended and carrier biomass. See Supporting Information for details.

### 4.2.3 Nitrogen Isotope Testing

Nitrogen stable isotope testing was performed on days 1,100, 1,112 and 1,128 to estimate the relative contributions of anammox and denitrification to N removal following Wang et al. (2015). Isotopes of  $^{15}\text{NH}_4^+$ ,  $^{15}\text{NO}_3^-$  and  $^{15}\text{NO}_2^-$  were spiked separately under initially anaerobic conditions (i.e. with no  $\text{O}_2$ ,  $^{14}\text{NO}_3^-$ , or  $^{14}\text{NO}_2^-$  present), with  $^{14}\text{NH}_4^+$  already present in solution, to quantify the percent contribution of anammox and denitrification by measuring the relative amounts of  $^{29}\text{N}_2$  and  $^{30}\text{N}_2$  produced, respectively. Further details can be found in the Supporting Information.

### 4.2.4 Biomass Sampling, DNA Extraction, qPCR and 16S rRNA Gene Sequencing

Suspended (floccular) and carrier (biofilm) biomass was sampled once or twice per month for 16S rRNA gene sequencing analyses. Suspended biomass was washed with Tris-EDTA buffer before archiving at  $-80\text{ }^\circ\text{C}$ , and whole K5 biocarriers were sampled and archived directly at  $-80\text{ }^\circ\text{C}$ . DNA extraction was performed in duplicate with the FastDNA SPIN kit for soil (MPBio, Santa Ana, CA, USA) per the manufacturer's instructions, and DNA concentration of the extracts was measured via 260 nm wavelength light absorption on an Eppendorf BioSpectrometer® fluorescence (Hauppauge, NY, USA).

Quantitative polymerase chain reaction (qPCR) was used to quantify anammox in carrier biomass via the hydrazine synthase (*hzsA*) gene. The 1597f/1829r primer set was used with reaction conditions described in Harhangi et al. (2012). *HzsA* gene copy numbers were normalized to ng DNA of the extracts.

For 16S rRNA gene sequencing, the V4–V5 region of the universal 16S rRNA gene was amplified on biological replicates for each sample via the 515F-Y/926R primer set (Parada et al., 2016) as previously described (Griffin and Wells, 2017). Raw sequence reads were deposited in GenBank with accession number PRJNA599569. Further details on biomass sampling, qPCR, and 16S rRNA gene sequencing can be found in the Supporting Information.

## 4.3 Results and Discussion

### 4.3.1 Phase 1 Reactor Performance

In the first 78 days of reactor operation, after biomass inoculation from a sidestream deammonification process on day 0, good performance of 69% TIN removal was observed (Figure 4.1). After day 78, effluent  $\text{NO}_3^-$  concentrations increased and TIN removal reduced to an average TIN removal of 46% over Phase 1. This reduction in N removal performance after day 78 coincided with an increase in the relative abundance of *Nitrospira* NOB (Figure 4.2 A&B) on both the carriers and in the suspended biomass according to 16S rRNA gene sequencing. Various efforts at NOB remediation during Phase 1 (outlined below) proved unsuccessful, and TIN removal did not improve until part of the influent was routed around the A-stage carbon removal reactor at the beginning of Phase 2 (day 900).

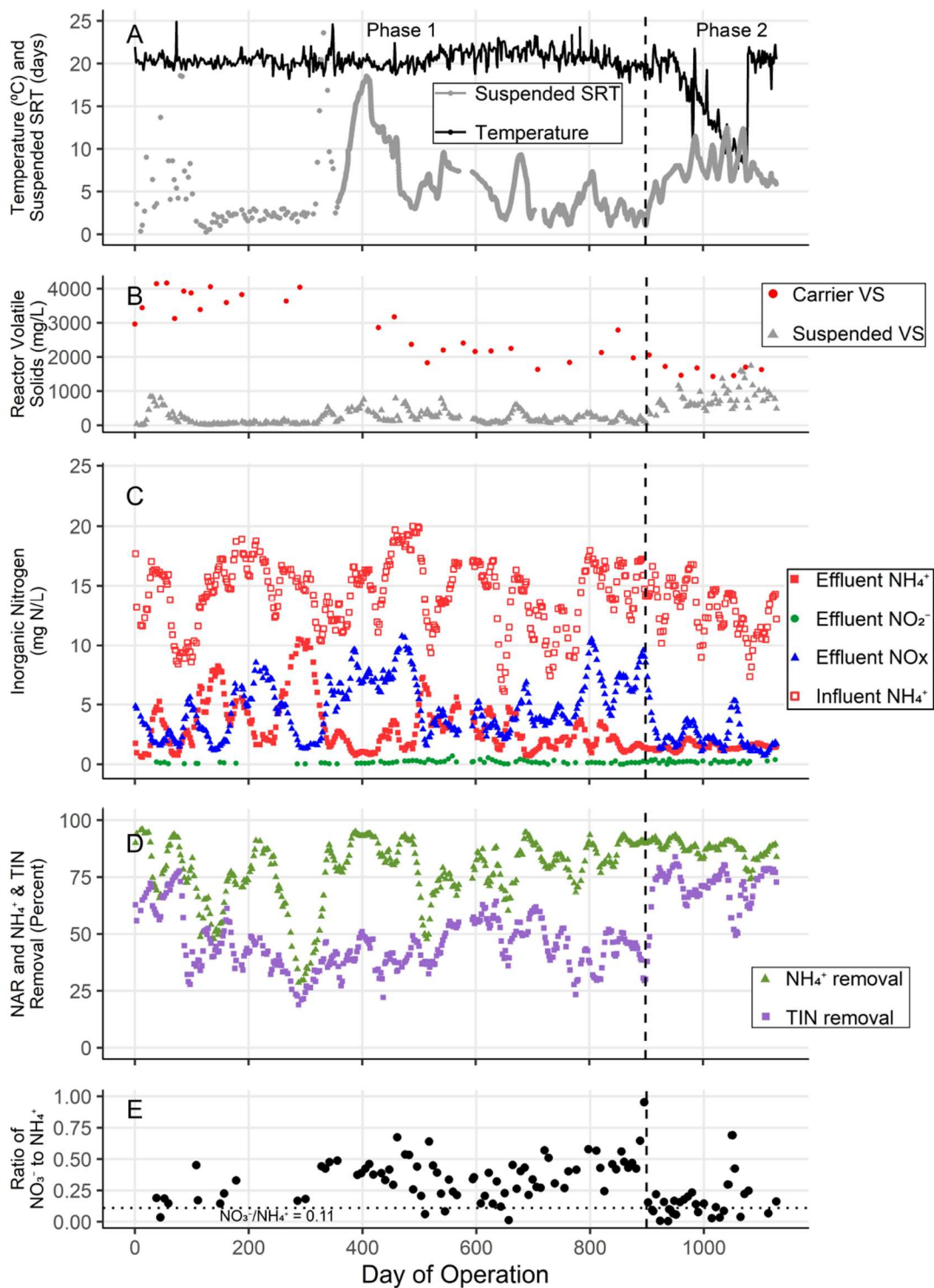


**Figure 4.1** Reactor temperature and performance over 1,128 days of reactor operation. A: Average daily reactor temperature and suspended SRT. The higher frequency of SRT data points

beginning on day 358 is due to implementation of variable react length based on the online ammonia sensor, at which point the SRT value was calculated on a per-cycle basis. **B**: Reactor volatile solids (VS) on the carriers and in the suspension. **C**: Influent  $\text{NH}_4^+$  and effluent  $\text{NH}_4^+$ ,  $\text{NO}_x$  ( $\text{NO}_2^- + \text{NO}_3^-$ ) (all shown as  $\sim 2$ -week rolling average) and  $\text{NO}_2^-$  (shown as discrete measurements) concentrations as measured from composite sampling. **D**:  $\text{NH}_4^+$  and total inorganic nitrogen (TIN) removal (both shown as  $\sim 2$ -week rolling averages) calculated from composite sampling measurements. **E**: Ratio of  $\text{NO}_3^-$  produced to  $\text{NH}_4^+$  removed as calculated from composite sampling measurements. The ratio of 0.11, shown in the graph, represents the theoretical combined stoichiometry of nitrification-anammox.

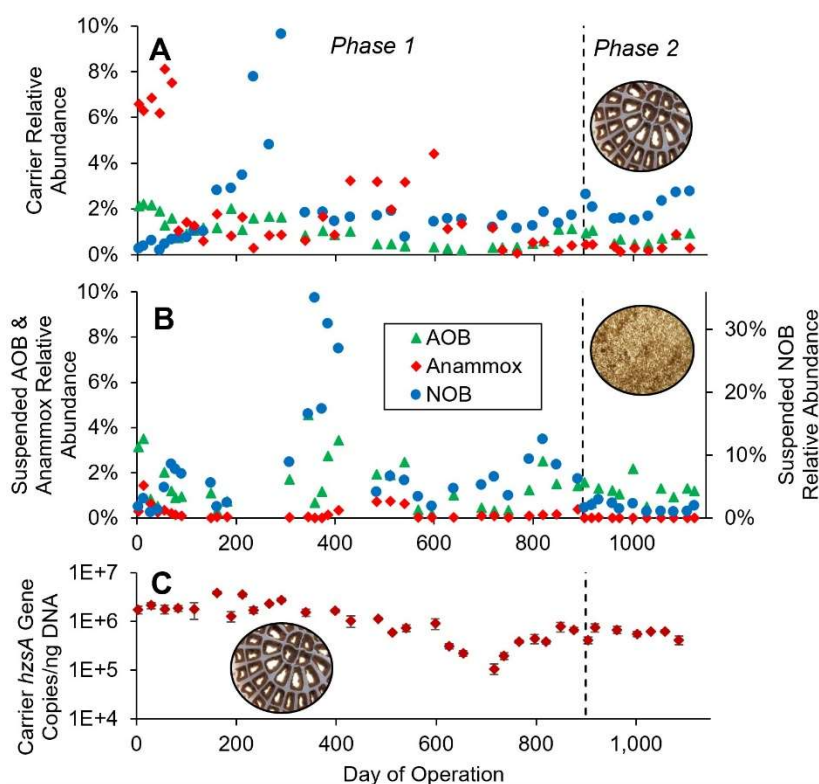


**Figure 4.2** Relative abundance of key functional groups in the attached growth biomass (panel A) and suspended growth biomass (panel B) according to 16S rRNA gene sequencing. Genera detected included *Nitrosomonas* for AOB, *Nitrospira*, *Nitrolancea* and *Nitrotoga* (in order of abundance) for NOB, and *Candidatus Brocadia* for anammox. Panel C shows the anammox hydrazine synthase (*hzsA*) gene copy number from carrier biomass according to qPCR, normalized to ng DNA.

### 4.3.2 Long term retention of robust anammox activity under low-concentration mainstream conditions

N removal performance issues during Phase 1 were related to excess  $\text{NO}_3^-$  production, and low TIN removal was not associated with low anammox activity. Retention of anammox biomass and activity was robustly maintained in this reactor for more than three years of operation in dilute mainstream conditions (average 16 mg TKN/L in the influent). After inoculation of the seeded K5 biocarriers on day 0 from a sidestream process with elevated ammonia concentrations, maximum anammox activity gradually declined as the biomass adapted to mainstream conditions (Figure 4.3). By day 435 the maximum activity had stabilized to an average of  $129 \pm 28$  mgN/L/d (days 435 – 937, before the temperature decline), almost double the average N loading rate of 67 mgN/L/d over the same period. qPCR measurements of anammox abundance confirmed the initial decline in anammox on the carriers followed by long-term maintenance to  $>10^5$  copies of the *hzsA* gene per ng DNA (Figure 4.2C). In contrast, 16S rRNA gene sequencing suggested a greater decline in the only detected anammox genus of *Candidatus Brocadia* (Figure 4.2A), though it has been noted that so-called universal 16S rRNA primer sets underrepresent anammox and Planctomycetes in general (Harhangi et al., 2012). Supplemental anammox biomass was added only once on day 849 in an attempt to increase N removal, but this had a minor impact on anammox activity and abundance and was not required to maintain process performance. In contrast, suspended or granular systems for mainstream deammonification have moved towards ongoing bioaugmentation from sidestream DEMON® processes to maintain anammox activity (Hoekstra et al., 2019; Le et al., 2019a). Taken together, these results indicate that anammox biomass and activity is robust and resilient to long term

mainstream conditions, and with appropriate means for biomass retention (here, growth in biofilms on carriers) do not limit performance of mainstream deammonification processes.

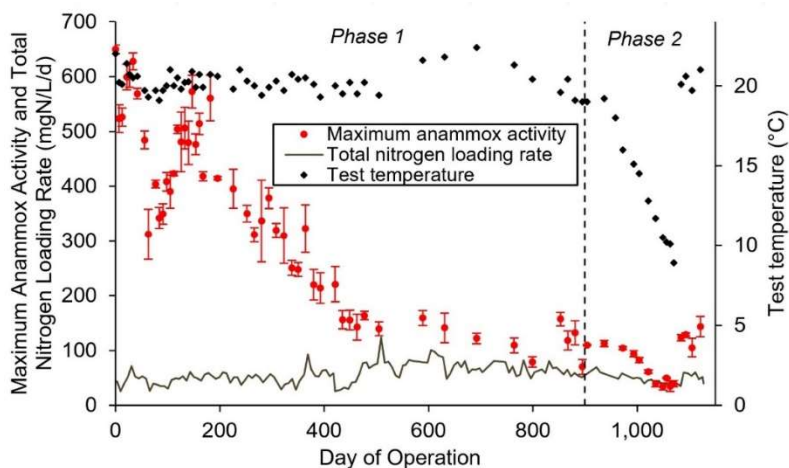


**Figure 4.3** Maximum anammox activity from *in situ* activity tests along with associated test temperatures. The reactor total N loading rate was calculated as a weekly average.

#### 4.3.3 Performance Improvement after Addition of 10% PE in Feed and Nitrifier Shift from Carriers to Suspension

On day 900 of operation, or the beginning of Phase 2, two operational changes were made:

(1) 10% of the influent volume was sourced directly from the primary effluent (by bypassing the A-stage reactor) in order to increase the influent sCOD:NH<sub>4</sub><sup>+</sup>-N ratio from 2.3 to 3.1 (Table 4.1) and (2) a one-time addition of 310 mg/L as VSS of suspended biomass was added from a bench-scale nitrification-denitrification reactor (as described in Roots et al., 2019a) in an effort to increase AOB abundance and VSS concentration. TIN removal performance immediately increased and was sustained throughout Phase 2 (days 900 – 1,128) at an average of 73%, an improvement from 46% TIN removal during Phase 1 (Figure 4.1). Interestingly, an increase in maximum nitrification activity in the suspended biomass (Figure 4.4), while expected due to the increased

suspended volatile solids (VS) concentration, was accompanied by a >70% decrease in maximum activity of both AOB and NOB on the carriers between activity tests on days 890 and 918 (Figure 4.4). Comparing the four maximum activity tests before and four maximum activity tests after day 900 (at 20 °C), both the AOB and NOB activity in the suspension was significantly higher after the influent change (t-test,  $p = 0.005$  and  $0.008$ , respectively), and both the AOB and NOB activity on the biofilm was significantly lower (t-test,  $p = 0.04$  and  $0.002$ , respectively). This shift of nitrification activity to the suspension ended a months-long domination of nitrification activity on the carriers.

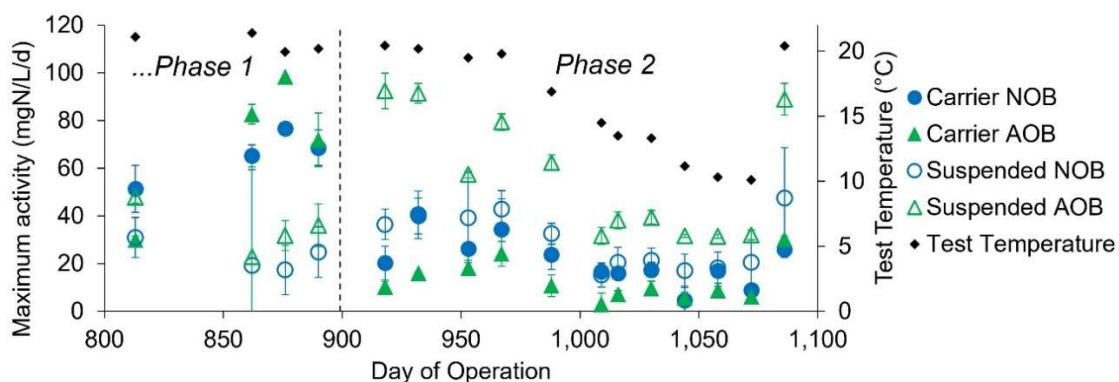


**Figure 4.4** Maximum AOB and NOB activities in the suspended biomass and on the carriers as measured in *ex situ* batch activity assays from day 800 to the end of the project. The entire dataset of AOB and NOB activity measurements is shown in Figure 4.S1.

**Table 4.1** Average reactor influent and effluent concentrations over the two phases.

	Phase 1: 0 - 899 d		Phase 2: 900 - 1128 d	
	Influent (A-stage effluent)	Reactor Effluent	Influent (90% A-stage 10% PE)	Reactor Effluent
TKN (mgN/L)	16.5 ± 5.0	4.4 ± 3.3	14.1 ± 4.1	2.3 ± 0.8
NH <sub>4</sub> <sup>+</sup> (mgN/L)	14.4 ± 4.1	3.2 ± 2.7	12.9 ± 3.6	1.5 ± 0.5
NO <sub>x</sub> <sup>-</sup> (mgN/L) <sup>a</sup>	0.4 ± 0.5	4.9 ± 2.9	0.3 ± 0.2	2.1 ± 1.5
NO <sub>2</sub> <sup>-</sup> (mgN/L) <sup>b</sup>	<i>not measured</i>	0.2 ± 0.1	<i>not measured</i>	0.2 ± 0.1
Total COD (mgCOD/L)	45 ± 30	27 ± 14	56 ± 17	32 ± 13
Soluble COD (mgCOD/L)	33 ± 13	21 ± 8	40 ± 12	26 ± 11
sCOD:NH <sub>4</sub> <sup>+</sup> (gCOD/gN)	2.3	<i>not applicable</i>	3.1	<i>not applicable</i>
alkalinity (meq/L)	4.7 ± 0.5	3.4 ± 0.6	5.0 ± 0.6	4.1 ± 0.6

*Values shown as arithmetic mean ± standard deviation*

<sup>a</sup>NO<sub>x</sub><sup>-</sup> = NO<sub>2</sub><sup>-</sup> + NO<sub>3</sub><sup>-</sup>

<sup>b</sup>NO<sub>2</sub><sup>-</sup> was measured less frequently (*n* = 110) than NH<sub>4</sub><sup>+</sup> and NO<sub>x</sub><sup>-</sup> (*n* = 425)

Higher influent organic carbon was critical to increasing the suspended biomass concentration to induce a shift of nitrification activity to the suspension and improving N removal. During Phase 1 from days 370 – 460, a strategy of increased suspended SRT and suspended VS was attempted (see in Figure 4.1-A&B) but with no associated process improvement. During that time, despite a high suspended SRT of 14 ± 3 days, only 430 ± 158 mg/L of suspended VS was sustained in the reactor, presumably due to low organic carbon in the influent. In contrast, with 10% primary effluent in the influent during Phase 2 (days 900 – 1128), an average of 771 ± 310 mg/L suspended VS was achieved with just a 7.3 ± 2.1 day SRT. This further suggests that the one-time addition of 310 mg VSS/L of suspended biomass on day 900 played a minor role in process improvement compared to the increase in organic carbon in the influent.

The difficulty in accumulating high concentrations of suspended solids under low organic

carbon loading conditions is corroborated by Laureni et al. (2019); in order to accumulate 3 g TSS/L in their IFAS reactor loaded with pretreated primary effluent at a 2.3 sCOD:NH<sub>4</sub><sup>+</sup>-N ratio, a greater than 150-day SRT was required. This very high SRT was achieved via effluent filtration and solids return to the reactor, which is unrealistic under full-scale operation. Achieving high suspended solids to induce a shift of nitrification from the biofilm to the suspension in an IFAS system (Hubaux et al., 2015), then, may require increased organic loading in a full-scale mainstream B-stage process (as in the present study, where a more realistic  $7.3 \pm 2.1$  day SRT was used). Moreover, MBBR systems that experience persistent NOB attachment and activity (Gustavsson et al., 2020) may benefit from such a transition to IFAS mode.

Certain methods for NOB suppression and process improvement that have been suggested in the literature were found, in this study, to be ineffective. The following unsuccessful strategies were attempted during Phase 1 to improve reactor performance:

- I. **MBBR vs. IFAS** (Gustavsson et al., 2020; Malovanyy et al., 2015; Veuillet et al., 2014): The reactor was operated in MBBR mode from days 132 – 314 via mixed liquor wasting to facilitate a low suspended SRT of  $2.1 \pm 0.5$  days and suspended VS concentration of  $63 \pm 32$  mg/L (Figure 4.1-A&B). While NOB were washed out of the suspension, NOB activity proliferated on the carriers (Figure 4.S1) and N removal did not improve (Figure 4.1-D). IFAS mode was utilized from day 315 to the end of the study.
- II. **Aeration regime**: On day 414 the aeration regime was switched from intermittent aeration (Gilbert et al., 2014a; Y. Ma et al., 2017b) with peak DO of 1 mgO<sub>2</sub>/L to low constant aeration (Laureni et al., 2016) to 0.05 – 0.2 mg O<sub>2</sub>/L. N removal did not

significantly improve (Figure 4.1-D), but low constant aeration was sustained for the remainder of the project due to simplicity of operation.

- III. **Anammox bioaugmentation:** Ongoing anammox bioaugmentation has been proposed for suspended and granular mainstream deammonification processes (Hoekstra et al., 2019; Le et al., 2019a). To test this strategy in our IFAS process as a means to increase anammox biomass/activity and aid NOB out-competition, on day 849 K5 carriers from the Egan WRP sidestream ANITA<sup>TM</sup> Mox process were added up to a fill ratio of 38%. However, the biofilms were thin, with average volatile solids of  $6.6 \pm 2.4$  mg/carrier, compared to  $20.4 \pm 3.9$  mg/carrier for the original carriers from James River (measurements averaged over days 849 – 1100), and their effect on total anammox activity was minimal (Figure 4.3). No significant change in N removal or NOB suppression was observed following the addition of carriers (Figure 4.1-D&E).

#### 4.3.4 Reactor Performance during the Phase 2 Temperature Decline

Robust N removal and anammox activity was demonstrated at 20 °C for 50 days after initiation of the A-stage bypass. To test process resilience under temperature stress typical of temperate climates, the temperature was decreased from 20 °C on day 950 down to 8 °C on day 1,076 (about -0.7 °C per week). Good TIN removal of  $72 \pm 9\%$  was sustained from days 950 to day 1,044 down to around 12 °C, and dropped to  $58 \pm 18\%$  for the remainder of the temperature decline due to higher effluent  $\text{NO}_3^-$  (days 951 – 1076, 12 °C to 8 °C, Figure 4.1). 12 °C was also the temperature at which the *ex situ* maximum anammox activity dropped below the N loading rate to the reactor (Figure 4.3), suggesting that the lower specific anammox activity may have limited N removal. A longer suspended SRT of  $8.7 \pm 1.7$  days was maintained during the

temperature decline to facilitate a higher biomass concentration (Figure 4.1) to prevent long react times caused by low metabolic rates at low temperatures. This strategy proved successful, as the HRT of  $7.6 \pm 2.3$  hours during the temperature decline was roughly equivalent to the HRT of  $7.5 \pm 2.5$  hours before (days 1 – 949, see Figure 4.S2). The higher biomass concentration also likely provided additional COD for denitrification via endogenous decay, thus aiding N removal at low temperatures. The overall good performance of this reactor is corroborated by other mainstream deammonification studies that have demonstrated the resiliency of surface-attached anammox biofilms and process performance down to  $10\text{ }^{\circ}\text{C}$  (Gilbert et al., 2015, 2014b), with superior performance at low temperatures compared to suspended/granular anammox processes (Gilbert et al., 2015; Lotti et al., 2014).

To estimate the effect of temperature on anammox activity, maximum activity assays were performed throughout Phase 2 between  $21.0$  and  $8.9\text{ }^{\circ}\text{C}$  to match the concurrent operating temperature (Figure 4.3). An activation energy  $E_a$  of  $71 \pm 8\text{ kJ/mol}$  was calculated from a least-squares linear regression of the Arrhenius plot of Phase 2 activity tests (Figure 4.S3). This result is not a direct measure of temperature sensitivity because the tests were performed over a seven-month period and may reflect temperature adaptation and population shifts in the community; however, it does allow a comparison point for anammox activation energies measured in the literature. 16S rRNA gene sequencing identified *Candidatus Brocadia* as the only known anammox genera in our reactor. Our activation energy of  $71 \pm 8\text{ kJ/mol}$  closely matches the  $70\text{ kJ/mol}$  activation energy measured by Strous et al. (1999) for *Candidatus Brocadia* anammoxidans, though that was measured with a temperature range of  $20 - 43\text{ }^{\circ}\text{C}$ . Lotti et al. (2015c) found that the Arrhenius coefficient of anammox increased with decreasing temperature,

though temperature sensitivity was least pronounced in granular biomass dominated by *Candidatus Brocadia fulgida* with a 6 month-long cultivation at 10 °C, with activation energies of 61 kJ/mol at 15 – 20 °C and 95 kJ/mol at 10 – 15 °C. This and other research (Zekker et al., 2016) demonstrates the importance of adaptation time for optimal anammox activity at low temperatures.

After the expected decline in anammox activity at low temperatures, recovery after resuming operation at 20 °C was rapid (Figure 4.3). The maximum activity test on day 1,084, seven days after the temperature increase, showed 123 mgN/L/d of anammox activity, close to the average of  $129 \pm 28$  mgN/L/d from days 435 – 937, before the temperature decline. The average of the last four activity tests at 20 °C was  $125 \pm 16$  mgN/L/d.

#### **4.3.5 Community analysis via 16S rRNA gene sequencing and qPCR**

Aggregate type significantly influenced population structure in this study; an analysis of similarities (ANOSIM) test on genus-level 16S rRNA gene sequencing data revealed a statistically significant difference between carrier and suspended biomass samples ( $R = 0.78$ ,  $p = 1E-4$ ). An accompanying non-metric multidimensional scaling (NMDS) ordination is shown in Figure 4.S4. Influent carbon also greatly impacted community structure, as further ANOSIM tests revealed statistically significant differences between Phases 1 and 2 carrier samples ( $R = 0.30$ ,  $p = 6E-4$ ), and Phases 1 and 2 suspension samples ( $R = 0.39$ ,  $p = 1E-4$ ). Together with the performance and activity data between the two phases, this demonstrates that small changes in influent organic carbon can induce significant and lasting changes in N removal and community structure.

*Candidatus* Brocadia was the only anammox genus identified in our reactor according to 16S rRNA gene sequencing. qPCR demonstrated anammox biomass maintenance on the carriers of  $>10^5$  *hzsA* copies/ng DNA throughout the study (Figure 4.2C). The qPCR trend, which demonstrated a 71% decline in relative abundance between the first four and last four sample dates, roughly paralleled the maximum anammox activity trend, which demonstrated a 78% decline between the first four and last four tests of the study (Figure 4.3), and a robust plateau over the last ~1.5 years of the study. *Nitrospira* was by far the most abundant NOB present according to 16S rRNA gene sequencing, and its very high abundance in both the suspended and carrier biomass during Phase 1 reflects the challenges in NOB suppression faced during that time. Interestingly, although nitrifier activity on the carriers was suppressed during Phase 2 (Figure 4.4), neither AOB nor NOB relative abundance on the carriers declined during Phase 2 relative to Phase 1. The average NOB (primarily *Nitrospira*) relative abundance in the suspension was significantly lower during Phase 2 at  $1.7 \pm 0.6\%$  than Phase 1 at  $8.6 \pm 8.6\%$  ( $p = 0.0001$ ), which may be due to increased abundance of heterotrophs with higher COD in the influent during Phase 2. *Nitrosomonas* was the only detected genus of AOB and its presence was consistent in both the suspended and carrier biomass at  $1.4 \pm 1.0\%$  and  $0.9 \pm 0.5\%$  relative abundance, respectively, over the entire study.

Given the importance of denitrification in this process (see next section), the heterotrophic community was essential to nitrogen removal, and indeed comprised most of the community according to 16S rRNA gene sequencing. On the carriers, the three most abundant amplicon sequence variants (ASVs) were of the class Ignavibacteria, one of which annotated to the genus *Ignavibacterium*, and together comprised an average of 23% relative abundance on the

carriers (Figure 4.S6). At least one species of *Ignavibacterium* is a known facultative denitrifier (Liu et al., 2012), indicating a likely role in N removal in this reactor. Other abundant heterotrophic genera included “UTCFX1” of the family Anaerolineaceae (3.6%) and *Limnobacter* (2.2%). The classes Ignavibacteria and Anaerolineae have also been found in high abundance in anoxic anammox granules (Lawson et al., 2017) and deammonification biofilms (Persson et al., 2017), suggesting a functional role in anammox processes. In the suspended biomass, abundant heterotrophic ASVs included the genus *Trichococcus* (average relative abundance = 3.4%), the family Anaerolineaceae (2.4%), and the genus *Terrimonas* (2.2%), among others. *Trichococcus*, a few species of which are capable of  $\text{NO}_3^-$  reduction and filamentous growth (Liu, 2002), were significantly higher during Phase 2 ( $8.6 \pm 5.1\%$ ) than Phase 1 ( $1.5 \pm 2.0\%$ , t-test:  $p = 0.0009$ ). Relative abundance plots of the most abundant genera according to 16S rRNA gene sequencing are shown in Figures 4.S6 and 4.S7.

#### 4.3.6 Quantification of anammox vs denitrification contribution to N removal

Nitrogen isotope testing during Phase 2 revealed that under anoxic conditions approximately 74% of N removal is routed through anammox when only  $\text{NO}_2^-$  (and not  $\text{NO}_3^-$ ) is present (Figure 4.5-B). However, in-cycle tests during Phase 2 revealed that  $\text{NO}_3^-$  was usually, though not always, at higher concentrations than  $\text{NO}_2^-$  (Figure 4.S5), indicating that denitrification-anammox may play an important role in this process. Indeed, when  $^{15}\text{N}$  labeled  $\text{NO}_3^-$  was dosed in the N isotope test, 47% was routed through the anammox metabolism (Figure 4.5-C), suggesting a substantial amount of cross feeding from denitrification to anammox. To translate *ex situ* N isotope tests to an estimation of the *in situ* anammox contribution to N removal, *in situ* concentrations of  $\text{NO}_2^-$  and  $\text{NO}_3^-$  are needed. The eight in-cycle tests (Figure 4.S5 shows 2 of

these tests) with average temperatures  $> 19\text{ }^{\circ}\text{C}$  during Phase 2 (nitrogen isotope testing was performed at  $23\text{ }^{\circ}\text{C}$ ) had an average in-cycle  $\text{NO}_2^-$  concentration of 22% that of total  $\text{NO}_X^-$ . N isotope testing indicates that 74% of  $\text{NO}_2^-$  (which comprises 22% of the  $\text{NO}_X^-$  present) removal is routed through anammox and 47% of the  $\text{NO}_3^-$  (which comprises 78% of the  $\text{NO}_X^-$  present) removal is routed through anammox, such that  $74\% \times 0.22 + 47\% \times (0.78) = 53\%$  of N removal occurred via anammox in this process during Phase 2, excluding the temperature decline.

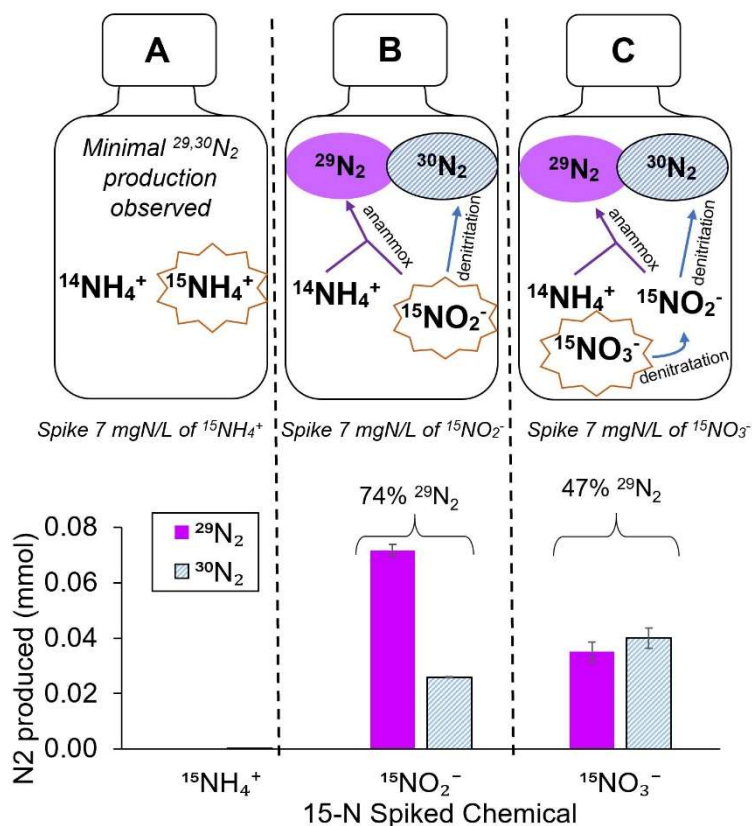


**Figure 4.5** Results from nitrogen isotope testing, which was performed to quantify relative contributions of anammox (which produce  $^{29}\text{N}_2$  in this test) and denitrification (which produce  $^{30}\text{N}_2$ ) to N removal. The testing schematic is shown in the top panel and results from day 1,128 are shown on the bottom panel.

Nitrogen isotope testing was only performed during Phase 2 with higher organic carbon in the influent than during Phase 1, so while N removal was lower during Phase 1, a greater proportion was likely routed through anammox. Conversely, it is likely that more N removal was routed through denitrification during the temperature decline. Indeed, only when the reactor temperature dropped below 13 °C did the maximum anammox activity drop below the N loading rate to the reactor (Figure 4.3), although good N removal performance was maintained for most of this period (Figure 4.1-D). An increased proportion of denitrification was likely possible due to the increased suspended solids concentration during this time (Figure 4.1-B) and organic carbon from endogenous decay.

While an excess of organic carbon can lead to anammox failure from out-competition for  $\text{NO}_2^-$  by denitrifiers (Tang et al., 2010), at least some anammox organisms, such as *Candidatus Brocadia fulgida* and *Candidatus Anammoxoglobus propionicus*, can use acetate or propionate to reduce  $\text{NO}_3^-$  to  $\text{NO}_2^-$  (Guvén et al., 2005; Kartal et al., 2008). The addition of organic carbon to an anammox process, therefore, does not necessarily imply increased activity of heterotrophic denitrifiers over that of anammox.

A note on terminology: it would be a metabolic oversimplification to call this process “partial nitrification/anammox” (because nitrification/denitrification was demonstrated via in-cycle  $\text{NO}_3^-$  concentrations and isotope testing) or “partial denitrification/anammox” (because of the likely presence of nitrification/anammox due to transient  $\text{NO}_2^-$  accumulation observed from in-cycle tests [Figure 4.S5]). The term “simultaneous partial nitrification, anammox and denitrification (SNAD),” as used by Zheng et al. (2016) is the most general and closest to the

truth, but “deammonification” has been chosen for simplicity with the stipulation that NOB and denitrification play key roles in the process.

### 4.3.7 Implications for Practice

The quantity of organic carbon relative to N in the influent is critical to the success of anammox processes, as too much can lead to the suppression of anammox (Chamchoi et al., 2008; Tang et al., 2010) and too little can limit the overall N removal (Chen et al., 2016; Malovanyy et al., 2015; Ni et al., 2012). However, adjusting the influent COD:N ratio at full scale remains challenging given that dosing of synthetic VFAs would compromise the energy- and chemical-saving goals of shortcut N removal processes. This study demonstrates a practical means for tuning the influent COD:N ratio of any anammox reactor with an upstream A-stage carbon removal process. Although the ratio of rerouted primary effluent to total reactor influent was fixed at 10% in this study, this ratio could be adjusted to optimize N removal performance of a given process. Moreover, this study demonstrated the importance of the COD:N ratio in tailoring aggregate type and architecture in mainstream deammonification processes, specifically by promoting the accumulation of suspended solids and the shift in nitrification activity from the biofilm to the suspension. This in turn improves our understanding of key controls and underlying mechanisms of IFAS systems for mainstream deammonification applications.

## 4.4 Supporting Information

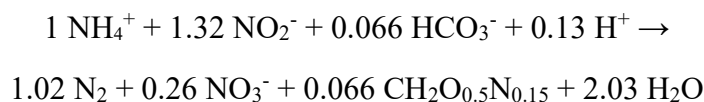
### 4.4.1 Batch Activity Assays

#### 4.4.1.1 *In situ* Maximum Anammox Activity Assays

Anammox maximum activity tests were performed *in situ* at the end of reactor cycles when sCOD was low to minimize interference from denitrifiers.  $\text{NH}_4^+$  and  $\text{NO}_2^-$  were spiked to

non-limiting conditions (20 – 40 mgN/L each) via ammonium chloride and sodium nitrite salt solutions and the reactor was mixed without aeration. To prevent oxygen intrusion, around day 540 several 1.4-inch diameter floating spheres (similar to ping pong balls) were added to cover the surface of the reactor and were left in place until end of the study. N<sub>2</sub> gas sparging was performed during the tests on days 800 and 867 but was not continued due to pH increase (from CO<sub>2</sub> sparging) and the lack of a discernable difference in activity. Five to six grab samples were taken in 30-minute intervals and analyzed for NH<sub>4</sub><sup>+</sup>, NO<sub>2</sub><sup>-</sup> and NO<sub>3</sub><sup>-</sup> by colorimetry (APHA, 2005).

According to stoichiometry from Strous et al. (1998) the anammox metabolic pathway removes N (as nitrogen gas + biomass) at a ratio of 2.05 moles N per mole NH<sub>4</sub><sup>+</sup> removed:



Anammox activity as N removal (in mg N/L/d) was therefore calculated as 2.05 times the slope of the NH<sub>4</sub><sup>+</sup> drawdown curve. Only linear trends with R<sup>2</sup> values above 0.8 were used. Stoichiometric ratios of NO<sub>2</sub><sup>-</sup> drawdown and NO<sub>3</sub><sup>-</sup> production to NH<sub>4</sub><sup>+</sup> drawdown were compared to anammox stoichiometry to check that anammox was the dominant metabolic pathway. Higher than expected NO<sub>2</sub><sup>-</sup> drawdown and lower than expected NO<sub>3</sub><sup>-</sup> production occasionally indicated the presence of denitrification in these tests, by which we inferred that use of the NH<sub>4</sub><sup>+</sup> drawdown curve alone (with anammox stoichiometry) was the most accurate method for calculating anammox activity.

#### 4.4.1.2 *Ex situ* Maximum AOB and NOB Activity Assays

AOB and NOB maximum activity assays were performed separately for carrier and suspended biomass (both in duplicate) via *ex situ* assays. For suspended biomass, 300 mL of mixed liquor from the end of a react cycle (to minimize sCOD concentration and interference from denitrifiers) was placed into each of two 500-mL Erlenmeyer flasks. For carrier biomass activity, K5 carriers were counted and placed into a final volume of 300 mL of reactor effluent in each of two 500-mL Erlenmeyer flasks to match the volumetric carrier filling ratio of the reactor (30 – 38% depending on date). The four flasks were placed on a shaker table with a water bath for temperature control between 10 – 22 °C to match the reactor temperature at the time. DO was monitored with a Hach LDO® optical DO probe and was maintained at or above 3 mgO<sub>2</sub>/L by shaking action and bubbling from small aquarium pumps. pH was monitored with the Hach PHC101® electrode and maintained between 7 and 8. NH<sub>4</sub><sup>+</sup> and NO<sub>2</sub><sup>-</sup> were spiked to non-limiting conditions (~20 mg NH<sub>4</sub><sup>+</sup>-N/L and ~10 mg NO<sub>2</sub><sup>-</sup>-N/L), and five grab samples were taken in 20-minute intervals and analyzed for NH<sub>4</sub><sup>+</sup>, NO<sub>2</sub><sup>-</sup> and NO<sub>3</sub><sup>-</sup> by colorimetry (APHA, 2005). AOB activity was taken as the slope of the NH<sub>4</sub><sup>+</sup> drawdown curve, and NOB was taken as the average of the (1) slope of the NO<sub>3</sub><sup>-</sup> production curve and (2) the sum of the slopes of NH<sub>4</sub><sup>+</sup> and NO<sub>2</sub><sup>-</sup> drawdown curves. Only linear trends with R<sup>2</sup> values above 0.8 were used. In some carrier tests (likely due to the presence of anoxic zones in the biofilm), a decline in TIN (i.e. NH<sub>4</sub><sup>+</sup> + NO<sub>2</sub><sup>-</sup> + NO<sub>3</sub><sup>-</sup> linear fit with R<sup>2</sup> > 0.8) over the course of the test indicated the presence of anammox activity, and AOB and NOB activities were adjusted accordingly via the anammox stoichiometry shown above.

#### 4.4.2 Nitrogen Isotope Testing

Isotopes of  $^{15}\text{NH}_4^+$ ,  $^{15}\text{NO}_3^-$  and  $^{15}\text{NO}_2^-$  were spiked separately under initially anaerobic conditions (i.e. with no  $\text{O}_2$ ,  $^{14}\text{NO}_3^-$ , or  $^{14}\text{NO}_2^-$  present), with  $^{14}\text{NH}_4^+$  already present in solution, to quantify the percent contribution of anammox and denitrification by measuring the relative amounts of  $^{29}\text{N}_2$  and  $^{30}\text{N}_2$  produced, respectively. In this test, the anammox metabolic pathway produces  $^{29}\text{N}_2$  by combining one molecule of  $^{14}\text{NH}_4^+$  and one molecule of  $^{15}\text{NO}_2^-$ , while the denitrification metabolic pathway produces  $^{30}\text{N}_2$  by combining two molecules of  $^{15}\text{NO}_2^-$  and/or  $^{15}\text{NO}_3^-$ . The  $^{15}\text{NH}_4^+$ -spiked test was used as a control to ensure anaerobic conditions (i.e. the absence of  $^{14}\text{NO}_3^-$  and  $^{14}\text{NO}_2^-$ ) such that minimal  $^{29}\text{N}_2$  and  $^{30}\text{N}_2$  production should be observed. A blank vial, with no  $^{15}\text{N}$  chemical spiked but all other conditions the same, was also included. Aside from the lack of aeration during isotope testing, test conditions were prepared to mimic in-cycle conditions as closely as possible. Carrier and suspended biomass were collected together in 250-mL vials in the middle of a typical cycle to mimic average organic carbon availability. Before spiking, the test vials were bubbled with Helium gas, capped, and shaken for 9 hours to ensure reduction of residual  $\text{O}_2$  and  $^{14}\text{NO}_X^-$  ( $^{14}\text{NO}_3^- + ^{14}\text{NO}_2^-$ ). 10 mgN/L of  $^{14}\text{NH}_4^+$  was chosen as a typical in-cycle  $\text{NH}_4^+$  concentration, and 7 mgN/L of  $^{15}\text{NH}_4^+$ ,  $^{15}\text{NO}_3^-$  or  $^{15}\text{NO}_2^-$  was spiked to separate bottles in duplicate to ensure that anammox would not become  $\text{NH}_4^+$ -limited during the test. After spiking  $^{15}\text{N}$  chemicals the vials were shaken for > 14 hours at room temperature (23 °C).

Mass spectrometry of the  $\text{N}_2$  isotopologues, in order to determine the relative abundance of  $^{28,29,30}\text{N}_2$ , was performed at the Stable Isotope Laboratory of the Earth and Planetary Sciences department of Northwestern, and with the help of lab manager Andrew Masterson. Mass spectrometry was performed immediately after sub-sampling the vials with a 100- $\mu\text{L}$  gas-tight

(Hamilton) syringe. Samples were withdrawn from the vials, immediately injected into a UHP He purged and septum sealed 12-mL Exetainer, and transferred to a thermo-stated (30C) incubation block of a GasBench II. Exetainers were sub-sampled further with the a double bore needle of a PAL autosampler, and loaded-injected into the GasBench II via a 100-uL injection loop at a flow-rate of 1.2 mL/min, dried 2X in a Nafion drier, and separated on a GC column (0.18 mm ID) held at 70 °C. The open-split of the GasBench II was further mated to a Thermo Delta V Plus isotope ratio mass-spectrometer, run in continuous flow mode (Thermo Scientific™, Waltham MA, USA), outfitted with three Faraday cup collectors ( $3 \times 10^8$ ,  $3 \times 10^{10}$ ,  $1 \times 10^{11}$  ohms). Pure N<sub>2</sub> gas (containing 99.634% of <sup>14</sup>N and 0.366% of <sup>15</sup>N typical of atmospheric N<sub>2</sub>) was used for calibration of <sup>28,29,&30</sup>N<sub>2</sub> (via independent collectors) with 5 injection volumes from 20 and 100 μL. 40 μL of gas was extracted from the headspace of each test vial for analysis; this volume was chosen to ensure that signal intensity remained well within the linear range (200 mV – 20 V) of the instrument and to avoid memory effects between samples. The quantity in mmol of each of <sup>28,29,&30</sup>N<sub>2</sub> for each sample injection was calculated from the calibration curve. The quantity in mmol of each of <sup>28,29,&30</sup>N<sub>2</sub> in the vial headspace was then inferred by multiplying by the ratio of the vial headspace volume to the injection volume (average multiplying factor = 795). The <sup>29</sup>N<sub>2</sub> and <sup>30</sup>N<sub>2</sub> produced for each sample was defined as the difference between the mmol of <sup>29</sup>N<sub>2</sub> or <sup>30</sup>N<sub>2</sub> in each sample vial headspace and the <sup>29</sup>N<sub>2</sub> or <sup>30</sup>N<sub>2</sub> in the blank vial headspace.

#### **4.4.3 Biomass sampling**

Suspended (floccular) and carrier (biofilm) biomass was sampled once or twice per month for 16S rRNA gene sequencing analyses. For the suspended biomass, four 1-mL aliquots of mixed liquor were centrifuged at 10,000g for 3 minutes, and the supernatant was replaced

with 1 mL of Tris-EDTA buffer. The biomass pellet was then vortexed and centrifuged at 10,000g for 3 minutes after which the supernatant was removed, leaving only the biomass pellet to be archived at -80 °C. For the carrier biomass whole K5 biocarriers were sampled and archived directly at -80 °C. Biofilm was scraped off a 1/8<sup>th</sup> section of the archived K5 biocarriers immediately before performing DNA extraction.

#### 4.4.4 16S rRNA Gene Sequencing

16S rRNA gene amplicon library preparations were performed using a two-step PCR protocol using the Fluidigm Biomark: Multiplex PCR Strategy as previously described (Griffin and Wells, 2017). In the first round of PCR, each 20 uL reaction contained 10 µL of FailSafe PCR 2X PreMix F (Epicentre, Madison, WI), 0.63 units of Expand High Fidelity PCR Taq Enzyme (Sigma-Aldrich, St. Louis, MO), 0.4 µM of forward primer and reverse primer modified with Fluidigm common sequences at the 5' end of each primer, 1 µL of gDNA (approximately 100 ng) and the remaining volume molecular biology grade water. The V4-V5 region of the 16S rRNA gene was amplified using the 515F-Y (5'-GTGYCAGCMGCCGCGGTAA-3') and 926R (5'-CCGYCAATTYMTTTRAGTTT-3') primer set (Parada et al., 2016). PCR reactions were run with a Biorad T-100 Thermocycler (Bio-Rad, Hercules, CA). Thermocycling conditions for the 515F-Y/926R primer set were 95°C for 5 minutes, then 28 cycles of 95°C for 30 seconds, 50°C for 45 seconds, and 68°C for 30 seconds, followed by a final extension of 68°C for 5 minutes. Specificity of amplification was checked for all samples via agarose gel electrophoresis.

Sample barcoding (i.e. second-stage PCR) and sequencing was performed at the University of Illinois at Chicago DNA Services Facility. Sequencing was done on an Illumina MiSeq sequencer (Illumina, San Diego, CA) using Illumina V2 (2x250 paired end) chemistry.

For amplicon sequence analysis, sequence quality control was performed through DADA2 (Callahan et al., 2016) integrated in QIIME2 version qiime2-2018.8 (Bolyen et al., 2018), which included quality-score-based sequence truncation, primer trimming, merging of paired-end reads, and removal of chimeras. Taxonomy was assigned to each individual sequence variation using the Silva database, release 132.

#### 4.4.5 qPCR

qPCR reactions were run on a Bio-Rad C1000 CFX96 Real-Time PCR system (Bio-Rad, Hercules, CA, USA). Each sample date included 2 technical replicates of 2 biological replicates (total of 4 replicates), and the standard series was generated in duplicate on each plate by tenfold serial dilutions of synthesized DNA (IDT Inc, Coralville, IA, USA). 20  $\mu$ L reactions included 10  $\mu$ L of the Bio-Rad SsoAdvanced Universal Inhibitor-Tolerant SYBR Green Supermix (Bio-Rad, Hercules, CA, USA), 0.5  $\mu$ M of each primer, 1  $\mu$ L of standard or 10-fold diluted DNA extracts, and the balance molecular biology grade water. Amplification specificity was verified for all samples via melt curve analysis, and for select samples via gel electrophoresis.

#### 4.4.6 Supplementary Figures

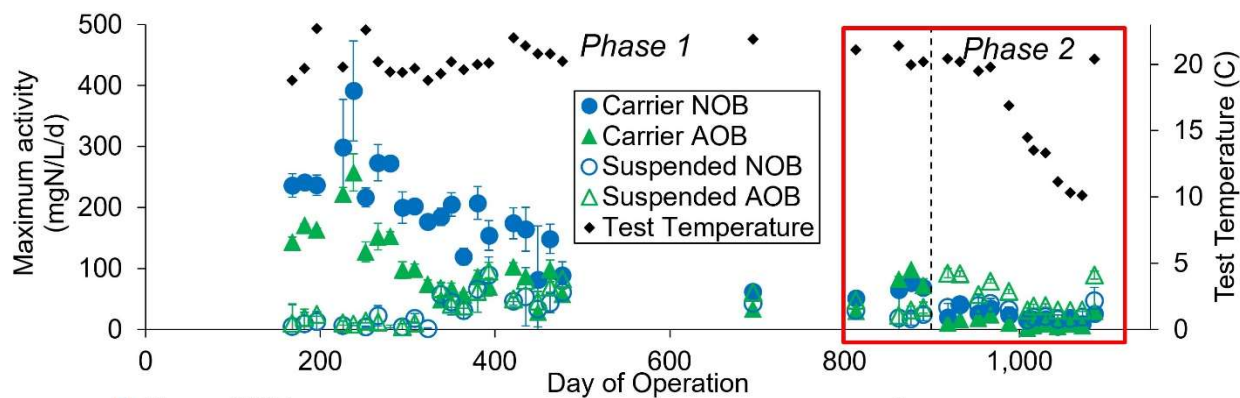


**Figure 4.S1** Maximum AOB and NOB activities in the suspended biomass and on the carriers as measured in *ex situ* batch activity assays over the entire project. The red box outlines the data shown in Figure 4.4.

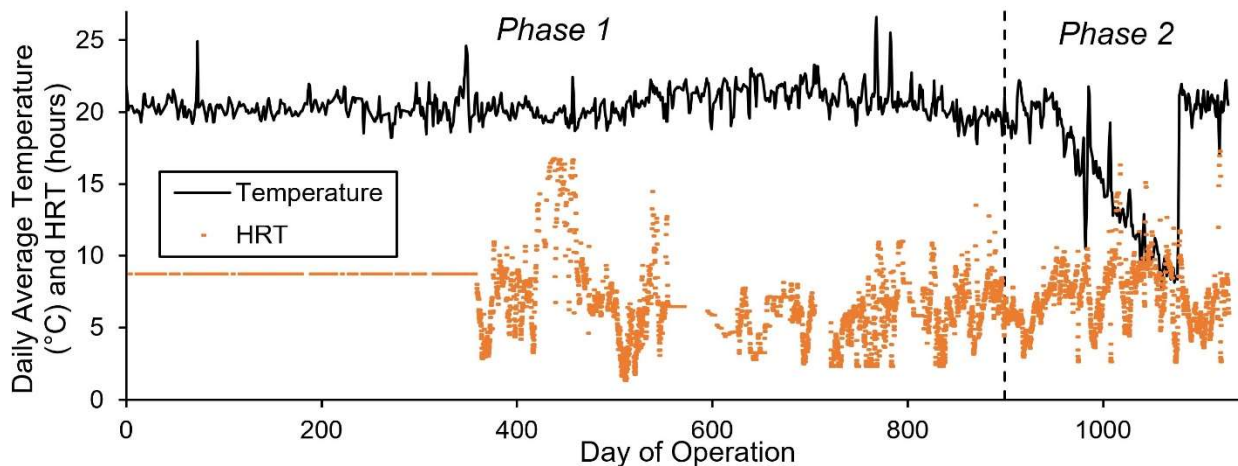


**Figure 4.S2** Hydraulic retention time (HRT) and daily average reactor temperature throughout the study. Variable HRT began on day 358 upon implementation of ammonia-based control, whereupon the aerated portion of the cycle was terminated when the target effluent ammonia concentration of 2 mg  $\text{NH}_4^+\text{-N/L}$  was reached. After day 358 the HRT was calculated on a per-cycle basis.

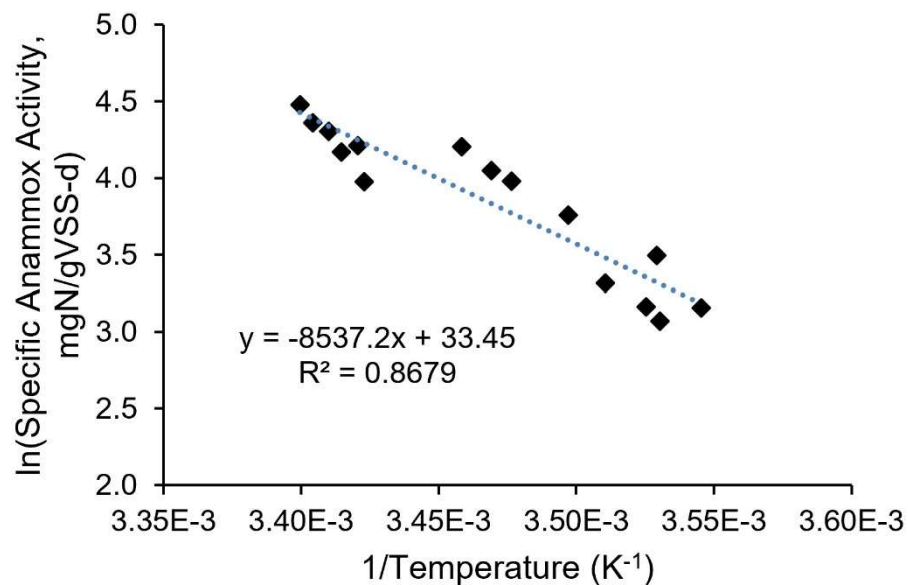


**Figure 4.S3** Arrhenius plot of 15 maximum specific anammox activity tests (normalized to total carrier biomass) during Phase 2 (days 904 – 1,121). The activation energy calculated from the slope was  $71 \pm 8$  kJ/mol ( $\pm$  standard error of the slope), though this should not be interpreted as a strict activation energy considering possible temperature adaptation and shifts in the microbial community over the 217 days.

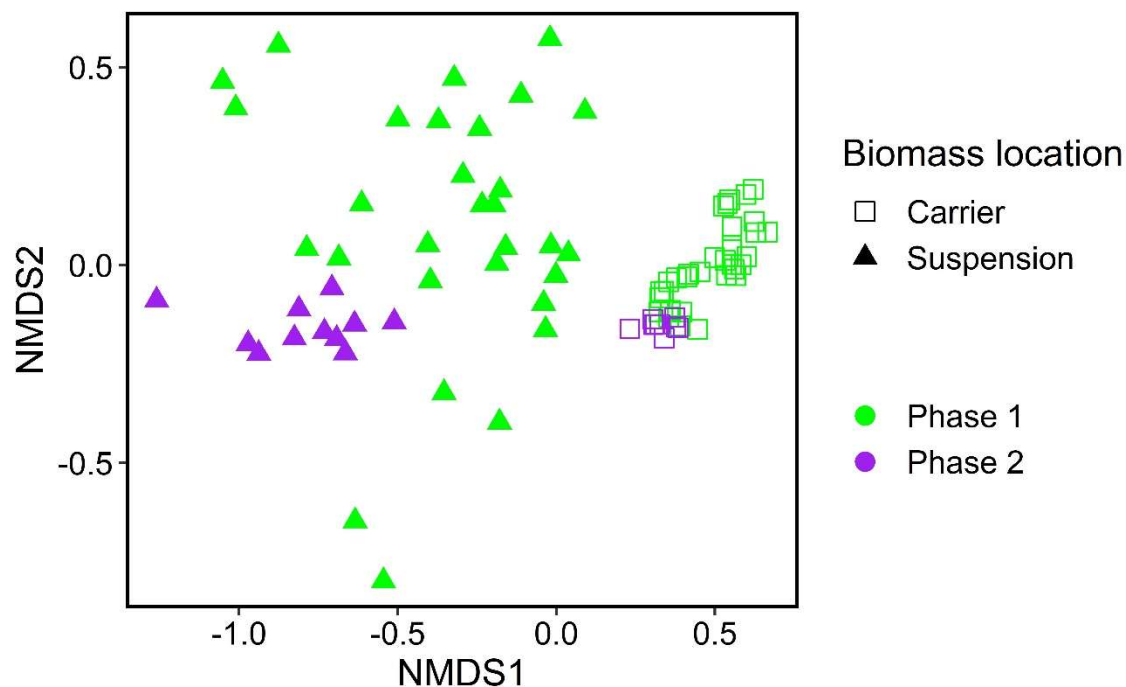


**Figure 4.S4** Non-metric multidimensional scaling (NMDS) ordination of all carrier and suspended biomass samples as calculated from genus-level 16S rRNA gene sequencing data. In order to facilitate convergence of the solution, the data was first trimmed to remove the least abundant genera comprising 0.09% of the total abundance. The significance of the ordination is represented by the stress value of 0.096.

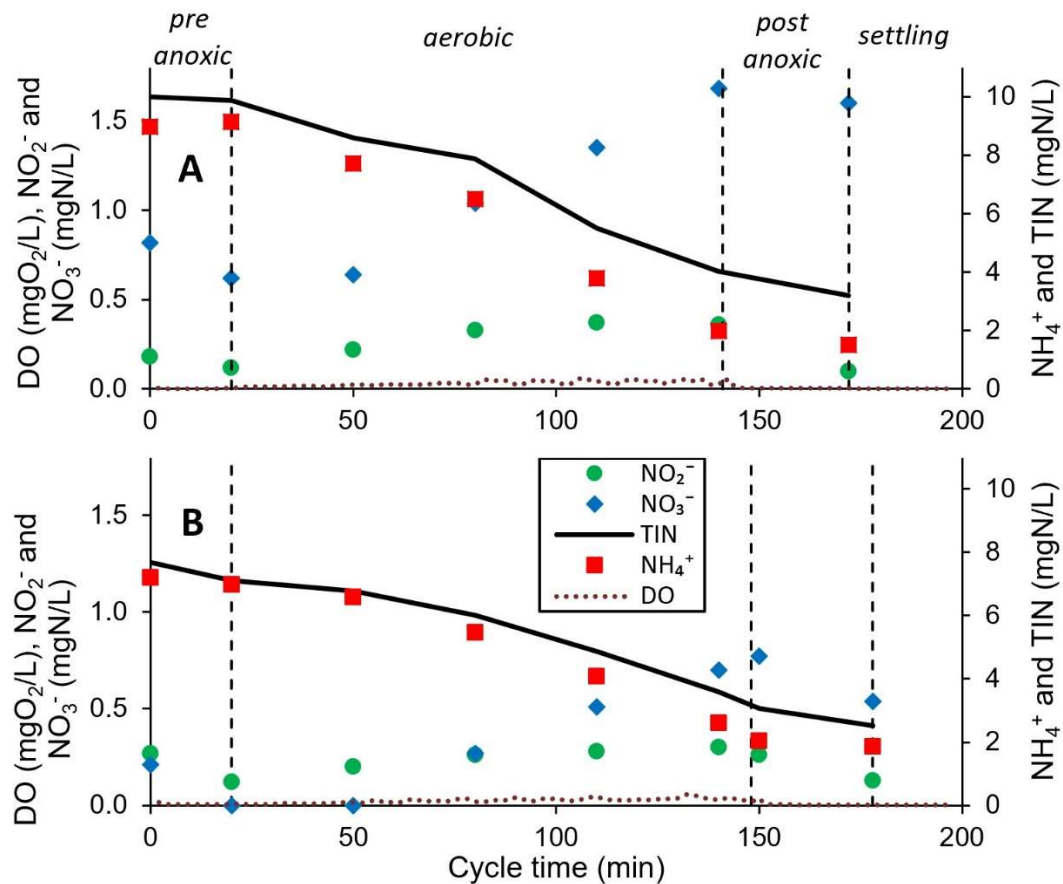


**Figure 4.S5** Two representative in-cycle tests during Phase 2 from (A) day 909 at 18.9 °C and (B) day 1107 at 21.1 °C. Reactor fill (not shown) occurred in less than 2 minutes, and cycle time = 0 is defined as the completion of fill.

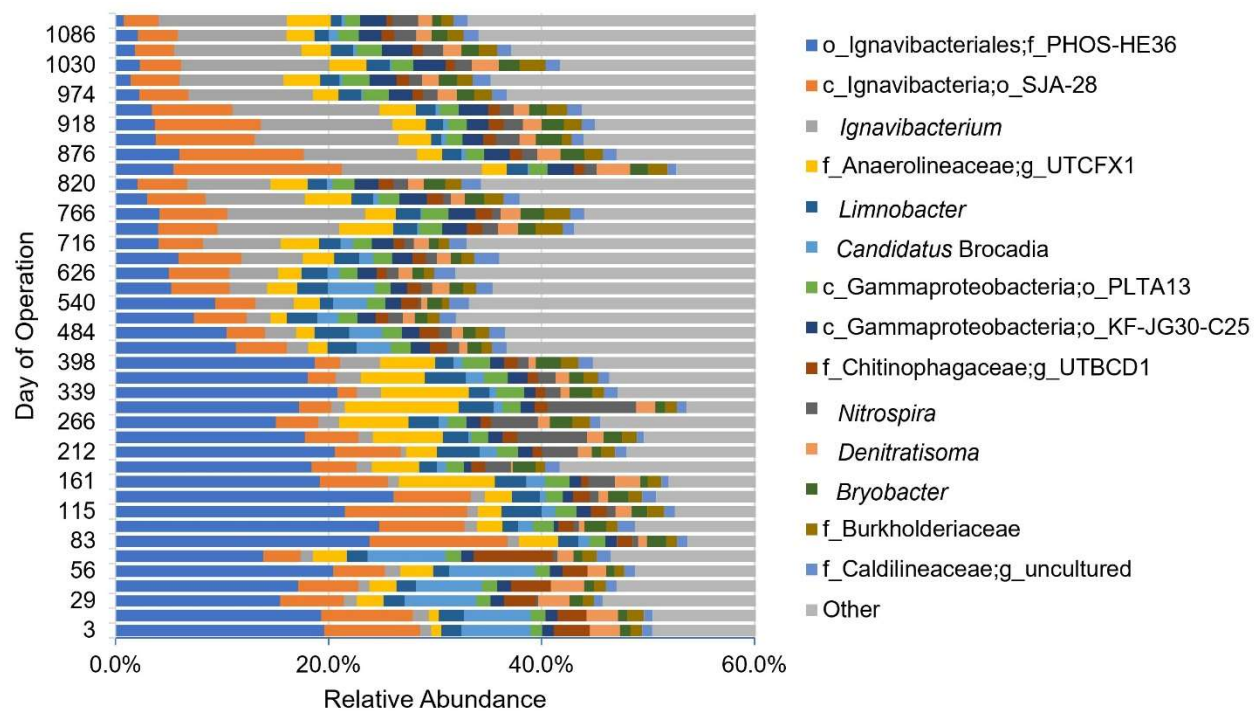


**Figure 4.S6** Relative abundance of the 14 most abundant bacterial genera in the carrier biomass according to 16S rRNA gene sequencing. Amplicon sequence variants that were unclassified at the genus level are presented with the corresponding lowest annotable taxonomy: p\_ = phylum, c\_ = class, o\_ = order, f\_ = family, g\_ = genus.

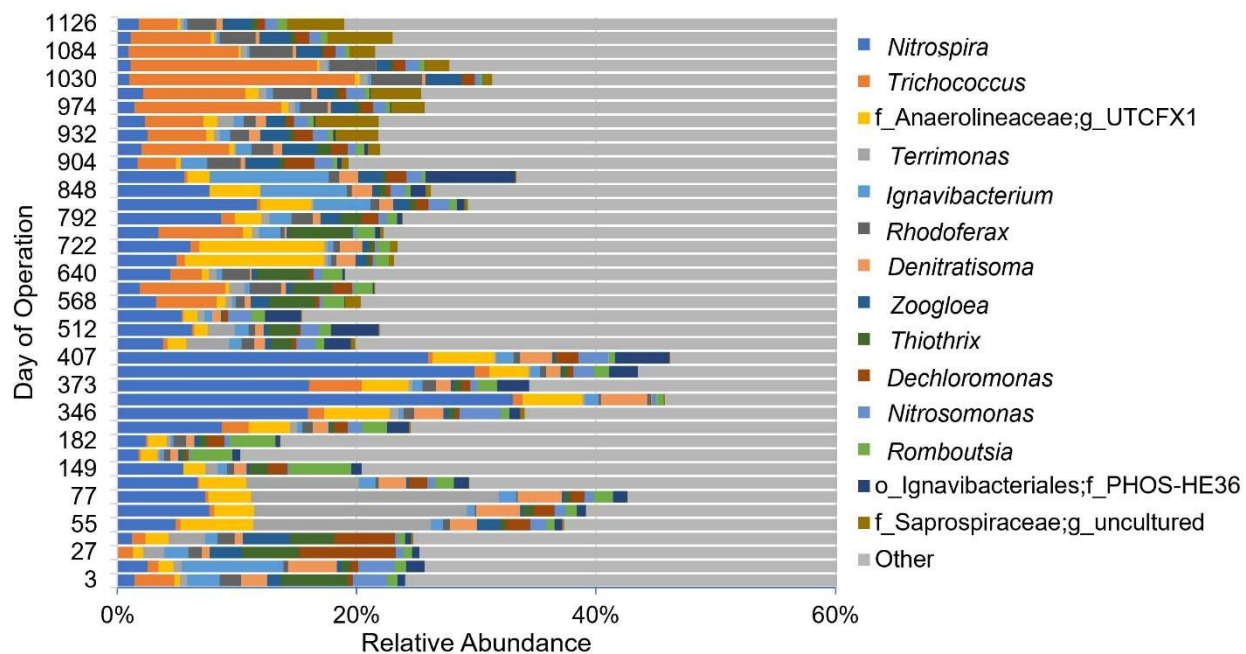


**Figure 4.S7** Relative abundance of the 14 most abundant bacterial genera in the suspended biomass according to 16S rRNA gene sequencing. Amplicon sequence variants that were unclassified at the genus level are presented with the corresponding lowest annotable taxonomy: o\_ = order, f\_ = family, g\_ = genus.

## CHAPTER 5: COMAMMOX NITROSPIRA ARE THE DOMINANT AMMONIA OXIDIZERS IN A MAINSTREAM LOW DISSOLVED OXYGEN NITRIFICATION REACTOR<sup>1</sup>

### Abstract

Recent findings show that a subset of bacteria affiliated with *Nitrospira*, a genus known for its importance in nitrite oxidation for biological nutrient removal applications, are capable of complete ammonia oxidation (comammox) to nitrate. Early reports suggested that they were absent or present in low abundance in most activated sludge processes, and thus likely functionally irrelevant. Here we show the accumulation of comammox *Nitrospira* in a nitrifying sequencing batch reactor operated at low dissolved oxygen (DO) concentrations. Actual mainstream wastewater was used as influent after primary settling and an upstream pre-treatment process for carbon and phosphorus removal. The ammonia removal rate was stable and exceeded that of the treatment plant's parallel full-scale high DO nitrifying activated sludge reactor. 16S rRNA gene sequencing showed a steady accumulation of *Nitrospira* to 53% total abundance and a decline in conventional ammonia oxidizing bacteria to <1% total abundance over 400+ days of operation. After ruling out other known ammonia oxidizers, qPCR confirmed the accumulation of comammox *Nitrospira* beginning around day 200, to eventually comprise 94% of all detected *amoA* and 4% of total bacteria by day 407. Quantitative fluorescence *in situ* hybridization confirmed the increasing trend and high relative abundance of *Nitrospira*. These results demonstrate that comammox can be metabolically relevant to nitrogen transformation in wastewater treatment, and can even dominate the ammonia oxidizing community. Our results suggest that comammox may be an important functional group in energy efficient nitrification systems designed to operate at low DO levels.

<sup>1</sup>Roots, P., Wang, Y., Rosenthal, A.F., Griffin, J.S., Sabba, F., Petrovich, M., Yang, F., Kozak, J.A., Zhang, H., Wells, G.F., 2019. Comammox *Nitrospira* are the dominant ammonia oxidizers in a mainstream low dissolved oxygen nitrification reactor. *Water Research* 157, 396–405. <https://doi.org/10.1016/j.watres.2019.03.060>

## 5.1 Introduction

Resource and energy-efficient nutrient removal methods from wastewater have gained increased attention in recent years due to utility goals of energy self-sufficiency and increasingly stringent effluent nitrogen (N) and phosphorus (P) standards. Such methods include partial nitrification/anammox (PN/A) and nitrification-denitrification, both of which require low dissolved oxygen (DO) or anoxic zones, as well as simply nitrification with low DO. These methods contrast with conventional nitrifying activated sludge operated at high, i.e.  $>2$  mg/L DO concentrations (Park and Noguera, 2004), which incur substantial energy costs due to aeration. When low DO methods are applied to mainstream wastewater, they may select for organisms that thrive under relatively low substrate (i.e. due to stringent effluent standards) and low oxygen conditions.

Comammox *Nitrospira*, discovered in late 2015 (Daims et al., 2015; van Kessel et al., 2015), may be such an organism. The name “comammox” is derived from their ability to perform complete ammonia oxidation all the way to nitrate ( $\text{NO}_3^-$ ). The comammox metabolism overturned a  $>100$ -year paradigm that nitrification is a two-step process requiring coordinated activity of ammonia oxidizing bacteria or archaea (AOB or AOA, ammonia  $[\text{NH}_3]$  to nitrite  $[\text{NO}_2^-]$ ) and nitrite oxidizing bacteria (NOB,  $\text{NO}_2^-$  to  $\text{NO}_3^-$ ). The presence of comammox could be detrimental to PN/A, nitrification, and nitrification-denitrification process performance, where accumulation of the intermediate  $\text{NO}_2^-$  via NOB suppression is a process requirement, and  $\text{NO}_3^-$  production is not desired. Early mining of shotgun metagenomics datasets revealed their presence (albeit low abundance) in conventional nitrifying activated sludge systems (Daims et al., 2015; van Kessel et al., 2015), as their unique ammonia monooxygenase (*amoA*) gene had

defined detection by previous quantitative polymerase chain reaction (qPCR) or sequencing assays targeting AOB. The extent of their importance to wastewater treatment, however, is currently unknown.

As demonstrated by substrate affinity tests on axenic cultures of *Nitrospira inopinata* (Kits et al., 2017), at least one comammox species is adapted to oligotrophic conditions due to its very high ammonia affinity (half-saturation coefficient  $K_{\text{NH}_3} = 0.049 \mu\text{M NH}_3$ ) and relatively low maximum rate of ammonia oxidation (Kits et al., 2017; Lawson and Lucker, 2018). While the oxygen affinity of comammox has yet to be measured, theoretical predictions and genomic studies alike indicate that they are likely adapted to environments with low DO (Costa et al., 2006; Lawson and Lucker, 2018). These characteristics are borne out in the conditions in which comammox has been discovered to date. Indeed, *N. inopinata* was originally cultured from a biofilm growing 1,200 m below the surface in an oil exploration well (Daims et al., 2015), while *Candidatus Nitrospira nitrosa* and *Candidatus Nitrospira nitrificans* were first found in biomass on an aquaculture system biofilter (van Kessel et al., 2015) exposed to ammonium ( $\text{NH}_4^+$ ) concentrations of 1.1 mg $\text{NH}_4^+$ -N/L or less. Comammox *Nitrospira* were also found in an aquaculture biofilter with low (0.1 mg $\text{NH}_4^+$ -N/L) substrate concentrations (Bartelme et al., 2017), and in this case outnumbered both AOA and AOB based on *amoA* quantification via qPCR. (Daims et al., 2015) and subsequent investigations found comammox in the oligotrophic environment of drinking water treatment plants (Fowler et al., 2018; Palomo et al., 2016; Pinto et al., 2016; Pjevac et al., 2017), where they were detected in 10 of 12 locations with metagenomic datasets (Wang et al., 2017). In four of the metagenomic samples from (Wang et al., 2017), comammox *amoA*-like sequences outnumbered the AOA and AOB *amoA*-like sequences,

suggesting that comammox may dominate nitrification activity in some drinking water treatment plants.

The “oligotrophic lifestyle” (Kits et al., 2017) of comammox suggests that, while they have been detected in wastewater treatment plants (WWTPs) (Daims et al., 2015; Pjevac et al., 2017; van Kessel et al., 2015), they may not be able to compete with other ammonia oxidizers in such nutrient-rich environments. Two surveys for comammox in WWTPs seem to confirm this (Annavaiahala et al., 2018; Gonzalez-Martinez et al., 2016). Gonzalez-Martinez et al. (2016) utilized 16S rRNA gene sequencing to survey 6 full-scale nitrifying activated sludge systems and 3 full-scale autotrophic nitrogen removal systems and found only one operational taxonomic unit (OTU) affiliated with comammox *Nitrospira* at a very low abundance of 0.08%, or five times less abundant than AOB. Annavaiahala et al. (2018) examined metagenomic data sets of 16 full-scale biological nitrogen removal systems and found comammox *Nitrospira* present in all reactors at a relative abundance of 0.28 – 0.64% (Annavaiahala et al., 2018). All samples had a ratio of comammox to AOB protein coding sequences of 0.18 or less, suggesting that comammox played a relatively minor role in  $\text{NH}_4^+$  oxidation in all systems. While the conclusion of Gonzalez-Martinez et al. (2016) was that comammox are not significant in nitrogen cycling, Annavaiahala et al. (2018) cautioned that their seeming ubiquity in WWTPs suggests that further research is warranted to understand their contribution to nitrogen transformations.

Increased research into low DO N removal systems for treatment of mainstream wastewater (as opposed to sidestream systems with high N concentrations > 300 mgN/L) to reduce energy consumption by aeration may produce environments more favorable to the oligotrophic comammox. Here, we demonstrate strong enrichment of comammox coupled to high rate

complete ammonia oxidation activity in a low DO nitrifying SBR operated for >400 days with real primary effluent as feed. While comammox *Nitrospira* have been previously detected in wastewater treatment systems, this study is the first to show it to be the dominant ammonia oxidizer in a mainstream wastewater treatment bioreactor without synthetic feed.

## 5.2 Methods

### 5.2.1 SBR operation/control, inoculation, online sensors, and batch activity assays

A 12-L suspended growth sequencing batch reactor (SBR) was fed pre-treated primary effluent at the Metropolitan Water Reclamation District of Greater Chicago Terrance J. O'Brien Water Reclamation Plant (WRP) in Skokie, Illinois, USA for 414 days. The SBR included online sensors (s::can, Vienna, Austria) for monitoring of temperature, DO, ammonium and pH every minute. The reactor was initially operated with the intent to select for mainstream suspended growth PN/A, but was transitioned over the course of reactor operation to a low DO complete nitrification reactor. Upstream treatment included primary settling tanks and a 56-L A-stage activated sludge sequencing batch reactor for COD and biological phosphorus removal. The 12-L reactor was seeded on May 24, 2016 (day 0) with ~1,800 mg/L of mixed liquor volatile suspended solids (MLVSS) suspended growth biomass from the full-scale sidestream DEMON® process at the York River treatment plant (Hampton Roads Sanitation District; HRSD) and ~200 mgVSS/L of scraped biofilm from the Kruger/Veolia Biofarm (ANITA™ Mox process) at James River, VA (equivalent to 10% of the initial VSS). The reactor was subsequently loaded with A-stage effluent (Table 5.1), temperature controlled to  $20.3 \pm 1.1^\circ\text{C}$ , and operated as a SBR to approximate plug flow reactor (PFR) behavior. Over the entire study, the average MLVSS was

$1.4 \pm 0.4$  g VSS/L and solids were not intentionally wasted from the reactor, resulting in an average SRT of  $99 \pm 44$  days (see Supporting Information for details on the SRT calculation).

**Table 5.1** Low DO nitrification reactor influent (A-stage effluent) and effluent average composition, along with primary effluent and parallel full-scale (O'Brien WRP) nitrifying activated sludge bioreactor effluent concentrations.

	Primary effluent	A-stage effluent	Reactor effluent	O'Brien effluent
TKN (mgN/L)	20.6 $\pm$ 4.4	16.5 $\pm$ 4.7	4.5 $\pm$ 2.7	1.9 $\pm$ 0.2
NH <sub>4</sub> <sup>+</sup> (mgN/L)	15.5 $\pm$ 3.6	14.3 $\pm$ 3.8	3.6 $\pm$ 2.6	0.7 $\pm$ 0.1
NO <sub>x</sub> (mgN/L)	--- <sup>a</sup> $\pm$ ---	0.5 <sup>b</sup> $\pm$ 0.7	7.2 $\pm$ 3.3	7.4 $\pm$ 2.1
COD (mgCOD/L)	141 $\pm$ 43	42 $\pm$ 32	24 $\pm$ 17	not available <sup>c</sup>
sCOD (mgCOD/L)	84 $\pm$ 21	29 $\pm$ 11	20 $\pm$ 7	not available
alkalinity (meq/L)	4.7 $\pm$ 0.5	4.6 $\pm$ 0.5	3.3 $\pm$ 0.6	not available
TSS (mg/L)	45 $\pm$ 25	15 $\pm$ 35	7 $\pm$ 8	6

<sup>a</sup>NO<sub>x</sub> in primary effluent was at or below detection limit of 0.15 mgN/L in 93% of samples

<sup>b</sup>NO<sub>x</sub> in A-stage effluent was at or below detection limit of 0.15 mgN/L in 54% of samples

<sup>c</sup>COD not measured, but BOD<sub>5</sub> in O'Brien WRP effluent =  $5.7 \pm 2.9$  mgBOD/L

SBR control of reactor equipment from inoculation to day 336 was managed with on-off circuit switching via ChronTrol programmable timers (4-circuit, 8-input XT Table Top unit, ChronTrol, San Diego, CA, USA). Sequences consisted of an initial fill + anaerobic react phase (4 - 30 minutes including 4-minute fill), an intermittently aerated react phase (240 - 270 minutes), settling (30 minutes), and decant (5 minutes). Aeration intervals were varied throughout the project depending on influent strength and aeration strategy from 1 – 2 minutes of aeration in a 2 – 30-minute interval. Target peak DO concentrations during aeration varied between 0.2 – 1.0 mgO<sub>2</sub>/L. Not including settling, the 50% volume decant resulted in a 9-hour hydraulic residence time (HRT).

Starting on day 337 and continuing to the end of the study (day 414), reactor equipment was controlled with code-based Programmable Logic Control (PLC) (Ignition SCADA software by Inductive Automation, Fulsom, CA, USA, and TwinCAT PLC software by Beckhoff, Verl,

Germany). Aeration control was switched to proportional-integral (PI) control based on the online oxygen sensor (s::can oxi::lyser™ optical probe) signal. On day 358, the length of the aerated react portion of the cycle switched from timer-based to ammonium sensor-based (s::can ammo::lyser™ ion selective electrode) control. The aerated react period ended when  $\text{NH}_4^+$  dropped to  $2 \text{ mgNH}_4^+ \text{-N/L}$ , resulting in variable HRT. Cycle phases from day 358 to day 414, the end of the study, consisted of fill (~2 minutes), anaerobic react (20 minutes), intermittently aerated react (average  $112 \pm 69$  minutes), polishing anaerobic react (20 minutes), settling (30 minutes), and decant (4.5 minutes). Not including settling and decant/fill, this resulted in a  $5.1 \pm 2.3$ -hour HRT.

Batch kinetic assays were performed to determine maximum activities of anammox, ammonia-oxidizing microorganisms (AOM), and NOB functional groups under non-limiting substrate conditions, as previously described (Laureni et al., 2016). See Supporting Information for details.

### **5.2.2 Full-scale secondary treatment at O'Brien WRP**

The bench-scale SBR described above for low DO nitrification was operated in parallel to a full-scale secondary treatment process at the O'Brien WRP consisting of one-stage conventional activated sludge in plug-flow configuration (O'Brien) targeting biochemical oxygen demand (BOD) removal and  $\text{NH}_4^+$  oxidation (nitrification). O'Brien received the same influent, or primary effluent (Table 5.1), as the A-stage to the bench-scale SBR (though in continuous feed mode vs. batch), offering a comparison point for the nitrifying community selected under similar influent but differing operating conditions. The O'Brien system was operated with an approximate average HRT of 7.3 hours, an SRT of 9.7 days, and MLVSS of 1.9 g/L. Wastewater temperature varied seasonally (low monthly average =  $11^\circ\text{C}$ , high monthly average =  $22^\circ\text{C}$ ) with

an average of 16.9°C. Aeration was provided throughout the basins (in contrast to intermittent aeration in the bench-scale reactor), and DO near the end of the basins was typically between 3 – 5 mgO<sub>2</sub>/L (in contrast to 0.2 – 1 mgO<sub>2</sub>/L in the bench-scale reactor). Average influent and effluent composition in the full-scale nitrifying activated sludge reactor is shown in Table 5.1.

### 5.2.3 Analytical methods

Total and soluble chemical oxygen demand (COD), total suspended solids (TSS), volatile suspended solids (VSS), alkalinity, total and soluble Kjeldahl nitrogen (TKN, sTKN), NH<sub>4</sub><sup>+</sup>-N, combined NO<sub>3</sub>+NO<sub>2</sub>-N (NO<sub>x</sub>-N), total phosphorus, and orthophosphate were monitored 3 to 5 times/week in influent and effluent samples, per Standard Methods (APHA, 2005).

### 5.2.4 Biomass sampling and DNA extraction

Reactor biomass was archived weekly to biweekly for PCR and sequencing-based analyses. Six 1 mL aliquots of mixed liquor were centrifuged at 10,000g for 3 minutes, and the supernatant was decanted and replaced with 1 mL of tris-EDTA buffer. The biomass pellet was then resuspended, and the aliquots were centrifuged again at 10,000g for 3 minutes and the supernatant decanted, leaving only the biomass pellet to be transferred to the -80°C freezer. All samples were kept at -80°C until DNA extraction was performed with the FastDNA SPIN Kit for Soil (MPBio, Santa Ana, CA, USA) per the manufacturer's instructions.

### 5.2.5 Quantitative PCR and comammox *amoA* cloning

Quantitative PCR (qPCR) assays were performed targeting AOB *amoA* via the *amoA*-1F and *amoA*-2R primer set (Rotthauwe et al., 1997), Nitrospira *nxB* via the 169f/638R primer set (Pester et al., 2014), comammox *amoA* via the Ntsp-*amoA* 162F/359R primer set (Fowler et al., 2018), AOA *amoA* via the Arch-*amoA*F/AR primer set (Francis et al., 2005), and total bacterial

(universal) 16S rRNA genes via the Eub519/Univ907 primer set (Burgmann et al., 2011). All assays employed thermocycling conditions reported in the reference papers, and were performed on a Bio-Rad C1000 CFX96 Real-Time PCR system (Bio-Rad, Hercules, CA, USA). Details on target genes, reaction volumes and reagents can be found in Supporting Information. After each qPCR assay, the specificity of the amplification was tested with melt curve analysis and agarose gel electrophoresis.

Comammox *amoA* genes were amplified, cloned, and sequenced on day 407 to generate standards for qPCR and confirm specificity of the comammox primer set, following previously described methods (Wells et al., 2009) (See Supporting Information for details).

#### **5.2.6 16S rRNA, *amoA*, and *nxB* gene amplicon sequencing**

16S rRNA and functional gene amplicon library preparations were performed using a two-step multiplex PCR protocol, as previously described (Griffin and Wells, 2017). All PCR reactions were performed using a Biorad T-100 Thermocycler (Bio-Rad, Hercules, CA). The V4-V5 region of the universal 16S rRNA gene was amplified in duplicate from 27 dates collected over the course of reactor operation using the 515F-Y/926R primer set (Parada et al., 2016). To characterize the overall *Nitrospira* and comammox *Nitrospira* microdiversity in the system, *Nitrospira nxB* gene amplicons were sequenced from duplicate biological samples from day 407 and comammox *amoA* gene amplicons were sequenced from duplicate biological samples of 6 time points (days 229, 262, 291, 370, 383, and 407) using primers mentioned in section 2.5 (Fowler et al., 2018; Pester et al., 2014). Further details on thermocycling conditions and primer sequences can be found in Supporting Information.

All amplicons were sequenced using a MiSeq system (Illumina, San Diego, CA, USA) with Illumina V2 (2x250 paired end) chemistry at the University of Illinois at Chicago DNA Services Facility and deposited in GenBank (accession number for raw data: PRJNA480047; also see Table 5.S2). Procedures for sequence analysis and phylogenetic inference can be found in Supporting Information.

### 5.2.7 Quantitative Fluorescence *in situ* Hybridization (qFISH)

Reactor biomass was fixed and archived biweekly to monthly for probe-based qFISH analyses, following previously described methods (Wells et al., 2017). Briefly, reactor biomass samples were fixed in a 4% formaldehyde solution for two hours at 4°C followed by storage at -20°C in a 1:1 solution of phosphate buffered saline (PBS) and ethanol. qFISH was performed to estimate the relative abundance of canonical *Nitrospira*, canonical ammonia oxidizing bacteria (AOB), putative comammox *Nitrospira*, and total bacteria (see Supporting Information and Table 5.S1 for probe sequences, staining procedure, imaging, and quantification methods).

## 5.3 Results

### 5.3.1 Bioreactor performance

The bench-scale reactor was initially assessed for its ability to remove total inorganic nitrogen (TIN) via the partial nitritation/anammox (PN/A) pathway. Effluent N concentrations over time are shown in Figure 5.1. The greatest TIN removal performance was observed in the first 77 days of operation after inoculation with sidestream PN/A biomass, where  $49 \pm 12\%$  of TIN and  $78 \pm 17\%$  of  $\text{NH}_4^+$  was removed from the reactor. A relatively low average ratio of  $\text{NO}_3^-$  production to  $\text{NH}_4^+$  removal of  $0.24 \text{ gNO}_3^- \text{-N/gNH}_4^+ \text{-N}$  during this time indicated moderate NOB suppression, as the theoretical nitritation-anammox pathway with no NOB activity produces a

ratio of 0.11 gNO<sub>3</sub><sup>-</sup>-N/gNH<sub>4</sub><sup>+</sup>-N. However, the activity and biomass of slow-growing anammox were rapidly lost from the system. Batch activity testing revealed that, by day 34, the maximum potential anammox activity had declined by 88% (Figure 5.2), and never appreciably recovered over the course of >400 days of operation. Subsequent molecular profiling demonstrated a parallel step decline in anammox abundance (described below).

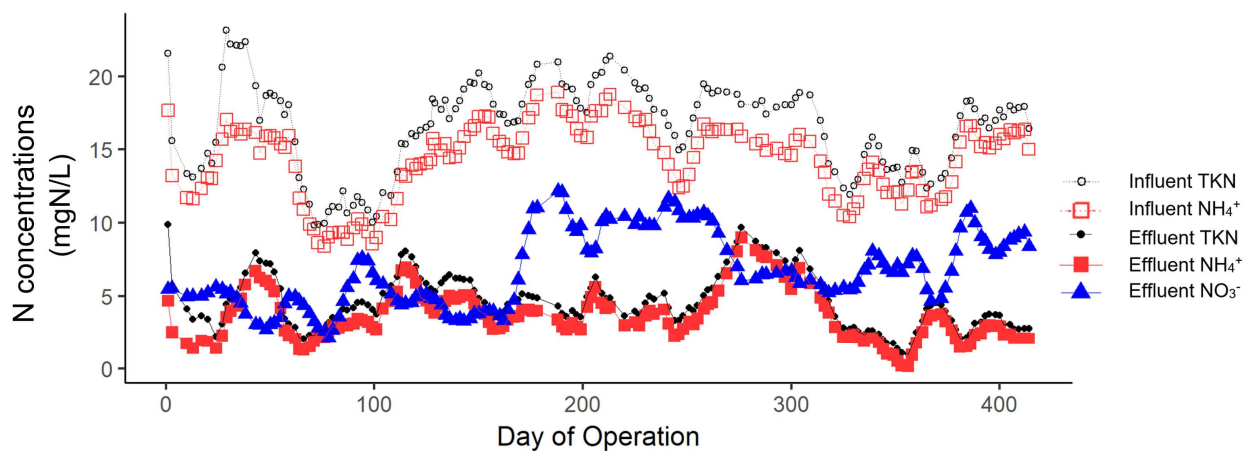


**Figure 5.1** Nitrogen concentrations in reactor influent and effluent over time. All parameters are shown as a two-week rolling average. “NO<sub>3</sub><sup>-</sup>” was measured as NO<sub>3</sub><sup>-</sup> + NO<sub>2</sub><sup>-</sup>, but weekly effluent NO<sub>2</sub><sup>-</sup> measurements revealed that NO<sub>2</sub><sup>-</sup> comprised <1% of NO<sub>3</sub><sup>-</sup> + NO<sub>2</sub><sup>-</sup> on average (max 6%).

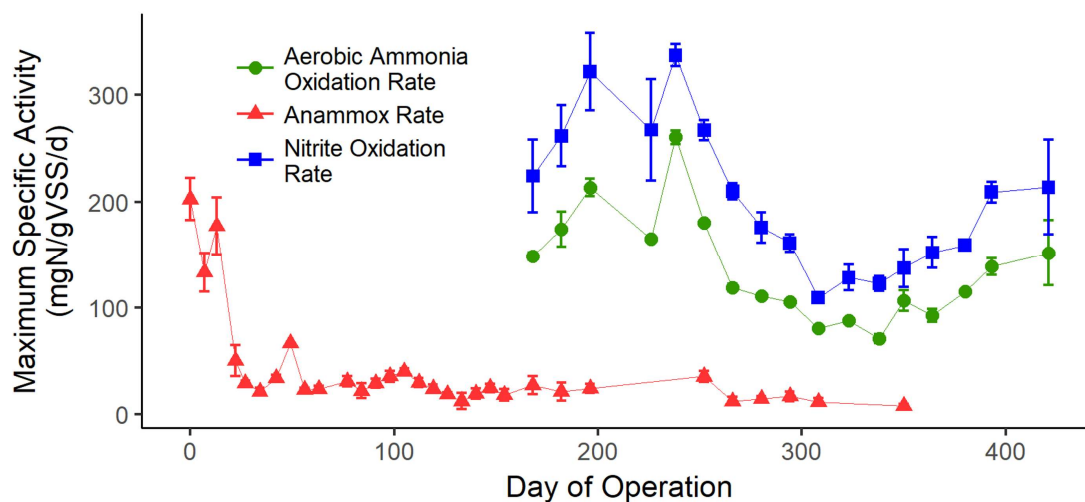


**Figure 5.2** Maximum specific activities for aerobic ammonia oxidation rate, nitrite oxidation rate, and anaerobic ammonia oxidation (anammox) rate in reactor biomass over time from batch assays. Rates were measured under non-limiting substrate concentrations.

Loss of anammox activity and abundance coincided with a decrease in TIN removal, but high rate complete  $\text{NH}_4^+$  oxidation was maintained in the presence of low DO with intermittent aeration. Between day 77 and the end of the study (day 414), TIN removal was  $21 \pm 19\%$ , less than half of that of the initial 77 days. During the same time period (day 78-414),  $\text{NH}_4^+$  removal did not decrease significantly, and averaged  $74 \pm 17\%$ . The length of intermittent aeration intervals was adjusted with changes in influent strength during this time period, and varied between 1 to 2 minutes of aeration in 2 to 30-minute intervals. Target peak DO was between 0.2 – 1.0  $\text{mgO}_2/\text{L}$ . This aeration strategy was originally chosen as a hypothesized means to suppress NOB activity and therefore achieve (partial) nitrification (Gilbert et al., 2014a). However, complete nitrification of  $\text{NH}_4^+$  to  $\text{NO}_3^-$ , rather than nitrification of  $\text{NH}_4^+$  to  $\text{NO}_2^-$ , was consistently achieved from days 78-414.  $\text{NO}_2^-$  accumulation in the effluent was not observed throughout the study, with average effluent  $\text{NO}_2^-$  of  $0.07 \pm 0.04 \text{ mgNO}_2^-/\text{N/L}$  (less than 1% of total effluent

$\text{NO}_2^- + \text{NO}_3^-$ ). Maximum aerobic  $\text{NH}_4^+$  oxidation and  $\text{NO}_2^-$  oxidation rates were first measured on day 168, and revealed a greater  $\text{NO}_2^-$  oxidation rate (Figure 5.2). This was consistently maintained throughout the experimental period, with an average ratio of 1.5:1 maximum  $\text{NO}_2^-$  oxidation to  $\text{NH}_4^+$  oxidation rate.

The bench scale low DO nitrifying SBR was operated in parallel to a full-scale conventional high DO nitrifying activated sludge bioreactor at the O'Brien WRP, offering an opportunity to compare performance characteristics between these systems. The O'Brien WRP achieved lower average effluent  $\text{NH}_4^+$  values of  $0.7 \pm 0.1 \text{ mgNH}_4^+ \text{-N/L}$  compared to  $3.6 \pm 2.6 \text{ mgNH}_4^+ \text{-N/L}$  for the bench-scale low DO reactor (Table 5.1), in large part because a high effluent  $\text{NH}_4^+$  residual was intentionally selected for the bench-scale system as a putative NOB out-selection strategy (Regmi et al., 2014) for PN/A operation. When the bench-scale reactor HRT was fixed at 9 hours from days 0 – 366, the  $\text{NH}_4^+$  loading and removal rate was greater in the full-scale system ( $\sim 42$  and  $40 \text{ mgNH}_4^+ \text{-N/L/d}$ , respectively) than in the bench scale system ( $40.1$  and  $28.8 \text{ mgNH}_4^+ \text{-N/L/d}$ , respectively). However, once PLC control of HRT was implemented on day 358, the average  $\text{NH}_4^+$  removal rate of  $58.6 \text{ mgNH}_4^+ \text{-N/L/d}$  in the bench-scale reactor exceeded that of the full-scale high DO system ( $\sim 38 \text{ mgNH}_4^+ \text{-N/L/d}$ ) from days 358 – 414. This was despite operation at significantly lower DO; the bench-scale reactor utilized intermittent aeration with a peak DO of  $\sim 1 \text{ mgO}_2/\text{L}$  (effectively ranging between 0 and  $1 \text{ mgO}_2/\text{L}$  throughout the react period), while the full-scale system utilized constant aeration with DO ranging from  $0 \text{ mgO}_2/\text{L}$  at the beginning to  $3 - 5 \text{ mgO}_2/\text{L}$  at the end of the aeration basins. The temperature of the bench-scale reactor during days 358 – 414 was only slightly higher than the full-scale system:  $20.8 \pm 0.8^\circ\text{C}$  vs.  $18.8 \pm 1.5^\circ\text{C}$ , respectively.

### 5.3.2 16S rRNA gene sequencing demonstrates strong enrichment of *Nitrospira* and decline in AOB

Results from 16S rRNA amplicon gene sequencing analyses over the course of reactor operation demonstrated a decline of anammox (which included all OTUs affiliated with the genus *Brocadia*; no other anammox genera were detected) relative abundance from 4% of total amplicons on day 13 to less than 0.1% by day 161 (Figure 5.3). This decline paralleled the rapid decline in maximum anammox activity (Figure 5.2) and TIN removal (Figure 5.1) in this system. While NOB abundance was expected to exceed that of AOM based on the maximum activity ratio (Figure 5.2) and the lack of a  $\text{NO}_2^-$  residual, 16S rRNA gene sequencing revealed an unexpected strong declining trend of canonical betaproteobacterial AOB (OTUs affiliated with the genus *Nitrosomonas*; no *Nitrospira*, AOA, or gammaproteobacterial AOB were detected) from 4.4% of total reads on day 3 to 0.8% of total reads by day 407, while putative NOB (which included only OTUs affiliated with the genus *Nitrospira*; *Nitrobacter* and *Nitrotoga* were not detected, and *Nitrolancea* was  $<0.2\%$  for all time points) steadily climbed from 3.1% of total reads on day 3 to an unusually high 53% of reads on day 407 (Figure 5.3). By clustering the *Nitrospira*-affiliated 16S rRNA gene sequences at the identity cutoff of 97%, the micro-diversity of the *Nitrospira* in the community appeared to be very low: just two OTUs (OTU2 and OTU4) contributed 95.4 – 99.8% (depending on time point) of all *Nitrospira* 16S rRNA gene amplicons. Around day 100 the less abundant of these two, OTU2, began to accumulate (Figure 5.3) and by day 407 accounted for 92% of total NOB and 49% of total 16S rRNA reads. This trend coincided with the strong decrease in canonical AOB abundance (Figure 5.3).

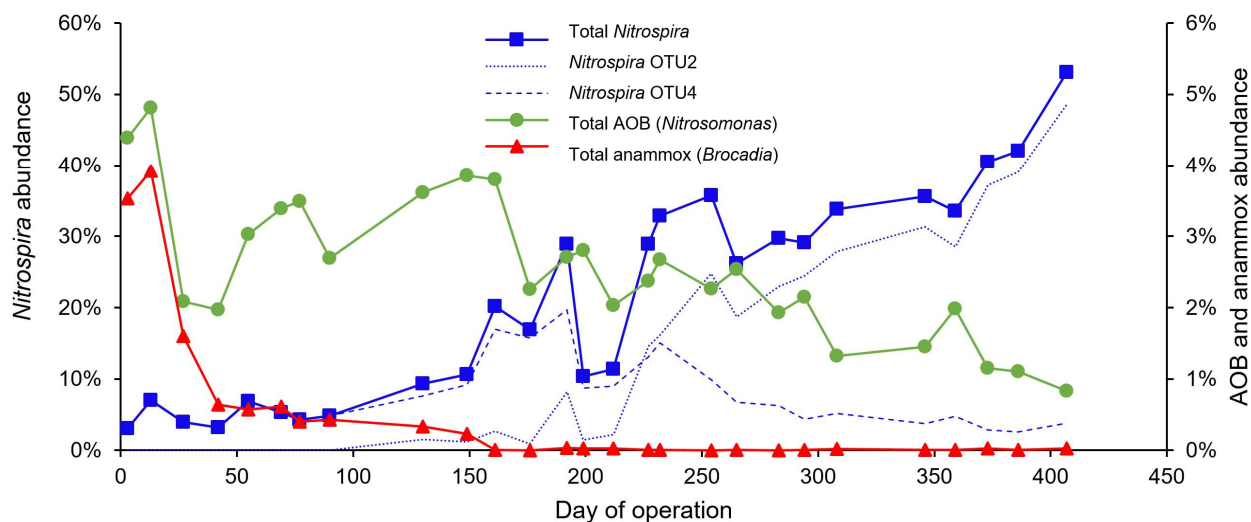


**Figure 5.3** Relative abundance of total *Nitrospira*, total AOB (all *Nitrosomonas*) and total anammox (all *Brocadia*), based on 16S rRNA gene amplicon sequence analysis. Relative abundance for *Nitrospira* is shown on the left y-axis, and AOB and anammox are shown on the right y-axis. *Nitrospira* OTU2 and OTU4 together comprise 95.3 – 99.8% of total *Nitrospira* for all time points.

Taken together, these patterns of relative abundance of *Nitrospira* and AOB-affiliated OTUs in 16S rRNA gene sequencing datasets led us to hypothesize the accumulation of comammox *Nitrospira* due to the consistent high ammonia oxidation activity and complete nitrification in the reactor. Moreover, for the period that maximum aerobic ammonia oxidation rates were measured (days 168 – 414), the average ratio of relative abundance of *Nitrospira* to canonical AOB was 19:1 according to 16S rRNA gene amplicon sequencing results, much higher than the aforementioned 1.5:1 maximum nitrite oxidation: ammonia oxidation rate. This finding reaffirmed the hypothesis that comammox may play a dominant role in ammonia oxidation in this low DO nitrification reactor. This hypothesis was further reinforced by a closer investigation of the phylogenetic affiliation of the amplicon sequence variants (ASV) in *Nitrospira* OTU2 and

OTU4 (Figure 5.S3), which suggested that ASV within OTU2 were phylogenetically affiliated with the 16S rRNA gene of *Ca. Nitrospira nitrosa*.

### 5.3.3 Functional gene quantification reveals dominance of comammox over canonical AOB

The presence or abundance of comammox *Nitrospira* cannot be resolved from 16S rRNA gene amplicon sequencing alone (Daims et al., 2015; Lawson and Lückner, 2018), and the unusually abundant *Nitrospira* population warranted the use of better tools for functional group quantification. For this purpose, qPCR was used to quantify comammox (targeting *amoA*), canonical AOB (*amoA*), total *Nitrospira* (*nxB*), and total bacteria (16S rRNA). Ammonia oxidizing archaea were also investigated via endpoint and qPCR targeting archaeal *amoA* genes, but were not detected on any samples dates based on the lack of detection or target bands in gel electrophoresis of qPCR products. *Nitrobacter* and *Nitrotoga* NOB were absent from 16S rRNA gene sequencing analysis and thus were not investigated with qPCR.

qPCR measurements confirmed broad NOB and AOB trends observed in the 16S rRNA gene sequencing results (Figure 5.4). Based on qPCR results, the average ratio of total *Nitrospira* to AOB for days 168 – 414 was 66:1 (*Nitrospira nxB*: AOB *amoA*), higher than the 19:1 ratio from 16S rRNA gene sequencing and the 1.5:1 ratio from maximum activity tests. The relative abundance of total *Nitrospira* based on qPCR measurements (*Nitrospira nxB* normalized to total bacterial 16S rRNA genes) increased over time to 55% on day 407, confirming trends and the surprisingly high total *Nitrospira* relative abundance we observed in 16S rRNA gene sequencing datasets at this time point (53%).

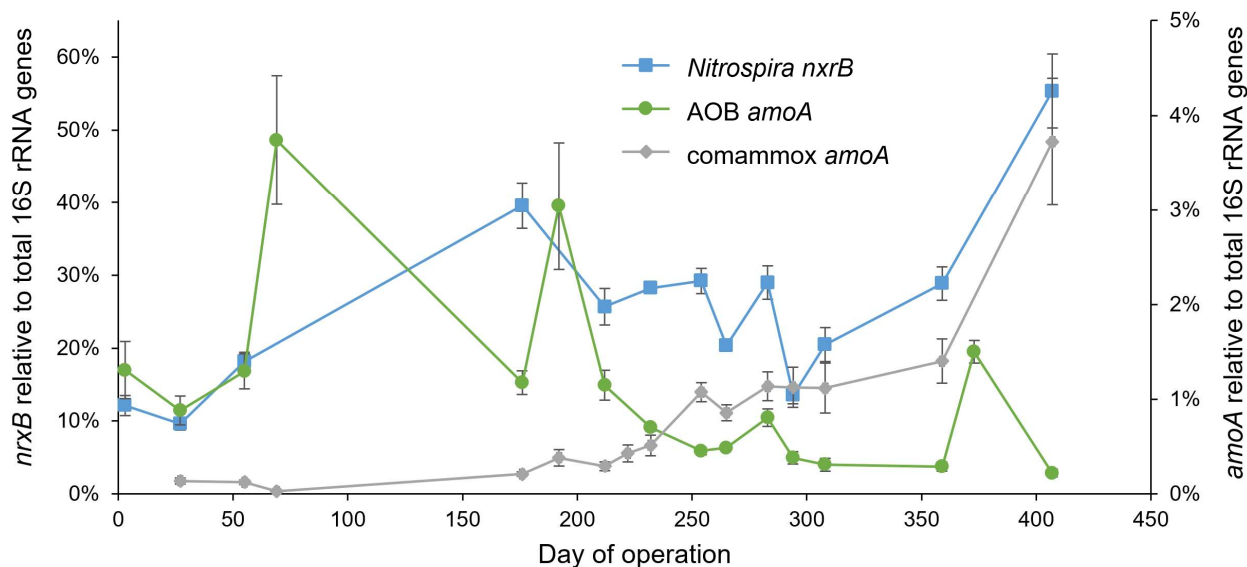


**Figure 5.4** Abundance of *Nitrospira nxrB* (squares), AOB *amoA* (circles), and comammox *amoA* (diamonds), as measured by qPCR. Results are normalized to total bacterial 16S rRNA gene copies. *Nitrospira* results are shown on the left y-axis, and AOB and comammox results are shown on the right y-axis.

Based on qPCR measurements, comammox was the dominant ammonia oxidizer from days 254 - 414 of reactor operation, with an average 79% of total *amoA*. By day 407, comammox comprised 94% of all detected *amoA*. qPCR measurements targeting comammox *amoA* revealed an increasing abundance in comammox *Nitrospira* beginning around day 222 (Figure 5.4), and a concurrent decline in AOB *amoA* abundance.

This increasing abundance of comammox *Nitrospira* coincided closely with the increase in the *Nitrospira* OTU2 from 16S rRNA gene sequencing (Figure 5.3), though the relative abundances did not match, suggesting that *Nitrospira* microdiversity was more complex than the two dominant *Nitrospira* OTUs (97% identity) documented via analysis of 16S rRNA gene sequence data. While *Nitrospira* OTU2 from 16S rRNA gene sequencing data accumulated to 49% of total reads by day 407, comammox *amoA* accumulated to just 4% of total bacteria when

measured relative to total bacterial 16S rRNA genes via qPCR. Interestingly, between days 254 and 414 of reactor operation, comammox *amoA* reads averaged just 5% relative to total *nxrB* reads. This result suggests that while comammox *Nitrospira* were the putative dominant ammonia oxidizers in this system (based on abundance relative to canonical AOB), a large fraction of the total *Nitrospira* community was incapable of comammox metabolism.

To verify specificity of comammox *amoA* primers and generate associated qPCR standards, three clones were generated from comammox *amoA* PCR products, sequenced, and phylogenetically analyzed. This analysis was employed for an initial assessment of relationship of comammox in this system to known comammox taxa. The results confirmed that all three clones affiliated with comammox *amoA* genes of comammox clade A and were most closely related to *Candidatus N. nitrosa* (van Kessel et al., 2015) and *Nitrospira* sp. UW LDO 01 (Camejo et al., 2017) (Figure 5.5b).

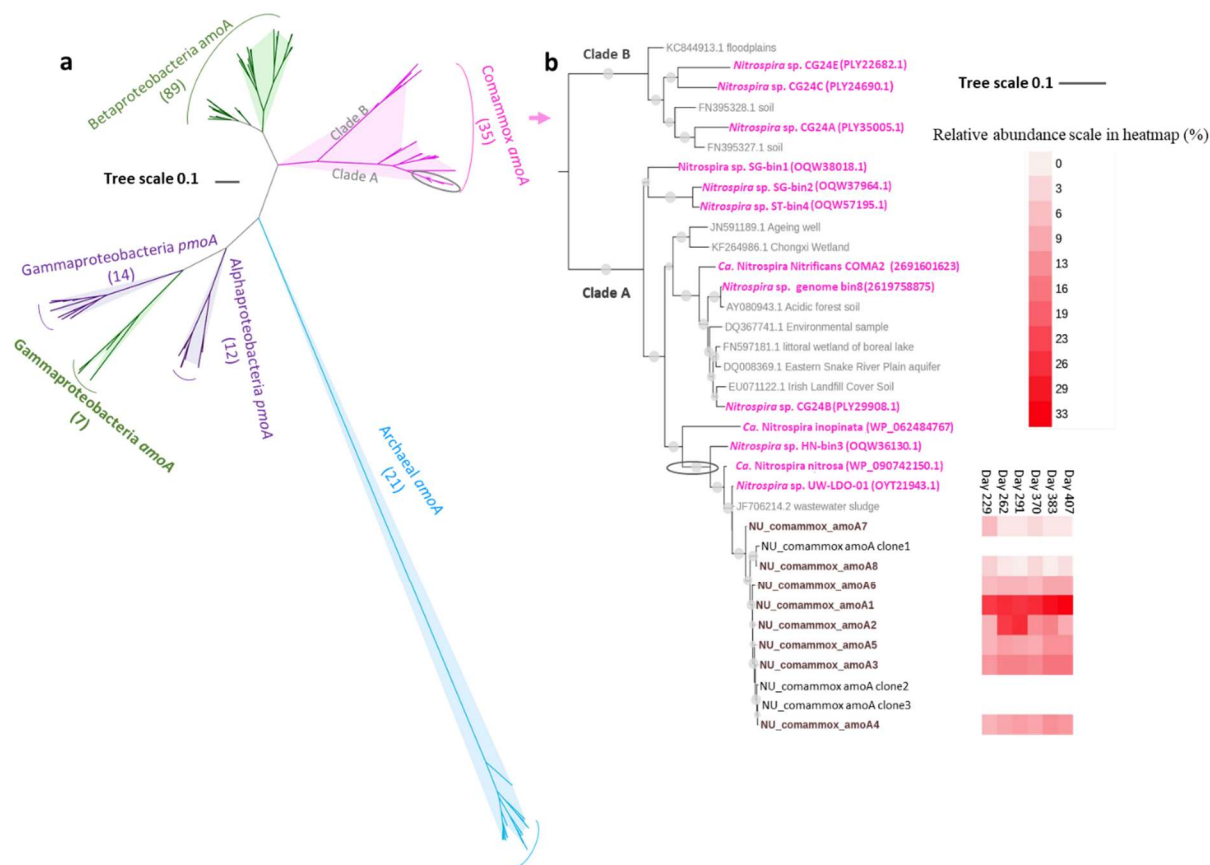


**Figure 5.5** Phylogenetic affiliation of comammox *amoA* gene sequences from the low DO nitrification reactor via cloning and sanger sequencing and via high throughput amplicon sequencing (173 bp fragment). Scale bars indicate estimated change per nucleotide sequence. a) Maximum likelihood tree showing the phylogenetic relationship of the 3 clone sequences and 8 amplicon sequence variants (ASV) from sequencing (circled in above tree) with other *amoA* gene superfamily members (167 sequences). b) Maximum likelihood tree showing phylogenetic relationship between the 3 comammox *amoA* clone sequences and 8 comammox *amoA* ASV from amplicon sequencing (black, names beginning with NU\_comammox) with NCBI database-derived comammox *amoA* gene sequences. The *amoA* gene from *Nitrosococcus watsonii* C-113 was applied as the outgroup. The heatmap indicates the relative abundance of the 8 comammox *amoA* ASV we detected in reactor biomass at the six time-points. Genome-derived comammox *amoA* genes are in magenta and other database-derived comammox *amoA* genes are in light gray. Nodes with the bootstrap value > 70% have all been marked with a gray circle, and the size of the circle is in positive correlation with the bootstrap value.

### 5.3.4 qFISH confirms *Nitrospira* enrichment

qFISH measurements of reactor biomass from three sample dates was used as a check on the trends and functional group abundances as observed by qPCR. The trend of the increasing ratio of NOB:AOB was confirmed; this ratio increased from 0.8:1 on day 35 to 15:1 on day 398 (Figure 5.6). A composite ratio reveals an enrichment of NOB from < 1% on day 35 to 35% of the overall bacterial community on day 398. This result confirms the strong increasing trend in total NOB documented via both 16S rRNA gene sequencing and qPCR analyses.

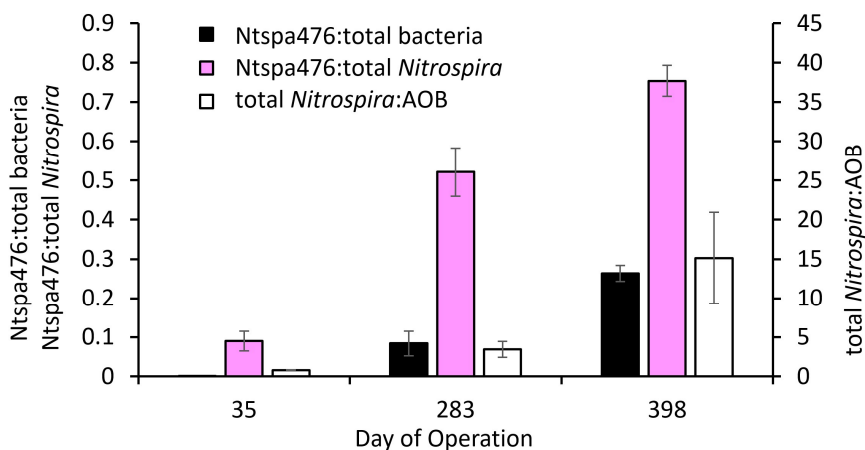


**Figure 5.6** qFISH results of Ntspa476 probe (see text section 3.4 and (van Kessel et al., 2015), total *Nitrospira*, total AOB, and total bacteria. See Supporting Information regarding the specificity of the Ntspa476 FISH probe to comammox.

The FISH probe Ntspa476 utilized in this study was previously developed to target putative comammox *Ca. N. nitrosa* and *Ca. N. Nitrificans* (van Kessel et al., 2015). The specificity and coverage of this probe set to our specific system was evaluated before conducting the qFISH assays (see Supporting Information). In brief, our analysis suggests that the probe is not capable of reliably resolving comammox from conventional nitrite-oxidizing *Nitrospira*; the inability of 16S rRNA gene-based methods to do so has been raised before (Lawson and Lückner, 2018). However, our analysis suggests that Ntspa476 targets a subset of lineage II *Nitrospira* that includes known comammox. 75% of the total *Nitrospira* on day 398 hybridized with Ntspa476 (Figure 5.6), substantially higher than the results of the qPCR analysis for comammox, which show 7% on day 407 as a fraction of total *nxrB* (Figure 5.4). These results and the analysis in Supporting Information suggest that a portion of *Nitrospira* targeted by Ntspa476 and prevalent in this reactor are non-comammox *Nitrospira*. The function of the surprisingly high abundance and putatively non-comammox *Nitrospira* taxa in this reactor warrants further investigation.

### 5.3.5 Functional gene sequencing

As described above, 16S rRNA gene sequencing suggested that a single OTU dominated the *Nitrospira* community by day 407 (Figure 5.3), while qPCR demonstrated that comammox comprised 7% of the *Nitrospira* community at this time point (Figure 5.4). To better resolve microdiversity within the *Nitrospira* community, *nxrB* functional gene sequencing was performed on the sample from day 407. 22,440 total *nxrB* sequences were generated from which 30 amplicon sequence variants (ASV) were identified with DADA2 (Callahan et al., 2016). The resulting *nxrB* phylogenetic tree (Figure 5.7) confirms that the *nxrB* gene cannot be reliably applied to distinguish comammox from canonical *Nitrospira* (i.e. see the top branch of Figure

5.7 for interspersed comammox and canonical *Nitrospira*; also see (Lawson and Lückner, 2018), but still offers insight into the diversity of the *Nitrospira* community. 15% of the *Nitrospira nxrB* sequences clustered with the *nrxB* gene in the comammox genomes of *Ca. N. nitrosa* and *Nitrospira* sp. UW LDO 01. Another 37% of *nrxB* sequences clustered with genomes of the canonical NOBs *Nitrospira defluvii* and *Nitrospira* sp. Strain ND1, of which two strains have been reported with a microaerophilic or hypoxic ecological niche (Lucker et al., 2010; Ushiki et al., 2017). Two additional clusters of *nrxB* sequences accounting for 10% and 38% of the total *nrxB* amplicons do not affiliate with currently available genomes, but a blast search in NCBI returned three sequences (indicated with “[*accession #*] activated sludge” labels in Figure 5.7) with 92 – 98% identity to the *nrxB* genes in these two clusters.

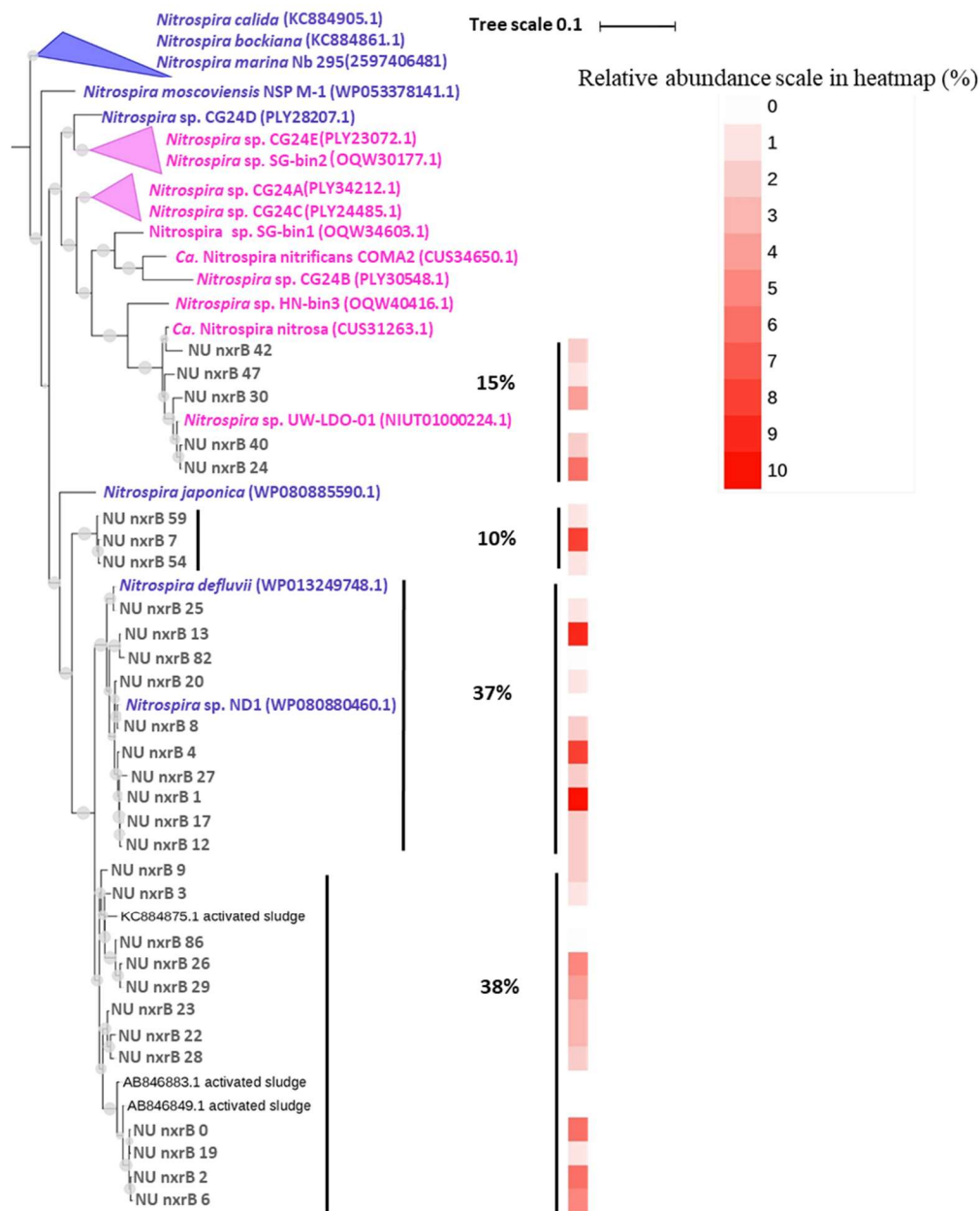


**Figure 5.7** Maximum-likelihood phylogenetic tree of *Nitrospira nxrB* gene sequences (453 bp fragment). The *nrxB* gene from *Nitrobacter hamburgensis* X14 was applied as the outgroup. Nodes with the bootstrap value > 70% have all been marked with a gray circle, and the size of the circle is in positive correlation with the bootstrap value. 30 *nrxB* ASV recovered in this study on day 407 of reactor operation are shown in bold as “NU nxrB ###”. In magenta are *nrxB* genes from known comammox *Nitrospira* genomes, and in purple are *nrxB* genes of known non-comammox *Nitrospira* genomes. Percentages to right of the tree indicate relative abundance of *nrxB* clusters relative to total *nrxB* in the low DO nitrification reactor. The red to white heatmap indicates the percentage of each NU nxrB ASV relative to the overall *Nitrospira* in the reactor.

No *nxB* genes from currently available genomes cluster with the 10 and 38% abundance NU *nxB* clusters, so the three closest non-genome database sequences are shown as “[*accession #*] activated sludge”.

Functional gene sequencing of the *amoA* gene of comammox *Nitrospira* on 6 sampling points from days 229 – 407 generated between 28,194 and 57,637 (depending on the time point) total *amoA* sequences from which 217 ASV were identified, and 8 of them accounted for 94 – 99% of the total. Phylogenetic analysis revealed that these 8 sequences cluster within comammox Clade A (see “NU\_comammox\_amoA” samples in Figure 5.5b). The close association of the comammox population in the low DO nitrification SBR with *Nitrospira* sp. UW LDO 01 (Camejo et al., 2017) and *Ca. Nitrospira nitrosa* (van Kessel et al., 2015) suggested by *nxB* sequencing (Figure 5.7) and sequencing of clones generated as qPCR standards (Figure 5.5b) was confirmed by this high throughput comammox *amoA* sequence analysis.

#### 5.4 Discussion

In this study, comammox *Nitrospira* were observed to accumulate over time in a low DO nitrification reactor treating mainstream municipal wastewater to eventually become the numerically dominant ammonia oxidizer as confirmed by sequencing, qPCR, and microscopy-based methods. This counters the prevailing assumption that comammox play a minor role in wastewater treatment bioreactors (Annavaiah et al., 2018; Gonzalez-Martinez et al., 2016). At least two previous studies have challenged this same assumption. In the original publication of the discovery of *N. inopinata* (Daims et al., 2015), metagenomic analysis revealed that comammox comprised 43 to 71% of the total *Nitrospira* population at the WWTP of the University of Veterinary Medicine in Vienna, Austria. A subsequent effort to develop

comammox-specific *amoA* qPCR primers revealed comammox at the same plant as comprising 14 to 35% of total *amoA* via qPCR (Pjevac et al., 2017), still a minority of the overall  $\text{NH}_4^+$  oxidizing community. In a separate study, while developing a bench-scale biological nutrient removal reactor with synthetic feed, researchers at the University of Wisconsin-Madison serendipitously enriched comammox to 38% of total *Nitrospira*, or 5.4% of total normalized metagenomic reads during the first stage of operation (Camejo et al., 2017). Comammox were far more abundant than AOA and AOB in this stage (which together comprised just 0.23% of total reads), suggesting that comammox was the dominant  $\text{NH}_4^+$  oxidizer. The enrichment was transient, however, as subsequent sampling revealed its absence, and was associated with synthetic rather than real wastewater feed.

Significantly, this study is the first to show comammox as the dominant  $\text{NH}_4^+$  oxidizer in a reactor using actual wastewater as influent, demonstrating that comammox may play an important role in biological nutrient removal systems in practice under certain conditions. Comammox *Nitrospira* was not detected in the parallel O'Brien WRP full-scale high DO nitrifying activated sludge system, indicating that operating parameters such as low DO and high SRT may be important for their selection. Of the two studies that have found comammox to (at least transiently) dominate the ammonia oxidizing community of a biological nutrient removal reactor – the present study and (Camejo et al., 2017), both of which selected for closely related comammox strains within Clade A – a few key similarities between the two SBRs stand out:

- Low in-reactor N concentrations: 0 – 12 mgN/L of  $\text{NH}_4^+$ ,  $\text{NO}_3^-$ , and  $\text{NO}_2^-$  (Camejo et al., 2017), and 0 – 14 mgN/L of  $\text{NH}_4^+$  and  $\text{NO}_3^-$ , 0 – 0.2 mgN/L of  $\text{NO}_2^-$  (present study)

- Low DO: 0 – 0.4 mgO<sub>2</sub>/L with constant aeration (Camejo et al., 2017), and 0 – 1.0 mgO<sub>2</sub>/L with intermittent aeration (present study)
- Very high average SRT: 80 days (Camejo et al., 2017) and 99 days (present study)

The above observations may help explain the low abundance of comammox measured to date in conventional activated sludge reactors, as such systems typically operate at high DO (> 3 mgO<sub>2</sub>/L) and moderate sludge ages (< 20 days) (Annavaajhala et al., 2018; Gonzalez-Martinez et al., 2016). However, the same observations are potentially unfavorable for applications targeting shortcut N removal processes, including PN/A. Low DO and high SRT are required to retain anammox activity and biomass in PN/A systems, but our results suggest that these conditions may inadvertently select for comammox when applied to the relatively low N concentrations typical of mainstream wastewater. However, while any NO<sub>2</sub><sup>-</sup> oxidation is considered unfavorable in PN/A systems, it is possible that the presence of comammox may still be compatible with their operation. Transient NO<sub>2</sub><sup>-</sup> accumulation produced by *N. inopinata* during oxidation of NH<sub>4</sub><sup>+</sup> has been observed (Daims et al., 2015; Kits et al., 2017), and FISH imaging revealed comammox *Candidatus N. nitrificans* and *Candidatus N. nitrosa* in co-aggregation with *Brocadia*-affiliated anammox (and in the absence of canonical AOM) (van Kessel et al., 2015). While this implies that comammox may be compatible with well-functioning PN/A systems, such systems may require a more careful control of redox conditions to ensure that reduction of NO<sub>2</sub><sup>-</sup> by anammox is favored over NO<sub>2</sub><sup>-</sup> oxidation by comammox or canonical NOB. Further studies involving the coordinated activity and cross-feeding of comammox and anammox will be required to better delineate these conditions.

In contrast, there are no obvious disadvantages to the presence of comammox in low DO nitrification systems, as in the present study. In fact, comammox may be especially suited to systems targeting very low effluent  $\text{NH}_4^+$  levels due to their high substrate affinity (Kits et al., 2017). In the present study, the  $\text{NH}_4^+$  oxidation rate in the bench-scale reactor exceeded that of the full-scale system when variable HRT was utilized on days 358 – 414, despite operation at much lower DO. This suggests that comammox *Nitrospira* may be well-suited to energy-efficient methods for complete ammonia oxidation, and thus offer an alternative to high-DO conventional nitrification systems. Low DO systems for nitrification have been shown to save up to 25% in energy use over conventional, high-DO systems (Keene et al., 2017) without sacrificing process stability (Fitzgerald et al., 2015; Park and Noguera, 2007, 2004).

#### **5.4.1 High NOB to AOM ratios**

A discrepancy between nitrite and ammonia oxidation rates and nitrite and ammonia oxidizing organism abundance in nitrifying activated sludge biomass, as in this study, has been observed before (Fitzgerald et al., 2015; Schramm et al., 1999; Wang et al., 2015). Wang et al. observed NOB:AOM ratios of anywhere from 9:1 to 5000:1 in five activated sludge reactors as measured by qPCR, and Schramm et al. observed an average NOB:AOM ratio of 24:1 on the surface of biomass aggregates as measured by FISH. *Nitrospira* was the most abundant NOB in both studies. Other researchers have speculated that undetected comammox *Nitrospira* may fill this gap (Daims et al., 2015), but even in this study, their presence does not fully explain the difference as measured by qPCR, as non-comammox *Nitrospira* still comprised ~50% of total bacteria by day 407, with an NOB: AOM ratio of about 14:1 on day 407 if comammox *Nitrospira* are counted as both NOB and AOM.

The most common explanations for high NOB:AOM ratios are (1) oversimplification of the metabolic versatility of NOB, particularly for *Nitrospira*, and (2) under-estimation of AOM.

With regards to explanation (1), the *Nitrospira* genus displays an impressive diversity in terms of metabolic capabilities (Daims et al., 2016; Koch et al., 2015). Koch et al. showed that *Nitrospira moscoviensis* contains genes encoding for urease and formate dehydrogenase, the latter of which need not be tied to nitrite oxidation. Daims et al., in their review of *Nitrospira* metabolic versatility, pointed out that *Nitrospira* are also capable of oxidizing hydrogen gas under oxic conditions and reducing  $\text{NO}_3^-$  in the presence of simple organics under anoxic conditions. Given this versatility, a portion of *Nitrospira* may not be oxidizing  $\text{NO}_2^-$  as their primary energy source. Additionally, NOB may proliferate in the presence of a nitrite oxidation/nitrate reduction loop in conjunction with heterotrophs (Winkler et al., 2012), facilitated by oxic-anoxic zones in space or time, as with intermittent aeration in the present study.

Fitzgerald et al. (Fitzgerald et al., 2015) suggest scenarios for the latter explanation (2), that AOM abundance may be underestimated. In a study of low DO nitrification systems, one nitrification reactor contained no known AOM despite the presence of complete nitrification to  $\text{NO}_3^-$ . Through batch experiments on pure culture isolates from the reactor they demonstrated  $\text{NH}_4^+$  removal beyond typical assimilation for five organisms previously not known to oxidize  $\text{NH}_4^+$ . The researchers suggest that heterotrophic nitrification may be especially important for low DO systems. It should also be noted that it is possible that currently available comammox *amoA* primers may underestimate comammox abundance.

Understanding of the relevance of comammox to diverse BNR systems is clearly in early stages, and diverse research questions remain. Looking forward, a key need for nutrient removal

researchers is for better specificity of maximum activity tests as performed in this study. Aerobic ammonia and nitrite oxidation as measured give a reasonable estimate of total potential oxidation rates, but do not distinguish between the activity of canonical AOM and comammox *Nitrospira*. Better delineation of *in situ* activities of key functional groups is needed to characterize these systems and could begin with measurements of gene expression within cycles.

## 5.5 Conclusions

- Comammox *Nitrospira* dominated the ammonia oxidizing community in a mainstream nitrification reactor fed with real municipal wastewater for >400 days. By the end of reactor operation, comammox *Nitrospira* accounted for 94% of the AOM community. This counters the notion that comammox are not relevant to wastewater treatment technologies.
- Efficient nitrification was demonstrated at low DO concentrations of 0.2 – 1.0 mg/L via intermittent aeration. Volumetric ammonium removal rates averaged 58.6 mgN/L-d during the final two months of operation when comammox abundance was particularly high. These rates were higher than in a parallel full-scale high DO (3-5 mg/L) nitrifying conventional activated sludge reactor, suggesting the potential for an energy-efficient and comammox-driven low DO alternative to conventional high-DO nitrification processes.
- *Nitrospira* increased in abundance during reactor operation to 53% of the overall microbial community. The presence of comammox does not fully explain the observed very high abundance nor high ratios of *Nitrospira* to AOM. Further research is needed to investigate the metabolic versatility within the *Nitrospira* genus and functional importance to reactor operation.
- Operational conditions (low DO, low  $\text{NH}_4^+$ , and high SRT) in this reactor mirror those commonly used or undergoing testing in mainstream partial nitrification/anammox reactors, suggesting that efforts to cultivate shortcut N removal bioprocesses in the mainstream may inadvertently select for comammox. These results further indicate that comammox may play an increasingly important role in low DO nutrient removal biotechnologies.

## 5.6 Supporting Information

### 5.6.1 Methods

#### 5.6.1.1 SRT calculation

No intentional wasting occurred throughout the study, so the average ( $\pm$  standard deviation) solids retention time (SRT) of  $99 \pm 44$  days was determined by effluent solids losses and reactor mixed liquor sampling. Effluent solids losses were minimized by 26-L downstream clarifiers which were used to return effluent solids to the reactor. Samples for effluent solids measurements were therefore sampled from the overflow of these clarifiers. SRT as discussed in this manuscript was calculated with the following formula:

$$SRT = \frac{X_R V}{X_E Q_E + X_R Q_S} \quad (Eq. 1)$$

$SRT$  = Solids retention time

$X_R$  = Suspended solids concentration in the reactor

$V$  = Volume of reactor

$X_E$  = Suspended solids concentration in clarifier overflow

$Q_E$  = Effluent flow rate

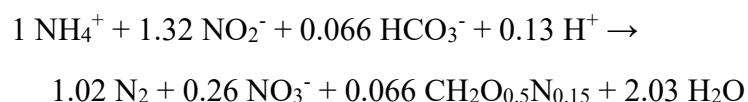
$Q_S$  = Sampling “flow rate,” i.e. volume & frequency of mixed liquor sampled from reactor

#### 5.6.1.2 Batch maximum activity assays

Batch kinetic assays were performed to determine maximum activities of anammox, ammonia-oxidizing microorganisms (AOM), and NOB functional groups under non-limiting substrate conditions, as previously described (Laureni et al., 2016). Anammox maximum activity

tests were performed *in situ* at the end of reactor cycles when sCOD was at a minimum to avoid potential interference from denitrifiers.  $\text{NH}_4^+$  and  $\text{NO}_2^-$  were spiked to non-limiting conditions (approximately 15 mgN/L each) via ammonium chloride and sodium nitrite salt solutions and the reactor was mixed without aeration. Five to six grab samples were taken in 30-minute intervals and analyzed for  $\text{NH}_4^+$ ,  $\text{NO}_2^-$  and  $\text{NO}_3^-$  by colorimetry (APHA, 2005).

According to stoichiometry from Strous et al. (Strous et al., 1998), the anammox metabolic pathway removes N (as nitrogen gas + biomass) at a ratio of 2.05 moles N per mole  $\text{NH}_4^+$  removed:



Anammox activity as N removal (in mg N/L/d) was therefore calculated as 2.05 times the slope of the  $\text{NH}_4^+$  drawdown curve. Only linear trends with  $R^2$  values above 0.8 were used. Stoichiometric ratios of  $\text{NO}_2^-$  drawdown and  $\text{NO}_3^-$  production to  $\text{NH}_4^+$  drawdown was checked against anammox stoichiometry to check that anammox was the dominant metabolic pathway in these batch assays.

AOM and NOB maximum activity assays were performed *ex situ* in duplicate 500-mL Erlenmeyer flasks, each containing 250 mL of mixed liquor. The flasks were placed on a shaker table with a water bath for temperature control between 19 – 21°C. DO was monitored with a Hach LDO<sup>®</sup> optical DO probe and were maintained at or above 3 mgO<sub>2</sub>/L by shaking action and bubbling from small aquarium pumps. pH was monitored with the Hach PHC101<sup>®</sup> electrode and maintained between 7 and 8.  $\text{NH}_4^+$  and  $\text{NO}_2^-$  were spiked to non-limiting conditions (~20 mgNH<sub>4</sub><sup>+</sup>-N/L and ~10 mgNO<sub>2</sub><sup>-</sup>-N/L), and five grab samples were taken in 20-minute intervals and analyzed for  $\text{NH}_4^+$ ,  $\text{NO}_2^-$  and  $\text{NO}_3^-$  by colorimetry (APHA, 2005).

For *ex situ* assays, AOM activity was taken as the slope of the  $\text{NH}_4^+$  drawdown curve, and NOB was taken as the average of the (1) slope of the  $\text{NO}_3^-$  production curve and (2) the sum of the slopes of  $\text{NH}_4^+$  and  $\text{NO}_2^-$  drawdown curves. Only linear trends with  $R^2$  values above 0.8 were used.

#### 5.6.1.3 qPCR gene targets, supermix and reaction conditions

qPCR gene targets included the AOB *amoA* gene (encoding the alpha subunit of ammonia monooxygenase in AOB) via the *amoA*-1F and *amoA*-2R primer set (Rotthauwe et al., 1997), the *Nitrospira nxrB* gene (encoding the beta subunit of nitrite oxidoreductase in *Nitrospira*) via the 169f/638R primer set (Pester et al., 2014), the comammox *amoA* gene (encoding the alpha subunit of ammonia monooxygenase specific to comammox *Nitrospira*) via the Ntsp-*amoA* 162F/359R primer set (Fowler et al., 2018), the AOA *amoA* gene (encoding the alpha subunit of ammonia monooxygenase specific to AOA) via the Arch-*amoA*F/AR primer set (Francis et al., 2005), and the total bacterial (universal) 16S rRNA gene via the Eub519/Univ907 primer set (Burgmann et al., 2011).

Bio-Rad iQ SYBR Green Supermix (Bio-Rad, Hercules, CA, USA) containing 50 U/ml iTaq DNA polymerase, 0.4 mM dNTPs, 100 mM KCl, 40 mM Tris-HCl, 6 mM MgCl<sub>2</sub>, 20 mM fluorescein, and stabilizers was used for all qPCR assays. The final volume of the reaction mix for each PCR and qPCR reaction was 20  $\mu\text{l}$ , in which the DNA template was  $\sim 1$  ng, and the primer concentrations were 0.2  $\mu\text{M}$ . All assays were performed in triplicate. For each assay, triplicate standard series were generated by tenfold serial dilutions ( $10^2$ - $10^8$  gene copies/ $\mu\text{l}$ ). All assays employed thermocycling conditions reported in the reference papers, and were performed on a Bio-Rad C1000 CFX96 Real-Time PCR system (Bio-Rad, Hercules, CA, USA).

#### *5.6.1.4 Comammox amoA cloning and sequencing*

198 bp fragments of the comammox *amoA* gene were amplified, cloned, and sequenced from DNA extracts of the sludge sampled on day 407 in order to generate standards for qPCR and confirm specificity of the comammox primer set (Fowler et al., 2018). Triplicate PCR products were pooled and purified via gel electrophoresis using the Qiagen QiaQUICK Gel Extraction Kit (Qiagen, Hilden, Germany). The purified PCR products were cloned using the TOPO<sup>®</sup> TA cloning<sup>®</sup> kits (Invitrogen/Thermo Fisher Scientific, Waltham, MA, USA) per the manufacturer's protocol. After blue/ white colony screening, three colonies were randomly selected and cultured overnight in LB medium containing 50 µg/ml ampicillin. The plasmids were isolated using the Invitrogen PureLink Quick Plasmid Miniprep Kit (Invitrogen/Thermo Fisher Scientific), and cloned inserts sequenced using the M13F-20 primer on the ABI 3730 automated Sanger sequencer at ACTG, Inc. (Wheeling, IL, USA). The acquired sequences were deposited in GenBank, and accession numbers can be found in SI Table 5.S2.

#### *5.6.1.5 16S rRNA, amoA, and nxrB gene PCR amplification, amplicon sequencing, analysis and phylogenetic inference*

16S rRNA and functional gene amplicon library preparations were performed using a two-step PCR protocol using the Fluidigm Biomark: Multiplex PCR Strategy. In the first round of PCR, each 20 µL reaction contained 10 µL of FailSafe PCR 2X PreMix F (Epicentre, Madison, WI), 0.63 units of Expand High Fidelity PCR Taq Enzyme (Sigma-Aldrich, St. Louis, MO), 0.4 µM of forward primer and reverse primer modified with Fluidigm common sequences at the 5' end of each primer, 1 µL of gDNA (approximately 100 ng) and the remaining volume molecular

biology grade water. The V4-V5 region of 16S rDNA was amplified in duplicate from 27 samples collected over the course of reactor operation using the 515F-Y (5'-GTGYCAGCMGCCGCGGTAA-3') and 926R (5'-CCGYCAATTYMTTTRAGTTT-3') (Parada et al., 2016) primer set. Thermocycling conditions for the 515F-Y/926R primer set were 95°C for 5 minutes, then 28 cycles of 95°C for 30 seconds, 50°C for 45 seconds, and 68°C for 30 seconds, followed by a final extension of 68°C for 5 minutes. Amplification was checked for all samples (including those described below) via agarose gel electrophoresis.

To characterize overall *Nitrospira* community structure in this system, *Nitrospira nxrB* amplicon sequencing was performed on samples from day 407 of reactor operation using the 169f (5'-TACATGTGGTGGAAACA) and 638R (5'-CGGTTCTGGTCRATCA) primer set (Pester et al., 2014). Thermocycling conditions were 95°C for 5 minutes, then 35 cycles of 95°C for 40 seconds, 56.2°C for 40 seconds, and 72°C for 90 seconds.

To assess community structure of comammox *Nitrospira*, comammox *amoA* amplicon sequencing was performed on samples from day 407 using the Ntsp-amoA 162F (GGATTTCTGGNTSGATTGGA) and Ntsp-amoA 359R (WAGTTNGACCACCASTACCA) primer set (Fowler et al., 2018). Thermocycling conditions were 94°C for 5 minutes, then 35 cycles of 94°C for 45 seconds, 56°C for 30 seconds, 72°C for 60 seconds, followed by a final extension of 72°C for 10 minutes. Amplification was checked for all samples on a 1% agarose gel.

Samples were then barcoded by sample via a second stage PCR amplification using Access Array Barcodes (Fluidigm, South San Francisco, CA)(Griffin and Wells, 2017). Each 20 uL PCR reaction consisted of 10 µL of FailSafe PCR 2X PreMix F, 0.63 units of Expand High Fidelity

PCR Taq Enzyme, 2  $\mu$ L of template from the first round of PCR, 4  $\mu$ L of sample-specific barcode primers and the remaining volume molecular biology grade water. The conditions for the second round of PCR were 95°C for 5 minutes, then 8 cycles of 95°C for 30 seconds, 60°C for 30 seconds, and 68°C for 30 seconds. Agarose gel electrophoresis was run again after the second round of PCR to verify correct amplification. Amplicons were pooled and then purified using Ampure XP bead cleanup, checked for quantity and quality using Qubit fluorescence analysis and TapeStation2200, respectively, and then diluted to appropriate concentration for sequencing. Sequencing was performed on an Illumina Miseq sequencer (Illumina, San Diego, CA) using Illumina V2 (2x250 paired end) chemistry.

For all amplicon sequence analysis, the primers were trimmed and the pair-end reads were merged using Trimmomatic. The 16S rRNA gene amplicons were initially clustered into operational taxonomic units (OTUs) at 97% identity in VSEARCH (Rognes et al., 2016). After de novo chimera filtering in VSEARCH, OTU taxonomy was assigned using the Silva database (Release 128) using the Quantitative Insights Into Microbial Ecology (QIIME) (Quast et al., 2013) command `align_seqs.py` with the Muscle option. To identify biologically distinct amplicons at sub-OTU resolution, 16S rRNA gene amplicons that were taxonomically assigned to *Nitrospira* were reclassified into unique sequences (also called `amplicon sequence variants` or ASV) using DADA2 with default settings (Callahan et al., 2016, p. 2). Functional gene amplicons (*nxB* and *amoA*) were also classified with DADA2.

Phylogenetic analyses were conducted on *Nitrospira* 16S rRNA, *Nitrospira nxB*, and comammox *amoA* gene amplicon sequences. The *Nitrospira* 16S rRNA genes (fragment length = 370 bp) were aligned in the ARB software package (Ludwig, 2004), and the maximum-

likelihood phylogenetic tree was constructed with RAxML (Stamatakis, 2014). The *nxB* (fragment length = 453 bp) and *amoA* (fragment length = 173 bp) gene sequences were aligned with MAFFT (Kato and Standley, 2013), and the maximum-likelihood phylogenetic trees were constructed with FastTreeMP (Price et al., 2010). All the trees were visualized in iTOL (Letunic and Bork, 2016). The *nxB* gene from *Nitrobacter hamburgensis* X14 and the *amoA* gene from *Nitrosococcus watsonii* C-113 were applied as outgroups in the *nxB* and *amoA* trees, respectively. The 16S rRNA gene from *Nitrobacter winogradskyi* ATCC 14123 was applied as outgroup in the *Nitrospira* 16S rRNA gene tree in Figure 5.S3; and the 16S rRNA gene from *Escherichia Coli* DE147 was applied as the outgroup in the phylogenetic tree for FISH probe evaluation in Figure 5.S5. The bootstrap value indicating the reliability of each split in the tree were all represented as gray circles in the inner nodes of the tree. FastTreeMP applies the Shimodaira-Hasegawa test and uses 1,000 resamples to generate the bootstrap value of each split, and RAxML applies 1,000 bootstrap runs and the GTR substitution model to generate the bootstrap value of each split in the tree.

#### 5.6.1.6 Fluorescent *in situ* Hybridization

Fluorescent *in situ* hybridization (FISH) was performed to estimate the relative abundance of canonical *Nitrospira*, canonical ammonia oxidizing bacteria (AOB), a subset of canonical *Nitrospira* that includes comammox, and total Eubacteria (see Table 5.S1 for probe sequences and corresponding references). Reactor biomass samples were chemically fixed in a 4% formaldehyde solution for two hours at 4°C followed by storage at -20°C in a 1:1 solution of phosphate buffered saline (PBS) and ethanol. Fixed biomass samples were diluted 6-fold in PBS and homogenized on ice in a Potter-Elvehjem tissue grinder (Kontes, Model# 886000-0020). 10

µl of the diluted homogenized samples were transferred to polytetrafluoroethylene (PTFE) printed 8-well slides and incubated at 60 °C for 1 hour to improve adhesion of the dehydrated biomass to the slide.

Samples underwent a dual-staining hybridization following protocols adapted from Nielsen et al. (Nielsen, 2009). For the “*Nitrospira*-AOB-Ntspa476” (see section S2. for discussion on probe Ntspa476 specificity) treatment, samples were first hybridized for four hours in a 35% formamide v/v hybridization buffer containing canonical *Nitrospira* probes (Ntspa662, Ntspa712; 6-FAM fluorophore) at concentrations of 0.83 µM and canonical Betaproteobacterial ammonia oxidizing bacteria probes (NEU, Nso1225, Cluster6a192; Cy3 fluorophore) at concentrations of 0.5 µM. Samples were then hybridized for four hours in a 20% formamide v/v hybridization buffer containing 0.5 µM Ntspa476 (Cy5 fluorophore), which was originally developed for the detection of the putative comammox organisms *Ca. N. nitrosa* and *Ca. N. Nitrificans* (van Kessel et al., 2015). For the “Eub-AOB-Ntspa476” treatment, the canonical *Nitrospira* probes were replaced with Eub338 I, Eub338 II, and Eub338 III (“Eub Mix”; 6-FAM fluorophore) at concentrations of 0.83 µM. The Eub mix was also added to the 20% formamide hybridization at concentrations of 0.83 µM. All probe mixes included equimolar concentrations of the recommended competitor oligonucleotides listed in Table 5.S1. Each sample was separately stained with the nonsense probe (Non-EUB338) tagged with 6-FAM, Cy3, and Cy5 fluorophores as a negative control for non-specific binding.

Hybridized cryosections were counterstained with DAPI at a concentration of 1 µg/mL in a glycerol based antifadent mounting media (Citifluor AF1). Image stacks were acquired on an inverted confocal laser scanning microscope (Model TCS SP5, Leica Microsystems) equipped

with an oil immersion 63× (1.44 NA) objective at a lateral resolution of 0.48 μm and an axial step size of 1 μm. DAPI, 6-FAM, Cy3, and Cy5 fluorophores were excited sequentially with 405nm, 488nm, 561nm, and 633nm laser lines, respectively. Ten fields of view were collected for each sample treatment.

Ratios of Ntspa476/AOB/*Nitrospira* and Ntspa476/AOB/total Eubacteria were calculated in the Fiji software package (Schindelin et al., 2012). Binary thresholds for each image channel were independently selected by a panel of three image analysts to distinguish hybridized biomass from background fluorescence. A given microbial quantity (e.g. AOB, *Nitrospira*) was calculated as the average thresholded pixel count in a given channel across ten fields of view averaged across the corresponding values reported by the three image analysts.

### 5.6.2 Analysis of FISH probe Ntspa476 specificity

The specificity and coverage of the putative comammox FISH probe Ntspa476 (van Kessel et al., 2015) and the *Nitrospira* FISH probe mix Ntspa662 and Ntspa712 (Daims et al., 2001) were evaluated by phylogenetic analysis on database-derived 16S rRNA gene sequences that could predictably hybridize with these probes. For this purpose, the Silva 132 SSURef NR99 database (695,171 sequences in total) was downloaded and imported into the ARB software (Ludwig, 2004). Probe\_server.arb was built on the whole SSU dataset. In this *in silico* analysis, we assumed database sequences with 0 mismatch to the FISH probe mix would hybridize with the probe. 726 sequences that had no nucleotide mismatches to either the Ntspa662 or the Ntspa712 probes were exported as sequences predicted to hybridize with the *Nitrospira*-specific FISH probe mix (Ntspa662 and Ntspa712). We also exported the 44 sequences that had no mismatches to the Ntspa476 FISH probe; 43 of these were a subset of the previous 726 sequences predicted

to also hybridize to the *Nitrospira* FISH probe mix (Ntspa662 and Ntspa712). All exported 16S rRNA gene sequences, together with the 5 dominant *Nitrospira* 16S rRNA gene ASV recovered via amplicon sequencing in this study, were aligned in ARB and the phylogenetic tree shown in Figure 5.S5 was generated with the RAxML software applying the GTR substitution model (Stamatakis, 2014).

43 out of the 44 sequences that we predicted would hybridize with Ntspa476 were also predicted to hybridize with the *Nitrospira* FISH probe mix (Ntspa662 and Ntspa712), and these sequences are shown in light magenta in Figure 5.S5. The 1 sequence predicted to hybridize to Ntspa476 but not to Ntspa662 or Ntspa712 is shown in dark magenta. The 673 (i.e.  $726 - 43 = 673$ ) 16S rRNA genes that hybridize only with the *Nitrospira* FISH probe mix (Ntspa662 and Ntspa712) but not with Ntspa476 are shown in blue in Figure 5.S5. As is indicated in Figure 5.S5, the specificity of the *Nitrospira* FISH probe mix (Ntspa662 and Ntspa712) is reasonably good, with minimal hybridizing sequences lying beyond the phylum of Nitrospirae. Of 726 total 16S rRNA sequences predicted to hybridize to either Ntspa662 or Ntspa712, only 19 (2.6%) did not affiliate with the Nitrospirae phylum (3 sequences from the phylum of Planctomycetes, 11 sequences from the phylum of Chloroflexi, 2 sequences from the phylum of Proteobacteria, and 3 sequences from the phylum of BRC1). All 44 sequences predicted to hybridize with the FISH probe Ntspa476 are in the genus *Nitrospira*, and 98% (43/44) of them are in *Nitrospira* lineage II. However, the resolution of FISH probe Ntspa476 in distinguishing the 16S rRNA genes between comammox and canonical NOBs is uncertain, based on the fact that gene sequences from known lineage II canonical *Nitrospira* (e.g. *Nitrospira lenta* (NR\_148573.1)) specific to the *Nitrospira* probe mix but not to Ntspa476 were interspersed with 16S rRNA gene sequences

predicted to hybridize to Ntspa476. Taken together, this analysis suggests that probe Ntspa476 is likely not capable of reliably resolving comammox from conventional nitrite-oxidizing *Nitrospira*, but is capable of specifically targeting a subset of lineage II *Nitrospira* that includes known comammox *Nitrospira*.

Regarding the dominant *Nitrospira* 16S rRNA gene ASV (black text, Figure 5.S5) identified in the present study, the three sequences in OTU4 that declined over time during reactor operation (see Figure 5.3) affiliated to *Nitrospira* lineage I. No *Nitrospira* 16S rRNA genes in lineage I are predicted to hybridize with probe Ntspa476. The two ASV in OTU2, i.e., ‘NU\_Nitrospira\_16S\_Rep\_Seq1’ and ‘NU\_Nitrospira\_16S\_Rep\_Seq2’, affiliated to *Nitrospira* lineage II, with the former phylogenetically closer to *Ca. Nitrospira nitrosa* and the latter much more abundant (as in shown in the heatmap of Figure 5.S5). Given the high abundance of taxa hybridized to probe Ntspa476 in qFISH quantification data (comprising 75% of all *Nitrospira* by day 398, see Figure 5.6), it is reasonable to suggest that both of the 16S rRNA genes in OTU2 were hybridized by the comammox FISH probe, but it is uncertain whether the more abundant one – ‘NU\_Nitrospira\_16S\_Rep\_Seq2’ – is, in fact, comammox *Nitrospira*.

## 5.6.2 Supporting Tables and Figures

**Table 5.S1** 16S rRNA-targeted oligonucleotide FISH probes used in this study.

Probe	Sequence (5' to 3')	FA (%)	Specificity	Reference
NEU	CCC CTC TGC TGC ACT CTA	35	Most halophilic and halotolerant <i>Nitrosomonas</i> spp.	(Wagner et al., 1995)
CTE (NEU Competitor)	TTC CAT CCC CCT CTG CCG	35	Unlabeled together with NEU <i>Comamonas</i> spp., <i>Acidovorax</i> spp., <i>Hydrogenophaga</i> spp., <i>Aquaspirillum</i> spp.	(Wagner et al., 1995)
Nso1225	CGC CAT TGT ATT ACG TGT GA	35	Ammonia-oxidizing $\beta$ -proteobacteria	(Mobarry et al., 1996)
Cluster6a192	CTT TCG ATC CCC TAC TTT CC	35	<i>Nitrosomonas oligotropha</i> lineage (Cluster 6a)	(Adamczyk et al., 2003)
Cluster6a 192 Competitor	CTT TCG ATC CCC TGC TTT CC	35	Competitor for Cluster6a192	(Adamczyk et al., 2003)
Ntspa662	GGA ATT CCG CGC TCC TCT	35	Genus <i>Nitrospira</i>	(Daims et al., 2001)
Ntspa662 Competitor	GGA ATT CCG CTC TCC TCT	35	Competitor for Ntspa662	(Daims et al., 2001)
Ntspa712	CGC CTT CGC CAC CGG CCT TCC	35	Most members of the phylum Nitrospirae	(Daims et al., 2001)
Ntspa712 Competitor	CGC CTT CGC CAC CGG TGT TCC	35	Competitor for Ntspa712	(Daims et al., 2001)
Ntspa476	CTG CAG GTA CCG TCC GAA	20	<i>Ca. N. nitrosa</i> , <i>Ca N. nitrificans</i>	(van Kessel et al., 2015)
Ntspa476 Competitor	CTG GAG GTA CCG TCC GAA	20	Competitor to Ntspa476	(van Kessel et al., 2015)
Eub338	GCT GCC TCC CGT AGG AGT	20, 35	Most Bacteria	(Amann et al., 1990)
Eub338 II	GCA GCC ACC CGT AGG TGT	20, 35	Planctomycetales	(Daims et al., 1999)
Eub338 III	GCT GCC ACC CGT AGG TGT	20, 35	Verrucomicrobiales	(Daims et al., 1999)
NON Eub	ACT CCT ACG GGA GGC AGC	20, 35	Negative control for nonspecific binding	(Wallner et al., 1993)

**Table 5.S2** GenBank accession numbers for *Nitrospira nxrB* and comammox *amoA* amplicon sequence variants, comammox *amoA* clone sequences, and raw sequencing data.

Amplicon sequence variant ID	GenBank accession number	Amplicon sequence variant ID	GenBank accession number
NU_nxrB_0	MH587129	NU_nxrB_40	MH587152
NU_nxrB_1	MH587130	NU_nxrB_42	MH587153
NU_nxrB_2	MH587131	NU_nxrB_47	MH587154
NU_nxrB_3	MH587132	NU_nxrB_54	MH587155
NU_nxrB_4	MH587133	NU_nxrB_59	MH587156
NU_nxrB_6	MH587134	NU_nxrB_82	MH587157
NU_nxrB_7	MH587135	NU_nxrB_86	MH587158
NU_nxrB_8	MH587136	NU_Commmox_amoA4	MH587119
NU_nxrB_9	MH587137	NU_Commmox_amoA5	MH587120
NU_nxrB_12	MH587138	NU_Commmox_amoA3	MH587121
NU_nxrB_13	MH587139	NU_Commmox_amoA7	MH587122
NU_nxrB_17	MH587140	NU_Commmox_amoA2	MH587123
NU_nxrB_19	MH587141	NU_Commmox_amoA8	MH587124
NU_nxrB_20	MH587142	NU_Commmox_amoA1	MH587125
NU_nxrB_22	MH587143	NU_Commmox_amoA_clone1	MH587126
NU_nxrB_23	MH587144	NU_Commmox_amoA_clone3	MH587127
NU_nxrB_24	MH587145	NU_Commmox_amoA_clone2	MH587128
NU_nxrB_25	MH587146	NU_Nitrospira_16S_rep_seq2	MH587159
NU_nxrB_26	MH587147	NU_Nitrospira_16S_rep_seq5	MH587160
NU_nxrB_27	MH587148	NU_Nitrospira_16S_rep_seq13	MH587161
NU_nxrB_28	MH587149	NU_Nitrospira_16S_rep_seq14	MH587162
NU_nxrB_29	MH587150	NU_Nitrospira_16S_rep_seq17	MH587163
NU_nxrB_30	MH587151	16S rRNA/ <i>amoA</i> / <i>nxrB</i> raw data	PRJNA480047

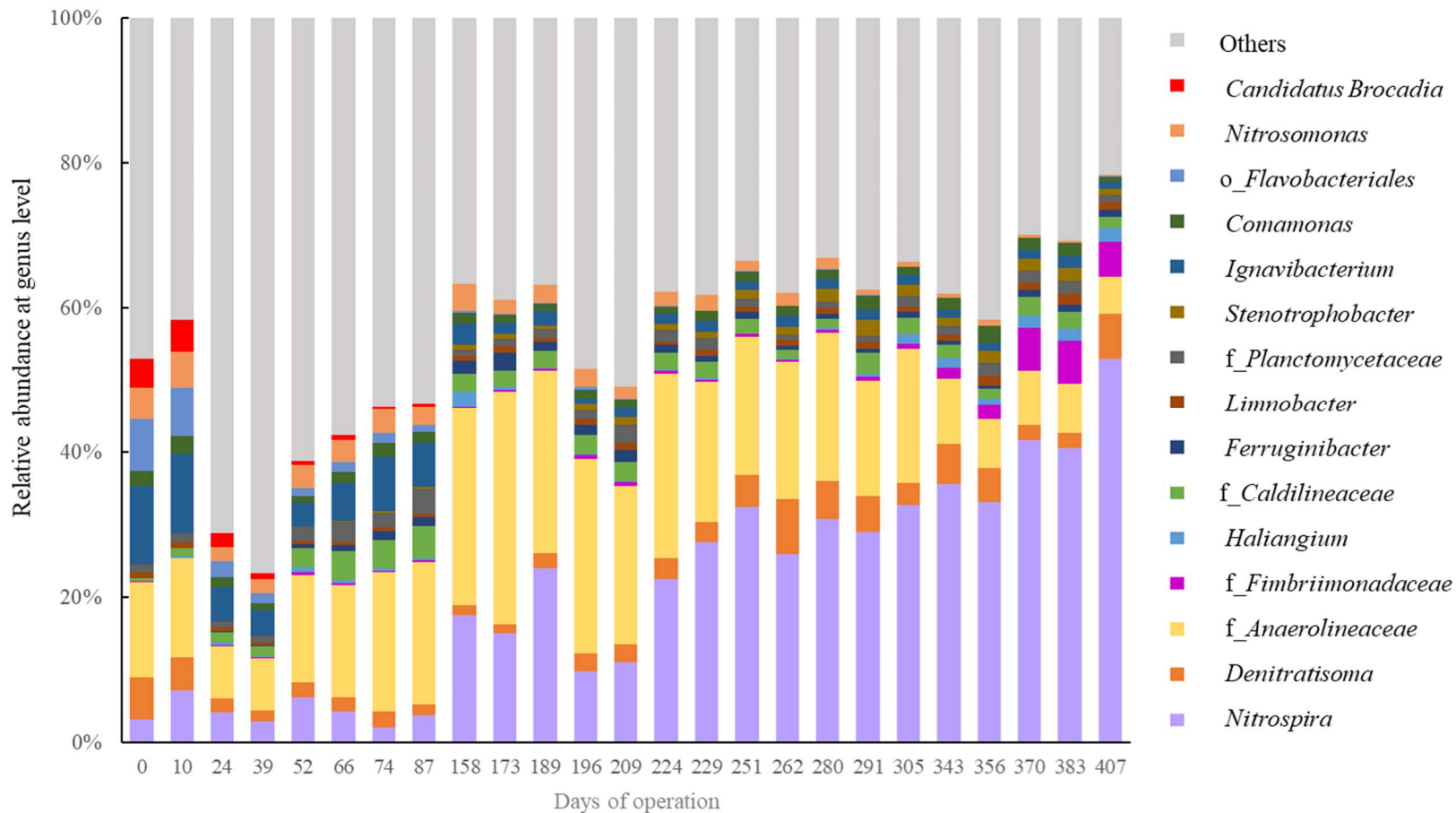


**Figure 5.S1** Relative abundance of the 15 most abundant bacterial genera at each time point according to 16S rRNA gene sequencing data. Sampling time point is shown on the x axis. The OTUs that were unclassified at the genus level are presented with the corresponding lowest annotable taxonomy names; ‘f\_’ indicate ‘Family’, and ‘o\_’ indicates ‘Order.’

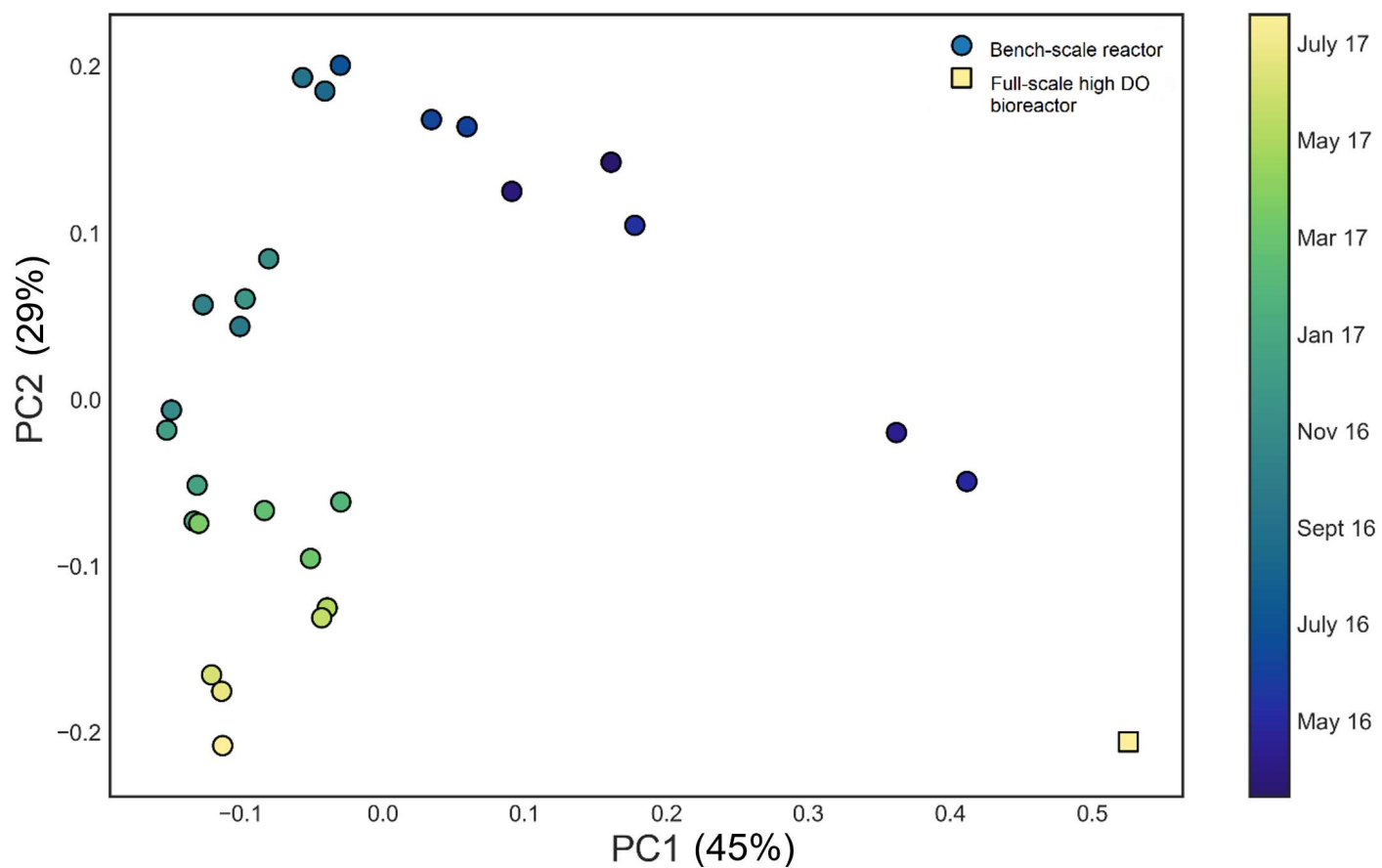


**Figure 5.S2** Principle Coordinate Analysis of weighted unifracs distances between samples, based on 16S rRNA gene amplicon sequencing analyses. Samples from the low DO bench-scale reactor are indicated by circles, and a single sample for comparison in the parallel full-scale high DO nitrifying activated sludge bioreactor is indicated by a square. Samples are color coded by time of sampling.

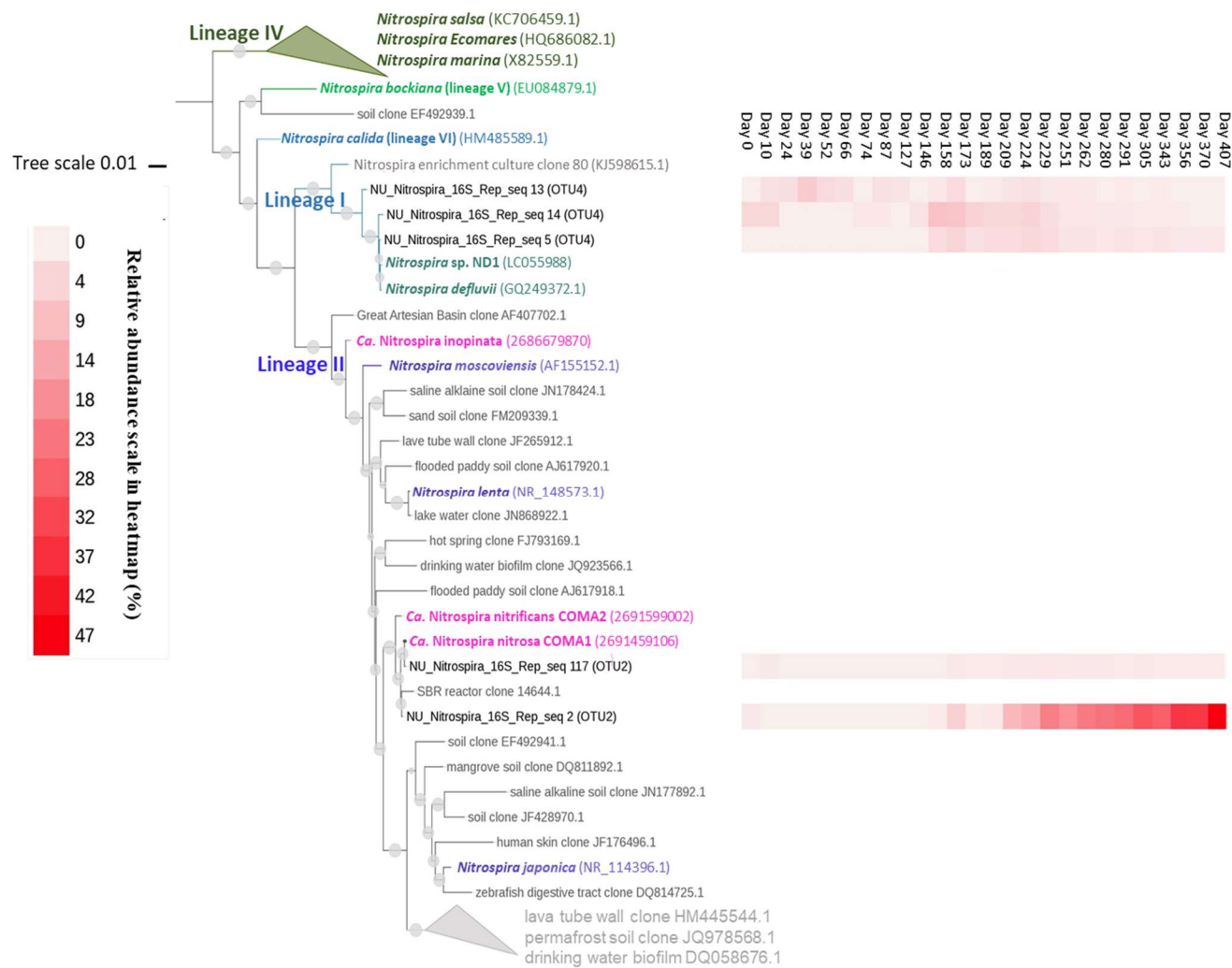


**Figure 5.S3** Maximum-likelihood phylogenetic tree of the 5 *Nitrospira* 16S rRNA gene amplicon sequence variants (ASV) (370 bp fragment) in the two dominant OTUs (OTU2 and OTU4, clustered to 97% identity). The heatmap shows the abundance of each of the 5 ASV against the total number of the 16S rRNA gene reads.

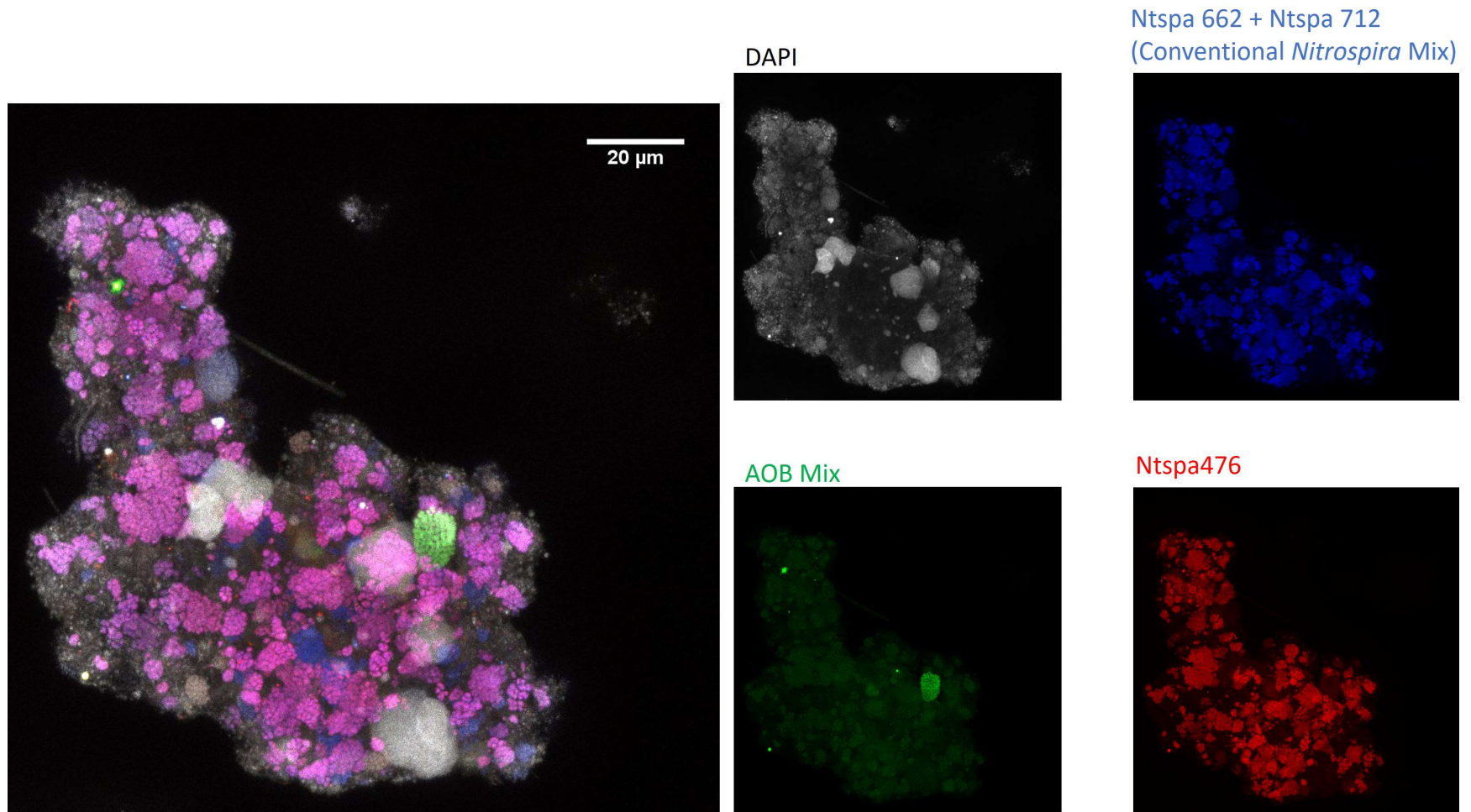


**Figure 5.S4** Representative FISH micrograph of showing co-aggregation of *Nitrospira*, *Nitrosomonas* and Ntspa476-hybridized *Nitrospira* in the low DO bench scale nitrification reactor consortium on day 407. DAPI counterstaining is in grey, and probes specific for *Nitrospira* (Ntspa662 and Ntspa712, blue), a subset of *Nitrospira* that includes known comammox (Ntspa476, red; red + blue = magenta), and *Nitrosomonas* (AOB mix: NEU, Nso1225, Cluster6a192; green)

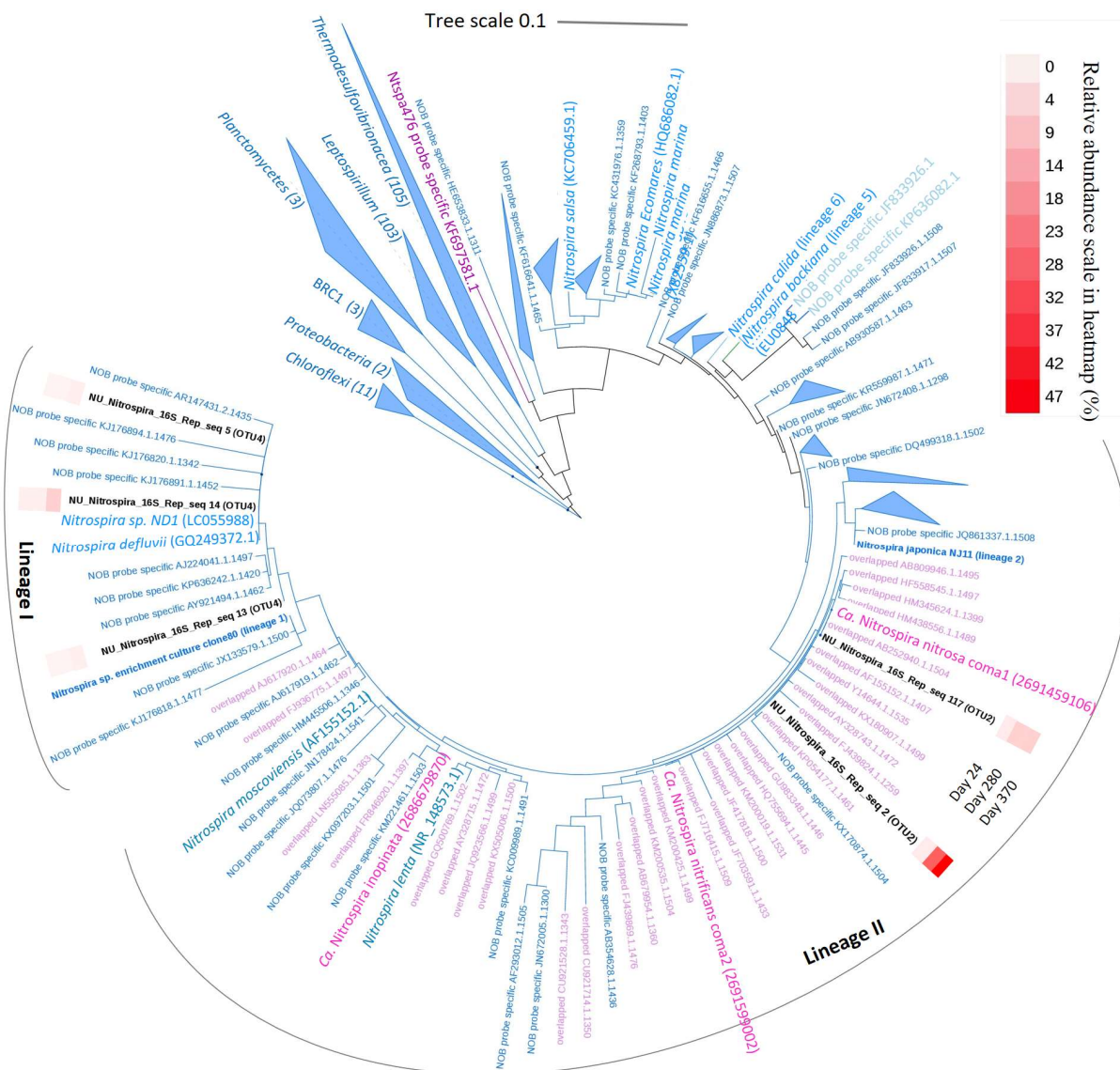


**Figure 5.S5** Maximum-likelihood phylogenetic tree of the 16S rRNA genes that could be targeted by FISH probe Ntspa476 (originally designed to target specific comammox taxa) and *Nitrospira* FISH probe mix (Ntspa662 and Ntspa712). Magenta indicates sequences predicted to hybridize with both Ntspa476 and the *Nitrospira* probe mix; blue indicates sequences predicted to hybridize with only the *Nitrospira* probe mix; pink indicates the 16S rRNA genes from three comammox genomes; and black indicates the five *Nitrospira* 16S rRNA gene ASV that were dominant in the reactor consortium of this study, with the relative abundance of each indicated in the heatmap. Numbers in parentheses after taxonomy names indicate the number of 16S rRNA genes that are predicted to hybridize with the *Nitrospira* FISH probes (Ntspa662 or Ntspa712) in the corresponding taxa. The heatmap indicates the abundance of each the *Nitrospira* 16S rRNA gene ASV against the total number of the 16S rRNA gene reads.

## CHAPTER 6: SUMMARY AND FUTURE WORK

### 6.1 Summary of Key Findings

In my research I investigated biological methods and underlying mechanisms for shortcut nitrogen and phosphorus removal from mainstream wastewater via two treatment trains and four lab-scale reactors. The major findings and scientific advances that resulted from this study are summarized here.

#### 6.1.1 Single Sludge Nitrification-Denitrification with EBPR

A single sludge method for combined shortcut nitrogen removal (via nitrification-denitrification) and enhanced biological phosphorus removal (EBPR) was presented in Chapter 2. This study was the first to demonstrate the compatibility and consistent performance of nitrification-denitrification and biological phosphorus removal at the moderate mainstream wastewater temperature of 20 °C.

Key lessons learned:

- The major takeaway is that the energy and carbon-saving shortcut nitrification-denitrification pathway for nitrogen removal is compatible with enhanced biological phosphorus removal in a single sludge system in temperate climates. In fact, nitrogen removal likely improved biological phosphorus removal due to the decreased recycle of oxidized reactive nitrogen (i.e.  $\text{NO}_2^-$  and  $\text{NO}_3^-$ ) to the anaerobic zone. Moreover, operation at low dissolved oxygen (DO) levels (intermittent aeration with peak DO = 1 mg  $\text{O}_2/\text{L}$ ) facilitated energy savings, provided consistent phosphorus removal and enabled rapid denitrification during anoxic intervals of intermittent aeration.

- The nitrification-denitrification method for nitrogen removal requires the suppression of nitrite oxidizing organisms (NOO). NOO were suppressed in this study by the combination of intermittent aeration and solids retention time (SRT) control. Intermittent aeration ensured constant substrate limitation for NOO, which need  $\text{NO}_2^-$  and DO simultaneously. Due to this limitation, NOO grew more slowly than ammonia oxidizing organisms (AOO), such that at an aerobic SRT of 3 to 4 days AOO activity was maintained while NOO activity was suppressed. While the specific aerobic SRT optimal for NOO out-competition and AOO maintenance will vary depending on influent characteristics, temperature, aeration intensity and more, the general approach of intermittent aeration in tandem with SRT control can be adjusted to optimize nitrification-denitrification performance for a given process.
- This process proved amenable to temperate climates with cold winter temperatures. Although the data is not included in Chapter 2, a gradual temperature reduction (about - 0.7 °C/week) down to 10 °C demonstrated that NOO out-competition was maintained down to 13 °C. NOB activity then proliferated due to a combination of the cold temperature (which has been shown to promote NOO activity over that of AOO) and the longer SRT, which was chosen to avoid long hydraulic retention times at cold temperatures. Importantly, NOO suppression was reestablished when operation at 20 °C was resumed along with low SRT control.
- Translation of process performance observed here to other wastewater flows is dependent on the influent organic carbon (especially volatile fatty acids, VFAs) to nutrient ratios. This process achieved 70% total N removal and 83% total P removal at influent ratios of

8.3 g tCOD/g TKN and 8.2 g VFA-COD/g TP. A higher COD:N ratio would have likely resulted in higher N removal, as the reactor became carbon limited at the end of sequencing batch reactor cycles, resulting in  $\text{NO}_2^-$  accumulation. On average, the influent VFA content was sufficient for biological P removal but became limiting during wet weather events due to dilution. Upsets in P removal, though transient, were consistently associated with wet weather flows.

- As a single-reactor activated-sludge process, many existing wastewater treatment facilities may be able to adapt this technology with minimal changes existing infrastructure. Translation of this process to full scale sequencing batch reactors would be relatively straightforward, as operation could be similar to that described in Chapter 2. If applying this technology to full scale plug flow reactors, achieving consistent aerobic/anoxic zones in intermittent aeration is expected to be the biggest challenge. Preliminary modeling results suggest that there is flexibility in the aerobic/anoxic times in intermittent aeration, with total interval times up to 40 minutes still maintaining NOO out-competition (in contrast to the shorter 10 – 20-minute total interval times used in the study). In a plug flow system this translates to larger aerobic/anoxic zones and less baffle walls to facilitate clear separation of redox zones.

### **6.1.2 High Rate EBPR**

Chapter 3 presented the results of the high rate biological phosphorus removal reactor for combined phosphorus and carbon removal. These results advanced understanding of low SRT biological phosphorus removal systems by being the first to demonstrate a washout SRT for

*Candidatus* Accumulibacter polyphosphate accumulating organisms (PAOs) in real mainstream wastewater.

Key lessons learned:

- This study demonstrated that Accumulibacter PAOs can be maintained at the low aerobic SRT of 1.4 days, and were washed out at an aerobic SRT between 0.8 and 1.4 days at 20 °C. This indicates that the dual goals of carbon diversion and phosphorus recovery in a high rate biological phosphorus removal reactor may be compatible, though further work needs to be done to quantify carbon diversion.
- This study was the first to investigate the diversity of PAOs in low SRT systems via the clade-level dynamics of Accumulibacter. Accumulibacter clades IIA, IIB and IID dominated the PAO community at the lowest SRT values, while clades IA and IC were washed out, suggesting that certain clades may have higher growth rates and thus be better adapted to low SRT operation.
- The ratio of readily biodegradable carbon (rbCOD) to total P in the influent of 16 g rbCOD/g TP (or 8.2 g VFA-COD/g TP) was just over the recommended lower limit of 15 g rbCOD/g TP. This was sufficient for good performance, but also indicated that the process was sensitive to influent dilution from wet weather flows. Later operation of a return sludge fermenter (data not shown) provided enough rbCOD for consistent P removal even during extended wet weather events, though operation of the fermenter increased the effective SRT.
- Glycogen accumulating organisms (GAOs), which are competitors to PAOs for rbCOD, were highly suppressed in this study. Both the low SRT and the relatively

low rbCOD:TP levels in the influent likely contributed to the competitive advantage of PAOs over GAOs.

### 6.1.3 Deammonification IFAS

The deammonification integrated fixed film activated sludge (IFAS) system described in Chapter 4 demonstrated the robust nature of anammox biofilms and their long-term compatibility with low temperature, low concentration environments, as well as the importance of influent organic carbon levels to mainstream deammonification performance.

Key lessons learned:

- Maximum activity tests of anammox stabilized to an N removal rate about double that of the N loading rate to the reactor and maintained such activity through the end of the study, which in total lasted longer than 3 years. Anammox activity was sensitive to temperature reduction (down to 10 °C) as expected, but activity quickly recovered to pre-temperature decline levels when operation at 20 °C was resumed.
- Nitrogen removal dramatically improved by rerouting 10% of the influent flow around the A-stage reactor, thus increasing the influent sCOD-to-ammonia ratio by 35%. This provided an additional nitrite sink via denitrification (the other being anammox) that, like the nitrification-denitrification reactor in Chapter 2, aided in NOO out-competition and contributed to total nitrogen removal. This reactor illustrated the critical role of organic carbon in mainstream deammonification, which lacks the usual selective pressures for AOO over NOO that exist in the sidestream: high temperatures and elevated free ammonia and nitrous acid.

- The challenge of NOO out-competition in mainstream deammonification was clearly illustrated in this process, which limited nitrogen removal due to excess nitrate production before the change in feeding strategy. Before that change, various strategies for NOO suppression proved unsuccessful: Washout of floccular biomass via low SRT control, various aeration strategies including intermittent aeration and constant low DO, and supplemental anammox biomass.
- Ultimately, both the anammox and denitrification pathways for N removal proved critical to the performance of the reactor. Nitrogen isotope testing indicated that anammox were responsible for about 53% of nitrogen removal, and that cross feeding of denitrifiers to anammox (via reduction of  $\text{NO}_3^-$  to  $\text{NO}_2^-$ ) played an important role.

#### 6.1.4 Comammox SG

The suspended growth (SG) reactor described in Chapter 5 was originally operated for N removal via mainstream deammonification, but loss of anammox biomass and activity within the first 100 days led to its operation as a low DO nitrification reactor. The serendipitous enrichment of complete ammonia oxidizing (comammox) *Nitrospira* led to its name of “comammox SG,” and was the first wastewater bioreactor to demonstrate the dominance of the ammonia oxidizing community by comammox.

Key lessons learned:

- The dominance of comammox in this reactor suggested that the very conditions of mainstream deammonification – low temperatures, long solids retention times, low dissolved oxygen and low ammonia concentrations – may inadvertently select for

- comammox. This could be problematic when NOO suppression is targeted for energy and carbon efficient N removal.
- However, comammox seem to offer a relatively low-energy path for nitrification due to their success in this low dissolved oxygen reactor. They may even be compatible with anammox and N removal given the increasing research into denitrification-anammox.
  - The enrichment of comammox in this reactor did not fully explain the very high abundance of *Nitrospira*. Namely, qPCR indicated that comammox comprised <10% of the total *Nitrospira* in the reactor, whereas *Nitrospira* comprised >50% of the total community as confirmed by qPCR, 16S rRNA gene amplicon sequencing, and Fluorescence In Situ Hybridization (FISH). The metabolic diversity of *Nitrospira* as demonstrated by other research suggests that they are capable of much more than linear  $\text{NO}_2^-$  oxidation to  $\text{NO}_3^-$ .

## 6.2 Future Work

Given the promising results of the nitritation-denitrification with EBPR reactor (Chapter 2), pilot scale testing is a logical next step. Translation of the SBR configuration used in my research to the plug-flow configuration typical of MWRDGC facilities is the primary challenge, particularly with regard to intermittent aeration. Preliminary process modeling suggest that aeration intervals could be extended considerably (to 40-minute total interval length) while maintaining NOB suppression, which should simplify process design. Nonetheless, achieving consistent redox zones at the pilot/full scale is anticipated to be the primary challenge.

A key unanswered question regarding the high rate EBPR system (Chapter 3) is the quantity (or percent of influent) of organic carbon redirected to anaerobic digestion. Unfortunately, I did not measure COD concentrations in the waste sludge during the timeline described in Chapter 3, and once I did start to perform sufficient COD measurements to perform a mass balance on the process, efforts to cultivate granules in the system compromised phosphorus removal performance. So, a better comparison of COD diversion efficiency at the range of SRT values used in the study (1 to 4 days) would help illuminate the impact of SRT on potential energy savings of the process. Moreover, a return activated sludge fermenter was eventually implemented to facilitate better P removal during rain events. This change effectively increased the SRT, and the implications of that change on carbon diversion efficiency have yet to be investigated. While investigation of the impact of the fermenter on the microbial community, particularly PAOs, in the reactor was outside the scope of this thesis, there is plenty of biomass from this process archived in the freezer that may warrant future investigation. Such an investigation of PAO diversity (including *Accumulibacter* clades) before and after implementation of the fermenter would offer a unique perspective on the impact of fermenters on the ecology of EBPR systems.

The diversity of organisms present in activated sludge is staggering, and microbial ecologists and environmental engineers alike have barely scratched the surface of understanding the phylogenetic or metabolic diversity present. From a more practical standpoint, however, the diversity of ammonia oxidizers in wastewater treatment is, in my experience, particularly poorly understood, and warrants further research. While our study of comammox (Chapter 5) shed some light onto the role of *Nitrospira* in ammonia oxidation, the results of Chapter 2, where the

abundance of both known ammonia oxidizers and *Nitrospira* approached zero during Phase 2 (while ammonia oxidation activity was high), only deepened the mystery. Some researchers have suggested that heterotrophic ammonia oxidation may play a role, but better tools and genomic knowledge are needed to identify and quantify such organisms. This, of course, is also true of comammox, wherein research is particularly needed to better understand their role in nitrogen removal biotechnologies. Gene expression assays may help differentiate comammox AOB activity from canonical AOB activity, as bulk activity assays from reactive nitrogen concentrations fails to make such a distinction. Another need in comammox research is measurement of ammonia, nitrite, and oxygen affinity of *Candidatus Nitrospira nitrosa*, to which most comammox found in wastewater treatment systems are closely related. Such data would facilitate modeling of comammox in nutrient removal bioreactors, and better predict the conditions that lead to their selection.

Partial denitrification/anammox (or denitrification/anammox) has been a growing area of research in mainstream deammonification studies, in part because it avoids the challenges of NOB out-competition. Much of my research was focused on strategies for NOB suppression, and while often successful (i.e. Chapter 2), also confirmed this difficulty (i.e. in the B-stage deammonification reactors, Chapters 4 and 5). Forgoing NOB suppression may reduce operational complexity, as for example in cases where SRT is used to maintain NOB washout. Whether such systems can maintain long-term anammox biomass and activity, however, and offer high total N removal at reduced energy and carbon demand over conventional processes, remains to be proven. If so, such processes may help move us towards high total nutrient removal at the full scale without VFA addition and at lower aeration (and energy) demand.

## REFERENCES

- Acevedo, B., Oehmen, A., Carvalho, G., Seco, A., Borrás, L., Barat, R., 2012. Metabolic shift of polyphosphate-accumulating organisms with different levels of polyphosphate storage. *Water Res.* 46, 1889–1900. <https://doi.org/10.1016/j.watres.2012.01.003>
- Adamczyk, J., Hesselsoe, M., Iversen, N., Horn, M., Lehner, A., Nielsen, P.H., Schloter, M., Roslev, P., Wagner, M., 2003. The isotope array, a new tool that employs substrate-mediated labeling of rRNA for determination of microbial community structure and function. *Appl. Environ. Microbiol.* 69, 6875–6887.
- Ahn, J., Daidou, T., Tsuneda, S., Hirata, A., 2001. Metabolic Behavior of Denitrifying Phosphate-Accumulating Organisms under Nitrate and Nitrite Electron Acceptor Conditions. *J. Biosci. Bioeng.* 92, 442–446.
- Ahn, J.H., Kim, S., Park, H., Rahm, B., Pagilla, K., Chandran, K., 2010. N<sub>2</sub>O Emissions from Activated Sludge Processes, 2008–2009: Results of a National Monitoring Survey in the United States. *Environ. Sci. Technol.* 44, 4505–4511. <https://doi.org/10.1021/es903845y>
- Amann, R.L., Devereux, R., Stahl, D.A., 1990. Combination of 16S rRNA-Targeted Oligonucleotide Probes with Flow Cytometry for Analyzing Mixed Microbial Populations. *APPL ENV. MICROBIOL* 56, 7.
- Annavaajhala, M.K., Kapoor, V., Santo-Domingo, J., Chandran, K., 2018. Comammox Functionality Identified in Diverse Engineered Biological Wastewater Treatment Systems. *Environ. Sci. Technol. Lett.* 5, 110–116. <https://doi.org/10.1021/acs.estlett.7b00577>
- Anthonisen, A.C., Loehr, R.C., Prakasam, T.B.S., Srinath, E.G., 1976. Inhibition of Nitrification by Ammonia and Nitrous Acid. *Water Pollut. Control Fed.* 48, 835–852.
- APHA, 2005. Standard methods for the examination of water and wastewater, 21st ed. American Public Health Association, Washington, D.C.
- Barat, R., Montoya, T., Borrás, L., Seco, A., Ferrer, J., 2006. Calcium effect on enhanced biological phosphorus removal. *Water Sci. Technol.* 53, 29–37. <https://doi.org/10.2166/wst.2006.403>
- Barker, P.S., Dold, P.L., 1997. General model for biological nutrient removal activated-sludge systems: model presentation. *Water Environ. Res.* 69, 969–984. <https://doi.org/10.2175/106143097X125669>
- Barnard, J.L., 1976. A review of biological phosphorus removal in the activated sludge process. *Water Sa* 2, 136–144.
- Barnard, J.L., Dunlap, P., Steichen, M., 2017. Rethinking the Mechanisms of Biological Phosphorus Removal. *Water Environ. Res.* 89, 2043–2054. <https://doi.org/10.2175/106143017X15051465919010>
- Bartelme, R.P., McLellan, S.L., Newton, R.J., 2017. Freshwater Recirculating Aquaculture System Operations Drive Biofilter Bacterial Community Shifts around a Stable Nitrifying Consortium of Ammonia-Oxidizing Archaea and Comammox Nitrospira. *Front. Microbiol.* 8. <https://doi.org/10.3389/fmicb.2017.00101>
- Bolyen, E., Rideout, J.R., Dillon, M.R., Bokulich, N.A., Abnet, C., Al-Ghalith, G.A., Alexander, H., Alm, E.J., Arumugam, M., Asnicar, F., Bai, Y., Bisanz, J.E., Bittinger, K., Brejnrod, A., Brislawn, C.J., Brown, C.T., Callahan, B.J., Caraballo-Rodríguez, A.M., Chase, J., Cope, E., Da Silva, R., Dorrestein, P.C., Douglas, G.M., Durall, D.M., Duvall, C.,

- Edwardson, C.F., Ernst, M., Estaki, M., Fouquier, J., Gauglitz, J.M., Gibson, D.L., Gonzalez, A., Gorlick, K., Guo, J., Hillmann, B., Holmes, S., Holste, H., Huttenhower, C., Huttley, G., Janssen, S., Jarmusch, A.K., Jiang, L., Kaehler, B., Kang, K.B., Keefe, C.R., Keim, P., Kelley, S.T., Knights, D., Koester, I., Kosciolk, T., Kreps, J., Langille, M.G., Lee, J., Ley, R., Liu, Y.-X., Loftfield, E., Lozupone, C., Maher, M., Marotz, C., Martin, B., McDonald, D., McIver, L.J., Melnik, A.V., Metcalf, J.L., Morgan, S.C., Morton, J., Naimey, A.T., Navas-Molina, J.A., Nothias, L.F., Orchanian, S.B., Pearson, T., Peoples, S.L., Petras, D., Preuss, M.L., Pruesse, E., Rasmussen, L.B., Rivers, A., Robeson, II, M.S., Rosenthal, P., Segata, N., Shaffer, M., Shiffer, A., Sinha, R., Song, S.J., Spear, J.R., Swafford, A.D., Thompson, L.R., Torres, P.J., Trinh, P., Tripathi, A., Turnbaugh, P.J., Ul-Hasan, S., van der Hooft, J.J., Vargas, F., Vázquez-Baeza, Y., Vogtmann, E., von Hippel, M., Walters, W., Wan, Y., Wang, M., Warren, J., Weber, K.C., Williamson, C.H., Willis, A.D., Xu, Z.Z., Zaneveld, J.R., Zhang, Y., Knight, R., Caporaso, J.G., 2018. QIIME 2: Reproducible, interactive, scalable, and extensible microbiome data science. *PeerJ*. <https://doi.org/10.7287/peerj.preprints.27295v1>
- Brdjanovic, D., Loosdrecht, M.C.M. van, Hooijmans, C.M., Alaerts, G.J., Heijnen, J.J., 1998. Minimal aerobic sludge retention time in biological phosphorus removal systems. *Biotechnol. Bioeng.* 60, 326–332. [https://doi.org/10.1002/\(SICI\)1097-0290\(19981105\)60:3<326::AID-BIT8>3.0.CO;2-J](https://doi.org/10.1002/(SICI)1097-0290(19981105)60:3<326::AID-BIT8>3.0.CO;2-J)
- Burgmann, H., Jenni, S., Vazquez, F., Udert, K.M., 2011. Regime Shift and Microbial Dynamics in a Sequencing Batch Reactor for Nitrification and Anammox Treatment of Urine. *Appl. Environ. Microbiol.* 77, 5897–5907. <https://doi.org/10.1128/AEM.02986-10>
- Callahan, B.J., McMurdie, P.J., Rosen, M.J., Han, A.W., Johnson, A.J.A., Holmes, S.P., 2016. DADA2: High-resolution sample inference from Illumina amplicon data. *Nat. Methods* 13, 581–583. <https://doi.org/10.1038/nmeth.3869>
- Camejo, P.Y., Owen, B.R., Martirano, J., Ma, J., Kapoor, V., Santo Domingo, J., McMahon, K.D., Noguera, D.R., 2016. *Candidatus Accumulibacter phosphatis* clades enriched under cyclic anaerobic and microaerobic conditions simultaneously use different electron acceptors. *Water Res.* 102, 125–137. <https://doi.org/10.1016/j.watres.2016.06.033>
- Camejo, P.Y., Oyserman, B.O., McMahon, K.D., Noguera, D.R., 2019. Integrated Omic Analyses Provide Evidence that a “*Candidatus Accumulibacter phosphatis*” Strain Performs Denitrification under Microaerobic Conditions. *mSystems* 4. <https://doi.org/10.1128/mSystems.00193-18>
- Camejo, P.Y., Santo Domingo, J., McMahon, K.D., Noguera, D.R., 2017. Genome-Enabled Insights into the Ecophysiology of the Comammox Bacterium “*Candidatus Nitrospira nitrosa*.” *mSystems* 2, e00059-17. <https://doi.org/10.1128/mSystems.00059-17>
- Cao, Y., Hong, K.B., van Loosdrecht, M.C.M., Daigger, G.T., Yi, P.H., Wah, Y.L., Chye, C.S., Ghani, Y.A., 2016. Mainstream partial nitritation and anammox in a 200,000 m<sup>3</sup>/day activated sludge process in Singapore: scale-down by using laboratory fed-batch reactor. *Water Sci. Technol.* 74, 48–56. <https://doi.org/10.2166/wst.2016.116>
- Cao, Y., van Loosdrecht, M.C.M., Daigger, G.T., 2017. Mainstream partial nitritation–anammox in municipal wastewater treatment: status, bottlenecks, and further studies. *Appl. Microbiol. Biotechnol.* <https://doi.org/10.1007/s00253-016-8058-7>

- Carvalho, M., 2014. The effect of key process operational conditions on enhanced biological phosphorus removal from wastewater.
- Carvalho, G., Lemos, P.C., Oehmen, A., Reis, M.A.M., 2007. Denitrifying phosphorus removal: Linking the process performance with the microbial community structure. *Water Res.* 41, 4383–4396. <https://doi.org/10.1016/j.watres.2007.06.065>
- Chamchoi, N., Nitisoravut, S., Schmidt, J.E., 2008. Inactivation of ANAMMOX communities under concurrent operation of anaerobic ammonium oxidation (ANAMMOX) and denitrification. *Bioresour. Technol.* 99, 3331–3336. <https://doi.org/10.1016/j.biortech.2007.08.029>
- Chan, C., Guisasola, A., Baeza, J.A., 2017. Enhanced Biological Phosphorus Removal at low Sludge Retention Time in view of its integration in A-stage systems. *Water Res.* 118, 217–226. <https://doi.org/10.1016/j.watres.2017.04.010>
- Chase, E.S., Eddy, H.P., 1944. High rate activated sludge treatment of sewage. *Sew. Works J.* 878–885.
- Chen, C., Sun, F., Zhang, H., Wang, J., Shen, Y., Liang, X., 2016. Evaluation of COD effect on anammox process and microbial communities in the anaerobic baffled reactor (ABR). *Bioresour. Technol.* 216, 571–578. <https://doi.org/10.1016/j.biortech.2016.05.115>
- Chen, H., Liu, S., Yang, F., Xue, Y., Wang, T., 2009. The development of simultaneous partial nitrification, ANAMMOX and denitrification (SNAD) process in a single reactor for nitrogen removal. *Bioresour. Technol.* 100, 1548–1554. <https://doi.org/10.1016/j.biortech.2008.09.003>
- Christensson, M., Ekström, S., Andersson Chan, A., Le Vaillant, E., Lemaire, R., 2013. Experience from start-ups of the first ANITA Mox plants. *Water Sci. Technol. J. Int. Assoc. Water Pollut. Res.* 67, 2677–2684. <https://doi.org/10.2166/wst.2013.156>
- Chung, Y.-C., Chung, M.-S., 2000. BNP test to evaluate the influence of C/N ratio on N<sub>2</sub>O production in biological denitrification. *Water Sci. Technol.* 42, 23–27. <https://doi.org/10.2166/wst.2000.0354>
- Corominas, L.I., Rieger, L., Takács, I., Ekama, G., Hauduc, H., Vanrolleghem, P.A., Oehmen, A., Gernaey, K.V., van Loosdrecht, M.C.M., Comeau, Y., 2010. New framework for standardized notation in wastewater treatment modelling. *Water Sci. Technol.* 61, 841–857. <https://doi.org/10.2166/wst.2010.912>
- Costa, E., Pérez, J., Kreft, J.-U., 2006. Why is metabolic labour divided in nitrification? *Trends Microbiol.* 14, 213–219. <https://doi.org/10.1016/j.tim.2006.03.006>
- Daims, H., Brühl, A., Amann, R., Schleifer, K.H., Wagner, M., 1999. The domain-specific probe EUB338 is insufficient for the detection of all Bacteria: development and evaluation of a more comprehensive probe set. *Syst. Appl. Microbiol.* 22, 434–444. [https://doi.org/10.1016/S0723-2020\(99\)80053-8](https://doi.org/10.1016/S0723-2020(99)80053-8)
- Daims, H., Lebedeva, E.V., Pjevac, P., Han, P., Herbold, C., Albertsen, M., Jehmlich, N., Palatinszky, M., Vierheilig, J., Bulaev, A., Kirkegaard, R.H., von Bergen, M., Rattei, T., Bendinger, B., Nielsen, P.H., Wagner, M., 2015. Complete nitrification by *Nitrospira* bacteria. *Nature* 528, 504–509. <https://doi.org/10.1038/nature16461>
- Daims, H., Lückner, S., Wagner, M., 2016. A New Perspective on Microbes Formerly Known as Nitrite-Oxidizing Bacteria. *Trends Microbiol.* <https://doi.org/10.1016/j.tim.2016.05.004>

- Daims, H., Nielsen, J.L., Nielsen, P.H.E.R.H., Wagner, M., Schleifer, K., Nielsen, P.H.E.R.H., Schleifer, K., 2001. In Situ Characterization of Nitrospira -Like Nitrite-Oxidizing Bacteria Active in Wastewater Treatment Plants. *Appl. Environ. Microbiol.* 67, 5273–5284. <https://doi.org/10.1128/AEM.67.11.5273>
- De Clippeleir, H., Vlaeminck, S.E., De Wilde, F., Daeninck, K., Mosquera, M., Boeckx, P., Verstraete, W., Boon, N., 2013. One-stage partial nitritation/anammox at 15 °C on pretreated sewage: feasibility demonstration at lab-scale. *Appl. Microbiol. Biotechnol.* 97, 10199–10210. <https://doi.org/10.1007/s00253-013-4744-x>
- Desloover, J., De Clippeleir, H., Boeckx, P., Du Laing, G., Colsen, J., Verstraete, W., Vlaeminck, S.E., 2011. Floc-based sequential partial nitritation and anammox at full scale with contrasting N<sub>2</sub>O emissions. *Water Res.* 45, 2811–2821. <https://doi.org/10.1016/j.watres.2011.02.028>
- Dold, P., Du, W., Burger, G., Jimenez, J., 2015. Is Nitrite-Shunt Happening in the System? Are Nob Repressed? *Proc. Water Environ. Fed.* 2015, 1360–1374. <https://doi.org/10.2175/193864715819540955>
- Domingo-Félez, C., Mutlu, A.G., Jensen, M.M., Smets, B.F., 2014. Aeration Strategies To Mitigate Nitrous Oxide Emissions from Single-Stage Nitritation/Anammox Reactors. *Environ. Sci. Technol.* 48, 8679–8687. <https://doi.org/10.1021/es501819n>
- Erdal, U.G., Erdal, Z.K., Daigger, G.T., Randall, C.W., 2008. Is it PAO-GAO competition or metabolic shift in EBPR system? Evidence from an experimental study. *Water Sci. Technol.* 58, 1329–1334. <https://doi.org/10.2166/wst.2008.734>
- Erdal, U.G., Erdal, Z.K., Randall, C.W., 2003. The competition between PAOs (phosphorus accumulating organisms) and GAOs (glycogen accumulating organisms) in EBPR (enhanced biological phosphorus removal) systems at different temperatures and the effects on system performance. *Water Sci. Technol.* 47, 1–8. <https://doi.org/10.2166/wst.2003.0579>
- Fitzgerald, C.M., Camejo, P., Oshlag, J.Z., Noguera, D.R., 2015. Ammonia-oxidizing microbial communities in reactors with efficient nitrification at low-dissolved oxygen. *Water Res.* 70, 38–51. <https://doi.org/10.1016/j.watres.2014.11.041>
- Foley, J., de Haas, D., Yuan, Z., Lant, P., 2010. Nitrous oxide generation in full-scale biological nutrient removal wastewater treatment plants. *Water Res.* 44, 831–844. <https://doi.org/10.1016/j.watres.2009.10.033>
- Fowler, S.J., Palomo, A., Dechesne, A., Mines, P.D., Smets, B.F., 2018. Comammox *Nitrospira* are abundant ammonia oxidizers in diverse groundwater-fed rapid sand filter communities: Comammox *Nitrospira* in drinking water biofilters. *Environ. Microbiol.* 20, 1002–1015. <https://doi.org/10.1111/1462-2920.14033>
- Francis, C.A., Roberts, K.J., Beman, J.M., Santoro, A.E., Oakley, B.B., 2005. Ubiquity and diversity of ammonia-oxidizing archaea in water columns and sediments of the ocean. *Proc. Natl. Acad. Sci.* 102, 14683–14688. <https://doi.org/10.1073/pnas.0506625102>
- Fux, C., Bohler, M., Huber, P., Brunner, I., Siegrist, H., 2002. Biological treatment of ammonium-rich wastewater by partial nitritation and subsequent anaerobic ammonium oxidation (anammox) in a pilot plant. *J. Biotechnol.* 99, 295–306.
- Gao, H., Mao, Y., Zhao, X., Liu, W.-T., Zhang, T., Wells, G., 2019. Genome-centric metagenomics resolves microbial diversity and prevalent truncated denitrification

- pathways in a denitrifying PAO-enriched bioprocess. *Water Res.* 155, 275–287. <https://doi.org/10.1016/j.watres.2019.02.020>
- Gao, H., Scherson, Y.D., Wells, G.F., 2014. Towards energy neutral wastewater treatment: methodology and state of the art. *Environ. Sci. Process. Impacts* 16, 1223. <https://doi.org/10.1039/c4em00069b>
- Ge, H., Batstone, D.J., Keller, J., 2015. Biological phosphorus removal from abattoir wastewater at very short sludge ages mediated by novel PAO clade Comamonadaceae. *Water Res.* 69, 173–182. <https://doi.org/10.1016/j.watres.2014.11.026>
- Ge, H., Batstone, D.J., Keller, J., 2013. Operating aerobic wastewater treatment at very short sludge ages enables treatment and energy recovery through anaerobic sludge digestion. *Water Res.* 47, 6546–6557. <https://doi.org/10.1016/j.watres.2013.08.017>
- Gilbert, E.M., Agrawal, S., Brunner, F., Schwartz, T., Horn, H., Lackner, S., 2014a. Response of Different *Nitrospira* Species To Anoxic Periods Depends on Operational DO. *Environ. Sci. Technol.* 48, 2934–2941. <https://doi.org/10.1021/es404992g>
- Gilbert, E.M., Agrawal, S., Karst, S.M., Horn, H., Nielsen, P.H., Lackner, S., 2014b. Low Temperature Partial Nitritation/Anammox in a Moving Bed Biofilm Reactor Treating Low Strength Wastewater. *Environ. Sci. Technol.* 48, 8784–8792. <https://doi.org/10.1021/es501649m>
- Gilbert, E.M., Agrawal, S., Schwartz, T., Horn, H., Lackner, S., 2015. Comparing different reactor configurations for Partial Nitritation/Anammox at low temperatures. *Water Res.* 81, 92–100. <https://doi.org/10.1016/j.watres.2015.05.022>
- Gonzalez-Martinez, A., Rodriguez-Sanchez, A., van Loosdrecht, M.C.M., Gonzalez-Lopez, J., Vahala, R., 2016. Detection of comammox bacteria in full-scale wastewater treatment bioreactors using tag-454-pyrosequencing. *Environ. Sci. Pollut. Res.* 23, 25501–25511. <https://doi.org/10.1007/s11356-016-7914-4>
- Griffin, J.S., Wells, G.F., 2017. Regional synchrony in full-scale activated sludge bioreactors due to deterministic microbial community assembly. *ISME J.* 11, 500–511. <https://doi.org/10.1038/ismej.2016.121>
- Gujer, W., Henze, M., Mino, T., Matsuo, T., Wentzel, M.C., Marais, G. v. R., 1995. The Activated Sludge Model No. 2: Biological Phosphorus Removal. *Water Sci. Technol.* 31, 1–11.
- Gustavsson, D.J.I., Suarez, C., Wilén, B.-M., Hermansson, M., Persson, F., 2020. Long-term stability of partial nitritation-anammox for treatment of municipal wastewater in a moving bed biofilm reactor pilot system. *Sci. Total Environ.* 714, 136342. <https://doi.org/10.1016/j.scitotenv.2019.136342>
- Guyen, D., Dapena, A., Kartal, B., Schmid, M.C., Maas, B., van de Pas-Schoonen, K., Sozen, S., Mendez, R., Op den Camp, H.J.M., Jetten, M.S.M., Strous, M., Schmidt, I., 2005. Propionate Oxidation by and Methanol Inhibition of Anaerobic Ammonium-Oxidizing Bacteria. *Appl. Environ. Microbiol.* 71, 1066–1071. <https://doi.org/10.1128/AEM.71.2.1066-1071.2005>
- Han, M., De Clippeleir, H., Al-Omari, A., Wett, B., Vlaeminck, S.E., Bott, C., Murthy, S., 2016a. Impact of carbon to nitrogen ratio and aeration regime on mainstream deammonification. *Water Sci. Technol.* <https://doi.org/10.2166/wst.2016.202>

- Han, M., Vlaeminck, S.E., Al-Omari, A., Wett, B., Bott, C., Murthy, S., De Clippeleir, H., 2016b. Uncoupling the solids retention times of flocs and granules in mainstream deammonification: A screen as effective out-selection tool for nitrite oxidizing bacteria. *Bioresour. Technol.* 221, 195–204. <https://doi.org/10.1016/j.biortech.2016.08.115>
- Harhangi, H.R., Le Roy, M., van Alen, T., Hu, B. -l., Groen, J., Kartal, B., Tringe, S.G., Quan, Z.-X., Jetten, M.S.M., Op den Camp, H.J.M., 2012. Hydrazine Synthase, a Unique Phylomarker with Which To Study the Presence and Biodiversity of Anammox Bacteria. *Appl. Environ. Microbiol.* 78, 752–758. <https://doi.org/10.1128/AEM.07113-11>
- Hellinga, C., Schellen, A.A.J.C., Mulder, J.W., van Loosdrecht, M.C.M., Heijnen, J.J., 1998. The sharon process: An innovative method for nitrogen removal from ammonium-rich waste water. *Water Sci. Technol.* 37, 135–142. [https://doi.org/10.1016/S0273-1223\(98\)00281-9](https://doi.org/10.1016/S0273-1223(98)00281-9)
- Hesselmann, R.P.X., von Rummell, R., Resnick, S.M., Hany, R., Zehnder, A.J.B., 2000. Anaerobic metabolism of bacteria performing enhanced biological phosphate removal. *Water Res.* 34, 3487–3494. [https://doi.org/10.1016/S0043-1354\(00\)00092-0](https://doi.org/10.1016/S0043-1354(00)00092-0)
- Hesselmann, R.P.X., Werlen, C., Hahn, D., van der Meer, J.R., Zehnder, A.J.B., 1999. Enrichment, Phylogenetic Analysis and Detection of a Bacterium That Performs Enhanced Biological Phosphate Removal in Activated Sludge. *Syst. Appl. Microbiol.* 22, 454–465. [https://doi.org/10.1016/S0723-2020\(99\)80055-1](https://doi.org/10.1016/S0723-2020(99)80055-1)
- Hocaoglu, S.M., Insel, G., Cokgor, E.U., Orhon, D., 2011. Effect of low dissolved oxygen on simultaneous nitrification and denitrification in a membrane bioreactor treating black water. *Bioresour. Technol.* 102, 4333–4340. <https://doi.org/10.1016/j.biortech.2010.11.096>
- Hoekstra, M., Geilvoet, S.P., Hendrickx, T.L.G., van Erp Taalman Kip, C.S., Kleerebezem, R., van Loosdrecht, M.C.M., 2019. Towards mainstream anammox: lessons learned from pilot-scale research at WWTP Dokhaven. *Environ. Technol.* 40, 1721–1733. <https://doi.org/10.1080/09593330.2018.1470204>
- Hubaux, N., Wells, G., Morgenroth, E., 2015. Impact of coexistence of flocs and biofilm on performance of combined nitrification-anammox granular sludge reactors. *Water Res.* 68, 127–139. <https://doi.org/10.1016/j.watres.2014.09.036>
- ifak, 2018. Simba# 3.0 Manual.
- Jenni, S., Vlaeminck, S.E., Morgenroth, E., Udert, K.M., 2014. Successful application of nitritation/anammox to wastewater with elevated organic carbon to ammonia ratios. *Water Res.* 49, 316–326. <https://doi.org/10.1016/j.watres.2013.10.073>
- Jimenez, J.A., Wise, G., Burger, G., Du, W., Dold, P., 2014. Mainstream nitrite-shunt with biological phosphorus removal at the city of St. Petersburg Southwest WRF. Presented at the WEFTEC, WEFTEC, New Orleans, LA.
- Joss, A., Salzgeber, D., Eugster, J., König, R., Rottermann, K., Burger, S., Fabijan, P., Leumann, S., Mohn, J., Siegrist, H., 2009. Full-scale nitrogen removal from digester liquid with partial nitritation and anammox in one SBR. *Environ. Sci. Technol.* 43, 5301–5306.
- Jubany, I., Lafuente, J., Baeza, J.A., Carrera, J., 2009. Total and stable washout of nitrite oxidizing bacteria from a nitrifying continuous activated sludge system using automatic control based on Oxygen Uptake Rate measurements. *Water Res.* 43, 2761–2772. <https://doi.org/10.1016/j.watres.2009.03.022>

- Kampschreur, M.J., van der Star, W.R.L., Wienders, H.A., Mulder, J.W., Jetten, M.S.M., van Loosdrecht, M.C.M., 2008. Dynamics of nitric oxide and nitrous oxide emission during full-scale reject water treatment. *Water Res.* 42, 812–826.  
<https://doi.org/10.1016/j.watres.2007.08.022>
- Kartal, B., Van Niftrik, L., Rattray, J., Van De Vossenberg, J.L.C.M., Schmid, M.C., Sinnighe Damsté, J., Jetten, M.S.M., Strous, M., 2008. Candidatus ‘*Brocadia fulgida*’: an autofluorescent anaerobic ammonium oxidizing bacterium: Autofluorescent anammox bacteria. *FEMS Microbiol. Ecol.* 63, 46–55. <https://doi.org/10.1111/j.1574-6941.2007.00408.x>
- Katoh, K., Standley, D.M., 2013. MAFFT Multiple Sequence Alignment Software Version 7: Improvements in Performance and Usability. *Mol. Biol. Evol.* 30, 772–780.  
<https://doi.org/10.1093/molbev/mst010>
- Keene, N.A., Reusser, S.R., Scarborough, M.J., Grooms, A.L., Seib, M., Santo Domingo, J., Noguera, D.R., 2017. Pilot plant demonstration of stable and efficient high rate biological nutrient removal with low dissolved oxygen conditions. *Water Res.* 121, 72–85.  
<https://doi.org/10.1016/j.watres.2017.05.029>
- Kern-Jespersen, J.P., Henze, M., 1993. Biological phosphorus uptake under anoxic and aerobic conditions.
- Kits, K.D., Sedlacek, C.J., Lebedeva, E.V., Han, P., Bulaev, A., Pjevac, P., Daebeler, A., Romano, S., Albertsen, M., Stein, L.Y., Daims, H., Wagner, M., 2017. Kinetic analysis of a complete nitrifier reveals an oligotrophic lifestyle. *Nature* 549, 269–272.  
<https://doi.org/10.1038/nature23679>
- Klaus, S., Printz, K., McCullough, K., Srinivasan, V., Wang, D., He, P., De Clippeleir, H., Gu, A., Bott, C.B., 2019. Integrating Bio-P and Shortcut Nitrogen Removal via RAS Fermentation and Partial Denitrification/Anammox, in: Proceedings of the WEF Nutrient Removal and Recovery Symposium. Presented at the WEF Nutrient Removal and Recovery Symposium, Water Environment Federation, Minneapolis, MN, USA.
- Koch, G., Egli, K., Van der Meer, J.R., Siegrist, H., 2000. Mathematical modeling of autotrophic denitrification in a nitrifying biofilm of a rotating biological contactor. *Water Sci. Technol.* 41, 191–198.
- Koch, H., Lücker, S., Albertsen, M., Kitzinger, K., Herbold, C., Spieck, E., Nielsen, P.H., Wagner, M., Daims, H., 2015. Expanded metabolic versatility of ubiquitous nitrite-oxidizing bacteria from the genus *Nitrospira*. *Proc. Natl. Acad. Sci.* 112, 11371–11376.  
<https://doi.org/10.1073/pnas.1506533112>
- Kouba, V., Widiayuningrum, P., Chovancova, L., Jenicek, P., Bartacek, J., 2016. Applicability of one-stage partial nitritation and anammox in MBBR for anaerobically pre-treated municipal wastewater. *J. Ind. Microbiol. Biotechnol.* 43, 965–975.  
<https://doi.org/10.1007/s10295-016-1766-2>
- Lackner, S., Gilbert, E.M., Vlaeminck, S.E., Joss, A., Horn, H., van Loosdrecht, M.C.M., 2014. Full-scale partial nitritation/anammox experiences – An application survey. *Water Res.* 55, 292–303. <https://doi.org/10.1016/j.watres.2014.02.032>
- Lackner, S., Welker, S., Gilbert, E.M., Horn, H., 2015. Influence of seasonal temperature fluctuations on two different partial nitritation-anammox reactors treating mainstream

- municipal wastewater. *Water Sci. Technol.* 72, 1358–1363.  
<https://doi.org/10.2166/wst.2015.301>
- Laureni, M., Falås, P., Robin, O., Wick, A., Weissbrodt, D.G., Nielsen, J.L., Ternes, T.A., Morgenroth, E., Joss, A., 2016. Mainstream partial nitrification and anammox: Long-term process stability and effluent quality at low temperatures. *Water Res.*  
<https://doi.org/10.1016/j.watres.2016.05.005>
- Laureni, M., Weissbrodt, D.G., Villez, K., Robin, O., de Jonge, N., Rosenthal, A., Wells, G., Nielsen, J.L., Morgenroth, E., Joss, A., 2019. Biomass segregation between biofilm and flocs improves the control of nitrite-oxidizing bacteria in mainstream partial nitrification and anammox processes. *Water Res.* 154, 104–116.  
<https://doi.org/10.1016/j.watres.2018.12.051>
- Law, Y., Matysik, A., Chen, X., Swa Thi, S., Ngoc Nguyen, T.Q., Qiu, G., Natarajan, G., Williams, R.B.H., Ni, B.-J., Seviour, T.W., Wuertz, S., 2019. High Dissolved Oxygen Selection against *Nitrospira* Sublineage I in Full-Scale Activated Sludge. *Environ. Sci. Technol.* 53, 8157–8166. <https://doi.org/10.1021/acs.est.9b00955>
- Law, Y., Ye, L., Pan, Y., Yuan, Z., 2012. Nitrous oxide emissions from wastewater treatment processes. *Philos. Trans. R. Soc. B Biol. Sci.* 367, 1265–1277.  
<https://doi.org/10.1098/rstb.2011.0317>
- Lawson, C.E., Lücker, S., 2018. Complete ammonia oxidation: an important control on nitrification in engineered ecosystems? *Curr. Opin. Biotechnol.* 50, 158–165.  
<https://doi.org/10.1016/j.copbio.2018.01.015>
- Lawson, C.E., Wu, S., Bhattacharjee, A.S., Hamilton, J.J., McMahon, K.D., Goel, R., Noguera, D.R., 2017. Metabolic network analysis reveals microbial community interactions in anammox granules. *Nat. Commun.* 8, 15416. <https://doi.org/10.1038/ncomms15416>
- Le, T., Peng, B., Su, C., Massoudieh, A., Torrents, A., Al-Omari, A., Murthy, S., Wett, B., Chandran, K., deBarbadillo, C., Bott, C., De Clippeleir, H., 2019a. Nitrate residual as a key parameter to efficiently control partial denitrification coupling with anammox. *Water Environ. Res.* 91, 1455–1465. <https://doi.org/10.1002/wer.1140>
- Le, T., Peng, B., Su, C., Massoudieh, A., Torrents, A., Al-Omari, A., Murthy, S., Wett, B., Chandran, K., DeBarbadillo, C., Bott, C., De Clippeleir, H., 2019b. Impact of carbon source and COD/N on the concurrent operation of partial denitrification and anammox. *Water Environ. Res.* 91, 185–197. <https://doi.org/10.1002/wer.1016>
- Lee, D.S., Jeon, C.O., Park, J.M., 2001. Biological nitrogen removal with enhanced phosphate uptake in a sequencing batch reactor using single sludge system. *Water Res.* 35, 3968–3976. [https://doi.org/10.1016/S0043-1354\(01\)00132-4](https://doi.org/10.1016/S0043-1354(01)00132-4)
- Letunic, I., Bork, P., 2016. Interactive tree of life (iTOL) v3: an online tool for the display and annotation of phylogenetic and other trees. *Nucleic Acids Res.* 44, W242–W245.  
<https://doi.org/10.1093/nar/gkw290>
- Lewis, W.M., Morris, D.P., 1986. Toxicity of Nitrite to Fish: A Review. *Trans. Am. Fish. Soc.* 115, 183–195. [https://doi.org/10.1577/1548-8659\(1986\)115<183:TONTF>2.0.CO;2](https://doi.org/10.1577/1548-8659(1986)115<183:TONTF>2.0.CO;2)
- Liu, J.R., 2002. Emended description of the genus *Trichococcus*, description of *Trichococcus collinsii* sp. nov., and reclassification of *Lactosphaera pasteurii* as *Trichococcus pasteurii* comb. nov. and of *Ruminococcus palustris* as *Trichococcus palustris* comb. nov. in the

- low-G+C Gram-positive bacteria. *Int. J. Syst. Evol. Microbiol.* 52, 1113–1126. <https://doi.org/10.1099/ijs.0.02085-0>
- Liu, Z., Frigaard, N.-U., Vogl, K., Iino, T., Ohkuma, M., Overmann, J., Bryant, D.A., 2012. Complete Genome of *Ignavibacterium album*, a Metabolically Versatile, Flagellated, Facultative Anaerobe from the Phylum Chlorobi. *Front. Microbiol.* 3. <https://doi.org/10.3389/fmicb.2012.00185>
- López-Vázquez, C.M., Hooijmans, C.M., Brdjanovic, D., Gijzen, H.J., van Loosdrecht, M.C.M., 2008. Factors affecting the microbial populations at full-scale enhanced biological phosphorus removal (EBPR) wastewater treatment plants in The Netherlands. *Water Res.* 42, 2349–2360. <https://doi.org/10.1016/j.watres.2008.01.001>
- Lopez-Vazquez, C.M., Oehmen, A., Hooijmans, C.M., Brdjanovic, D., Gijzen, H.J., Yuan, Z., van Loosdrecht, M.C.M., 2009. Modeling the PAO–GAO competition: Effects of carbon source, pH and temperature. *Water Res.* 43, 450–462. <https://doi.org/10.1016/j.watres.2008.10.032>
- Lotti, T., Kleerebezem, R., Abelleira-Pereira, J.M., Abbas, B., van Loosdrecht, M.C.M., 2015a. Faster through training: The anammox case. *Water Res.* 81, 261–268. <https://doi.org/10.1016/j.watres.2015.06.001>
- Lotti, T., Kleerebezem, R., Hu, Z., Kartal, B., de Kreuk, M.K., van Erp Taalman Kip, C., Kruit, J., Hendrickx, T.L.G., van Loosdrecht, M.C.M., 2015b. Pilot-scale evaluation of anammox-based mainstream nitrogen removal from municipal wastewater. *Environ. Technol.* 36, 1167–1177. <https://doi.org/10.1080/09593330.2014.982722>
- Lotti, T., Kleerebezem, R., Hu, Z., Kartal, B., Jetten, M.S.M., van Loosdrecht, M.C.M., 2014. Simultaneous partial nitrification and anammox at low temperature with granular sludge. *Water Res.* 66, 111–121. <https://doi.org/10.1016/j.watres.2014.07.047>
- Lotti, T., Kleerebezem, R., van Loosdrecht, M.C.M., 2015c. Effect of temperature change on anammox activity: Temperature Effect on Anammox Bacteria. *Biotechnol. Bioeng.* 112, 98–103. <https://doi.org/10.1002/bit.25333>
- Lucker, S., Wagner, M., Maixner, F., Pelletier, E., Koch, H., Vacherie, B., Rattei, T., Damste, J.S.S., Spieck, E., Le Paslier, D., Daims, H., 2010. A *Nitrospira* metagenome illuminates the physiology and evolution of globally important nitrite-oxidizing bacteria. *Proc. Natl. Acad. Sci.* 107, 13479–13484. <https://doi.org/10.1073/pnas.1003860107>
- Ludwig, W., 2004. ARB: a software environment for sequence data. *Nucleic Acids Res.* 32, 1363–1371. <https://doi.org/10.1093/nar/gkh293>
- Ma, B., Bao, P., Wei, Y., Zhu, G., Yuan, Z., Peng, Y., 2015. Suppressing Nitrite-oxidizing Bacteria Growth to Achieve Nitrogen Removal from Domestic Wastewater via Anammox Using Intermittent Aeration with Low Dissolved Oxygen. *Sci. Rep.* 5, 13048. <https://doi.org/10.1038/srep13048>
- Ma, B., Qian, W., Yuan, C., Yuan, Z., Peng, Y., 2017a. Achieving Mainstream Nitrogen Removal through Coupling Anammox with Denitrification. *Environ. Sci. Technol.* 51, 8405–8413. <https://doi.org/10.1021/acs.est.7b01866>
- Ma, B., Qian, W., Yuan, C., Yuan, Z., Peng, Y., 2017b. Achieving mainstream nitrogen removal through coupling anammox with denitrification. *Environ. Sci. Technol.* <https://doi.org/10.1021/acs.est.7b01866>

- Ma, B., Wang, S., Zhang, S., Li, X., Bao, P., Peng, Y., 2013. Achieving nitrification and phosphorus removal in a continuous-flow anaerobic/oxic reactor through bio-augmentation. *Bioresour. Technol.* 139, 375–378. <https://doi.org/10.1016/j.biortech.2013.02.077>
- Ma, B., Zhang, S., Zhang, L., Yi, P., Wang, J., Wang, S., Peng, Y., 2011. The feasibility of using a two-stage autotrophic nitrogen removal process to treat sewage. *Bioresour. Technol.* 102, 8331–8334. <https://doi.org/10.1016/j.biortech.2011.06.017>
- Ma, Y., Domingo-Félez, C., Plósz, B.Gy., Smets, B.F., 2017a. Intermittent Aeration Suppresses Nitrite-Oxidizing Bacteria in Membrane-Aerated Biofilms: A Model-Based Explanation. *Environ. Sci. Technol.* <https://doi.org/10.1021/acs.est.7b00463>
- Ma, Y., Domingo-Félez, C., Plósz, B.Gy., Smets, B.F., 2017b. Intermittent Aeration Suppresses Nitrite-Oxidizing Bacteria in Membrane-Aerated Biofilms: A Model-Based Explanation. *Environ. Sci. Technol.* 51, 6146–6155. <https://doi.org/10.1021/acs.est.7b00463>
- Malovanyy, A., Trela, J., Plaza, E., 2015. Mainstream wastewater treatment in integrated fixed film activated sludge (IFAS) reactor by partial nitrification/anammox process. *Bioresour. Technol.* 198, 478–487. <https://doi.org/10.1016/j.biortech.2015.08.123>
- Mamais, D., Jenkins, D., 1992. The Effects of MCRT and Temperature on Enhanced Biological Phosphorus Removal. *Water Sci. Technol.* 26, 955–965. <https://doi.org/10.2166/wst.1992.0537>
- Mamais, D., Jenkins, D., Prrr, P., 1993. A rapid physical-chemical method for the determination of readily biodegradable soluble COD in municipal wastewater. *Water Res.* 27, 195–197. [https://doi.org/10.1016/0043-1354\(93\)90211-Y](https://doi.org/10.1016/0043-1354(93)90211-Y)
- Mao, Y., Graham, D.W., Tamaki, H., Zhang, T., 2015. Dominant and novel clades of *Candidatus Accumulibacter phosphatis* in 18 globally distributed full-scale wastewater treatment plants. *Sci. Rep.* 5, 11857. <https://doi.org/10.1038/srep11857>
- Mao, Y., Yu, K., Xia, Y., Chao, Y., Zhang, T., 2014. Genome Reconstruction and Gene Expression of “*Candidatus Accumulibacter phosphatis*” Clade IB Performing Biological Phosphorus Removal. *Environ. Sci. Technol.* 48, 10363–10371. <https://doi.org/10.1021/es502642b>
- McClintock, S.A., Randall, C.W., Pattarkine, V.M., 1993. Effects of temperature and mean cell residence time on biological nutrient removal processes. *Water Environ. Res.* 65, 110–118. <https://doi.org/10.2175/WER.65.2.3>
- Melcer, H., 2004. *Methods for Wastewater Characterization in Activated Sludge Modelling*. IWA Publishing.
- Mobarry, B.K., Wagner, M., Urbain, V., Rittmann, B.E., Stahl, D.A., 1996. Phylogenetic probes for analyzing abundance and spatial organization of nitrifying bacteria. *Appl. Environ. Microbiol.* 62, 2156–2162.
- Nguyen, H.T.T., Le, V.Q., Hansen, A.A., Nielsen, J.L., Nielsen, P.H., 2011. High diversity and abundance of putative polyphosphate-accumulating Tetrasphaera-related bacteria in activated sludge systems: Tetrasphaera-related bacteria in activated sludge systems. *FEMS Microbiol. Ecol.* 76, 256–267. <https://doi.org/10.1111/j.1574-6941.2011.01049.x>
- Ni, B.-J., Chen, Y.-P., Liu, S.-Y., Fang, F., Xie, W.-M., Yu, H.-Q., 2009. Modeling a granule-based anaerobic ammonium oxidizing (ANAMMOX) process. *Biotechnol. Bioeng.* 103, 490–499. <https://doi.org/10.1002/bit.22279>

- Ni, S.-Q., Ni, J.-Y., Hu, D.-L., Sung, S., 2012. Effect of organic matter on the performance of granular anammox process. *Bioresour. Technol.* 110, 701–705. <https://doi.org/10.1016/j.biortech.2012.01.066>
- Nielsen, P.H., 2009. FISH Handbook for Biological Wastewater Treatment. *Water Intell.* Online 8. <https://doi.org/10.2166/9781780401775>
- Nowka, B., Daims, H., Spieck, E., 2015. Comparison of Oxidation Kinetics of Nitrite-Oxidizing Bacteria: Nitrite Availability as a Key Factor in Niche Differentiation. *Appl. Environ. Microbiol.* 81, 745–753. <https://doi.org/10.1128/AEM.02734-14>
- Pagilla, K.R., Urgan-Demirtas, M., Ramani, R., 2006. Low effluent nutrient technologies for wastewater treatment. *Water Sci. Technol.* 53, 165–172. <https://doi.org/10.2166/wst.2006.089>
- Palomo, A., Jane Fowler, S., Gülay, A., Rasmussen, S., Sicheritz-Ponten, T., Smets, B.F., 2016. Metagenomic analysis of rapid gravity sand filter microbial communities suggests novel physiology of *Nitrospira* spp. *ISME J.* 10, 2569–2581. <https://doi.org/10.1038/ismej.2016.63>
- Pambrun, V., Paul, E., Spérandio, M., 2006. Modeling the partial nitrification in sequencing batch reactor for biomass adapted to high ammonia concentrations. *Biotechnol. Bioeng.* 95, 120–131. <https://doi.org/10.1002/bit.21008>
- Parada, A.E., Needham, D.M., Fuhrman, J.A., 2016. Every base matters: assessing small subunit rRNA primers for marine microbiomes with mock communities, time series and global field samples: Primers for marine microbiome studies. *Environ. Microbiol.* 18, 1403–1414. <https://doi.org/10.1111/1462-2920.13023>
- Park, H.-D., Noguera, D.R., 2007. Characterization of two ammonia-oxidizing bacteria isolated from reactors operated with low dissolved oxygen concentrations. *J. Appl. Microbiol.* 102, 1401–1417. <https://doi.org/10.1111/j.1365-2672.2006.03176.x>
- Park, H.-D., Noguera, D.R., 2004. Evaluating the effect of dissolved oxygen on ammonia-oxidizing bacterial communities in activated sludge. *Water Res.* 38, 3275–3286. <https://doi.org/10.1016/j.watres.2004.04.047>
- Persson, F., Suarez, C., Hermansson, M., Plaza, E., Sultana, R., Wilén, B.-M., 2017. Community structure of partial nitrification-anammox biofilms at decreasing substrate concentrations and low temperature. *Microb. Biotechnol.* 10, 761–772. <https://doi.org/10.1111/1751-7915.12435>
- Pester, M., Maixner, F., Berry, D., Rattei, T., Koch, H., Lückner, S., Nowka, B., Richter, A., Spieck, E., Lebedeva, E., Loy, A., Wagner, M., Daims, H., 2014. *NxrB* encoding the beta subunit of nitrite oxidoreductase as functional and phylogenetic marker for nitrite-oxidizing *Nitrospira*: Functional and phylogenetic marker for *Nitrospira*. *Environ. Microbiol.* 16, 3055–3071. <https://doi.org/10.1111/1462-2920.12300>
- Piciooreanu, C., Pérez, J., van Loosdrecht, M.C.M., 2016. Impact of cell cluster size on apparent half-saturation coefficients for oxygen in nitrifying sludge and biofilms. *Water Res.* 106, 371–382. <https://doi.org/10.1016/j.watres.2016.10.017>
- Pijuan, M., Ye, L., Yuan, Z., 2010. Free nitrous acid inhibition on the aerobic metabolism of poly-phosphate accumulating organisms. *Water Res.* 44, 6063–6072. <https://doi.org/10.1016/j.watres.2010.07.075>

- Pinto, A.J., Marcus, D.N., Ijaz, U.Z., Bautista-de los Santos, Q.M., Dick, G.J., Raskin, L., 2016. Metagenomic Evidence for the Presence of Comammox *Nitrospira* -Like Bacteria in a Drinking Water System. *mSphere* 1, e00054-15. <https://doi.org/10.1128/mSphere.00054-15>
- Pjevac, P., Schaubberger, C., Poghosyan, L., Herbold, C.W., van Kessel, M.A.H.J., Daebeler, A., Steinberger, M., Jetten, M.S.M., Lückner, S., Wagner, M., Daims, H., 2017. AmoA-Targeted Polymerase Chain Reaction Primers for the Specific Detection and Quantification of Comammox *Nitrospira* in the Environment. *Front. Microbiol.* 8. <https://doi.org/10.3389/fmicb.2017.01508>
- Poot, V., Hoekstra, M., Geleijnse, M.A.A., van Loosdrecht, M.C.M., Pérez, J., 2016. Effects of the residual ammonium concentration on NOB repression during partial nitrification with granular sludge. *Water Res.* 106, 518–530. <https://doi.org/10.1016/j.watres.2016.10.028>
- Price, M.N., Dehal, P.S., Arkin, A.P., 2010. FastTree 2 – Approximately Maximum-Likelihood Trees for Large Alignments. *PLOS ONE* 5, e9490. <https://doi.org/10.1371/journal.pone.0009490>
- Quast, C., Pruesse, E., Yilmaz, P., Gerken, J., Schweer, T., Yarza, P., Peplies, J., Glöckner, F.O., 2013. The SILVA ribosomal RNA gene database project: improved data processing and web-based tools. *Nucleic Acids Res.* 41, D590-596. <https://doi.org/10.1093/nar/gks1219>
- Rahman, A., De Clippeleir, H., Winckel, T.V., Le, T., Riffat, R., Wett, B., Jimenez, J.A., Bott, C., Al-Omari, A., Murthy, S., 2015. Does Optimization of Carbon Redirection Always Imply Energy Recovery? *Proc. Water Environ. Fed.* 2015, 4432–4443.
- Regmi, P., Holgate, B., Miller, M.W., Park, H., Chandran, K., Wett, B., Murthy, S., Bott, C.B., 2015. Nitrogen polishing in a fully anoxic anammox MBBR treating mainstream nitrification-denitrification effluent: Nitrogen Polishing in a Fully Anoxic Anammox MBBR. *Biotechnol. Bioeng.* n/a-n/a. <https://doi.org/10.1002/bit.25826>
- Regmi, P., Miller, M.W., Holgate, B., Bunce, R., Park, H., Chandran, K., Wett, B., Murthy, S., Bott, C.B., 2014. Control of aeration, aerobic SRT and COD input for mainstream nitrification/denitrification. *Water Res.* 57, 162–171. <https://doi.org/10.1016/j.watres.2014.03.035>
- Rittmann, B., McCarty, P.L., 2001. *Environmental Biotechnology: Principles and Applications*. McGraw-Hill Higher Education.
- Rognes, T., Flouri, T., Nichols, B., Quince, C., Mahé, F., 2016. VSEARCH: a versatile open source tool for metagenomics. *PeerJ* 4. <https://doi.org/10.7717/peerj.2584>
- Roots, P., Sabba, F., Rosenthal, A.F., Wang, Y., Yuan, Q., Rieger, L., Yang, F., Kozak, J.A., Zhang, H., Wells, G.F., 2019a. Integrated shortcut nitrogen and biological phosphorus removal from mainstream wastewater: process operation and modeling. *Environ. Sci. Water Res. Technol.* 6, 566–580. <https://doi.org/10.1039/C9EW00550A>
- Roots, P., Wang, Y., Rosenthal, A.F., Griffin, J.S., Sabba, F., Petrovich, M., Yang, F., Kozak, J.A., Zhang, H., Wells, G.F., 2019b. Comammox *Nitrospira* are the dominant ammonia oxidizers in a mainstream low dissolved oxygen nitrification reactor. *Water Res.* 157, 396–405. <https://doi.org/10.1016/j.watres.2019.03.060>
- Rothauwe, J.-H., Witzel, K.-P., Liesack, W., 1997. The ammonia monooxygenase structural gene amoA as a functional marker: molecular fine-scale analysis of natural ammonia-oxidizing populations. *Appl. Environ. Microbiol.* 63, 4704–4712.

- Rumble, J.R., 2018. CRC Handbook of Chemistry and Physics 99th Edition [WWW Document]. URL [http://hbcponline.com/faces/documents/05\\_24/05\\_24\\_0003.xhtml](http://hbcponline.com/faces/documents/05_24/05_24_0003.xhtml) (accessed 10.9.18).
- Sabba, F., Terada, A., Wells, G., Smets, B.F., Nerenberg, R., 2018. Nitrous Oxide Emissions from Biofilm Processes for Wastewater Treatment. *Appl Microbiol Biotechnol* 36.
- Sales, C.M., Lee, P.K., 2015. Resource recovery from wastewater: application of meta-omics to phosphorus and carbon management. *Curr. Opin. Biotechnol., Environmental biotechnology • Energy biotechnology* 33, 260–267. <https://doi.org/10.1016/j.copbio.2015.03.003>
- Scherson, Y.D., Criddle, C.S., 2014. Recovery of Freshwater from Wastewater: Upgrading Process Configurations To Maximize Energy Recovery and Minimize Residuals. *Environ. Sci. Technol.* 48, 8420–8432. <https://doi.org/10.1021/es501701s>
- Schindelin, J., Arganda-Carreras, I., Frise, E., Kaynig, V., Longair, M., Pietzsch, T., Preibisch, S., Rueden, C., Saalfeld, S., Schmid, B., Tinevez, J.-Y., White, D.J., Hartenstein, V., Eliceiri, K., Tomancak, P., Cardona, A., 2012. Fiji: an open-source platform for biological-image analysis. *Nat. Methods* 9, 676–682. <https://doi.org/10.1038/nmeth.2019>
- Schraa, O., Rieger, L., Alex, J., Miletić, I., 2019. Ammonia-based aeration control with optimal SRT control: improved performance and lower energy consumption. *Water Sci. Technol.* 79, 63–72. <https://doi.org/10.2166/wst.2019.032>
- Schramm, A., de Beer, D., van den Heuvel, J.C., Ottengraf, S., Amann, R., 1999. Microscale Distribution of Populations and Activities of *Nitrosospira* and *Nitrospira* spp. along a Macroscale Gradient in a Nitrifying Bioreactor: Quantification by In Situ Hybridization and the Use of Microsensors. *Appl. Environ. Microbiol.* 65, 3690–3696.
- Seuntjens, D., Van Tendeloo, M., Chatzigiannidou, I., Carvajal-Arroyo, J.M., Vandendriessche, S., Vlaeminck, S.E., Boon, N., 2018. Synergistic Exposure of Return-Sludge to Anaerobic Starvation, Sulfide, and Free Ammonia to Suppress Nitrite Oxidizing Bacteria. *Environ. Sci. Technol.* 52, 8725–8732. <https://doi.org/10.1021/acs.est.7b06591>
- Shao, Y.J., Wada, F., Abkian, V., Crosse, J., Horenstein, B., Jenkins, D., 1992. Effects of MCRT on Enhanced Biological Phosphorus Removal. *Water Sci. Technol.* 26, 967–976. <https://doi.org/10.2166/wst.1992.0538>
- Skalsky, D.S., Daigger, G.T., 1995. Wastewater solids fermentation for volatile acid production and enhanced biological phosphorus removal. *Water Environ. Res.* 67, 230–237. <https://doi.org/10.2175/106143095X131402>
- Smolders, G.J.F., Van der Meij, J., Van Loosdrecht, M.C.M., Heijnen, J.J., 1994. Model of the anaerobic metabolism of the biological phosphorus removal process: stoichiometry and pH influence. *Biotechnol. Bioeng.* 43, 461–470.
- Stamatakis, A., 2014. RAxML version 8: a tool for phylogenetic analysis and post-analysis of large phylogenies. *Bioinformatics* 30, 1312–1313. <https://doi.org/10.1093/bioinformatics/btu033>
- Steffen, W., Richardson, K., Rockstrom, J., Cornell, S.E., Fetzer, I., Bennett, E.M., Biggs, R., Carpenter, S.R., de Vries, W., de Wit, C.A., Folke, C., Gerten, D., Heinke, J., Mace, G.M., Persson, L.M., Ramanathan, V., Reyers, B., Sorlin, S., 2015. Planetary boundaries: Guiding human development on a changing planet. *Science* 347, 1259855–1259855. <https://doi.org/10.1126/science.1259855>

- Stinson, B., Murthy, S., Bott, C., Wett, B., Al-Omari, A., Bowden, G., Mokhyerie, Y., De Clippeleir, H., 2013. Roadmap Toward Energy Neutrality & Chemical Optimization at Enhanced Nutrient Removal Facilities. *Proc. Water Environ. Fed.* 2013, 702–731.
- Stokholm-Bjerregaard, M., McIlroy, S.J., Nierychlo, M., Karst, S.M., Albertsen, M., Nielsen, P.H., 2017. A Critical Assessment of the Microorganisms Proposed to be Important to Enhanced Biological Phosphorus Removal in Full-Scale Wastewater Treatment Systems. *Front. Microbiol.* 8. <https://doi.org/10.3389/fmicb.2017.00718>
- Strous, M., Heijnen, J.J., Kuenen, J.G., Jetten, M.S.M., 1998. The sequencing batch reactor as a powerful tool for the study of slowly growing anaerobic ammonium-oxidizing microorganisms. *Appl. Microbiol. Biotechnol.* 50, 589–596.
- Strous, M., Kuenen, J.G., Jetten, M.S.M., 1999. Key Physiology of Anaerobic Ammonium Oxidation. *Appl. Environ. Microbiol.* 65, 3248–3250.
- Takács, I., Stricker, A.-E., Achleitner, S., Barrie, A., Rauch, W., Murthy, S., 2008. Do You Know Your Sludge Age? *Proc. Water Environ. Fed.* 2008, 3639–3655. <https://doi.org/10.2175/193864708788733486>
- Tang, C., Zheng, P., Wang, C., Mahmood, Q., 2010. Suppression of anaerobic ammonium oxidizers under high organic content in high-rate Anammox UASB reactor. *Bioresour. Technol.* 101, 1762–1768. <https://doi.org/10.1016/j.biortech.2009.10.032>
- Tang, C.-J., Zheng, P., Chai, L.-Y., Min, X.-B., 2013. Thermodynamic and kinetic investigation of anaerobic bioprocesses on ANAMMOX under high organic conditions. *Chem. Eng. J.* 230, 149–157. <https://doi.org/10.1016/j.cej.2013.06.047>
- Tasli, R., Orhon, D., Artan, N., 1999. The effect of substrate composition on the nutrient removal potential of sequencing batch reactors. *Water A* 25, 337–344.
- Tsuneda, S., Ohno, T., Soejima, K., Hirata, A., 2006. Simultaneous nitrogen and phosphorus removal using denitrifying phosphate-accumulating organisms in a sequencing batch reactor. *Biochem. Eng. J.* 27, 191–196. <https://doi.org/10.1016/j.bej.2005.07.004>
- Ushiki, N., Jinno, M., Fujitani, H., Suenaga, T., Terada, A., Tsuneda, S., 2017. Nitrite oxidation kinetics of two *Nitrospira* strains: The quest for competition and ecological niche differentiation. *J. Biosci. Bioeng.* 123, 581–589. <https://doi.org/10.1016/j.jbiosc.2016.12.016>
- Valverde-Pérez, B., Wágner, D.S., Lóránt, B., Gülay, A., Smets, B.F., Plósz, B.G., 2016. Short-sludge age EBPR process – Microbial and biochemical process characterisation during reactor start-up and operation. *Water Res.* 104, 320–329. <https://doi.org/10.1016/j.watres.2016.08.026>
- van Kessel, M.A.H.J., Speth, D.R., Albertsen, M., Nielsen, P.H., Op den Camp, H.J.M., Kartal, B., Jetten, M.S.M., Lücker, S., 2015. Complete nitrification by a single microorganism. *Nature* 528, 555–559. <https://doi.org/10.1038/nature16459>
- Větrovský, T., Baldrian, P., 2013. The Variability of the 16S rRNA Gene in Bacterial Genomes and Its Consequences for Bacterial Community Analyses. *PLoS ONE* 8, e57923. <https://doi.org/10.1371/journal.pone.0057923>
- Veuillet, F., Lacroix, S., Bausseron, A., Gonidec, E., Ochoa, J., Christensson, M., Lemaire, R., 2014. Integrated fixed-film activated sludge ANITA™Mox process – a new perspective for advanced nitrogen removal. *Water Sci. Technol.* 69, 915. <https://doi.org/10.2166/wst.2013.786>

- Vlaeminck, S.E., De Clippeleir, H., Verstraete, W., 2012. Microbial resource management of one-stage partial nitritation/anammox: MRM on OLAND. *Microb. Biotechnol.* 5, 433–448. <https://doi.org/10.1111/j.1751-7915.2012.00341.x>
- Volcke, E.I.P., Picioreanu, C., De Baets, B., van Loosdrecht, M.C.M., 2010. Effect of granule size on autotrophic nitrogen removal in a granular sludge reactor. *Environ. Technol.* 31, 1271–1280. <https://doi.org/10.1080/09593331003702746>
- Wagner, M., Rath, G., Amann, R., Koops, H.-P., Schleifer, K.-H., 1995. In situ Identification of Ammonia-oxidizing Bacteria. *Syst. Appl. Microbiol.* 18, 251–264. [https://doi.org/10.1016/S0723-2020\(11\)80396-6](https://doi.org/10.1016/S0723-2020(11)80396-6)
- Wallner, G., Amann, R., Beisker, W., 1993. Optimizing fluorescent in situ hybridization with rRNA-targeted oligonucleotide probes for flow cytometric identification of microorganisms. *Cytometry* 14, 136–143. <https://doi.org/10.1002/cyto.990140205>
- Wan, J., Gu, J., Zhao, Q., Liu, Y., 2016. COD capture: a feasible option towards energy self-sufficient domestic wastewater treatment. *Sci. Rep.* 6. <https://doi.org/10.1038/srep25054>
- Wang, J.C., Park, J.K., Whang, L.M., 2001. Comparison of Fatty Acid Composition and Kinetics of Phosphorus-Accumulating Organisms and Glycogen-Accumulating Organisms. *Water Environ. Res.* 73, 704–710. <https://doi.org/10.2175/106143001X143448>
- Wang, Shanyun, Peng, Y., Ma, B., Wang, Shuying, Zhu, G., 2015. Anaerobic ammonium oxidation in traditional municipal wastewater treatment plants with low-strength ammonium loading: Widespread but overlooked. *Water Res.* 84, 66–75. <https://doi.org/10.1016/j.watres.2015.07.005>
- Wang, Y., Ma, L., Mao, Y., Jiang, X., Xia, Y., Yu, K., Li, B., Zhang, T., 2017. Comammox in drinking water systems. *Water Res.* 116, 332–341. <https://doi.org/10.1016/j.watres.2017.03.042>
- Wastewater Treatment [WWW Document], 2017. . METHANOL Inst. URL <http://www.methanol.org/wastewater-treatment/> (accessed 11.7.17).
- Welles, L., Lopez-Vazquez, C.M., Hooijmans, C.M., van Loosdrecht, M.C.M., Brdjanovic, D., 2014. Impact of salinity on the anaerobic metabolism of phosphate-accumulating organisms (PAO) and glycogen-accumulating organisms (GAO). *Appl. Microbiol. Biotechnol.* 98, 7609–7622. <https://doi.org/10.1007/s00253-014-5778-4>
- Wells, G.F., Park, H.-D., Yeung, C.-H., Eggleston, B., Francis, C.A., Criddle, C.S., 2009. Ammonia-oxidizing communities in a highly aerated full-scale activated sludge bioreactor: betaproteobacterial dynamics and low relative abundance of Crenarchaea. *Environ. Microbiol.* 11, 2310–2328. <https://doi.org/10.1111/j.1462-2920.2009.01958.x>
- Wells, G.F., Shi, Y., Laurenzi, M., Rosenthal, A., Szivák, I., Weissbrodt, D.G., Joss, A., Buergermann, H., Johnson, D.R., Morgenroth, E., 2017. Comparing the Resistance, Resilience, and Stability of Replicate Moving Bed Biofilm and Suspended Growth Combined Nitritation–Anammox Reactors. *Environ. Sci. Technol.* 51, 5108–5117. <https://doi.org/10.1021/acs.est.6b05878>
- Wett, B., Omari, A., Podmirseg, S.M., Han, M., Akintayo, O., Gómez Brandón, M., Murthy, S., Bott, C., Hell, M., Takács, I., Nyhuis, G., O’Shaughnessy, M., 2013. Going for mainstream deammonification from bench to full scale for maximized resource efficiency. *Water Sci. Technol.* 68, 283. <https://doi.org/10.2166/wst.2013.150>

- Wett, B., Podmirseg, S.M., Gómez-Brandón, M., Hell, M., Nyhuis, G., Bott, C., Murthy, S., 2015. Expanding DEMON Sidestream Deammonification Technology Towards Mainstream Application. *Water Environ. Res.* 87, 2084–2089. <https://doi.org/10.2175/106143015X14362865227319>
- Wiesmann, U., 1994. Biological nitrogen removal from wastewater, in: *Biotechnics/Wastewater, Advances in Biochemical Engineering/Biotechnology*. Springer Berlin Heidelberg, Berlin, Heidelberg, pp. 113–154. <https://doi.org/10.1007/BFb0008736>
- Winkler, M.K.H., Bassin, J.P., Kleerebezem, R., Sorokin, D.Y., van Loosdrecht, M.C.M., 2012. Unravelling the reasons for disproportion in the ratio of AOB and NOB in aerobic granular sludge. *Appl. Microbiol. Biotechnol.* 94, 1657–1666. <https://doi.org/10.1007/s00253-012-4126-9>
- Wrage, N., Velthof, G.L., van Beusichem, M.L., Oenema, O., 2001. Role of nitrifier denitrification in the production of nitrous oxide. *Soil Biol.* 10.
- Xiaojin Li, Stephanie Klaus, Charles Bott, Zhen He, 2018. Status, Challenges and Perspectives of Mainstream Nitritation-Anammox for Wastewater Treatment. *Water Environ. Res.* <https://doi.org/10.2175/106143017X15131012152870>
- Yang, Y., Zhang, L., Shao, H., Zhang, S., Gu, P., Peng, Y., 2017. Enhanced nutrients removal from municipal wastewater through biological phosphorus removal followed by partial nitritation/anammox. *Front. Environ. Sci. Eng.* 11. <https://doi.org/10.1007/s11783-017-0911-0>
- Yuan, Z., Pratt, S., Batstone, D.J., 2012. Phosphorus recovery from wastewater through microbial processes. *Curr. Opin. Biotechnol.* 23, 878–883. <https://doi.org/10.1016/j.copbio.2012.08.001>
- Zekker, I., Rikmann, E., Mandel, A., Kroon, K., Seiman, A., Mihkelson, J., Tenno, Taavo, Tenno, Toomas, 2016. Step-wise temperature decreasing cultivates a biofilm with high nitrogen removal rates at 9°C in short-term anammox biofilm tests. *Environ. Technol.* 37, 1933–1946. <https://doi.org/10.1080/09593330.2015.1135995>
- Zekker, I., Rikmann, E., Tenno, Toomas, Seiman, A., Loorits, L., Kroon, K., Tomingas, M., Vabamäe, P., Tenno, Taavo, 2014. Nitritating-anammox biomass tolerant to high dissolved oxygen concentration and C/N ratio in treatment of yeast factory wastewater. *Environ. Technol.* 35, 1565–1576. <https://doi.org/10.1080/09593330.2013.874492>
- Zeng, R.J., Lemaire, R., Yuan, Z., Keller, J., 2003a. Simultaneous nitrification, denitrification, and phosphorus removal in a lab-scale sequencing batch reactor. *Biotechnol. Bioeng.* 84, 170–178. <https://doi.org/10.1002/bit.10744>
- Zeng, R.J., Saunders, A.M., Yuan, Z., Blackall, L.L., Keller, J., 2003b. Identification and comparison of aerobic and denitrifying polyphosphate-accumulating organisms. *Biotechnol. Bioeng.* 83, 140–148. <https://doi.org/10.1002/bit.10652>
- Zeng, R.J., van Loosdrecht, M.C.M., Yuan, Z., Keller, J., 2003c. Metabolic model for glycogen-accumulating organisms in anaerobic/aerobic activated sludge systems. *Biotechnol. Bioeng.* 81, 92–105. <https://doi.org/10.1002/bit.10455>
- Zeng, W., Li, B., Wang, X., Bai, X., Peng, Y., 2014. Integration of denitrifying phosphorus removal via nitrite pathway, simultaneous nitritation–denitrification and anammox treating carbon-limited municipal sewage. *Bioresour. Technol.* 172, 356–364. <https://doi.org/10.1016/j.biortech.2014.09.061>

- Zhang, M., Qiao, S., Shao, D., Jin, R., Zhou, J., 2018. Simultaneous nitrogen and phosphorus removal by combined anammox and denitrifying phosphorus removal process. *J. Chem. Technol. Biotechnol.* 93, 94–104. <https://doi.org/10.1002/jctb.5326>
- Zhao, J., Wang, X., Li, X., Jia, S., Peng, Y., 2018. Combining partial nitrification and post endogenous denitrification in an EBPR system for deep-level nutrient removal from low carbon/nitrogen (C/N) domestic wastewater. *Chemosphere* 210, 19–28. <https://doi.org/10.1016/j.chemosphere.2018.06.135>
- Zhao, J., Wang, X., Li, X., Jia, S., Wang, Q., Peng, Y., 2019. Improvement of partial nitrification endogenous denitrification and phosphorus removal system: Balancing competition between phosphorus and glycogen accumulating organisms to enhance nitrogen removal without initiating phosphorus removal deterioration. *Bioresour. Technol.* 281, 382–391. <https://doi.org/10.1016/j.biortech.2019.02.109>
- Zheng, Z., Li, J., Ma, J., Du, J., Bian, W., Li, Y., Zhang, Y., Zhao, B., 2016. Nitrogen removal via simultaneous partial nitrification, anammox and denitrification (SNAD) process under high DO condition. *Biodegradation* 27, 195–208. <https://doi.org/10.1007/s10532-016-9766-5>
- Zhou, X., Zhang, Z., Zhang, X., Liu, Y., 2018. A novel single-stage process integrating simultaneous COD oxidation, partial nitritation-denitritation and anammox (SCONDA) for treating ammonia-rich organic wastewater. *Bioresour. Technol.* 254, 50–55. <https://doi.org/10.1016/j.biortech.2018.01.057>
- Zhou, Y., Pijuan, M., Zeng, R.J., Lu, H., Yuan, Z., 2008. Could polyphosphate-accumulating organisms (PAOs) be glycogen-accumulating organisms (GAOs)? *Water Res.* 42, 2361–2368. <https://doi.org/10.1016/j.watres.2008.01.003>